

AD-A080 567

WESTINGHOUSE RESEARCH AND DEVELOPMENT CENTER PITTSBU--ETC F/G 9/1
OPTICALLY ACTIVATED SWITCH.(U)
APR 78 L R LOWRY

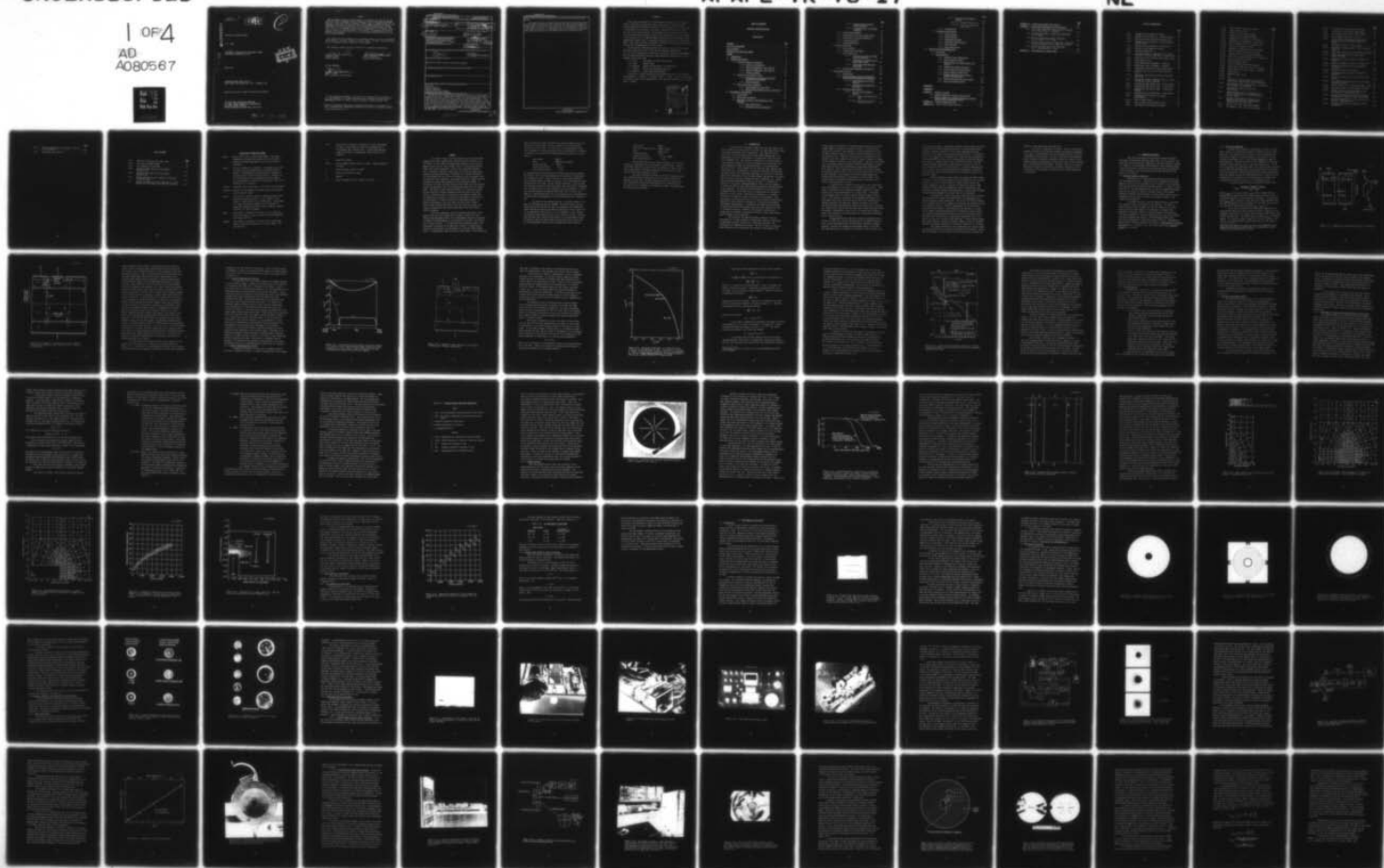
F33615-74-C-2029

UNCLASSIFIED

AFAPL-TR-78-17

NL

1 OF 4
AD
A080567



ADA080567

✓
AFAPL-TR-78-17

LEVEL

2

OPTICALLY ACTIVATED SWITCH

L. R. LOWRY

WESTINGHOUSE RESEARCH AND DEVELOPMENT CENTER
PITTSBURGH, PENNSYLVANIA 15235

DDC
RECEIVED
FEB 11 1980
E

FILE COPY

APRIL 1978

TECHNICAL REPORT AFAPL-TR-78-17
FINAL REPORT FOR PERIOD APRIL 1974 - FEBRUARY 1978

Approved for public release; distribution unlimited

AIR FORCE AERO PROPULSION LABORATORY
AIR FORCE WRIGHT AERONAUTICAL LABORATORIES
AIR FORCE SYSTEMS COMMAND
WRIGHT-PATTERSON AIR FORCE BASE, OHIO 45433

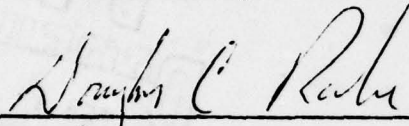
80 2 8 021

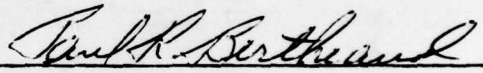
NOTICE

When Government drawings, specifications, or other data are used for any purpose other than in connection with a definitely related Government procurement operation, the United States Government thereby incurs no responsibility nor any obligation whatsoever; and the fact that the government may have formulated, furnished, or in any way supplied the said drawings, specifications, or other data, is not to be regarded by implication or otherwise as in any manner licensing the holder or any other person or corporation, or conveying any rights or permission to manufacture, use, or sell any patented invention that may in any way be related thereto.

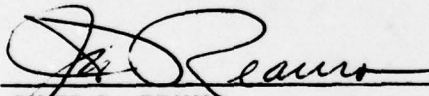
This report has been reviewed by the Information Office (OI) and is releasable to the National Technical Information Service (NTIS). At NTIS, it will be available to the general public, including foreign nations.

This technical report has been reviewed and is approved for publication.


DOUGLAS C. RABE
Project Engineer


PAUL R. BERTHEAUD
Technical Area Manager

FOR THE COMMANDER


JAMES D. REAMS
Chief, Aerospace Power Division

"If your address has changed, if you wish to be removed from our mailing list, or if the addressee is no longer employed by your organization please notify AFAPL/POP-2, W-PAFB, OH 45433 to help us maintain a current mailing list".

Copies of this report should not be returned unless return is required by security considerations, contractual obligations, or notice on a specific document.

UNCLASSIFIED

SECURITY CLASSIFICATION OF THIS PAGE (When Data Entered)

| 19 REPORT DOCUMENTATION PAGE | | READ INSTRUCTIONS BEFORE COMPLETING FORM |
|--|---|---|
| 1. REPORT NUMBER (18) AFAPL-TR-78-17 | 2. GOVT ACCESSION NO. | 3. RECIPIENT'S CATALOG NUMBER |
| 4. TITLE (and Subtitle) (6) OPTICALLY ACTIVATED SWITCH | 5. TYPE OF REPORT & PERIOD COVERED (9) Final Technical Report 1 Apr 1974 - 1 Feb 1978 | 6. PERFORMING ORG. REPORT NUMBER |
| 7. AUTHOR(s) (10) L. R. Lowry | 8. CONTRACT OR GRANT NUMBER(s) (15) F33615-74-C-2029 | |
| 9. PERFORMING ORGANIZATION NAME AND ADDRESS Westinghouse Electric Corporation Research and Development Center 1310 Beulah Road, Churchill Borough Pittsburgh PA 15235 | 10. PROGRAM ELEMENT, PROJECT, TASK AREA & WORK UNIT NUMBERS Project 3145 Task 314532, Work Unit 31453223 (17) 32 | |
| 11. CONTROLLING OFFICE NAME AND ADDRESS | 12. REPORT DATE (11) Apr 1978 | 13. NUMBER OF PAGES |
| 14. MONITORING AGENCY NAME & ADDRESS (if different from Controlling Office) (12) 349 | 15. SECURITY CLASS. (of this report) Unclassified | 15a. DECLASSIFICATION/DOWNGRADING SCHEDULE |
| 16. DISTRIBUTION STATEMENT (of this Report) Approved for public release; distribution unlimited. | | |
| 17. DISTRIBUTION STATEMENT (of the abstract entered in Block 20, if different from Report) | | |
| 18. SUPPLEMENTARY NOTES | | |
| 19. KEY WORDS (Continue on reverse side if necessary and identify by block number) Thyristor Optical Thyristor Optical Triggering High Repetition Rate Switches Laser Activated Silicon Switch | | |
| 20. ABSTRACT (Continue on reverse side if necessary and identify by block number) There has been a growing need for improved switches for very high energy pulsed power systems. Conventional switches such as thyratons, spark gaps, and ignitrons have deficiencies in one or more of the desired parameters. A new solid state device, the Laser Activated Silicon Switch (LASS), appears to have the potential of meeting simultaneously all of the desired parameters including life and reliability of an extremely fast, high power, pulsed power switch. The LASS is a silicon pnpn structure similar to an electrically gated thyristor, but it is triggered by a beam from a Nd:YAG laser. The laser trigger causes the | | |

DD FORM 1 JAN 73 1473 EDITION OF 1 NOV 65 IS OBSOLETE

UNCLASSIFIED

SECURITY CLASSIFICATION OF THIS PAGE (When Data Entered)

346 625

JP

UNCLASSIFIED

SECURITY CLASSIFICATION OF THIS PAGE(When Data Entered)

device to turn on orders of magnitude faster than does an electrically gated device.

This report describes the development and experimental verification of an analytic model of a high power LASS. Switches were fabricated and tested that achieved dI/dt values greater than 40000 A/ μ sec to peak currents of 25000 A for a pulse width of 40 μ sec. It is concluded that the LASS indeed has the potential to meet the needs for a pulsed power switch, but considerable research and development work is required. Recommendations are given for future work.

UNCLASSIFIED

SECURITY CLASSIFICATION OF THIS PAGE(When Data Entered)

FOREWORD

This report was prepared by the Westinghouse Research and Development Center, Pittsburgh, Pennsylvania 15235, under Contract F33615-74-C-2029, Project/Task/Work Unit numbers 3145/32/23. The objective of the program was to investigate the potential of the Laser Activated Silicon Switch (LASS) for use in pulse power systems. The program's major thrusts consisted of: 1) an analytical and theoretical study of the principles of operation leading to the construction of a computer model that would predict performance of an experimental design, and 2) experimental fabrication and tests to verify the model. The report describes, in detail, the various tasks and program results and provides recommendations for future work.

The program was administered under the direction of the Air Force Aero Propulsion Laboratory by Mr D. Rabe, Project Engineer (AFAPL/POP). Mr L. R. Lowry, Manager Device Technology was the Westinghouse Program Manager. The following Westinghouse personnel made significant contributions to the program in the areas cited:

| | |
|----------------|---|
| J. R. Davis | Development of LASS Analytic Model |
| L. R. Lowry | Thermal Model |
| J. B. Brewster | Design and Fabrication of 40 PFN Pulser |
| J. S. Roberts | Electrical Experiments with LASS |
| P. E. McMullin | Light Scattering Experiment |

In addition, valuable assistance was rendered from time to time during the program by L. E. Hohn, L. V. Rohall, and R. J. Fiedor. Useful contributions to the theory and to the interpretation of the data were supplied by D. J. Page and P. L. Hower.

| | |
|--------------------|--|
| Accession For | |
| NTIS General | <input checked="checked" type="checkbox"/> |
| DDC TAB | <input type="checkbox"/> |
| Unannounced | <input type="checkbox"/> |
| Justification | |
| By | |
| Distribution/ | |
| Availability Codes | |
| Dist | Availand/or special |
| A | |

TABLE OF CONTENTS

OPTICALLY ACTIVATED SWITCH

Final Report

| | <u>Page</u> |
|---|-------------|
| <u>ABSTRACT</u> | v |
| <u>LIST OF ILLUSTRATIONS</u> | vi |
| <u>LIST OF TABLES</u> | x |
| <u>DEFINITION OF TERMS AND SYMBOLS</u> | xi |
| <u>SUMMARY</u> | 1 |
| 1.0 <u>INTRODUCTION</u> | 4 |
| 2.0 <u>THEORETICAL ANALYSIS</u> | 8 |
| 2.1 <u>Thyristor Theory of Operation</u> | 8 |
| 2.1.1 <u>Electrical Triggering</u> | 9 |
| 2.1.2 <u>Optical Triggering - Slow Turn-on</u> | 13 |
| 2.1.3 <u>Optical Triggering - Fast Turn-on</u> | 13 |
| 2.1.4 <u>Plasma Spreading</u> | 22 |
| 2.2 <u>Analytical and Computer Model</u> | 23 |
| 2.2.1 <u>Development of Optically Activated Thyristor Turn-on Model</u> | 24 |
| 2.2.2 <u>Thermal Analysis</u> | 30 |
| 2.3 <u>Other Analytical Information</u> | 43 |
| 2.3.1 <u>Air Breakdown by Laser Beam</u> | 43 |
| 2.3.2 <u>Minimum Light Needed to Turn-on Thyristor</u> | 44 |
| 3.0 <u>EXPERIMENTAL VERIFICATION</u> | 46 |
| 3.1 <u>Introduction</u> | 46 |
| 3.2 <u>Fabrication of Devices</u> | 49 |
| 3.3 <u>Equipment, Circuits, Instrumentation, and Technique</u> | 53 |
| 3.3.1 <u>Laser Light Source</u> | 53 |
| 3.3.2 <u>Spreading Velocity Measurement</u> | 56 |

| | <u>Page</u> |
|--|-------------|
| 3.3.2.1 <u>Infrared image converter camera technique</u> | 56 |
| 3.3.2.2 <u>Photomultiplier - light-pipe technique</u> | 70 |
| 3.3.3 <u>Pulsed Power Supplies</u> | 82 |
| 3.3.4 <u>Attenuation of the Laser Light Energy</u> | 86 |
| 3.3.5 <u>Variation of the Area Illuminated</u> | 88 |
| 3.3.6 <u>Current Monitoring</u> | 90 |
| 3.3.7 <u>Voltage Monitoring</u> | 90 |
| 3.4 <u>Problems Encountered</u> | 92 |
| 3.4.1 <u>Laser Problems</u> | 94 |
| 3.4.2 <u>Instrumentation Problems</u> | 95 |
| 3.4.3 <u>Device Under Test</u> | 96 |
| 3.4.3.1 <u>Non-uniform contact and high lateral resistance</u> | 96 |
| 3.4.3.2 <u>Shadowing of a portion of the light input window</u> | 102 |
| 3.4.3.3 <u>Stray light from laser and laser beam</u> | 104 |
| 3.4.4 <u>40 PFN Pulser Shakedown and Operation</u> | 104 |
| 3.5 <u>Experimental Results</u> | 106 |
| 3.5.1 <u>Introduction</u> | 106 |
| 3.5.2 <u>Plasma Spreading Velocity Measurements Using Infrared Recombination Radiation</u> | 107 |
| 3.5.2.1 <u>Observations at low dI/dt and low J</u> | 107 |
| 3.5.2.2 <u>Observations at high dI/dt and high J</u> | 116 |
| 3.5.3 <u>Electrical Measurements</u> | 122 |
| 3.5.3.1 <u>Tests on 23 mm diameter devices</u> | 124 |
| 3.5.3.1.1 <u>Light scattering experiments</u> | 124 |
| 3.5.3.1.2 <u>Other tests on 23 mm diameter devices</u> | 134 |

| | <u>Page</u> |
|---|-------------|
| 3.5.3.2 <u>Tests on 50 mm diameter devices</u> | 134 |
| 3.5.3.2.1 <u>Voltage-current data</u> | 142 |
| 3.5.3.2.2 <u>Effect of varying the light input</u> | 142 |
| 3.5.4 <u>Extended Work</u> | 147 |
| 3.6 <u>Packaging Considerations</u> | 154 |
| 3.6.1 <u>Optical Design</u> | 155 |
| 3.6.2 <u>Thermal Design</u> | 158 |
| 3.6.3 <u>Equalization Design</u> | 160 |
| 3.6.4 <u>Inductance Considerations</u> | 160 |
| 3.6.5 <u>Switch Package</u> | 161 |
| 3.6.6 <u>Laser Light Source</u> | 161 |
| 4.0 <u>CONCLUSIONS AND RECOMMENDATIONS</u> | 163 |
| 4.1 <u>Conclusions</u> | 163 |
| 4.2 <u>Recommendations</u> | 165 |
| 4.2.1 <u>Determine Light Requirements</u> | 165 |
| 4.2.2 <u>Improve Analytic Model</u> | 166 |
| 4.2.3 <u>Explore Means of Coupling Light into Silicon</u> | 166 |
| 4.2.4 <u>Improve Heat Removal Technique</u> | 166 |
| 4.2.5 <u>Develop Improved Instrumentation</u> | 167 |
| 4.2.6 <u>Measure Dynamic Forward Drop</u> | 167 |
| 4.2.7 <u>Design, Fabricate, and Evaluate a Complete Switch System</u> | 167 |
| 4.2.8 <u>Increase Thyristor Blocking Voltage</u> | 168 |
| 4.2.9 <u>Create True ON-OFF Switch</u> | 168 |
| <u>REFERENCES</u> | 169 |
| <u>APPENDICES</u> | 170 |
| <u>APPENDIX I - Computer Listings</u> | 170 |
| I-1 <u>Thermal Program for Infinite Silicon Slab</u> | 171 |
| I-2 <u>Thermal Program for Composite Material, Infinite Lateral Extent, Repetitive Pulses</u> | 176 |
| <u>APPENDIX II - Voltage Clamping Circuit</u> | 192 |
| <u>APPENDIX III - Laser Purchase Specifications</u> | 196 |

| | <u>Page</u> |
|---|-------------|
| <u>APPENDIX IV - Pulsed Power Supply Test Circuit</u> | 202 |
| <u>APPENDIX V - Papers Published Related to this Contract</u> | 224 |
| V-1 "Ultra-fast, High-power Laser-activated Switches" by J. R. Davis and J. S. Roberts | 225 |
| V-2 "A Theoretical Model of Light-Fired Thyristors" by J. R. Davis | 233 |
| V-3 "Light Activated Semiconductor Switches" by L. R. Lowry and D. J. Page | 242 |
| V-4 "Future Prospects for Fast, High Power, Long Life, Solid State Switches" by D.J.Page and L.R.Lowry . . . | 250 |
| V-5 "Solid State High Power Pulse Switching" by P. F. Pittman and D. J. Page | 265 |
| <u>APPENDIX VI - Oscillograms of Original Data</u> | 278 |

LIST OF ILLUSTRATIONS

| | | <u>Page</u> |
|-------|--|-------------|
| 2.1-1 | Diagrams for two-transistor analog | 10 |
| 2.1-2 | Diagram of power thyristor - forward blocking . . | 11 |
| 2.1-3 | Electron and hole distribution in thyristor . . . | 14 |
| 2.1-4 | Diagram of power thyristor - forward blocking, optical drive | 15 |
| 2.1-5 | Absorption characteristics of bulk silicon . . . | 17 |
| 2.1-6 | Optical carrier generation profile | 20 |
| 2.2-1 | Completed LASS device | 31 |
| 2.2-2 | Calculated change in temperature of a silicon slab after a 40 μ sec heat pulse, infinite slab . | 33 |
| 2.2-3 | Conceptual view of infinite slab physical model . | 35 |
| 2.2-4 | Nodal geometry plot | 37 |
| 2.2-5 | Node-element mesh arrangement - primitive | 38 |
| 2.2-6 | Node-element mesh arrangement - realistic | 39 |
| 2.2-7 | Temperature variation for double sided device . . | 40 |
| 2.2-8 | Isothermal plot at the end of the twentieth cycle | 41 |
| 2.2-9 | Temperature excursion of silicon at one-fifth heat input | 43 |
| 3.1-1 | Voltage and current waveforms of device at full voltage and current conditions | 47 |
| 3.2-1 | Experimental LASS emitter mask. H-type design . | 50 |
| 3.2-2 | Experimental LASS emitter mask. K-type design . | 51 |
| 3.2-3 | Experimental LASS emitter mask. J and R-type designs | 52 |
| 3.2-4 | Cathode metallization patterns - 23 mm devices . | 54 |
| 3.2-5 | Illumination port patterns in cathode metallization | 55 |
| 3.3-1 | Photo of laser output | 57 |
| 3.3-2 | View of inside laser head-adj. mirror | 58 |
| 3.3-3 | View inside laser head-lamp changing | 59 |

| | <u>Page</u> |
|--------|---|
| 3.3-4 | Front panel of laser power supply 60 |
| 3.3-5 | Laser cooling system 61 |
| 3.3-6 | Schematic of I-R image equipment. 63 |
| 3.3-7 | Typical data from image equipment 64 |
| 3.3-8 | Schematic of IR image conv. with laser 66 |
| 3.3-9 | Calibration of transmission of glan prism 68 |
| 3.3-10 | Device mounting jig for IR observations 69 |
| 3.3-11 | Photo of IR system with laser 71 |
| 3.3-12 | Schematic of PM-IR test set-up with PFN's 72 |
| 3.3-13 | Photo of PM-IR test set-up with PFN's 73 |
| 3.3-14 | Cathode contact with slotted IR windows 74 |
| 3.3-15 | Plan view of cathode showing grid of 005 holes 76 |
| 3.3-16 | Photo of cathode electrodes 77 |
| 3.3-17 | Photomultiplier signal 81 |
| 3.3-18 | Photo of system with 20 PFN's exposed 84 |
| 3.3-19 | Pulse shape of PFN test circuit, 10 μ sec/div 85 |
| 3.3-20 | Pulse shape of PFN test circuit, 1 μ sec/div 85 |
| 3.3-21 | Hammer switch 86 |
| 3.3-22 | Modified hammer switch 87 |
| 3.3-23 | FOC 89 |
| 3.3-24 | Comparison of current signal from 0.001 ohm resistor and Pearson model current transformer 91 |
| 3.3-25 | Oscilloscope traces showing effects of different gain settings on oscilloscope 93 |
| 3.4-1 | Failed device showing arcing in the metallization 97 |
| 3.4-2 | Sketch defining contact configuration for lateral voltage drop in the metallization of the LASS device 99 |
| 3.4-3 | Sketches illustrating the effects of poor geometric and electrical configurations associated with the light input 103 |
| 3.5-1 | Cathode view of the structures examined 109 |
| 3.5-2 | I-R emission, laser fired, H-type design 110 |

| | <u>Page</u> |
|--------|--|
| 3.5-3 | I-R emission, laser fired, K-type design 112 |
| 3.5-4 | I-R emission, laser fired, J-type design 113 |
| 3.5-5 | I-R emission, laser fired, R-type design 114 |
| 3.5-6 | 23 mm diameter device with 4 slots 118 |
| 3.5-7 | 23 mm diameter LASS devices showing overall pattern of 0.127 mm diameter observation windows 119 |
| 3.5-8 | Spreading velocity vs current density 120 |
| 3.5-9 | Comparison of hammer switch to LASS in coaxial capacitor 123 |
| 3.5-10 | Experimental set-up for studying beam spreading . 126 |
| 3.5-11 | Images from sample #1 with laser beam at normal incidence 128 |
| 3.5-12 | Dimensions of mask aperture and thickness of sample #1 130 |
| 3.5-13 | Images from sample #2, angle of incidence 60° . . 131 |
| 3.5-14 | Dimensions of mask aperture and thickness of sample #2 134 |
| 3.5-15 | Hexifurcated fiber optics cable 135 |
| 3.5-16 | Illumination parts used with 50 mm devices initially 137 |
| 3.5-17 | Pattern of fiber optics cable end burned into silicon 138 |
| 3.5-18 | 50 mm diameter semiconductor device with eight rectangular windows 140 |
| 3.5-19 | Current waveform for 40 paralleled PFN's, 1700V . 141 |
| 3.5-20 | Illumination parts in 50 mm diameter devices . . 143 |
| 3.5-21 | Change in current waveform between one and two branches of fiber optics cable 146 |
| 3.5-22 | Multiple exposure showing effect of reducing the number of branches of fiber optics cable . . 148 |
| 3.5-23 | Forward voltage drop at 2 μ sec as function of initially illuminated area 150 |
| 3.5-24 | Forward voltage drop as a function of beam attenuation 152 |

| | <u>Page</u> |
|---|-------------|
| 3.5-25 Forward voltage drop as a function of time at 77.3% attenuation | 153 |
| 3.6-1 Conceptual switch design | 156 |

LIST OF TABLES

| | <u>Page</u> |
|--|-------------|
| 2.2-1 Thyristor model input and output data | 29 |
| 2.2-2 Input data to WECAN program | 40 |
| 2.3-1 Air breakdown by laser beam | 45 |
| 3.5-1 Voltage-currents data for 50 mm diameter thyristor 2G-4 | 144 |
| 3.5-2 Voltage-current data for 50 mm diameter thyristor 2G6 | 145 |
| 3.5-3 Forward voltage drop as a function of initially illuminated area | 147 |
| 3.5-4 Effect of varying the ports, taken four at a time, keeping the fiber optics cable branches constant | 149 |

DEFINITION OF TERMS AND SYMBOLS

- device - Usually used to mean a single LASS element. Used interchangeably with element and fusion; also used to denote a completely packaged semiconductor such as a thyristor or transistor.
- fusion - The active element of a thyristor. It consists of the silicon wafer (with the proper impurity diffusions) bonded (fused) to a molybdenum plate for mechanical strength and then metallized on the free silicon surface. Patterns are cut as appropriate in the metallization and the edges of the fused assembly are bevelled and passivated. This is the working part of a thyristor.
- element - Frequently used to mean fusion. Also called "active element."
- thyristor - Properly the environmentally packaged fusion but sometimes used to mean the fusion.
- switch - An electrical component capable of completing and/or interrupting an electrical circuit. In the context of this report it usually refers to the closing type. It can refer to a single functioning component or to a plurality of components arranged to provide a higher capability (usually referred to as "switch system").
- gate - The process of turning-on a thyristor. It is usually an electrical signal of control (rather than power) magnitude. See trigger and fire.
- trigger - The process of turning-on a thyristor in the conventional manner either with an electrical or optical signal. See gate and fire.

- fire - The process of turning-on a thyristor in a very fast manner by using a strong light of the proper wavelength such as that obtained from a Nd:YAG laser. Contrast with gate and trigger which imply a conventional, slower turn-on of the thyristor.
- I - electrical current.
- dI/dt - rate of change (usually rise) of current. Usually specified in A/ μ sec.
- J - current density, usually in A/cm²
- V - electrical potential in volts.
- A - amperes
- v_s - plasma spreading velocity, usually in μ m/ μ sec.

SUMMARY

For several years it has been apparent that the pulsed power community will need a significantly improved electrical switch in the late 1970's or early 1980's for high energy programs such as electromagnetic pulse testors, laser weapons, laser or electron-beam induced fusion, and isotope separation. Each of the conventional switches (e.g., thyratrons, ingitrons, spark gaps, etc.) that are being used to perform preliminary experiments to checkout the technical feasibility of these systems have one or more deficiencies such as inadequate life, low repetition rate capability, low average current, or trigger stability problems that render them unsuitable for an operational system. A new device, the laser activated silicon switch (LASS), has the potential to meet simultaneously all of the desired performance and life requirements. The LASS is a pnpn structure similar to a thyristor and would have the long life and high reliability associated with solid state devices. Thyristors that can control over one megawatt steady-state are commercially available, and typically such devices can operate in the pulse mode at 10 times or more of the steady-state rating. In addition experiments in the late 1960's and early 1970's showed that by using a Nd:YAG laser beam to fire the thyristor, rather than using the conventional electrical gating signal, very fast turn-on could be achieved.

With this background, the Aero Propulsion Laboratory of the United States Air Force entered into a research contract with the Research and Development Center of the Westinghouse Electric Corporation to advance the understanding of the operation of the LASS. The contract had two major thrusts: 1) an analytical and theoretical study of the principles of operation of the LASS, with the goal of constructing a model that would predict the performance of a particular LASS design; and 2) an experimental study that would provide inputs to the theoretical

model for data that cannot be derived in a practical manner from first principles, and also that would be a vehicle for the experimental verification of the model. A further goal of the experimental study was to demonstrate a significant advance in the performance of the LASS; specifically, to achieve the following performance goals with a single device.

| | | |
|-----------------------|---|----------------------------|
| peak current | - | 20000 A |
| dI/dt | - | 20000 A/ μ sec minimum |
| blocking voltage | - | 2000 V |
| current pulse width | - | 40 μ sec |
| pulse repetition rate | - | 1 pps |

The ultimate pulse rate desired with the other specifications constant was 500 pps, but for the experimental study there were two limitations on the repetition rate. First, there was not sufficient controlled power (800 kW) readily available to operate at full specification values and 500 pulses per second. Second, and more important, it was believed that the peak current and pulse width goals were sufficiently challenging that the added burden of a high repetition rate was premature. It would have required extensive design and fabrication time to build a test fixture to simultaneously meet all of the optical, power, instrumentation, and heat removal requirements for the LASS operating at full repetition rate.

The goals of the contract were met. An analytic model of the LASS was developed and coded in FORTRAN. This model accepts various design and operational data as input, and generates three dimensional curves showing the temporal and spatial distribution of the current and of the temperature in the device. It also generates a curve showing the forward voltage drop of the device as a function of time. The data from the model were verified by the results of the experimental study. In addition, LASS units were fired in the special pulse circuit built for the experimental study and the following values were achieved:

| | |
|-----------------------------|---------------------|
| peak current | >25000 A |
| flat top of pulse current - | 20000 A nominal |
| dI/dt | >40000 A/ μ sec |
| blocking voltage | >2000 V |
| current pulse width | 40 μ sec (FWHM) |
| pulse repetition rate | 1 pps |

Several LASS devices, each 50 mm in diameter, met the above values and considerable data was obtained on these devices. However, the thermal design of the test fixture was adequate to remove heat for only a few seconds of continuous operation at one pulse per second, and all devices were eventually failed.

The report describes in detail the various tasks and results. It is concluded that the LASS does have the potential capabilities desired in a very fast, extremely high power, long life switch, but that considerable research and development work is required before the LASS will be a candidate for operational systems. Recommendations for future work are provided.

1.0 INTRODUCTION

There has been increasing evidence over the past several years that an improved electrical switch is needed for high energy lasers, electron beams, and plasma physics experiments. Such switches will be used in the control of capacitively stored energy ranging from a few kilojoules up to tens of kilojoules at voltages from a few tens of kV up to hundreds of kV. The pulse rate required will be of the order of a few pulses per second up to tens of kilopulses per second with rise times ranging from about one microsecond down to a few nanoseconds. The switch should also be capable of very long life under adverse operating conditions. Traditionally, thyratrons, spark gaps, and ignitrons have been used for such high power switching, but each type of available switch has limitations so that the high voltage, high current, low jitter, high rise time, long life, freedom from false triggering, etc., cannot all be achieved simultaneously from any one type. In contrast the thyristor, a four-layer (pnpn) semiconductor device, has the longevity of solid state devices and a power-switching capability approaching that of the spark gap. The inherent switching speed of the electrically triggered device is relatively slow, but experimental and theoretical work prior to this contract indicated the possibility of a dramatic increase in the switch-on speed of thyristor type structures. This improvement is achieved by the use of the laser activated silicon switch (LASS) which shows promise of meeting all of the desired performance requirements simultaneously. In addition, the LASS has the advantage of being fabricated from reasonably sized and rated components so that it is modular in nature. Therefore, its rating in current and/or voltage may be increased or decreased in modest or large steps without major redesign of every component.

The reason for the expected dramatic increase in turn-on performance of the LASS compared to conventional solid state thyristors is described in detail in Section II, Theoretical Analysis. The reasoning can be summarized as follows: The rate of rise of current in most thyristors must be limited by the external circuit because only

a small region of the device is initially turned on when an electrical trigger signal is applied to the gate electrode. If the full load current were allowed to rise instantly, the heat generated locally in the small turned-on region in the device could be sufficient to cause the silicon to melt. External circuitry must be incorporated in the system to limit the current rise until the turned-on region, or plasma, in the thyristor has spread to the entire device. The size of the region that is initially turned-on has been increased substantially on modern high speed thyristors by incorporating an amplifying interdigitated gate structure. Here a small built-in thyristor is initially turned on and anode current is used to turn on a much larger area of the device. By this technique, turn-on speeds of several thousand amperes per microsecond can be obtained. Unfortunately, series strings of the devices cannot be conveniently operated because of variations in the turn-on speed from device to device.

A superior way to turn-on the device is to use a laser beam with a wavelength that is matched to the bandgap of the silicon. Large areas of the device can be turned-on extremely rapidly and a series string can be fired simultaneously by a single laser. In addition, this arrangement does not require complex isolated trigger circuits. Prior to this contract, scientists at the Westinghouse Research and Development Center had constructed devices which were modifications of standard thyristors and which were switched on using a laser beam. Only limited design and parametric studies were carried out to optimize the initial area of turn-on and the pulse rate at which the device could be operated. Nevertheless, rates of rise of 20,000 A/ μ sec rising to 3000 A were observed at a low repetition rate, indicating a substantial area of initial turn-on.

Recognizing that the LASS was a potential candidate device to fulfill the needs for a greatly improved switch, the United States Air Force and the Westinghouse Electric Corporation undertook a research program to increase the demonstrated performance levels of the LASS. The long range goal, not intended to be achieved in this contract, was

to develop an efficient, lightweight, high power, high voltage, optically triggered switch using the general approach of stacking high voltage, optically triggered thyristors in series and triggering them simultaneously with a single, Q-switched, neodymium YAG laser. The ultimate goal of the program was to determine how a single thyristor triggered by a Q-switched Nd^{3+} :YAG laser can be fabricated which can achieve performance levels of 20,000 A peak current, 20,000 A/ μsec dI/dt , and 2000 V forward blocking voltage with a pulse duration as long as 40 μsec at pulse repetition rates up to 500 pulses/sec. A specific immediate goal of the contract was to design, fabricate, and demonstrate a thyristor that meets this electrical performance but at a repetition rate of one pulse per second.

Towards meeting the above goals, the program had three primary objectives: (1) to develop parametric design information, (2) to extend the state of the art of these devices to improve their current and voltage capability, and (3) to maintain the high dI/dt value at high current and pulse repetition frequencies. While accomplishing these objectives, potential problems (and approaches to solving these problems) in the eventual packaging of the device were to be considered.

The approach to achieve the primary objectives was as follows: The LASS device was studied both theoretically and experimentally to develop parametric design information. The area of the device switched on was examined using a new technique that observed the radiation emitted by recombining carriers. From this measurement the carrier density distribution was obtained. This information was applied as one input to the computer program developed from the theoretical analytic model. The computer program generated tables or plots of the voltage-current characteristics and the local, instantaneous temperature rise of the device for each set of current pulse conditions. Various device designs were constructed and evaluated to generate empirical data for parameters needed by the analytic model and to verify the predictions of the model.

The primary objectives of the program were met, and the target performance objectives for the fabricated devices were exceeded. However, much work remains to be done before it will be practical to design and

construct a very high power, very fast LASS.

The report is organized as follows: Section 2, Theoretical Analysis, describes the theoretical analysis and computer programming of the LASS. The experimental work is discussed in detail in Section 3, Experimental Verification. Section 4, Conclusions and Recommendations, contains the specific conclusions reached as a result of this research program, and addresses the major areas that require additional work to advance the LASS technology. Finally, copies of the original data plus an extensive collection of peripheral information that is of interest to this program are contained in the various Appendices to this report.

2.0 THEORETICAL ANALYSIS

This section describes the theoretical analysis and model development and evaluation performed under Task 1 of the contract. The three major sections describe, respectively, the basic theory of turn-on of a thyristor, the development and evaluation of the theoretical model to describe optically activated turn-on under high dI/dt and high peak current conditions, and other theoretical analyses performed in the course of the contract.

2.1 Thyristor Theory of Operation.

The thyristor is a three-terminal bistable device with a low and a high impedance state. The device can be triggered from the high impedance state to the low impedance state ("turn-on") by an electrical pulse applied between the gate and cathode contacts. In order to return the device to the high impedance state, it must be commutated externally since once the device is turned on the gate contact loses control. Although the dynamic characteristics of turn-on differ with the type of triggering, once the device is fully on the manner in which it was triggered is unimportant.

The primary concern of the work reported herein is extremely fast turn-on by optical activation of the thyristor. In order to understand why an optical signal can turn-on a thyristor much faster than an electrical gate signal, it is necessary to examine three mechanisms of thyristor turn-on: electrical gating, optical gating with slow (comparable to electrical gating) turn-on, and optical gating to achieve extremely fast turn-on. The following discussion will describe the mechanisms of these three types of turn-on. Supplementary material about thyristor operation is available in Semiconductor Controlled Rectifiers by F. E. Gentry, et al., and a more recent book, Thyristor Physics by A. Blicher.¹

2.1.1 Electrical Triggering.

A simple way of looking at the thyristor is with a two transistor analog. Two transistors comprise the thyristor; the collector region of an npn transistor is the n-base of the pnp transistor and the collector region of the pnp transistor is the p-base of the npn transistor (see Figure 2.1-1). The collector junction is common to both transistors. Then the collector of each transistor is "driving" the base of the other and there is a positive feedback loop. If one of the transistors has sufficient gain to drive the other into saturation and the other has sufficient gain in the saturated state to drive the first into saturation, then both transistors will remain in saturation until the external current is reduced sufficiently to bring one of the transistors out of saturation. For this reason, the thyristor must be commutated externally to revert to a high impedance state.

It is easily shown from the two transistor analog⁽¹⁾ that

$$I_{\text{Anode}} = \frac{\alpha_{\text{nnp}} I_{\text{gate}} + I_{\text{CBOnpn}} + I_{\text{CBOpnp}}}{1 - (\alpha_{\text{nnp}} + \alpha_{\text{pnp}})}$$

where I_{Anode} is the anode current, I_{CBO} is the collector junction leakage current (emitter open) of the respective transistors, and α is the grounded base gain of the respective transistors. It can be seen that I_{Anode} tends to infinity as the sum of the alphas approaches one, and this corresponds to the low impedance or "on" state of the device. The criterion of switching is then that $\alpha_{\text{nnp}} + \alpha_{\text{pnp}} \geq 1$.*

Let us look in some detail at electrical triggering of an npnp thyristor where the p-base is used as the gate. Figure 2.1-2 is a schematic cross-section of a typical power thyristor shown biased in the forward blocking state. The common collector junction, J_2 , is reversed biased. If a positive voltage is applied to the gate relative to the cathode, the forward biased n-p emitter junction, J_1 , will begin to

*The sum of the alphas can exceed one only in the transient turn on during which the "excess current" goes into compensating the space charge of the common collector junction.

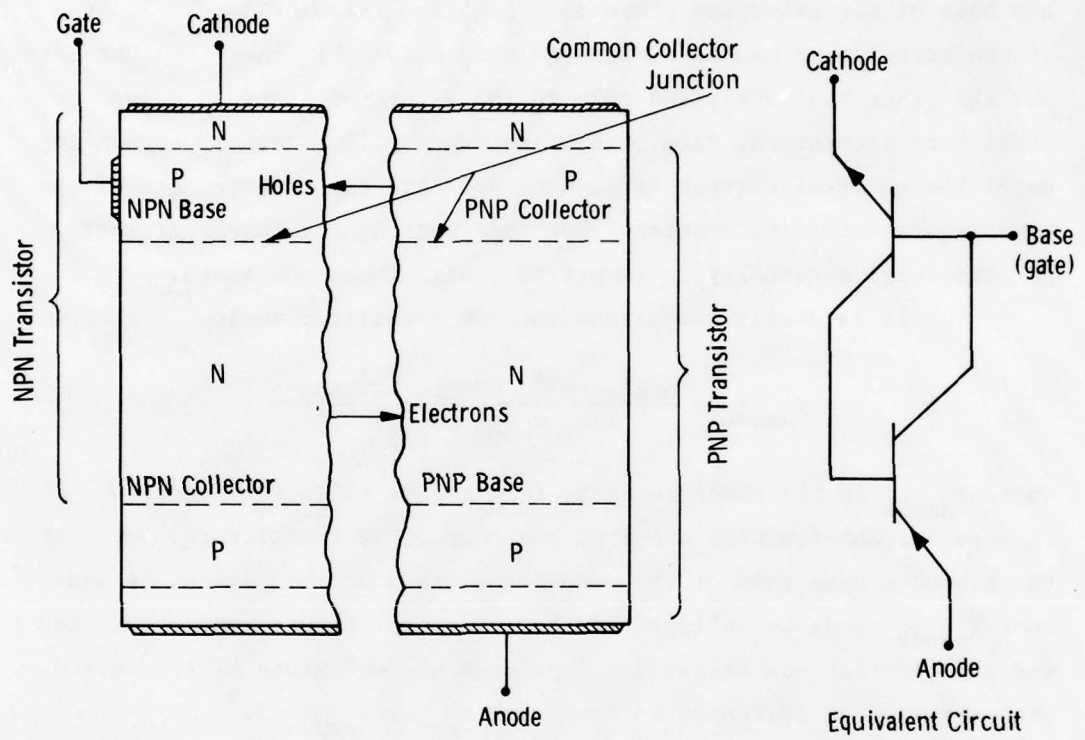


Figure 2.1-1. Diagrams for two-transistor analog of a thyristor.

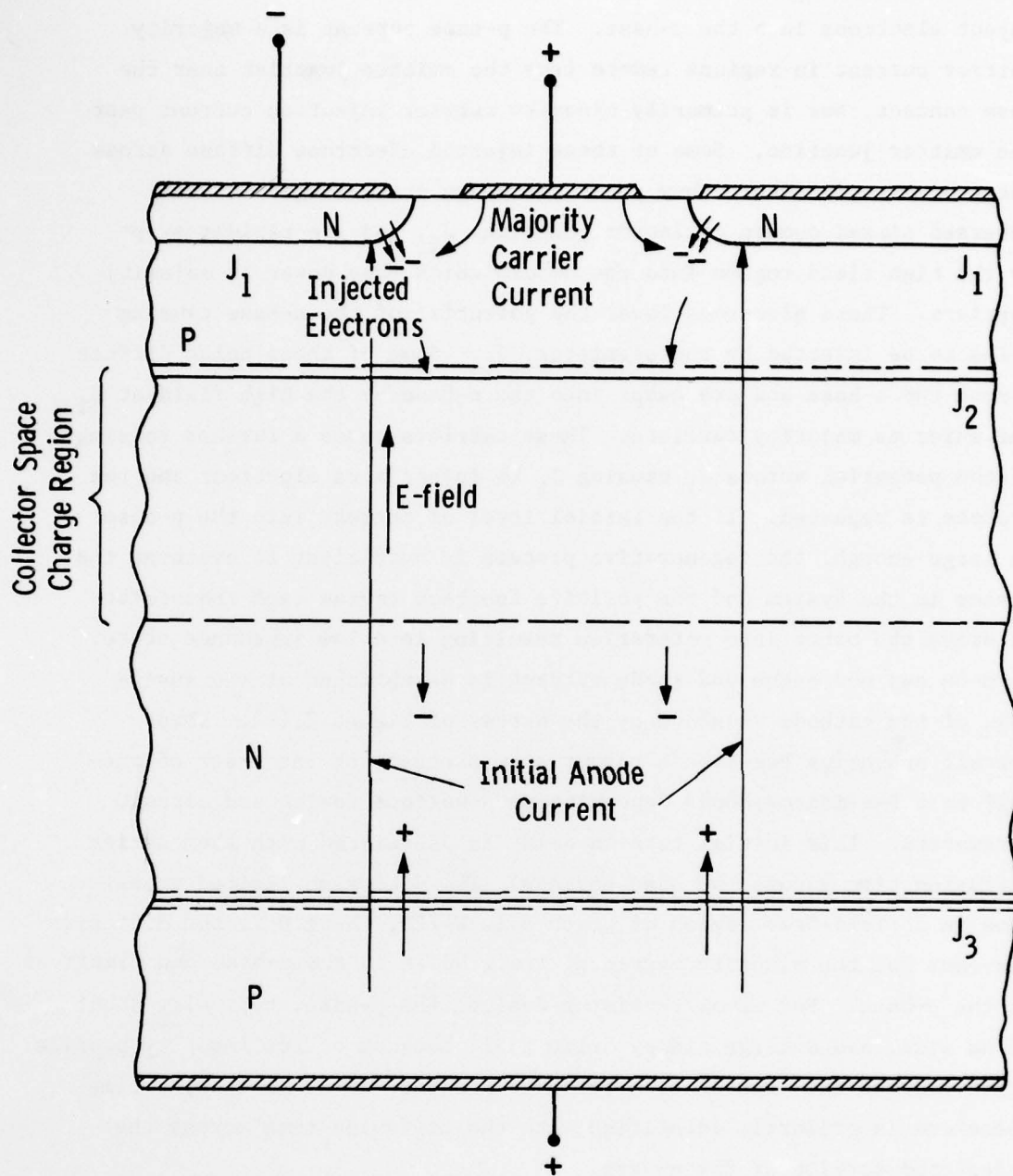


Figure 2.1-2. Diagram of a power thyristor in the forward blocking state during the early stage of turn-on. (Electrical gate drive.)

inject electrons into the p-base. The p-base current is a majority carrier current in regions remote from the emitter junction near the base contact, but is primarily minority carrier injection current near the emitter junction. Some of these injected electrons diffuse across the p-base region where they enter the space charge region of the reversed biased common collector junction, J_2 , and are rapidly swept by the high field region into the n-base which they enter as majority carriers. These electrons lower the potential of the n-base causing holes to be injected by the p-emitter, J_3 . Some of these holes diffuse across the n-base and are swept into the p-base by the high field at J_2 and enter as majority carriers. These carriers cause a further raising of the potential across J_1 causing J_1 to inject more electrons and the process is repeated. If the initial level of current into the p-base is large enough, the regenerative process is sufficient to overcome the losses in the system and the positive feedback causes each transistor to drive the other into saturation resulting in a low impedance state. Turn-on has now begun and anode current is established at the inside edge of the cathode as shown by the arrows of Figure 2.1-2. This overall operation has been a rather slow process, of the order of one-half to a few microseconds depending upon various device and circuit parameters. This initial turn-on delay is associated with the carrier diffusion time across the base regions. The diffusion limited transit time in a field-free region of width W is $W^2/2D$, where D is the diffusion constant for the minority carriers, i.e., holes in the n-base and electrons in the p-base. For usual thyristor designs the p-base, typically about 50 μm wide, has a large aiding drift field because of its impurity profile which reduces the transit time by about a factor of 3. The delay time therefore is primarily identified with the diffusion time across the undepleted portion of the n-base.

The "on" region will spread laterally at some velocity in the range of 40 to 100 μm per μsec . This will be discussed further in Section 2.1.4. In order not to cause damage by excessive current density, the anode current must be limited by the external circuit until substantial

spreading of the "on" region has taken place. When the turn-on process is completed, a plasma of electrons and holes exists in the base regions of the device with a density distribution as shown by the upper curves of Figure 2.1-3.

2.1.2 Optical Triggering--Slow Turn-On.

The thyristor can be optically triggered in a manner analogous to the electrical trigger. Assume that the gate region of the thyristor is illuminated with light that is absorbed in the silicon. Look at the cross-section of the thyristor (Figure 2.1-4). The absorption of the light generates hole-electron pairs in the bulk of the device. In the p-type base region, the minority carrier electrons which do not recombine through surface states diffuse away from the surface until they recombine with holes. The hole-electron pairs do not constitute base drive since their charges neutralize each other. If, however, the diffusion length of minority carriers in the p-base is sufficiently long (long lifetime) for electrons to reach a junction such as the collector junction, J_2 , the electrons are quickly accelerated out of the p-base region leaving excess holes behind. These excess holes effectively raise the potential in the p-base region causing the emitter junction, J_1 , to inject electrons into the base region. If the electrons are "collected" by the collector junction, J_2 , the separation of a hole-electron pair constitutes an excess majority carrier appearing in the base region of each transistor (see also Figure 2.1-1); whereas "collection" of a hole by the emitter junction constitutes an excess majority carrier appearing in only one base region. Therefore, it is desirable to generate as many carriers as possible within a diffusion length of the common collector junction, J_2 in order to most effectively drive the thyristor with light. From this it is apparent that the geometry of the device and the absorption characteristics of the light are important factors in achieving effective light drive of a thyristor.

2.1.3 Optical Triggering--Fast Turn-On.

A temporary digression is now in order to examine in detail how light is absorbed in silicon. A further investigation of what happens

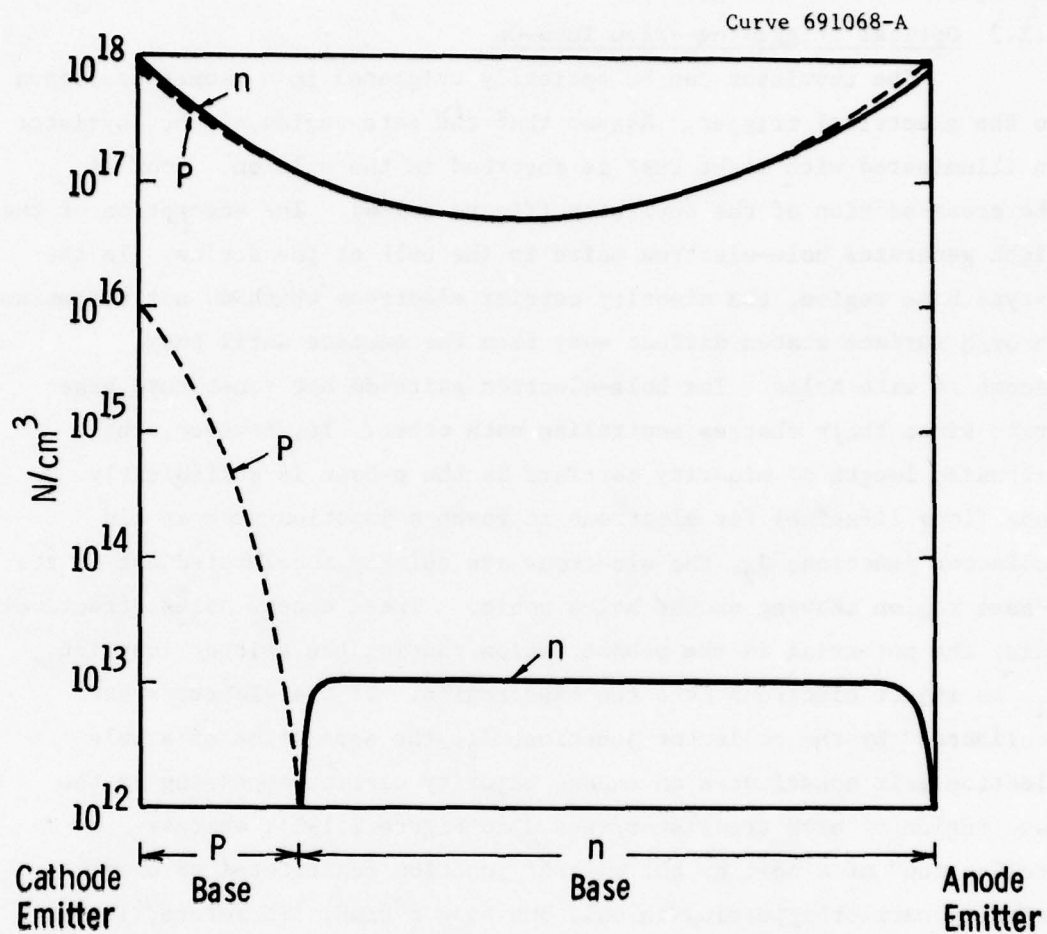


Figure 2.1-3. Electron and hole distribution in the base regions of a thyristor in the conducting state (upper curves) and in the unbiased state (lower curves). Figure truncated on both sides to eliminate the cathode and anode emitter regions.

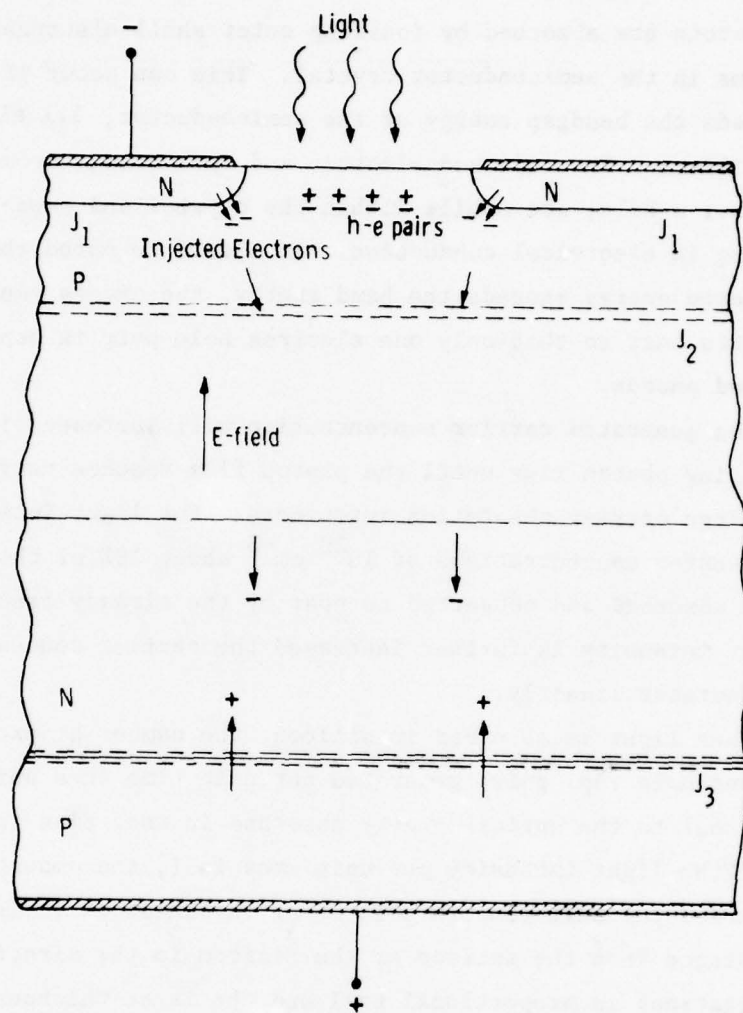


Figure 2.1-4. Diagram of a power thyristor in the forward blocking state. (Optical activation.)

when light is absorbed in the silicon of an operating thyristor will lead to an appreciation of how extremely fast turn-on can be achieved.

The absorption of light by a semiconductor is for our purposes dependent on two mechanisms. In the first and most important process incident photons are absorbed by ionizing outer shell electrons of the lattice atoms in the semiconductor crystal. This can occur if the photon energy exceeds the bandgap energy of the semiconductor, 1.1 electron volts for silicon. The released electron and the vacancy from which it came, i.e.; a hole, are mobile within the crystal and capable of participating in electrical conduction. It should be noted that if the incident photon energy exceeds the band energy, the excess energy is converted into heat so that only one electron hole pair is generated for each absorbed photon.

The generated carrier concentration will increase linearly with increasing photon flux until the photon flux reaches very high levels and free carrier absorption intervenes. For light intensities producing carrier concentrations of 10^{20} cm^{-3} about 10% of the incident photons are absorbed and converted to heat by the already free carriers, and as light intensity is further increased the carrier concentration ceases to increase linearly.

When light is absorbed in silicon, the number of excess electron (Δn) and hole (Δp) pairs generated per unit time in a unit volume is proportional to the optical energy absorbed in that time in the unit volume. If the light intensity per unit area is I , the amount of light energy absorbed per unit time in a layer of thickness dx (x is the perpendicular distance from the surface of the silicon in the direction of the light propagation) is proportional to I and the layer thickness dx :

$$-dI = \alpha I dx,$$

where α is a coefficient of proportionality, known as the optical absorption coefficient. Figure 2.1-5 shows how the absorption coefficient, α , varies with wavelength of the incident radiation.

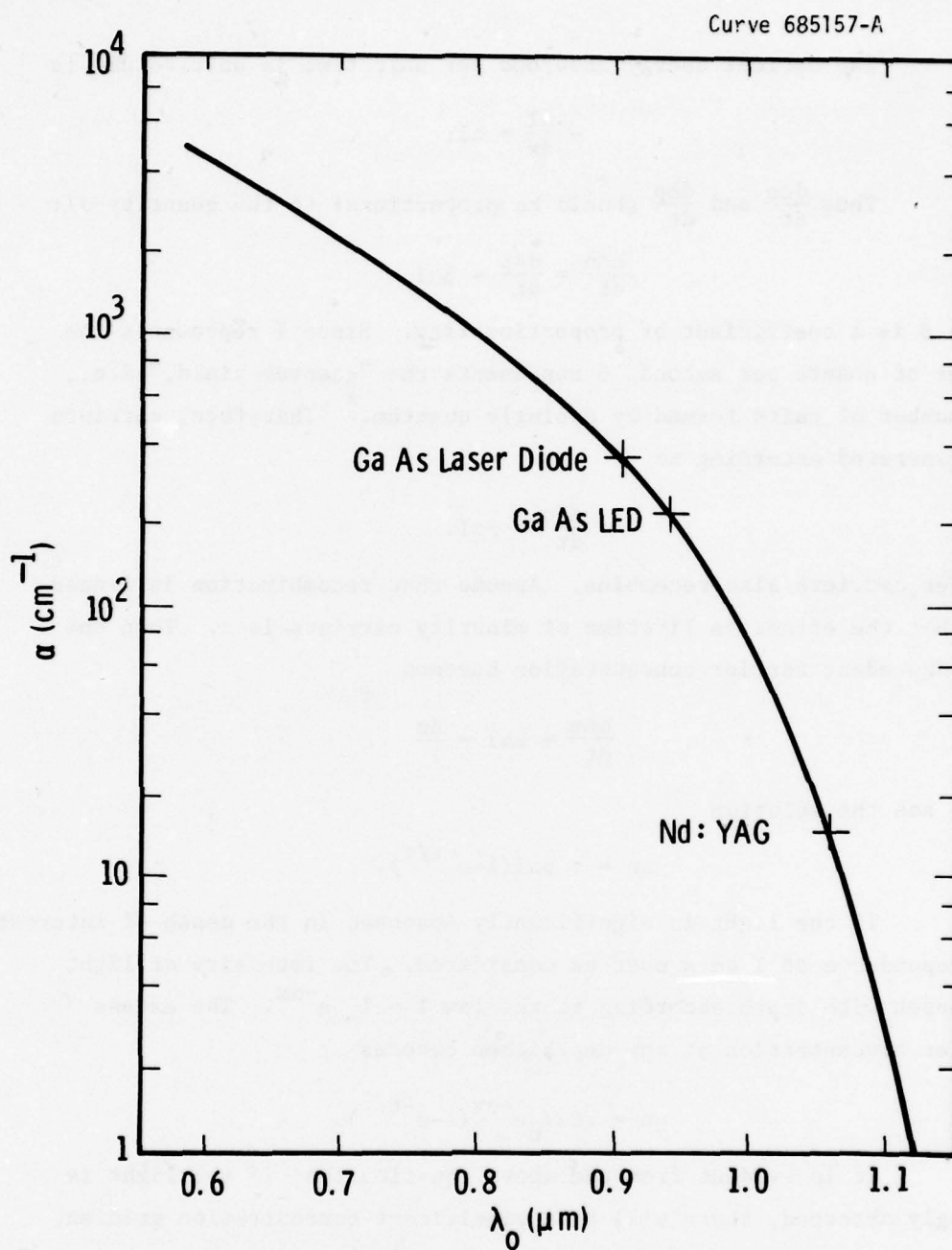


Figure 2.1-5. Absorption coefficient, α , of bulk silicon as a function of the wavelength of light. Data from H. Y. Fan and M. Becker, "Infrared Optical Properties of Silicon and Germanium", pp. 132-147 in Semiconducting Materials, Butterworth Scientific Publications, London, edited by H. K. Henish (1950).

The optical energy absorbed per unit time in unit volume is

$$-\frac{dI}{dx} = \alpha I.$$

Thus $\frac{d\Delta n}{dt}$ and $\frac{d\Delta p}{dt}$ should be proportional to the quantity αI :

$$\frac{d\Delta n}{dt} = \frac{d\Delta p}{dt} = \beta \alpha I,$$

where β is a coefficient of proportionality. Since I represents the number of quanta per second, β represents the "quantum yield," i.e., the number of pairs formed by a single quantum.* Therefore, carriers are generated according to

$$\frac{d\Delta n}{dt} = \beta \alpha I.$$

However, carriers also recombine. Assume that recombination is linear and that the effective lifetime of minority carriers is τ . Then the time dependent carrier concentration becomes

$$\frac{d\Delta n}{dt} = \beta \alpha I - \frac{\Delta n}{\tau}$$

which has the solution

$$\Delta n = \tau \beta \alpha I (1 - e^{-t/\tau}).$$

If the light is significantly absorbed in the depth of interest the dependence of I on x must be considered. The intensity of light decreases with depth according to the law $I = I_0 e^{-\alpha x}$. The excess carrier concentration at any depth then becomes

$$\Delta n = \tau \beta \alpha I_0 e^{-\alpha x} (1 - e^{-t/\tau}).$$

It is evident from the above equation that if the light is strongly absorbed, there will be a significant concentration gradient set up in the silicon and the carriers must then redistribute themselves

*The quantum yield, β , is close to 1 for the wavelengths which will be of interest.

with time through diffusion. It is not necessary to solve the time dependent equation for the diffusion of these carriers to get some feel for the effectiveness of different wavelengths and intensities of light in triggering the LASS as a result of penetration depth and generated carrier concentration. It will be seen that in the case of primary interest (i.e., generation by a short pulse from a Nd^{3+} :YAG laser), a carrier concentration corresponding to an "on" state of the LASS can be generated before diffusion effects can become significant.

Figure 2.1-6 is a plot of the carrier concentration profile as a result of photon absorption in silicon for three different wavelengths which have been used in triggering experiments. The total energy in the pulse is the same for curves A through F. The carriers are "frozen" in the plots to show the number of carriers generated at a given x at the end of the light pulse. Surface recombination is of little consequence and has been ignored because the surface region is greater than a diffusion length from the collector junction. Collection by the emitter junction is not negligible in the LASS design where light passes through the emitter junction into the p-base region. However, if the p-base region is brought to the surface and collection by the emitter junction is now a result of lateral diffusion only, the effective gate drive becomes negligible because the emitter junction is greater than a diffusion length (L_n) from the region of light absorption (see Figure 2.1-4). Therefore only carriers generated within a diffusion length of the collector junction are effective light drive for the thyristor.

In Figure 2.1-6 the diffusion length is indicated on the p-base side of the metallurgical junction. The space charge region (i.e., effective junction location) depends on the bias on the junction and is shown approximately for a 10 volt bias on the common collector. The lifetime in the n-base (i.e., τ_p) is assumed to be 20 microseconds. Diffusion lengths in the p-base are shown for $\tau_n = 1$ microsecond and $\tau_n = 0.3$ microseconds. The lifetime in the n-base (i.e., τ_p) is assumed to be 20 microseconds for computation of the curves; therefore, the n-base is approximately equal to L_p .

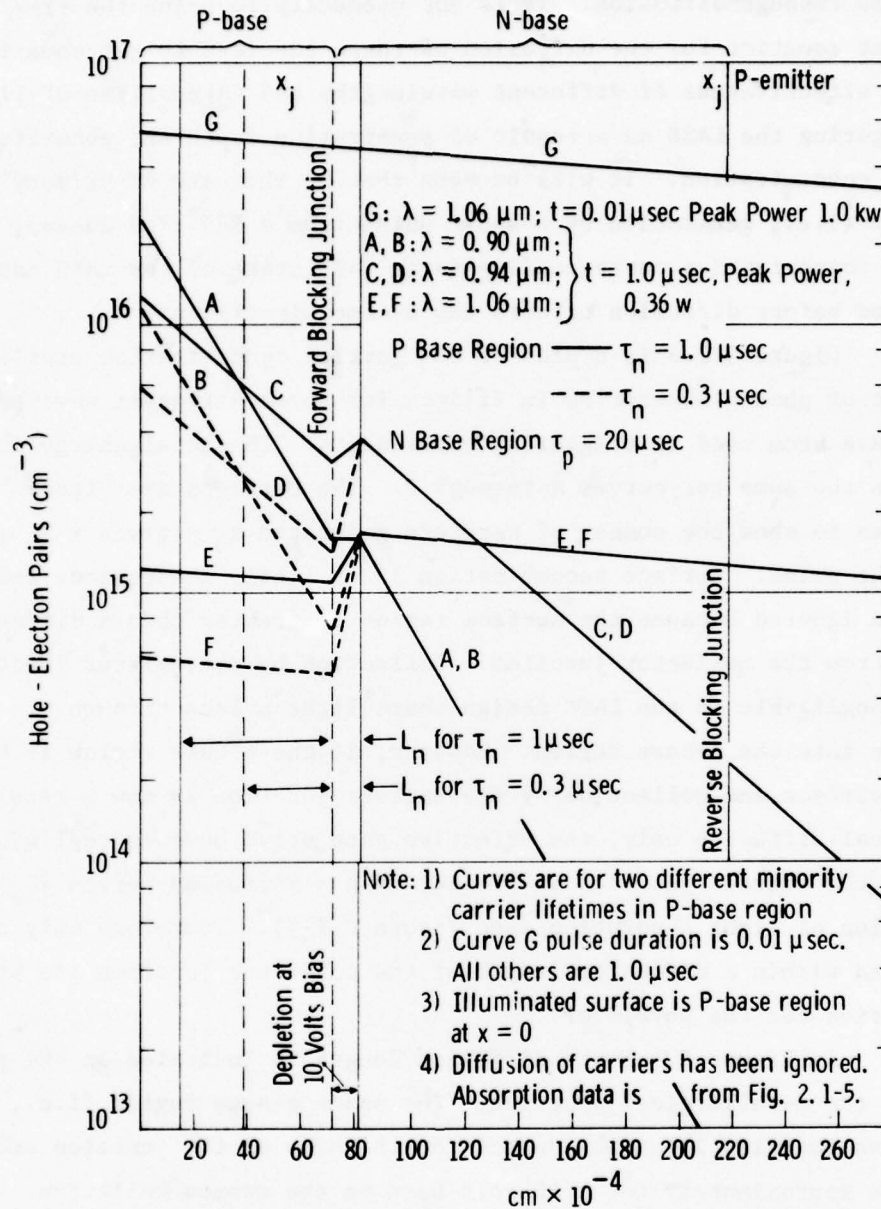


Figure 2.1-6. Optical carrier generation profile in a typical thyristor blocking 10 volts forward bias for different radiation wavelengths and times.

The slope of the curves is determined by the absorption coefficient α , so that as the wavelength is decreased (i.e., higher energy photons) more of the energy is absorbed and more carriers are generated near the surface (Refer to Figure 2.1-5). These carriers are effective if they are within a diffusion length of a junction; however, surface recombination now becomes important and a significant number of generated carriers may be lost through surface recombination and the light becomes less effective as a trigger. In addition, the transit time of more of the generated carriers in the p-base is increased as the point of generation approaches the surface; consequently, the turn-on delay time is increased. Conversely, as the radiation wavelength is increased the carriers are generated more uniformly in the silicon (decreased slope); however, the absorption coefficient α is also decreased so that the absolute level of carrier generation is decreased and the light again becomes less effective for triggering. For wavelengths longer than the band edge of silicon (about 1.150 μm), the silicon is transparent and no carriers are generated.

The plot of Figure 2.1-6 clearly shows that if τ_n (lifetime in p-base) $< 0.3 \mu\text{sec}$, then 0.94 μm radiation is more efficient as a trigger source than 0.90 μm since within a diffusion length of the collector junction the generated concentration is always greater for 0.94 μm than for 0.90 μm radiation. It is also apparent from the curves that the 0.94 μm radiation appears to be more effective than the 1.06 μm radiation at low power levels. The carrier concentration is significantly greater in the p-base region and remains greater to a depth of 125 microns for the 0.94 μm radiation compared to the 1.06 μm radiation.

Curve G shows a different type of phenomena occurring. In this case the pulse duration and power level are comparable to that of a Q-switched Nd^{3+} :YAG laser. The carrier concentration clear across the device is now of the order of the "on" state equilibrium concentration in the device 10 nanoseconds after initiation of the pulse. In other words, the device is "on" in the radiated area. One can now clearly see why the turn-on performance of the device is superior with this type

of optical gating. The device is no longer being triggered on; it is being conductivity modulated on by optical generation. Note also that the concentration level is a smooth curve from the p-base to the n-base since the generation level is independent of lifetime for times short compared to the lifetime. Curve G is the type of optical gating with which this contract work was primarily concerned.

2.1.4 Plasma Spreading.

As mentioned in Section 2.1.1, a small region near the edge of the cathode is carrying all of the anode current early in the turn-on process. Although the thyristor has a low impedance under these conditions, the current density can be very high unless the current is limited by external circuit components. Excessive current density leads to severe local heating and eventual destruction of the device (the silicon literally melts). There are three mechanisms that can alleviate this situation:

1. If the current pulse is short enough, the temperature rise caused by the heat generation will not be large enough to damage the silicon or degrade the performance characteristics.
2. The plasma of electrons and holes spreads laterally into the nonconducting regions of the device, turning them on and effectively reducing the current density and thus the rate of heat generation.
3. There is a small but finite area under the metal which is also turned on by optical scatter; its width was estimated to be about equal to the device thickness. The experimental work reported in Section 3.5.3.1.1 shows that the scattering is much less than this value. This affects the numerical results but not the approach. The initial conduction area is therefore this scatter lighted width multiplied by the total perimeter of the window.

A large portion of the experimental effort in this program was to determine the rate at which the conducting plasma spread under

the high dI/dt and peak current densities encountered. It was previously known from the work of Yamasaki and others that the velocity of the plasma front (spreading velocity) is a weak function of the current density.⁽²⁾ It was also known that the spreading velocity is essentially independent of the temperature. This information was incorporated into the physical model with provisions to modify the spreading velocity as future data might indicate.

The apparatus, technique, and experimental results of the spreading velocity measurements are described in detail in Sections 3.3 and 3.5.

2.2 Analytical and Computer Model.

The experimental determination of how a given semiconductor device will respond to variations in design (including geometry, impurity concentration profile, and packaging) and operation (including gating stimulus and numerous circuit controlled variations in voltage and current and rates of change of voltage and current) is a very long and costly procedure. Because of the large number of parameters involved in a thyristor, huge quantities of test units must be fabricated and evaluated under carefully controlled conditions. When it is desired to provide sufficient units to allow for failures and for adequate data at each step to provide statistical significance, the number of thyristors involved with all of their parameters that must be recorded becomes unwieldy. This is the situation that faced the LASS investigators. Fortunately, a considerable body of theory has been developed in the literature, and portions of this theory are applicable to portions of the LASS problem. It was therefore a contract task that a computer model be developed so that a theoretical parametric study could be carried out to predict the performance of the LASS over a range of operating conditions. An experimental verification program would then be used to confirm the predictions of the theoretical study or to provide information for corrective action in the computer model.

It was expected that the computer model would accept input data concerning the initial conditions, the geometry and design of the

device, the blocking voltage and the current pulse width and magnitude, the rate of current rise and fall, and the length of time between pulses. The model would provide the spatial and temporal distributions of current density and temperature and the forward voltage drop as a function of time and current. These expectations have been met as illustrated in the two papers by Davis and by Davis and Roberts in Appendix V.

It was realized early that there were three major tasks to accomplish the development of a meaningful computer model. Two of these, the model development itself and thermal analysis, properly are portions of the analytical work and are discussed in the next two sections of this report. The third, the determination of the plasma spreading velocity under conditions of very high current densities, is covered in Sections 3.3 and 3.5 under the major section on Experimental Verification.

2.2.1. Development of Optically Activated Thyristor Turn-on Model,

The computer model of the light fired thyristor assumes a light source such as a high peak power Q-switched neodymium:YAG laser. Such a light pulse generates excess carrier concentrations throughout the illuminated base regions of the device which are of the same order of magnitude (10^{17} - 10^{19} per cm^3) as those which occur in the device in the normal on-state. (Refer to Figure 2.1-3). The time required for these carriers to be generated is a combination of the transit time of the light through the device (~ 1 picosecond) and the duration of the light pulse (~ 10 nanoseconds in cases examined thus far). A thyristor turned on in a conventional manner such as electrical gate drive or "light triggering" (as opposed to "light firing" which is under discussion here) takes the order of a microsecond because it depends on comparatively slow drift and diffusion mechanisms to establish a conduction plasma in the device. Therefore the voltage collapse across a Q-switched $\text{Nd}^3\text{:YAG}$ laser fired device is orders of magnitude faster than that of a conventionally triggered device and can, consequently, sustain a much higher time rate of change of current (dI/dt) through the device. For this

reason, this technique of light activation of the solid state switch is of great interest in any power circuit with high dI/dt requirements.

A preliminary computer program was stepwise constructed that utilized an arbitrary number of circular spots as the illuminated geometry. It was known that a large initial periphery is desired in order to maximize the initial conduction area. The functions of this model were to point out trends which would be the guide to other geometries with superior properties, and to provide the basis for developing a more sophisticated and realistic model.

The preliminary model assumes that at time zero the thyristor starts on with the on area equal to the illuminated area. The load current is constant at I_0 . The conduction area is a function of the original area, A_0 , and plasma spreading velocity v_s . It is known that the plasma spreading velocity is a function of the current density J :

$$v_s(J) = bJ^c.$$

For a quantity N_0 of circular apertures of radius R_0

$$\pi N_0 J (R_0 + bJ^c t)^2 - I_0 = 0.$$

The program solves this equation for $J(t)$ and then determines $r(t)$.

Data from diodes and thyristors on forward voltage drop were available for current densities up to about 1500 A/cm^2 . This was used to extrapolate to high current densities according to the relationship

$$V = A + BJ.$$

The product of the instantaneous values of $V(J,t)$ and $J(t)$ provides a determination of the incremental power density $P(t)$. By summing the incremental power dissipations and absorbing the heat totally within the silicon in the conducting region (adiabatic case), one can calculate the temperature T at the end of the pulse as a function of the radius R_0 .

The output data from this program was supplied to the thermal analysis as input data for initial evaluation of the thermal analysis program.

The efforts to achieve a more realistic model were based on

the approach of the preliminary model, but with attention to several important details that were ignored in that model. To aid the development of the new model, the over-all model was broken into five major subsections which could be worked on independently. These were identified as:

- (1) EFFWO Mathematical model of the effective conduction width of the laser illuminated, unmetallized area of the thyristor structure. Provision is also made for the area under the metal adjacent to the window which is illuminated by scattered light. This computation provides the $t = 0^+$ boundary condition for conduction area and current density for the spreading-turn-on calculations. This calculates the current density $J(x)$ at $t = 0$. The light pulse is considered to be a delta function which generates a plasma in the device. The carriers redistribute spatially in a dielectric relaxation time in a manner depending on the lateral resistance of the illuminated area near the surface and the electrical contact. This redistribution is integrated in EFFWO and then divided by the peak current to give an effective "on" width and current density for use as the initial condition in the SPREAD program.
- (2) HIJVC Model of the voltage-current characteristic versus temperature under very high current density conditions where Auger recombination dominates. Model is based on literature and experimental data taken in this laboratory. This model was subsequently expanded to include carrier-carrier scattering and the temperature dependence of lifetimes and mobilities. Short pulse V-J characteristics with J up to $1,000 \text{ A/cm}^2$ show that Auger recombination process is dominant at high values of J .

- (3) SPREAD Model for calculating current and voltage versus time for the LASS device which includes the effect of conduction area spreading as a function of instantaneous current density. Model is based on extrapolation of infrared study of turn-on plasma spreading in this laboratory. This program was revised from the circular type of conduction of the preliminary model to a perimeter type of conduction to improve the initial "on" region available for spreading.
- (4) TMPRO This calculation determines the distribution of energy dissipation and temperature distribution spatially across the device as a function of time during the conduction pulse.
- (5) CURDIS A calculation of the spatial distribution of current as a function of time. The results obtained with the previous four model elements imply that the temperature across the device will be highly non-uniform and since the voltage-current characteristic is temperature dependent it follows that the current distribution at any given instant will be non-uniform. A self-consistent iterative algorithm was devised which determines this current distribution for each point on the time grid. Inputs for this calculation are the time dependent terminal current, the conduction area as determined by SPREAD and EFFWO, and the temperature distribution obtained for the previous time interval. The iterative loop includes HIJVC and TMPRO; and thereby obtains, in addition to the current distribution, the terminal voltage and the new temperature distribution.

Provisions were made to modify the above programs as experimental data became available for turn-on and for plasma spreading. These five programs were developed more or less independently (although simultan-

eously by the same worker) on an interactive time-share computer. Inputs from the thermal analysis work (Section 2.2.2) were incorporated as appropriate, especially in the TMPRO program. The five programs were assembled into one program that required the input data and provided the output data listed in Table 2.2-1. The data obtained from this analysis provided excellent insight into device and optical system design requirements. One of the most significant was the prediction that rectangular illumination ports would be superior to circular ports.

Some input parameters cannot be derived from first principles and must be correlated to empirical data. This is particularly true of the spreading velocity, the voltage-current density relationship, and various temperature dependent parameters. The spreading velocity and the voltage-current measurements constituted the major portion of the experimental work on this contract and are reported in Section 3.

The working program was translated from the small, time-share computer system to the UNIVAC computer system using FORTRAN compatible with CDC6600 Scope 3.4 OS as required by the contract. At this time an improved terminal voltage-current density (V-J) relationship was incorporated. The initial V-J data was from small diodes and thyristors with current densities up to about 1500 amperes per square centimeter. These data were fit to a two segment curve of the form $V = A + BJ$. New data to $10,000 \text{ A/cm}^2$ were added, and the relationship was restructured with three segments of the same form. Examples of the output data are given in the two papers by Davis and by Davis and Roberts in Appendix V. These papers also discuss the model development and usage in some detail.

Although the program is working well, there are some improvements that should be made. First, although provisions were incorporated in the programing to permit the thermal analysis of the device over a train of current pulses, their operation has not been confirmed on the UNIVAC because insufficient funds and time remained on the contract. Therefore, the program presently calculates the effect of one current pulse on the device. Second, under some conditions the FORTRAN program does not converge. This can be solved by dividing the current pulse

TABLE 2.2-1 THYRISTOR MODEL INPUT AND OUTPUT DATA.

Inputs

1. $I(t)$ - The time dependent current waveform of the circuit
2. $T(x)$ - The initial temperature distribution across the device
3. Geometric parameters of the device
4. Material parameters of the device
5. v_s spreading velocity

Outputs

1. $T(t,x)$ Temperature as a function of time and location
2. $J(t,x)$ Current density as a function of time and location
3. $I(t)$ Current as a function of time
4. $V(t)$ Terminal voltage as a function of time
5. $A(t)$ Conducting area as a function of time

into 72 or more time increments, but this seems excessive. The conditions under which this occurs and how to correct them are described in the program documentation delivered with the program to the USAF. This shortcoming is more of a nuisance than a major fault. Third, the experimental V-I data for large devices with a multiplicity of windows did not track the calculated V-I curve. The measured values of V were higher than the calculated ones. The model assumes that the electron-hole plasma can spread laterally without limit. In the large device, the windows are slots with a radial pattern (Figure 2.2-1) and the spreading plasma fronts meet early in the pulse near the center of the device. Once they start to overlap, the actual conducting area is less than the calculated area, the actual current density is therefore higher than that calculated, and the actual terminal voltage will be higher than that predicted by the model. When this was discovered, there were insufficient funds remaining on the contract to add the additional task of providing means to modify the area calculation based on device geometry. This is an important point whenever the illumination windows are to be located close enough together that portions of the plasma fronts will overlap during the current pulse. Fourth, the heat flow calculations are based on one dimensional flow along the axis of the device. Certainly for long pulses or trains of pulses the lateral heat flow will be important. The model should be modified in any extended work to consider lateral heat flow. Fifth, it would be very desirable to perform some thermal measurements to confirm the accuracy of the calculated temperatures. This would be a difficult experimental task, but it seems essential if further work is to be done in the application of the LASS.

2.2.2 Thermal Analysis.

When this program started, there was conjecture, but no supporting data in the literature, that the thermal conditions in the silicon slice during a 40 microsecond pulse were adiabatic. The dynamics of the heat generation and flow during and after the conducting pulse were central to the theoretical model desired for the LASS. Therefore, a substantial effort was mounted to determine these dynamics.

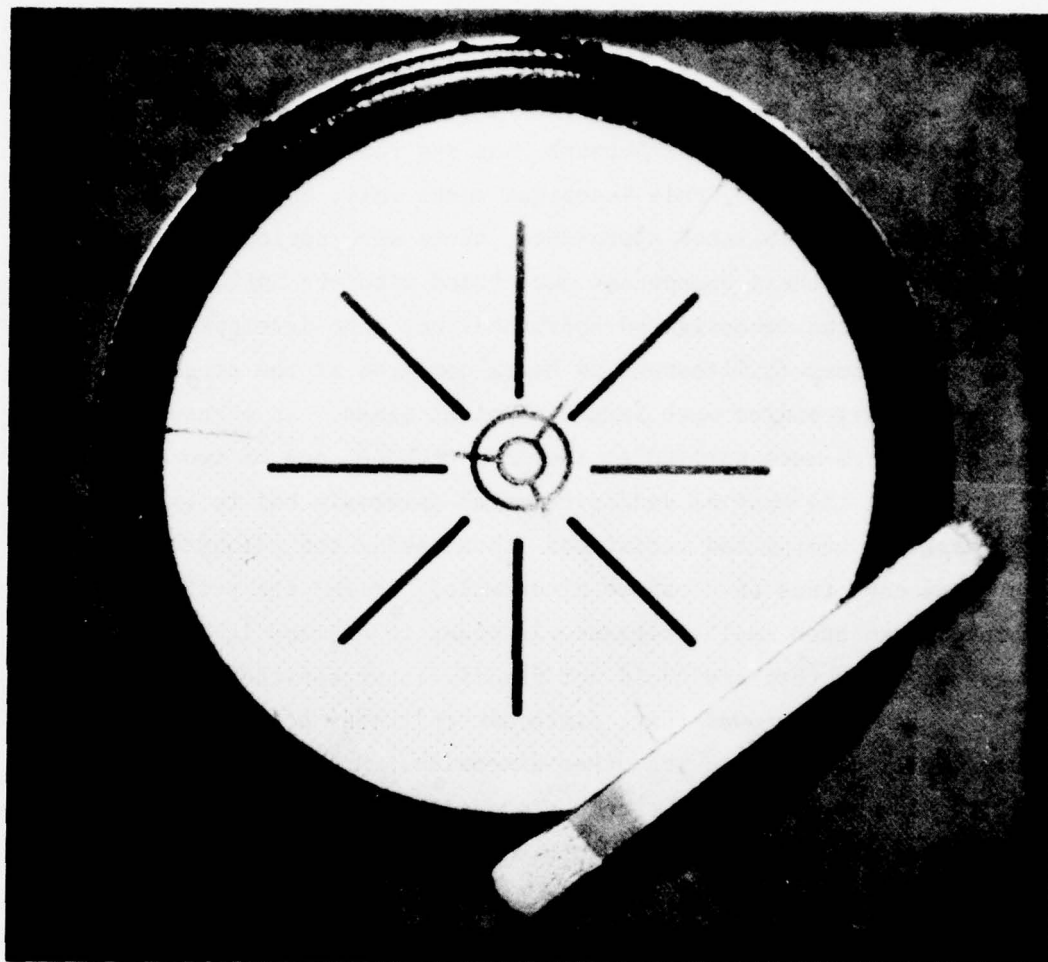


Figure 2.2-1. Completed light activated semiconductor switch element designed for fast turn-on.

Initially, attempts were made to apply well-established techniques for the computation of transient heat flow. One of these, for which considerable experience was available, was the use of the ECAP computer program. This Electrical Circuit Analysis Program, designed by IBM for users of their computers, permits the solution of transient problems for electrical networks. By merely making an electrical analog of the thermal network, one can readily solve thermal problems. In principle, this technique works well; but, as was also found for other established approaches, there were serious, unacceptable limitations when these approaches were tried with the LASS. This is because all of the investigated approaches had been developed for much larger time frames (millisecond to hours compared to the present interest of microseconds) and/or much larger physical sizes. As a result, when these techniques were applied to the LASS problem, one of two conditions occurred: (a) the spatial and/or temporal intervals had to be so large as to mask any unexpected variations (thus making the adiabatic assumption come true as a matter of default), or (b) the problem had to be broken into such small fragments in order to examine it in the necessary detail that one could not readily interpret the overall results.

Analysis showed that, since the thickness of the silicon slice is very small compared to its other dimensions (0.05 cm vs. ~ 5 cm), an infinite slab approximation should provide insight into the characteristics of the heat flow in the silicon. This approximation should also be reasonable for the contacting plates of molybdenum or tungsten, but less so for subsequent, and presumable thicker, materials such as copper which form the final heat conducting path to the ultimate coolant. Since the primary concern was what happened in the silicon, the possible loss of validity in the copper was acceptable. The heat flow in the copper could probably be treated on an average power basis. Accordingly, the problem was reduced to a complicated version of a standard textbook problem in transient heat flow. The initial model was a semi-infinite silicon slab; i.e., a sheet of silicon of finite thickness with one dimensional heat flow perpendicular to the plane of the sheet. Figure 2.2-2

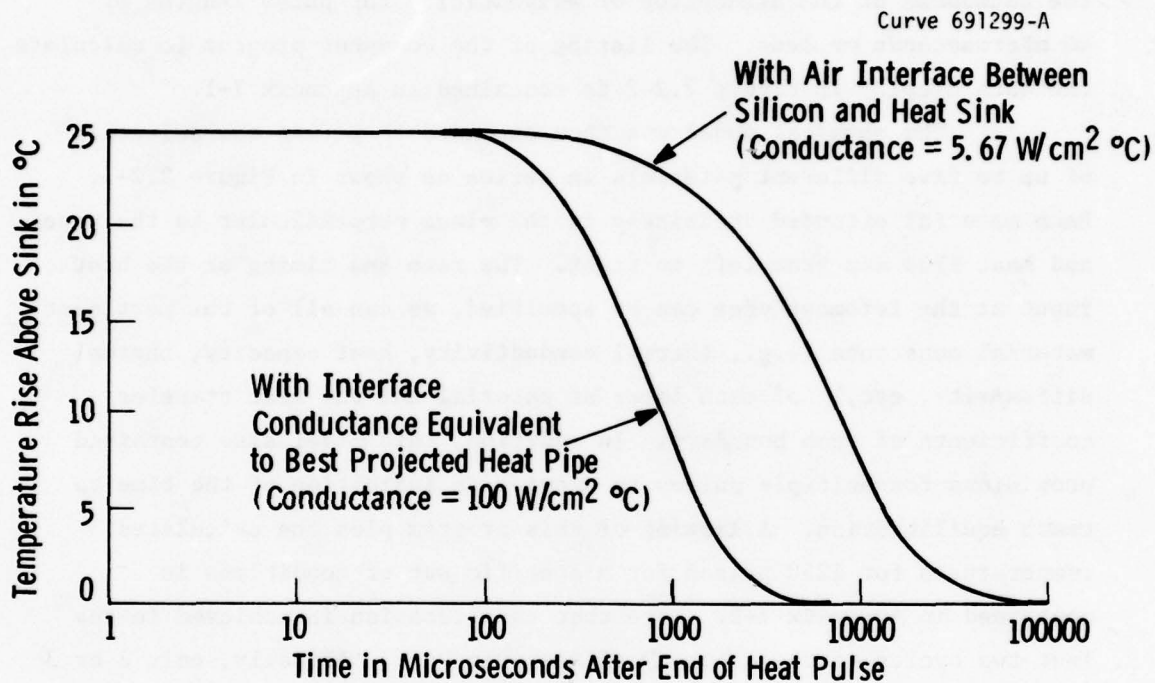


Figure 2.2-2. Calculated change in temperature at the center of a silicon slab after a 40 $\mu\text{sec.}$ heat pulse. Infinite slab model. Thickness of silicon=0.05cm. Thermal conductivity of silicon=1.25W/cm $^{\circ}\text{C}$. Thermal diffusivity of silicon=0.681cm 2 /sec. Initial temperature above ambient at end of 40 $\mu\text{sec.}$ pulse=25 $^{\circ}\text{C}$.

is a plot of the decrease in temperature with time after a delta function of heat input raised the temperature 25°C. The value of 25° was estimated as a reasonable one from the preliminary turn-on model. This curve shows how the temperature decreases with time for a wide range of values for thermal interface conductance. Note that there is no perceptible decrease in temperature until 100 microseconds. This confirmed the soundness of the assumption of adiabaticity for pulse lengths of 40 microseconds or less. The listing of the computer program to calculate the data display in Figure 2.2-2 is contained in Appendix I-1.

The physical model was then expanded to permit the selection of up to five different materials in series as shown in Figure 2.2-3. Each material extended infinitely in the plane perpendicular to the paper, and heat flow was from left to right. The rate and timing of the heat input at the leftmost edge can be specified, as can all of the pertinent material constants (e.g., thermal conductivity, heat capacity, thermal diffusivity, etc,) of each layer of material and the heat transfer coefficients of each boundary. In addition, this model also contained provisions for multiple pulses to provide an indication of the time to reach equilibration. A listing of this program plus the calculated temperatures for 1250 pulses for a specific set of conditions is contained in Appendix I-2. Note that equilibration is achieved in the last two cycles to the accuracy of the print-out. Actually, only 2 or 3 figures are significant, and on this basis equilibration is attained after 1800 μ sec, or 450 pulses. In spite of the many obvious simplifications, this scheme accomplished the desired objective of providing a feeling for the magnitude and location of the problem areas as was confirmed later by the following more sophisticated approach.

With the improved understanding of the problem obtained from the above described infinite-slab, multimaterial investigation, it was practical to increase the level of sophistication of the investigation. A finite element computer program, identified proprietarily as WECAN, was employed to make a detailed analysis of the problem. This type of program is capable of handling real thermal transient problems in

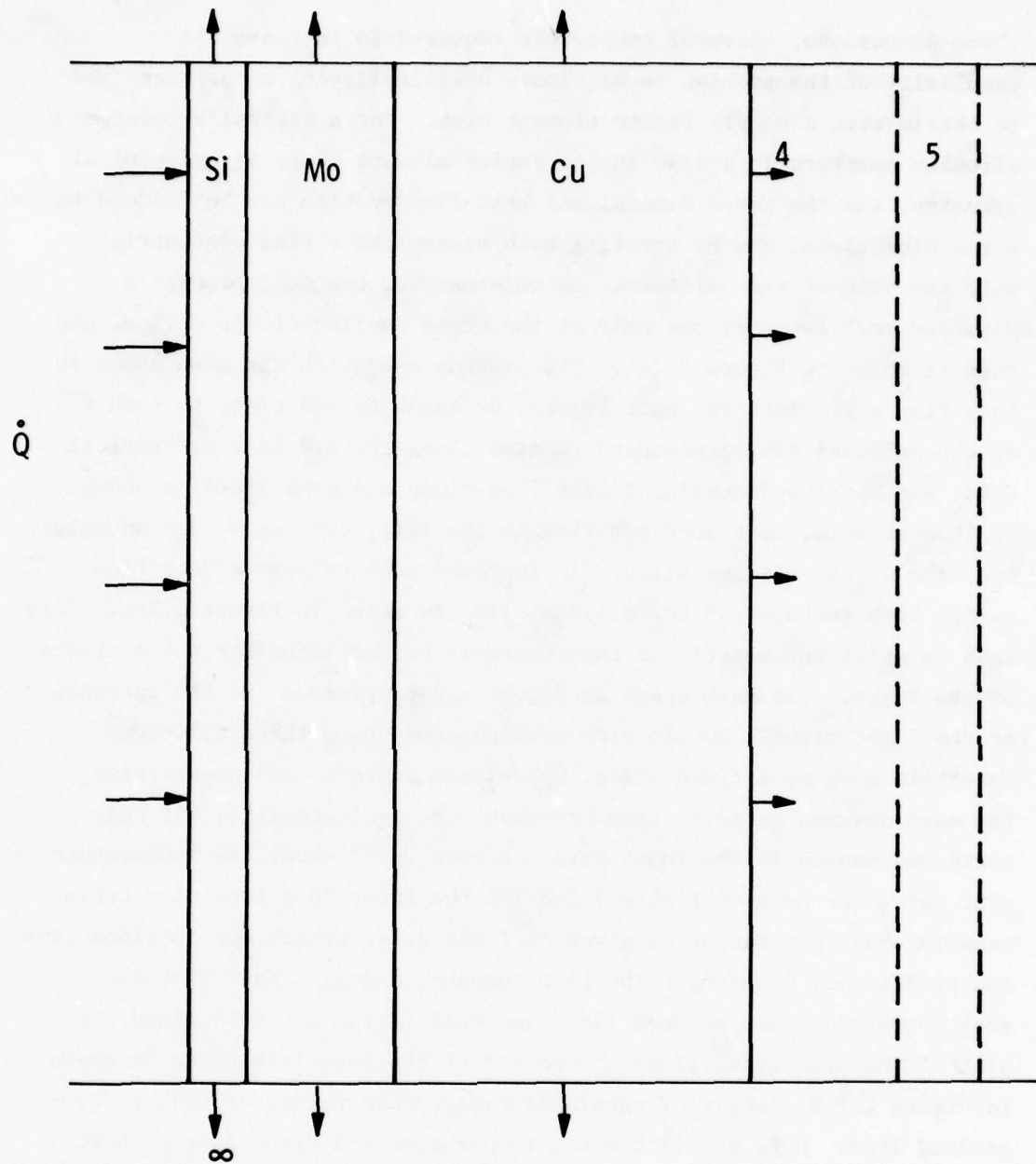


Figure 2.2-3. Conceptual view of physical model for infinite slab transient heat flow calculation.

three dimensions. Several steps were required to increase the complexity of the problem to eliminate oversimplifying assumptions and to obtain even a simple finite element mesh. For a centrally located circular aperture in a disc shaped active element there is cylindrical symmetry, and the three dimensional heat flow problem can be reduced to a two dimensional one by treating each element as a ring concentric with the axis of the cylinder. In this manner, one need prepare a detailed mesh for only one half of the cross section of the device, and this is shown in Figure 2.2-4. The program used with the mesh shown in this figure provides for heat inputs, by quantity and time, to each of the selected finite elements located along the ordinate or vertical axis, and for two dimensional heat flow along the mesh lines as shown. In this example, heat does not flow to the left; cooling occurs on only one side of the silicon slice. An improved mesh to permit heat flow out of both surfaces of the silicon slice is shown in Figure 2.2-5. This mesh is still unrealistic in that there is no provision for the entrance of the light. The mesh shown in Figure 2.2-6 provides for the entrance of the light signal, double side cooling, and up to three different materials such as silicon slice, molybdenum support, and copper sink. The mesh assumes material symmetry about the ordinate axis, but this could be changed in the input data. Figure 2.2-7 shows the temperature plot using the mesh of Figure 2.2-6 for the first 20 pulses of a train assuming heat generation as given in Table 2.2-2 (which was obtained from the preliminary version of the LASS computer model). Note that the peak temperature has reached 126°C and that it has not stabilized. A plot of the isothermal lines at the end of the twentieth pulse is shown in Figure 2.2-8 along with tabulated temperature values of each corresponding line. Note how little the temperature has risen over a short distance away from the illuminated area.

Because the maximum temperature at which a thyristor will reliably block rated voltage is about 125°C , it is clear that the temperature and therefore the current density is unacceptably high in the illustrated case. The results of a rerun with the heat input at

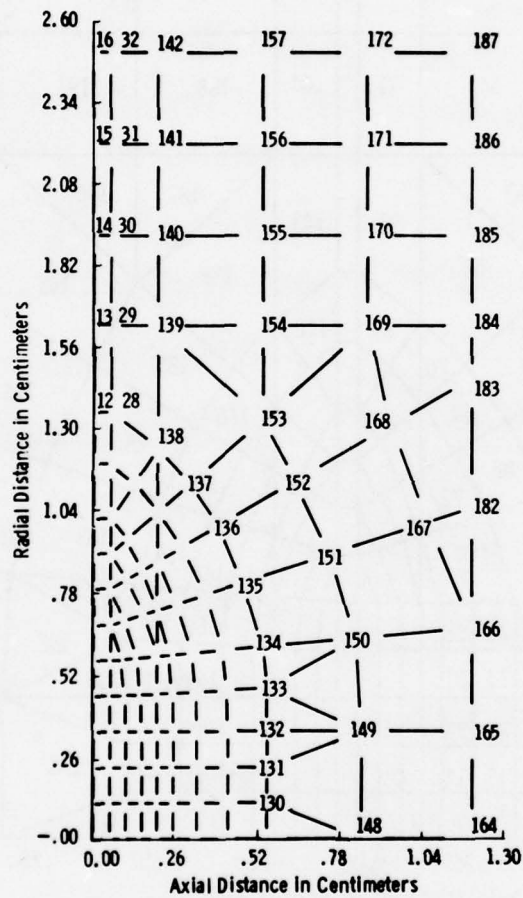
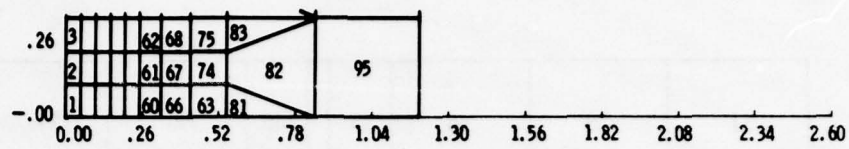


Figure 2.2-4. Nodal geometry plot of thyristor heat-up time history. Dimensions on axis in cm.

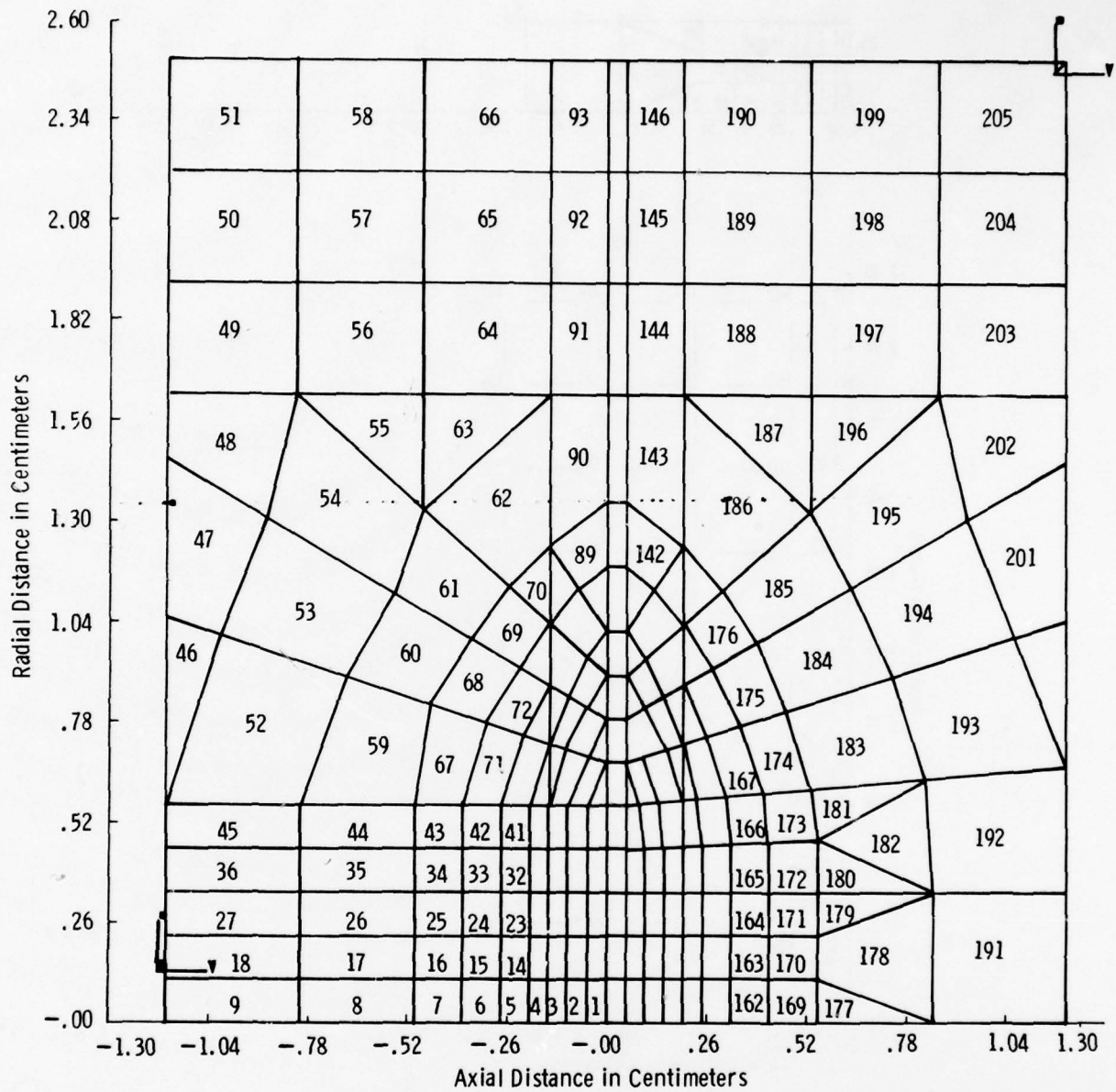


Figure 2.2-5. Node-element mesh arrangement for 2-sided finite element computer analysis. Circular symmetry is assumed.

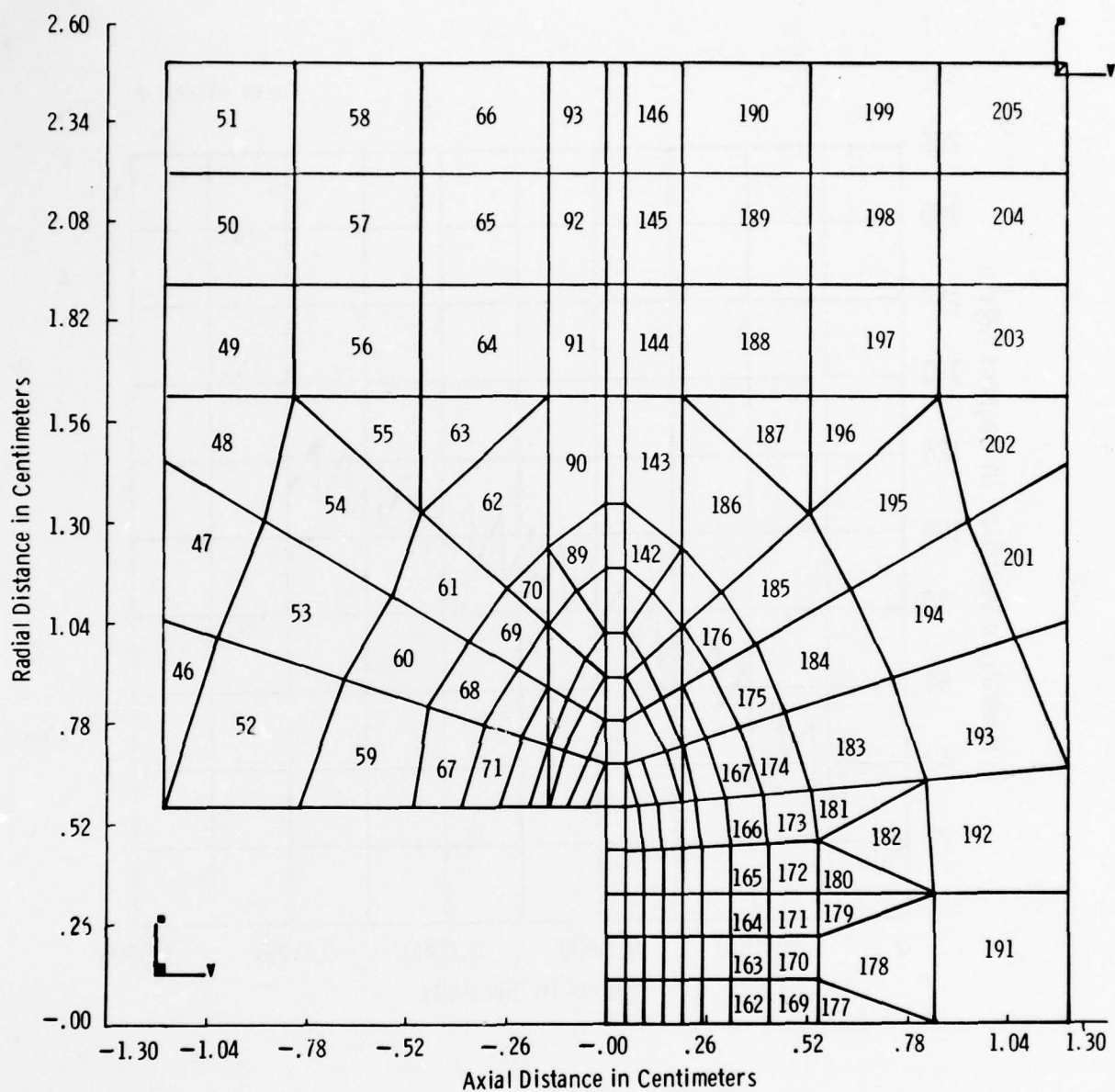


Figure 2.2-6. Node-element mesh with elements 1 through 45 removed to account for path of laser beam. Left edge of slice is zero reference.

Curve 690680-A

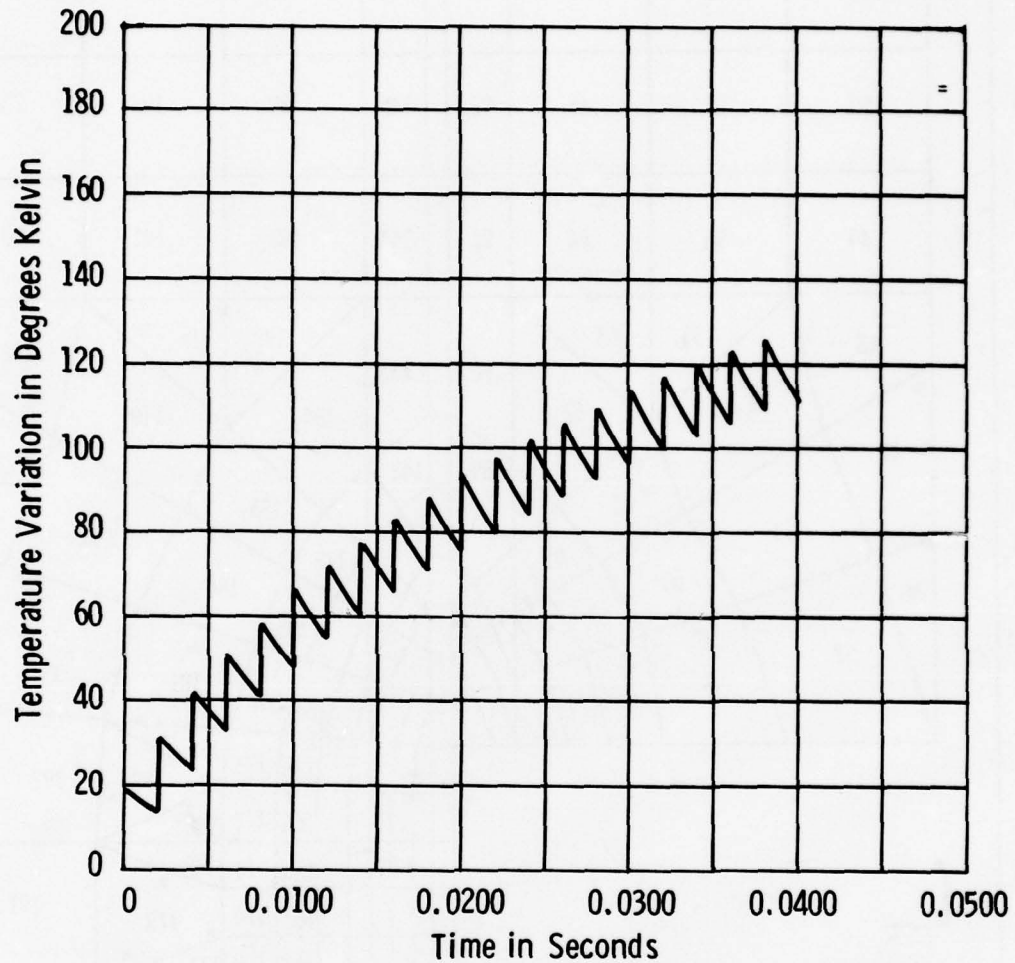


Figure 2.2-7. Temperature variation of the interface between elements 1 and 97 (surface of silicon slice) for double-sided device. Zero temperature is starting temperature of the silicon.

Curve 690682-A

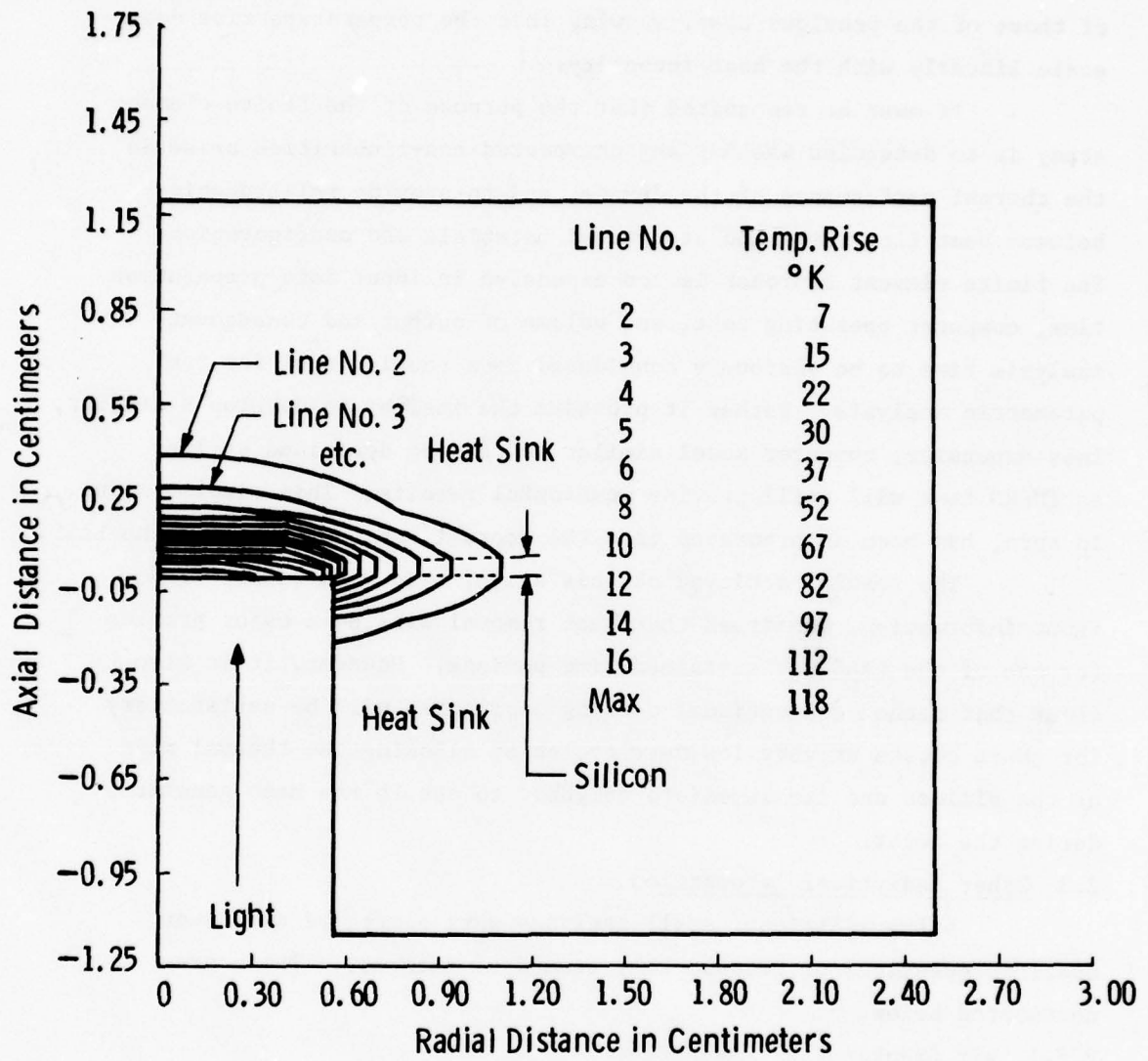


Figure 2.2-8. Isothermal plot at end of 20th cycle. Note 90° rotation in orientation from that of Figure 2.2-6.

one-fifth of the previous levels are shown in Figure 2.2-9. Although the temperature still has not equilibrated, the peak values are one-fifth of those of the previous case, showing that the temperature rise does scale linearly with the heat intensity.

It must be recognized that the purpose of the finite element study is to determine whether any unexpected non-linearities arise in the thermal performance of the device, and to provide relationships between heat flow rates and structural materials and configuration. The finite element approach is too expensive in input data preparation time, computer operating cost, and volume of output and consequent analysis time to be seriously considered as a routine tool for the parametric analysis. Rather it provides the insight to develop a simpler, less expensive, computer model similar to the one described earlier as TMPRO that will still provide meaningful results. This simpler model, in turn, has been incorporated into the overall turn-on model for the LASS.

The results achieved at this stage, even with rather crude input information, confirmed that heat removal will be a major problem for use of the LASS for sustained time periods. However, it is also clear that rather conventional cooling approaches will be satisfactory for short bursts at very low duty cycles by allowing the thermal mass of the silicon and its immediate neighbor to absorb the heat generated during the burst.

2.3 Other Analytical Information.

A few additional small analyses were performed to answer specific questions or because they seemed of interest. These are documented below.

2.3.1 Air Breakdown by Laser Beam.

The possibility of air breakdown from the intense electromagnetic fields in the laser beam was investigated. According to Lencioni the measured breakdown in air at $1.06 \mu\text{m}$ for 100 nsec pulse lengths has a threshold of $2 \times 10^{10} \text{ w/cm}^2$ for large ($> 10^{-1} \text{ cm}^2$) spot sizes.⁽³⁾ The threshold is considerably larger at smaller spot sizes as given in the right hand column of Table 2.3-1.

Curve 690681-A

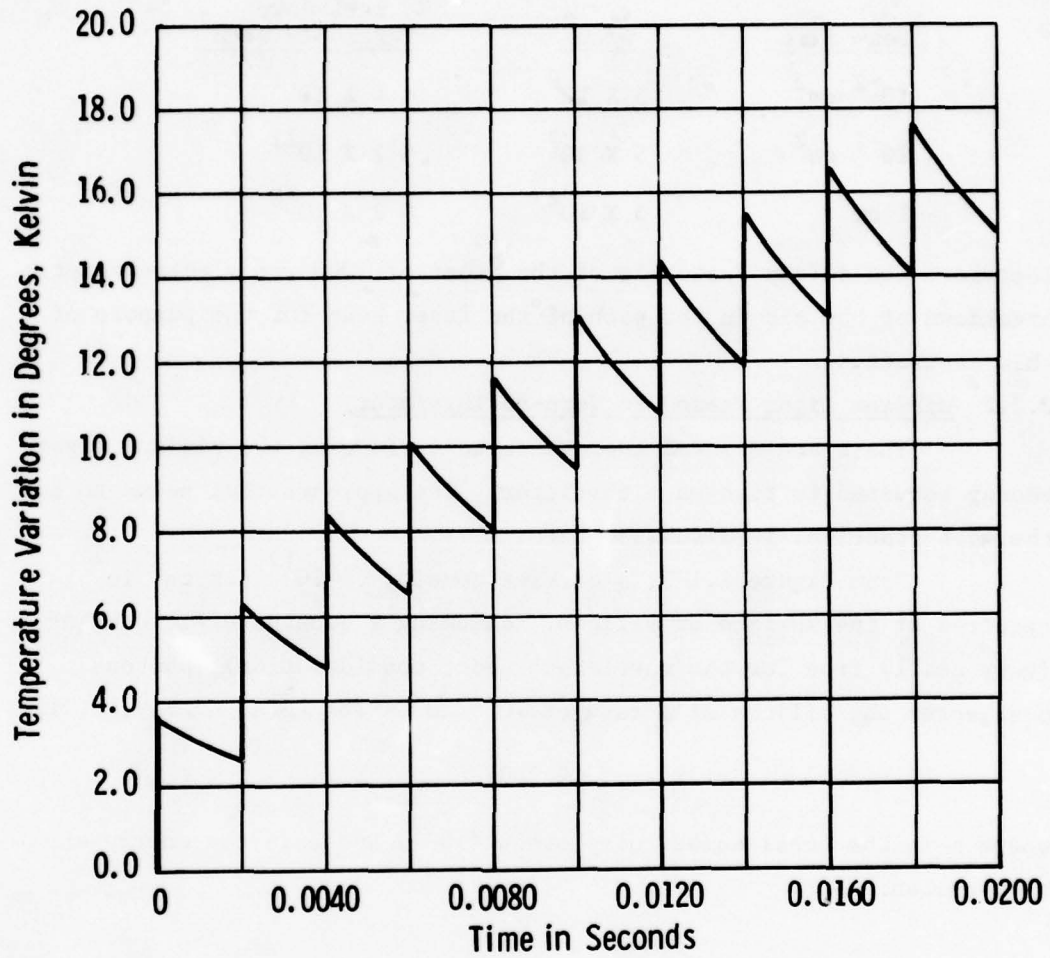


Figure 2.2-9. Temperature excursion of silicon element for 10 pulses with only 1/5 the input heat of Figures 2.2-7 and 2.2-8.

The laser obtained for this contract produces 100 mJ, 20 nsec pulses with a peak power of 5×10^6 watts. Then for a beam size of:

TABLE 2.3-1. AIR BREAKDOWN BY LASER BEAM.

| <u>Laser Output</u> | | <u>Breakdown Threshold w/cm^2</u> |
|------------------------|----------------------------|--|
| <u>Beam Size</u> | <u>w/cm^2</u> | |
| 10^{-2} cm^2 | 5×10^8 | $\sim 4 \times 10^{11}$ |
| 10^{-1} cm^2 | 5×10^7 | $\sim 2 \times 10^{11}$ |
| 1 cm^2 | 5×10^6 | $\sim 2 \times 10^{10}$ |

Therefore the safety factor is of the order of 1000 for electromagnetic breakdown of the air in the path of the laser beam for the purpose of this contract.

2.3.2 Minimum Light Needed to Turn-on Thyristor.

There are several approaches to estimating the minimum light energy required to turn-on a thyristor. The approach that seems to be the most practical is discussed here.

From Figure 2.1-3, a carrier density of 10^{17} per cm^3 is required at the surface of silicon. Assuming a quantum efficiency of 1 (very nearly true for the wavelength under consideration), photons must enter the silicon at a rate of $10^{17}/\text{cm}^3$. The total energy, E, is

$$E = n\epsilon$$

where n is the total number of photons (10^{17}) and ϵ is the energy of each photon. But

$$\epsilon = hc/\lambda$$

where λ is the wavelength of the light ($1.06 \times 10^{-6} \text{ m}$), h is Planck's constant ($6.6 \times 10^{-34} \text{ J-sec}$), and c is the velocity of light ($3 \times 10^8 \text{ m/sec}$). Then

$$E = nhc/\lambda$$

and substituting the above values gives $E = 19 \text{ mJ/cm}^3$. This much energy

must be absorbed by the silicon in the manner shown in Figure 2.1-3. To allow for non-preferential absorption characteristics, reflection at the surface, and transmission losses, the light delivered from the laser should be at least an order of magnitude greater, say 200 mJ/cm^3 of silicon activated.

For the 20,000 A, 2000 volt device of this contract one can estimate the light needed. To obtain a reasonable voltage drop, say about 20 volts at the 10 μsec point in the pulse (from Appendix V-2), approximately one square cm of silicon must be illuminated. The silicon is 0.05 cm thick; therefore, 0.05 cm^3 of silicon must be illuminated at the desired level. This would indicate that a minimum of 10 mJ is required from the laser. As will be seen in Section 3.5, this is within a factor of perhaps 2 of the experimental results.

3.0 EXPERIMENTAL VERIFICATION

3.1 Introduction.

One of the major tasks of the Optically Activated Switch program was that of experimental verification of the projections of the analytic study. As is usually the case, the division between the tasks was not clean, because the analytic study needed experimental inputs for several parameters--especially plasma spreading velocity and the forward-drop current-density relationship. Some general comments about the experimental results are in order before examining them in detail.

The electrical testing conducted for the low dI/dt infrared plasma spreading experiments are not of any new significance in themselves since devices have been tested to these levels with electrical gating without undue stress. These tests served as a reference point for the infrared measurements. On the other hand, the performance levels achieved by the laser light fired thyristor in the specially constructed pulse forming network test system are orders of magnitude greater than those achieved with electrically gated thyristors and will be discussed here in some detail. The results and the problems encountered will also be discussed and interpreted for the purpose of making recommendations for future encapsulation and application of the LASS.

Thyristor elements or devices were tested at various voltages and currents. The tests were performed stepwise. The voltage was increased across the device in steps of approximately 425 volts by changing the taps on the main transformer--usually starting each voltage level with 20 pulse forming networks connected to the device under test and increasing the current and voltage level until the device failed for one reason or another. The most significant achievement was the testing of two devices at maximum operating voltage and current without device failure. Figure 3.1-1 shows the voltage and current waveforms. The voltage was measured using the clamping circuit. The full voltage waveform cannot be shown at high speed because the

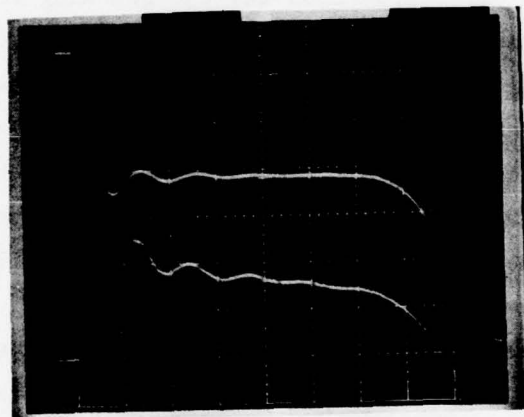


Figure 3.1-1. Voltage (lower) and current (upper) waveforms of device 2G4 at full voltage (1700 V) and current conditions (40 PFN's). Scales: Vertical 5000 A/cm and 5 V/cm; Horizontal 5 μ sec/cm. Current and voltage zero 1 cm above bottom line. Voltage measured using the clamp circuit.

fast probes will not sustain the operating voltage of the device.

These devices were 50 mm diameter gold plated units and were operated at a blocking voltage of 1700 volts with all 40 PFN's connected. Under these conditions the flat portion of the current pulse was approximately 19,300 amperes. The full width half maximum value of the current was approximately 40 μ sec in duration. The leading edge of the current waveform was purposely made to overshoot in the test circuit by removing the first inductor in each of the 40 pulse forming networks to maximize the dI/dt available from the system. This overshoot value reaches 24,300 amperes in one microsecond. dI/dt measured from the 10% to 90% of the flat portion of the curve gives a value of 40,000 amperes/ μ second. The pulse repetition rate was one pulse per second.

In summary, the peak current achieved was 24,300 amperes. The pulse current was 19,300 amperes for a 40 μ sec duration at one pulse/sec. The dI/dt was 40,000 amperes/ μ second and the blocking voltage was 1700 volts.

It was found in general that a failure point for the devices could not be empirically predicted. The reason is that there are so many different parameters to consider that if any one is wrong, the device may fail. However, it was shown that extremely high performance levels can be achieved if certain conditions are achieved. First, the electrical contact must be sufficiently thick and metallurgically attached to the silicon. The electrical-optical configuration should not give rise to current channelling which will unduly stress a region. The laser light must be of sufficient intensity and activate a sufficiently large area so that the current will not exceed a critical current density.

The major questions are, what are these values or combination of values? We believe that the analytic computer program provides the basic approach to the answers. We have found that the experimental voltage and current waveforms can be closely approximated by the single slit or circular geometry patterns from the computer program. By combining these inputs, device performance has been predicted far above the experimental failures. The fact that failures occur in some cases and not in others shows that the limit has not been empirically found. The tests

at Lawrence Livermore Laboratories described in Section 3.5.4 indicate extremely high dI/dt and current density capability. We believe that by proper extension of the computer program it can be used to predict the ultimate capability of the LASS.

Some additional empirical data should be obtained to complete the work, however. Some thermal measurements are needed to correlate to the temperatures predicted by the program, and the relationship of the intensity level of the light (J/cm^2) to the forward voltage drop or switching power loss needs to be better understood. These points are discussed in Section 4, CONCLUSIONS AND RECOMMENDATIONS.

3.2 Fabrication of Devices.

Two approaches were used to obtain thyristor or LASS devices for experimental testing. First, devices which had been fabricated for electrical gating (i.e., designed and fabricated to be triggered by a conventional electrical signal as opposed to an optical signal) were modified by etching away the electrical gate contact and also by etching patterns (windows or ports) into the cathode metallization to observe the infrared recombination radiation (see Section 3.5.2). The etching was accomplished by typical photoresist and aluminum contact etching techniques used throughout the semiconductor industry. Second, devices were designed and fabricated specifically for optical firing so that the passivation of the surface took place after the cathode electrical contact optical window patterns were defined. High voltage power thyristor processing is a relatively low yield manufacturing process, and many problems were experienced with the specially designed runs. Most of the devices tested were modified "conventional" devices; however, the specially prepared devices provided some interesting data also.

Figures 3.2-1 through 3.2-5 are some typical designs used in the electrical testing. Figures 3.2-1, 3.2-2, and 3.2-3 are plan views of three of the emitter designs used in the low dI/dt test system. The fourth design used was the same as that of Figure 3.2-3 except that the shunt pattern appeared over the entire device surface (i.e., in the

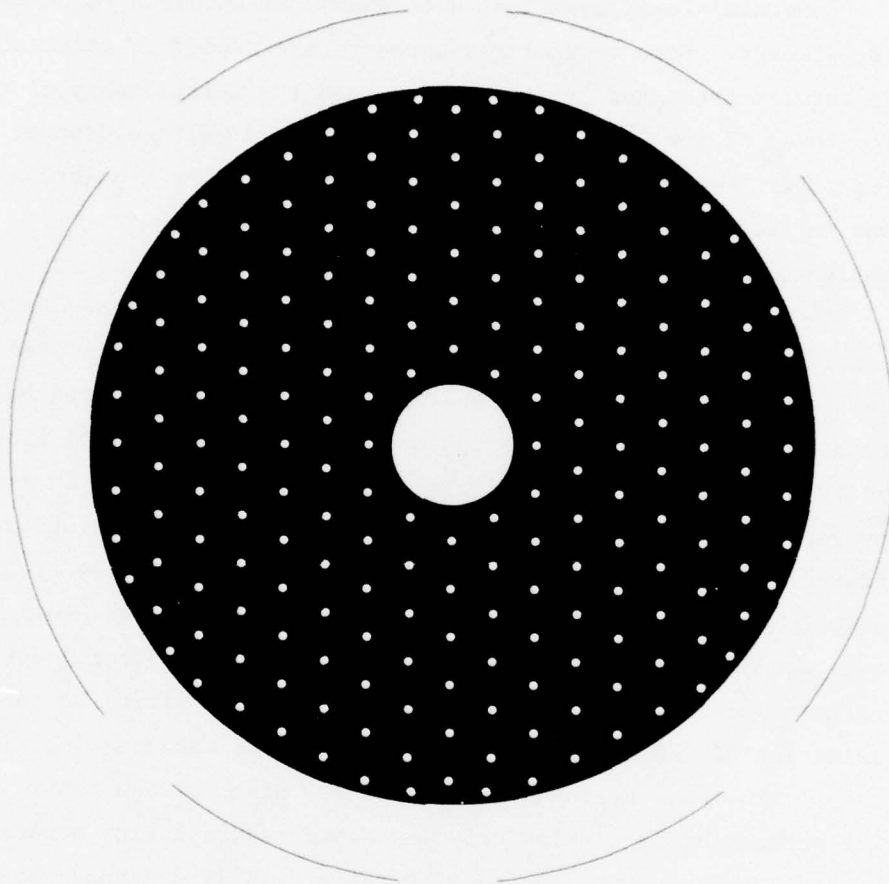


Figure 3.2-1. Experimental LASS emitter mask. H-type design. Dark regions are N-type. Light regions are P-type.

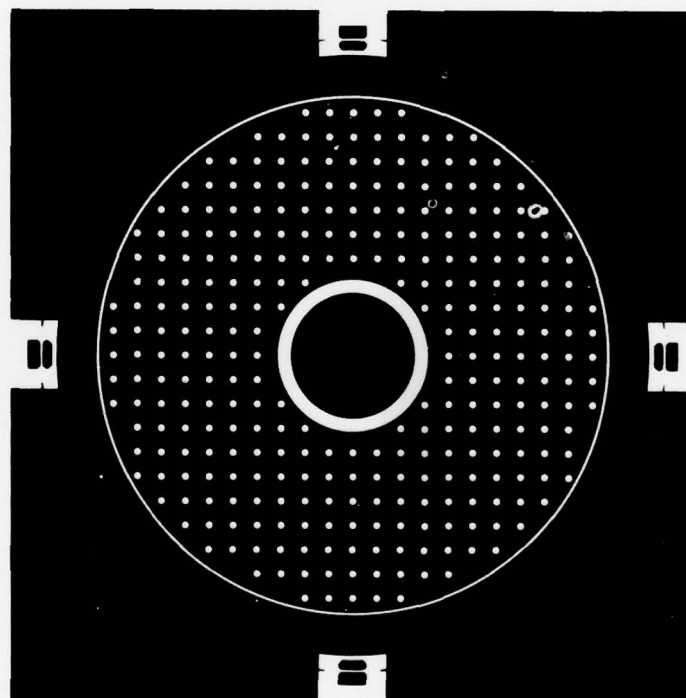


Figure 3.2-2. Experimental LASS emitter mask. K-type design. Dark regions are N-type. Light regions are P-type.

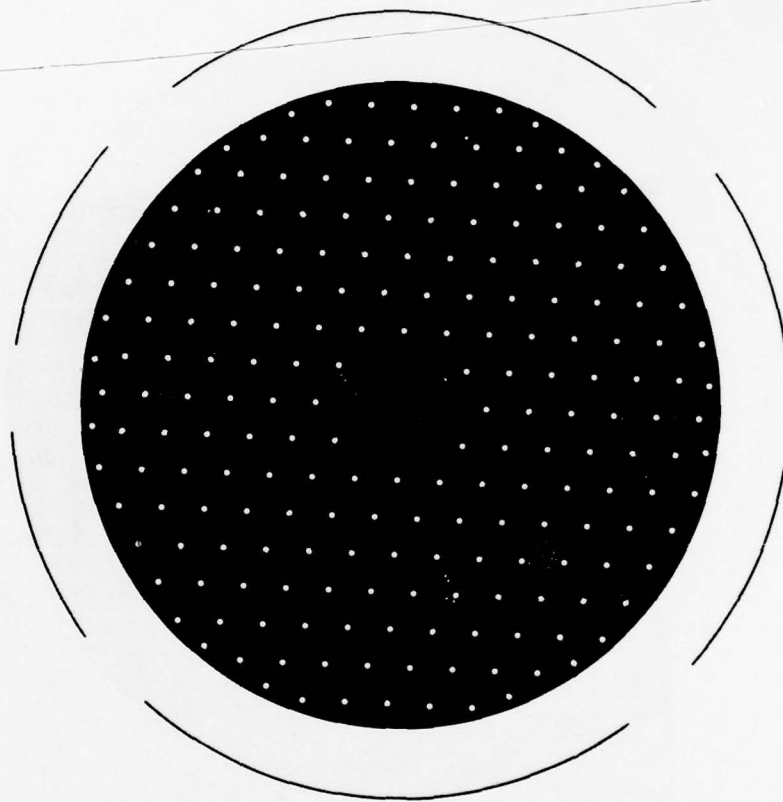


Figure 3.2-3. Experimental LASS emitter mask. J-type design. Dark regions are N-type. Light regions are P-type. This pattern was used also for the R-type design except the shunt pattern (white dots) continued over the central region.

center region also) and the n-base region was thinner than those tested with the Figure 3.2-3 emitter design. These structures were designated II, J, K, and R, respectively.

In all three figures, the dark regions are n-type and the light regions are p-type.

Figures 3.2-4 and 3.2-5 show the various cathode metallization patterns that were used on various devices for low and high dI/dt testing. For the LASS tests, the central gate metal was removed from the three commercially available device types shown at the right in Figure 3.2-4. An additional type of device design in the 23 mm diameter size, the Reverse Blocking Diode Thyristor or RBDT (formerly Reverse Switching Rectifier, or RSR), was modified for use in the high dI/dt tests by having a centrally located round or rectangular port etched into the cathode metallization. Three port patterns were used with the 50 mm diameter devices as shown. In several of the devices the overall pattern of very small windows for observation of the infrared recombination radiation can be seen. These geometric patterns were used on device designs to block either 1000 volts or over 2000 volts in order to compare the effect of base width (i.e. different impurity profiles) on plasma spreading velocity.

The results of the testing of these various configurations are discussed, as applicable, in Section 3.5.

3.3 Equipment, Circuits, Instrumentation, and Techniques.

The following seven subsections describe the important circuits and techniques (along with special instrumentation where applicable) used to obtain the experimental data. Special considerations and rationale for the approaches adopted are developed where appropriate. Discussions of particular problems encountered are deferred to Section 3.4, Problems Encountered.

3.3.1 Laser Light Source .

The source of light activation for the experimental testing was a neodymium doped yttrium aluminum garnet (Nd^{3+} :YAG) laser purchased from the GTE Sylvania Corporation as Government furnished

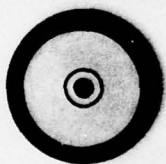
Special Designs
Showing Central
Optical Window



H-Type

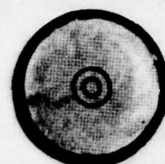


J-Type
R-Type



K-Type

Commerically Available
Designs - Central Gate
Metal Not Removed



Conventional Amplifying Gate



Inside-Outside Amplifying Gate



Snowflake Amplifying Gate

Figure 3.2-4. Cathode metallization patterns used on 23 mm devices designed for LASS experiments (left) and commercially available patterns (right).

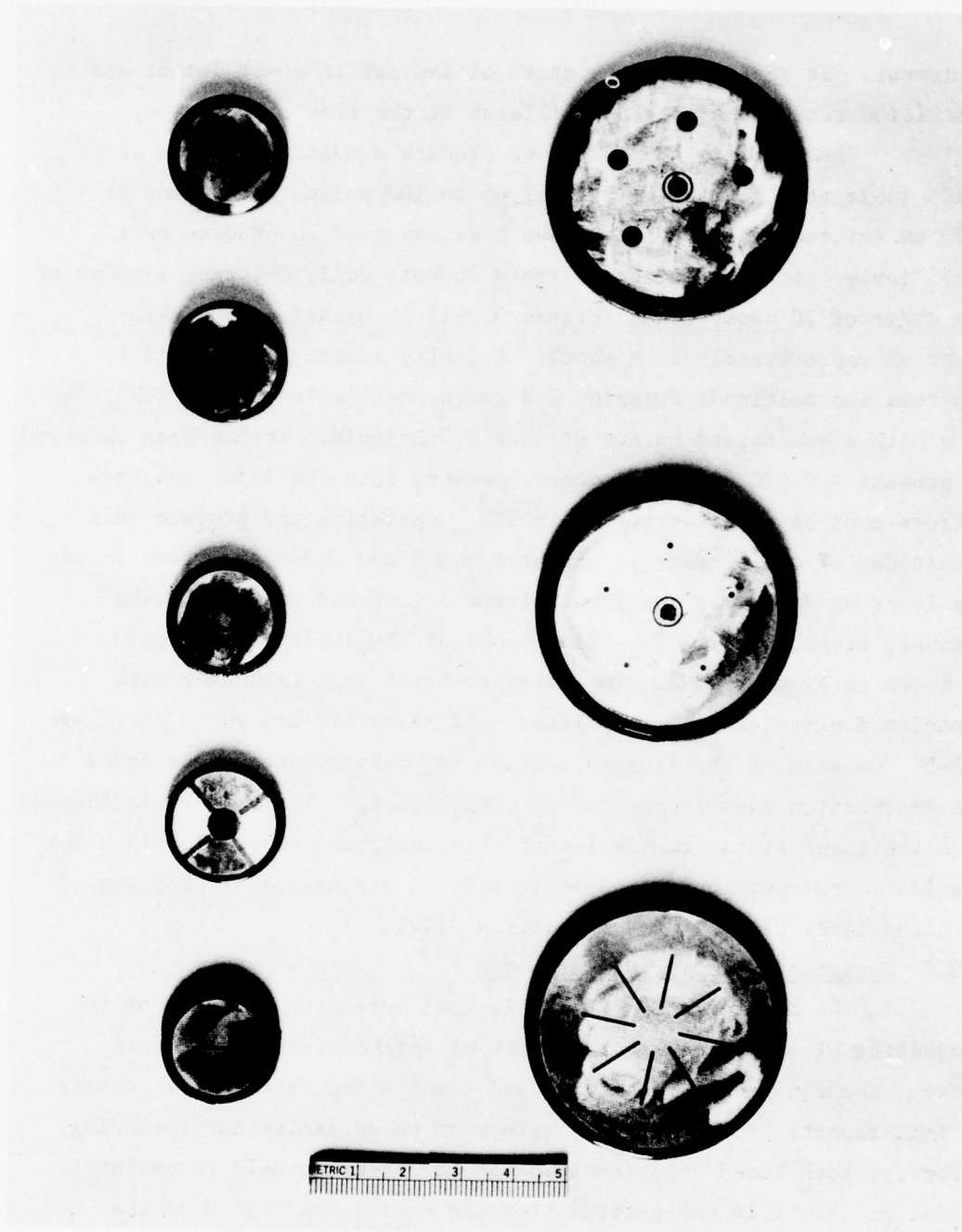


Figure 3.2-5. Illumination port patterns in the cathode metallization for LASS experiments.

equipment. It represented the state of the art in power output and repetition rate for a single oscillator at the time of purchase.

The laser is guaranteed to produce a multimode pulse of 0.125 joule at a repetition rate of up to 100 pulses per second at 1.06 μm emitted wavelength. It has been observed to produce over 0.150 joule. It is Q-switched with a Pockels cell, emitting a pulse of the order of 10 nanoseconds (Figure 3.3-1) in duration to a peak power of approximately 15 M watts. A cavity insert is provided to suppress the multimode emission and cause oscillation in the TEM_{00} mode with a guaranteed output of over 0.010 joule. It has been observed to produce > 0.020 J in this mode; however, both the front and back mirrors must be adjusted to obtain TEM_{00} operation and produce this magnitude of output energy. Figures 3.3-2 and 3.3-3 are views inside the laser head showing the front mirror adjustment and flash lamp removal, respectively. The front panel of the laser power supply is shown in Figure 3.3-4. The water-to-water heat exchanger with associated circulating pump, filter, and reservoir are shown in Figure 3.3-5. Details of the laser operation and maintenance can be found in the instruction manual provided by GTE Sylvania. The manual was shipped with the laser at the completion of this contract. Specifications for the laser are contained in Appendix III. A discussion of problems with the laser can be found in Section 3.4.1.

3.3.2 Spreading Velocity Measurement.

The determination of the lateral spreading velocity of the conducting plasma was a major subtask of this contract. For this reason, the equipment, technique, and results are discussed in detail in this report. Two approaches were used to determine the spreading velocity, both based on observation of the electron-hole recombination radiation ($\lambda = 1.14 \mu\text{m}$) emitted from the conducting region of the thyristor. These approaches are described in the following subsections.

3.3.2.1 Infrared image converter camera technique. It is well known that thyristors turn-on locally and the conducting or "on" region plasma then spreads over the entire active area of the device at

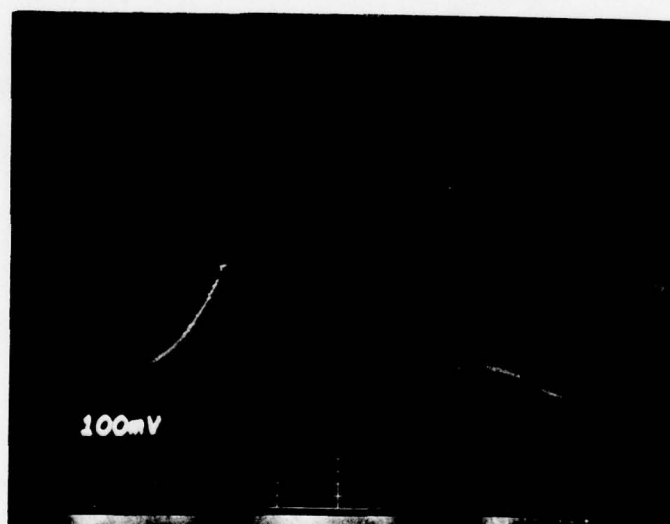


Figure 3.3-1. Oscillograph of laser output. Time scale is 5 nsec per major scale division. Oscilloscope used was Tektronics type 7904.

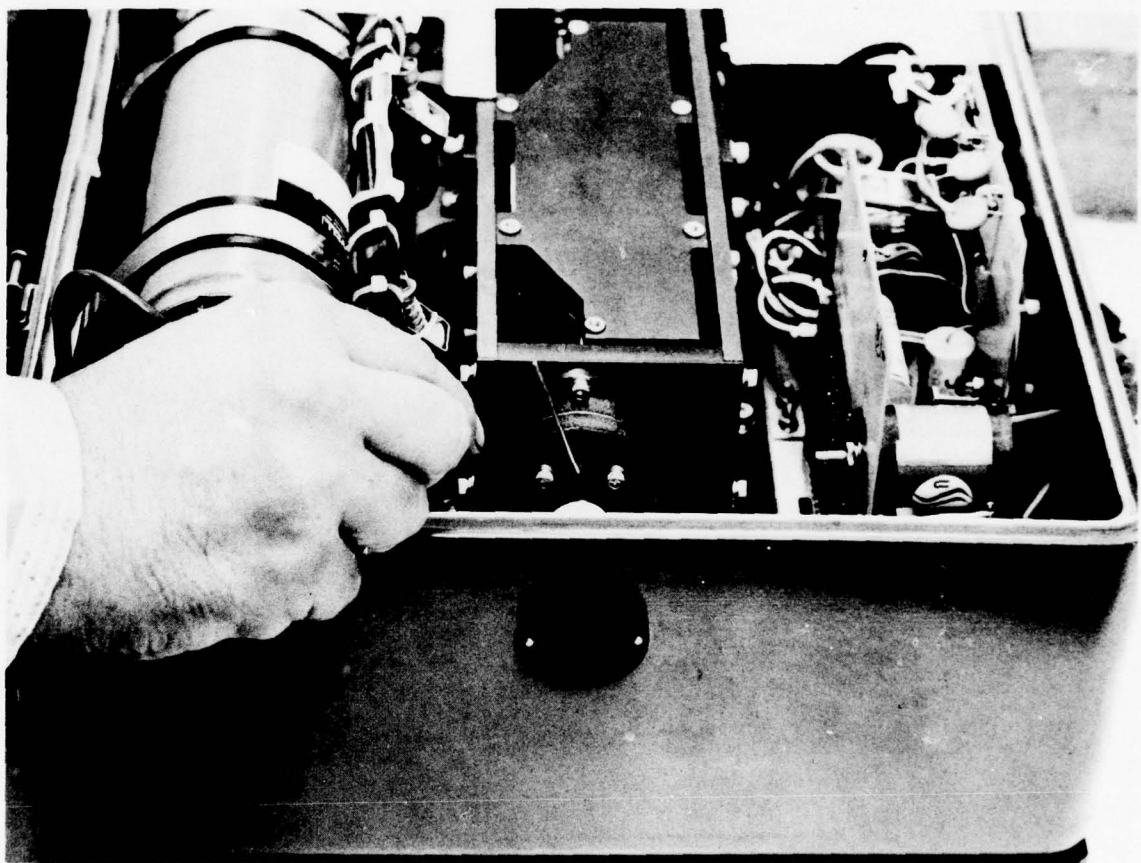


Figure 3.3-2. View inside the laser head showing adjustment of front mirror.

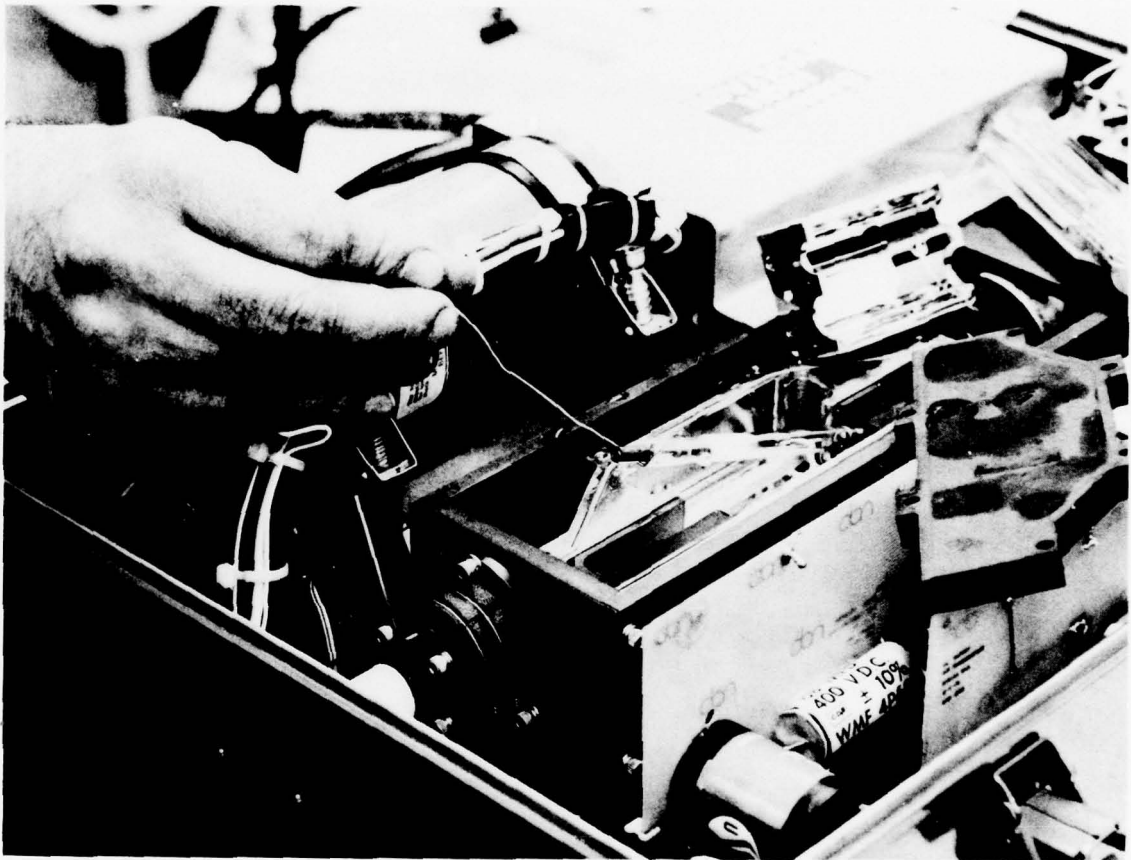


Figure 3.3-3. View inside laser head showing flash lamp removal.

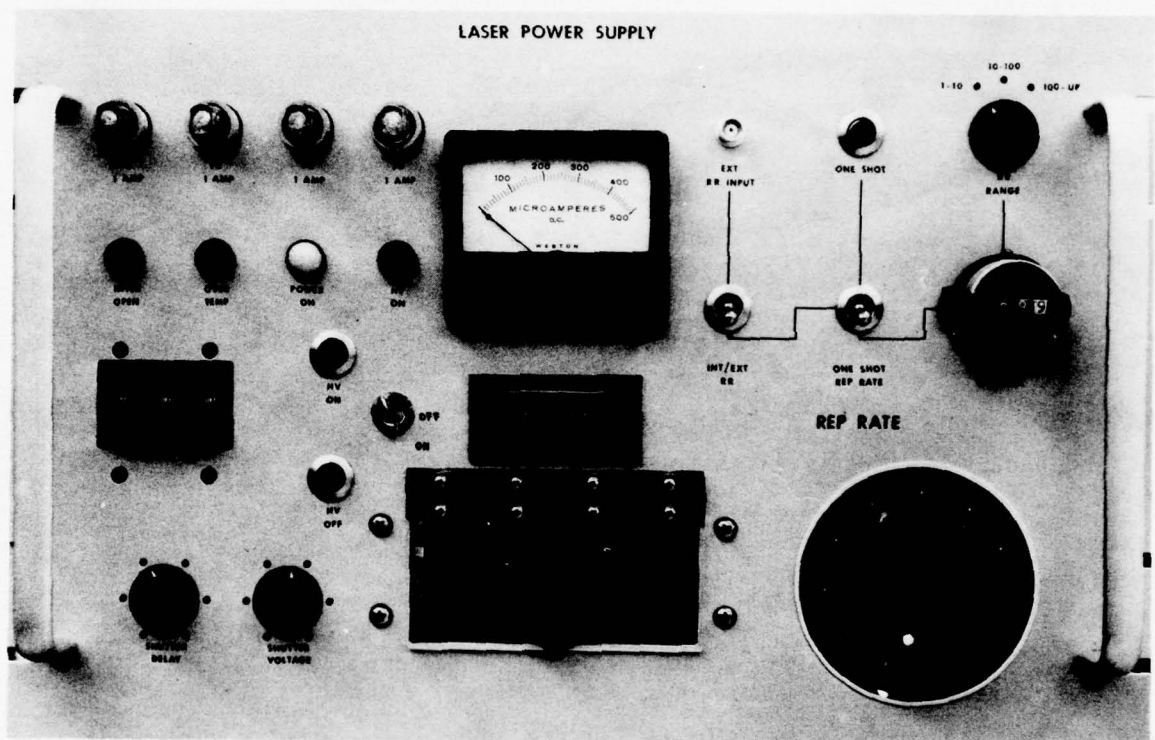


Figure 3.3-4. Front panel of laser power supply.

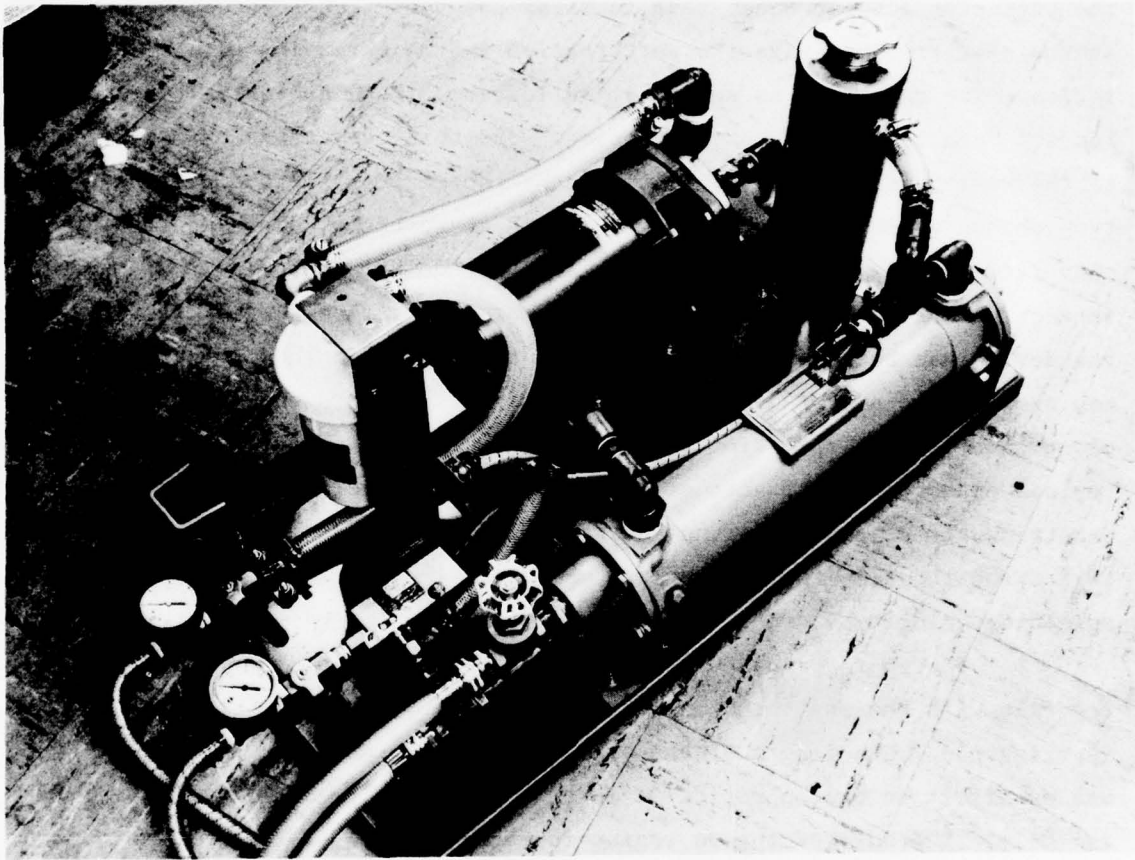


Figure 3.3-5. View of water circulating/cooling pump and water-to-water heat exchanger with sheet metal cabinet removed.

some rate.⁽¹⁾ The rate of lateral spreading of the plasma is called the spreading velocity, v_s . A technique that has been used to observe the spreading velocity is to observe the recombination radiation emitted in the conducting region of a device. This technique is discussed in detail in references (1). The system is shown schematically in Figure 3.3-6.

Observation windows are etched into the cathode contact of the thyristor element under test to allow the radiation to escape and at the same time minimize the perturbation in the spreading of the "on" region. The radiation is sensed by an infrared image converter tube focused onto the cathode of the device. The tube converts the image to the visible where it is intensified by tandem image intensifiers and then photographed for permanent record and measurement. The image converter tube is constructed with a variable delay shutter so that the area of plasma spreading can be observed at some variable time after the device has been fired. In this way, the area which has turned on can be observed at various times after triggering, thus enabling measurement of the spreading velocity of the plasma. Figure 3.3-7 shows typical examples of the sort of photographs which are obtained. By measuring the physical distance between different diameters of the on region and the time the shutter is opened after device triggering, the spreading velocity v_s is obtained.

The photographs obtained are a multiplicity of exposures of the film with the shutter opened at the same time each time the device is triggered. The length of the exposure (i.e., number of exposures) has an effect on the on region diameter because of the sensitivity of the film. The edge of the on region is not conducting as heavily as those regions which have been on for a time so that the intensity of the recombination radiation is not as great at the edge of the conduction region. Even if the number of exposures at each time frame were kept the same (that is, the exposure time at some fixed repetition rate), the intensity of the recombination radiation is a function of the current density which changes (decreases) as the shutter position is

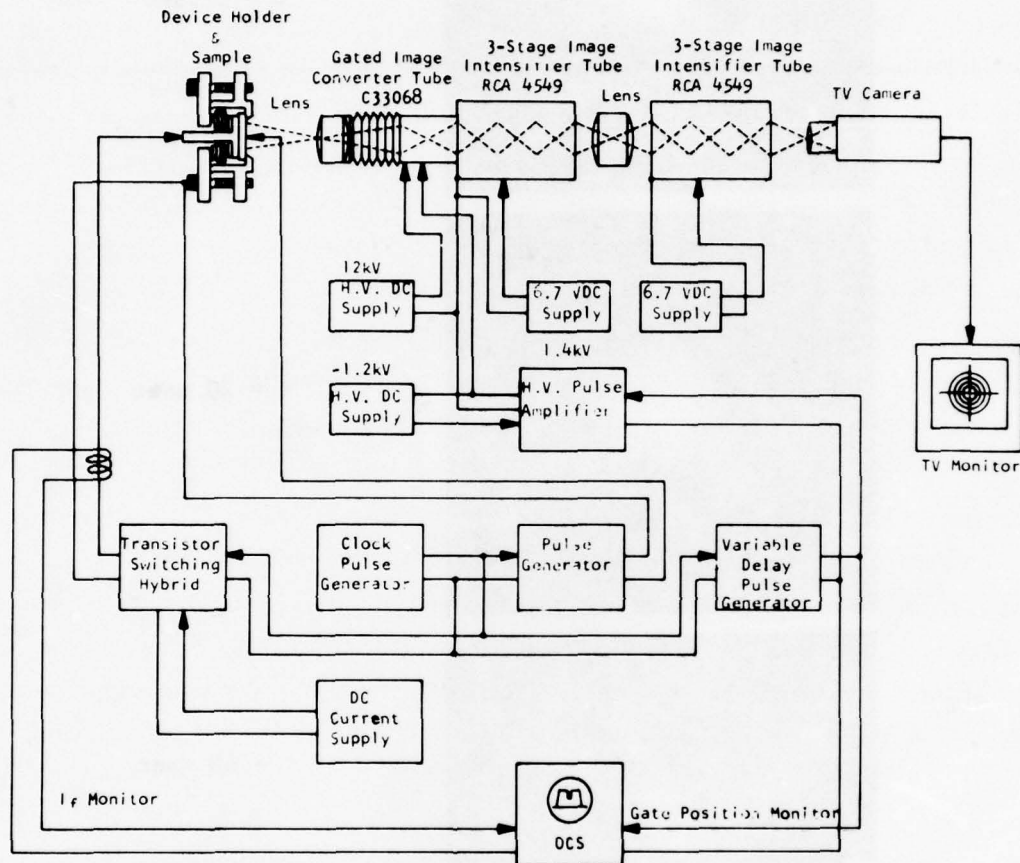
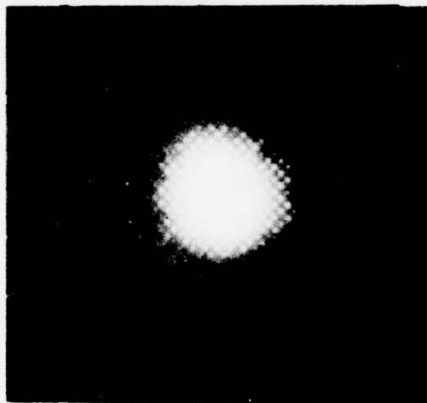


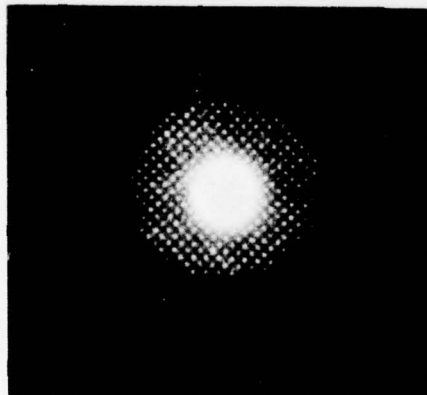
Figure 3.3-6. Schematic representation of the infrared image converter camera technique for measuring the lateral spreading velocity of the electron-hole plasma.



$t = 2 \mu\text{sec}$



$t = 10 \mu\text{sec}$



$t = 40 \mu\text{sec}$

Figure 3.3-7. Typical example of raw data obtained from infrared image converter camera technique. Current pulse width 100 μsec ; shutter pulse width $\approx 2 \mu\text{sec}$. Anode current 600 A.

moved farther in time from the initiation of turn-on. This contributes to errors in two ways. The turned-on area is determined as being somewhat smaller than is really the case. As a first result, the effective radius measured at each interval in the current pulse is less than the true value; and to the extent that this difference varies with the spreading velocity value or current density value, it contributes to an error in the determination of Δr and thereby the spreading velocity. Second, because the measured area is too small, there is an apparent increase in the current density. This factor would cause a shift in the spreading velocity-current density relationship toward higher values of current density for a given spreading velocity; and it also increases the scatter of the experimental data taken with different values of anode current.

There are additional uncertainties in the value of v_s obtained by this means. First, it has been observed for both electrically triggered and laser fired devices that the gate region or optical window for the laser pulse conduct current only during the early stages of conduction; consequently, the assumed area of conduction from which the current density is derived is only approximate. Second, an unknown factor results from the fact that conducting region of many devices does not spread radially in a uniform manner and actual current density is therefore unknown. This may be a matter of technique in contacting the cathode of the device because the devices tested on this program demonstrated very uniform spreading.

The neodymium laser was set up with the plasma spreading equipment to observe turn-on spreading of devices fired with the laser. Figure 3.3-8 is a diagram of the pertinent parts of the set-up. The laser pulse was directed into the center of the device with a glass prism at an angle approximately 45° to the normal. Although the image converter tube is electronically shuttered off during the laser pulse, a pass band light filter was found to be necessary between the silicon surface and the image converter tube. Continuing radiation from the laser pump flash lamp (after the laser pulse is over) is scattered from

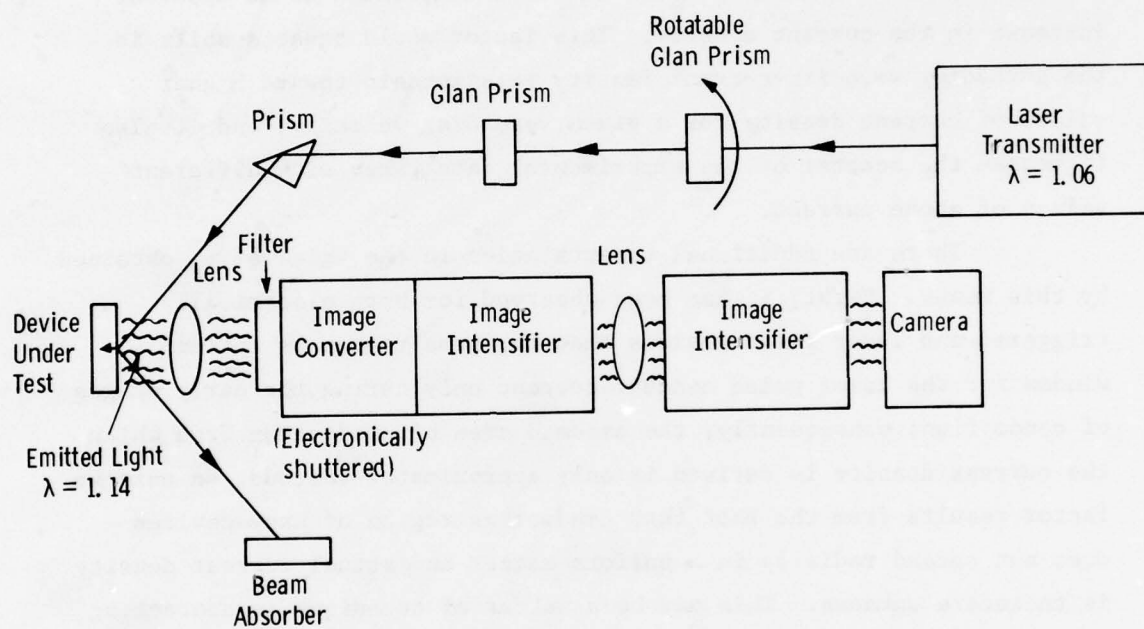


Figure 3.3-8. Diagram of infrared recombination radiation system for studying plasma spreading with laser light activation of device under test.

the silicon and metal contact surface and saturates the image converter tube. The pass band filter is centered on 11,400 Å (silicon band-to-band recombination radiation peak) with a half power bandwidth of ± 300 Å. Because of the change in optical path length introduced by insertion of the band pass filter, the focusing must be carefully checked at this point.

Fluorescence from the laser rod prior to Q-switching is effectively blocked by the image converter and is apparently at a low enough level after the laser Q-switches that feed-through does not present a problem. The only restriction on the system is that the shutter cannot be open during the laser Q-switched pulse.

An attenuator consisting of two crossed glan prisms was inserted into the beam path. Two glan prisms are used so that the plane of polarization of the output beam remains unchanged while the amplitude is varied. The attenuator is set up by aligning the second prism for maximum transmission of the laser beam, which is linearly polarized by the use of a Pockels cell Q-switch. The first prism is placed between the laser and the second prism. When the first prism is rotated, the output power will vary as $\cos^4 \theta$, rather than $\cos^2 \theta$ as would result if the second prism were omitted.

Figure 3.3-9 is a calibration curve run on the system using a Coherent Radiation Labs calorimeter with the laser running at 50 pps. The excellent agreement between theory and the measured value indicates that the laser output is highly plane polarized, as it should be. Maximum output through the attenuator and prism with the laser running in the TEM₀₀ mode was found to be 13 mjoule/pulse.

The thyristor element to be tested is mounted in a jig which contacts the device at the periphery, allowing the major portion of the cathode contact surface to be focused onto an image converter tube for observation of infrared recombination radiation emitting from the "on" regions of the device. (See Figure 3.3-10.) Small holes were etched into the metal contact surface to expose the bare silicon surface and, thus, allow the infrared radiation to reach the converter tube.

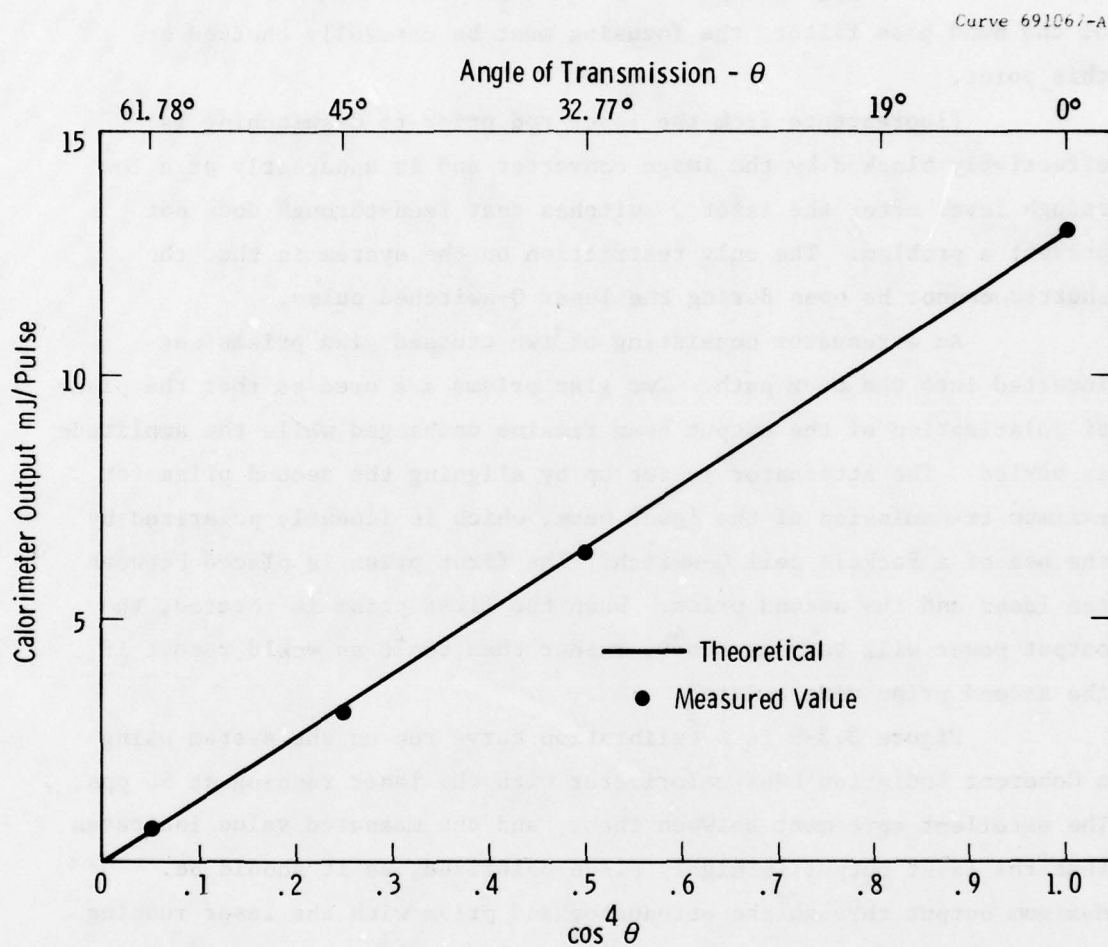


Figure 3.3-9. Calibration of glan prism attenuator.

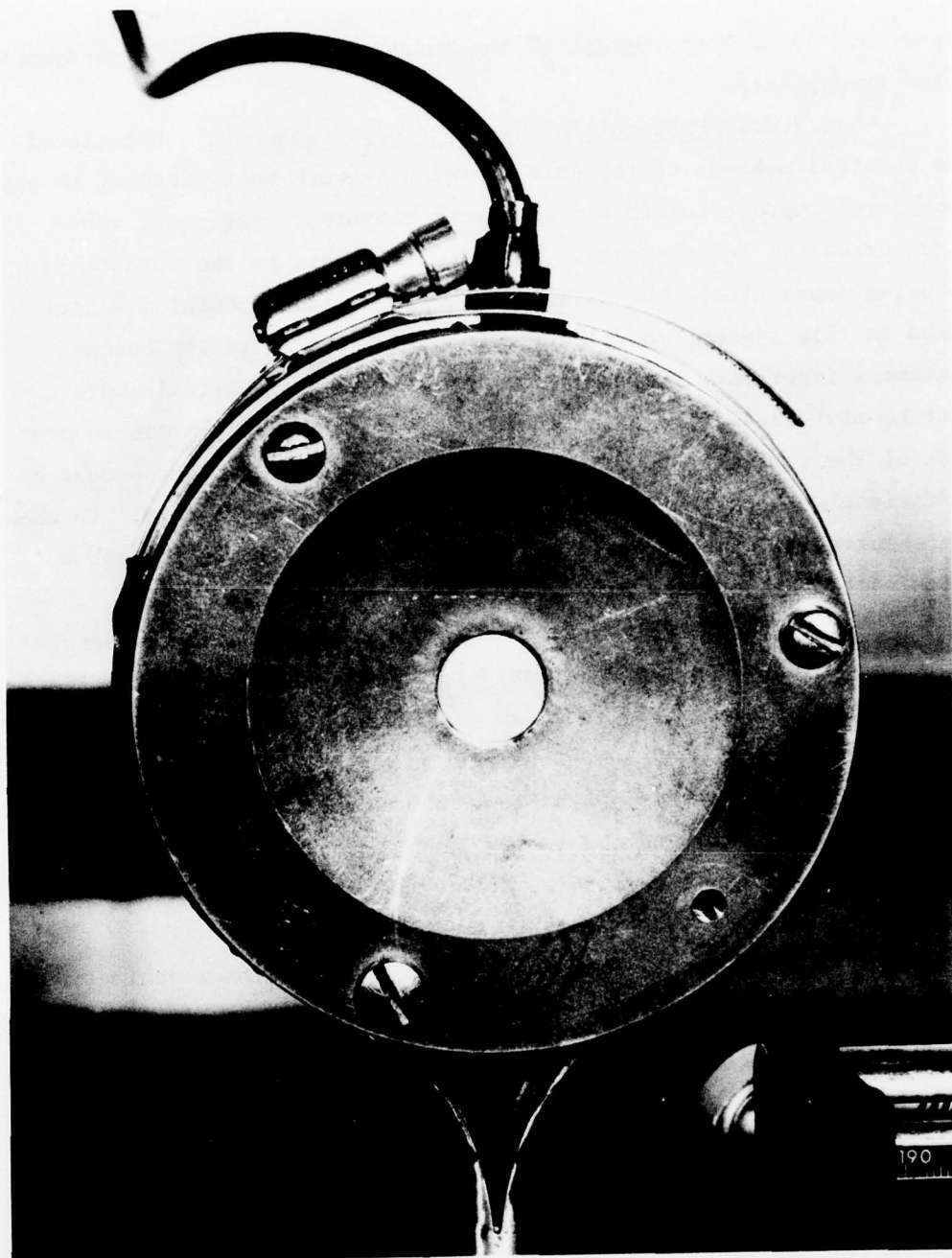


Figure 3.3-10. Infrared recombination radiation observation. Note pattern in device to permit radiation to escape. Device shown in jig is not optically activated.

Figure 3.3-11 is a photograph of the infrared system and the neodymium laser transmitter.

3.3.2.2 Photomultiplier-light pipe technique Because of the physical make-up of the pulse forming network test circuit, it was considered impractical to use the image converter system for very high current v_s measurements. Not only is access to the cathode for focusing impractical, but also at the high current densities anticipated in this system, the electrical contact configuration becomes extremely important. Perturbations to very good electrical contact must be minimized. The cathode electrode must be under pressure over most of the surface of the device or the device metallization must be sufficiently thick that lateral voltage drops are negligible. To keep the observation windows small and at the same time focus through a thick contact layer is impractical.

Figure 3.3-12 is a schematic of the system used to measure spreading velocity in the PFN test circuit described in Section 3.3.3. A photograph of the set-up is shown in Figure 3.3-13. The photomultiplier (PM) tube has an S-1 surface and is not highly sensitive in the very near infrared (silicon band-to-band recombination radiation peaks at $1.14 \mu\text{m}$). In order to obtain low level signals from the PM, the tube was inclosed in a commercial dewar and cooled to dry ice-methanol temperature (-72°C).

Two types of observation windows in the cathode contact were used. The first consisted of four radial rectangular regions etched 90° apart as shown in Figure 3.3-14. A light pipe was inserted into a hole in the cathode contact pole piece which was aligned with the radial slot. This light pipe was used to transmit the recombination radiation to the photomultiplier tube input. This technique was needed because a large observation port was required to obtain an adequate signal with the original photomultiplier system. Catastrophic failure of devices became common with this approach and always occurred in the same spot (See Figure 3.3-14). The reason for the failure is obvious. The thin region of metallization between the circular illuminated

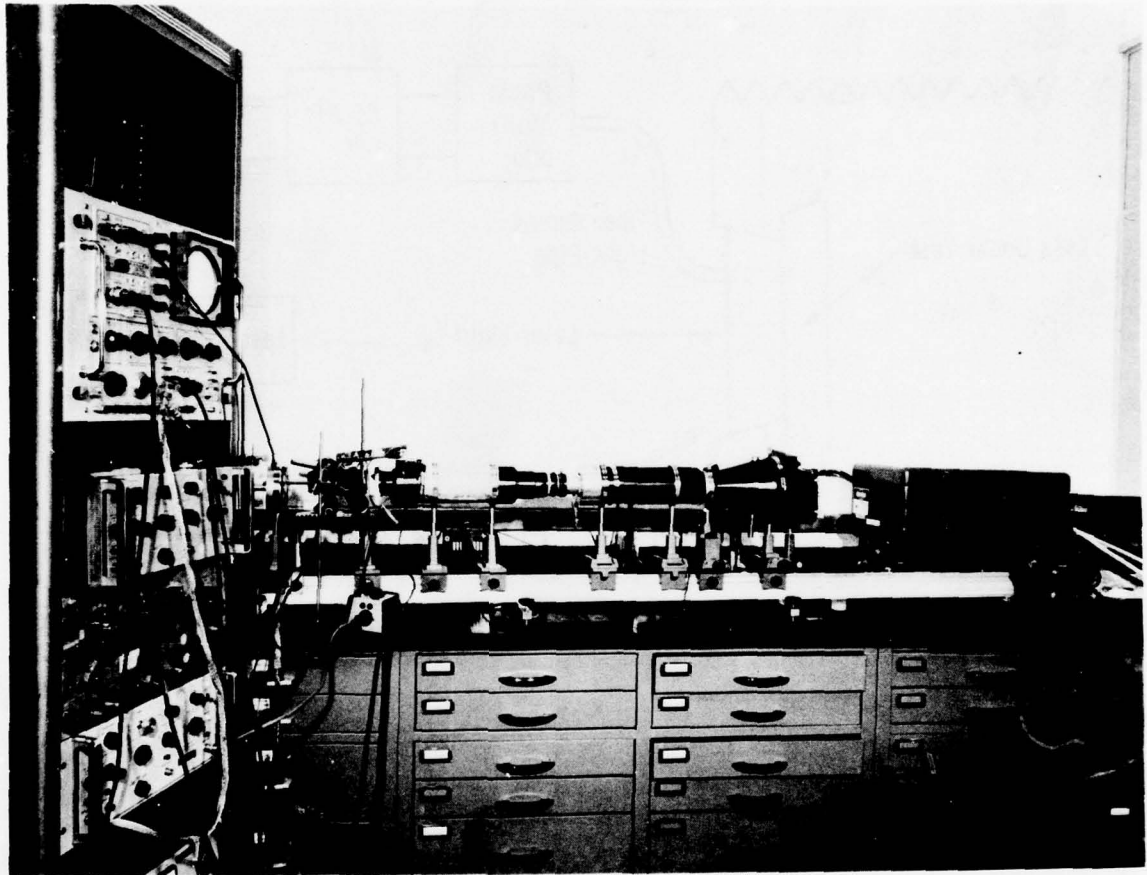


Figure 3.3-11. Infrared recombination radiation observation system showing electronic control optical system. Neodymium laser transmitter is located at far right. (Refer to Figure 3.3-7.)

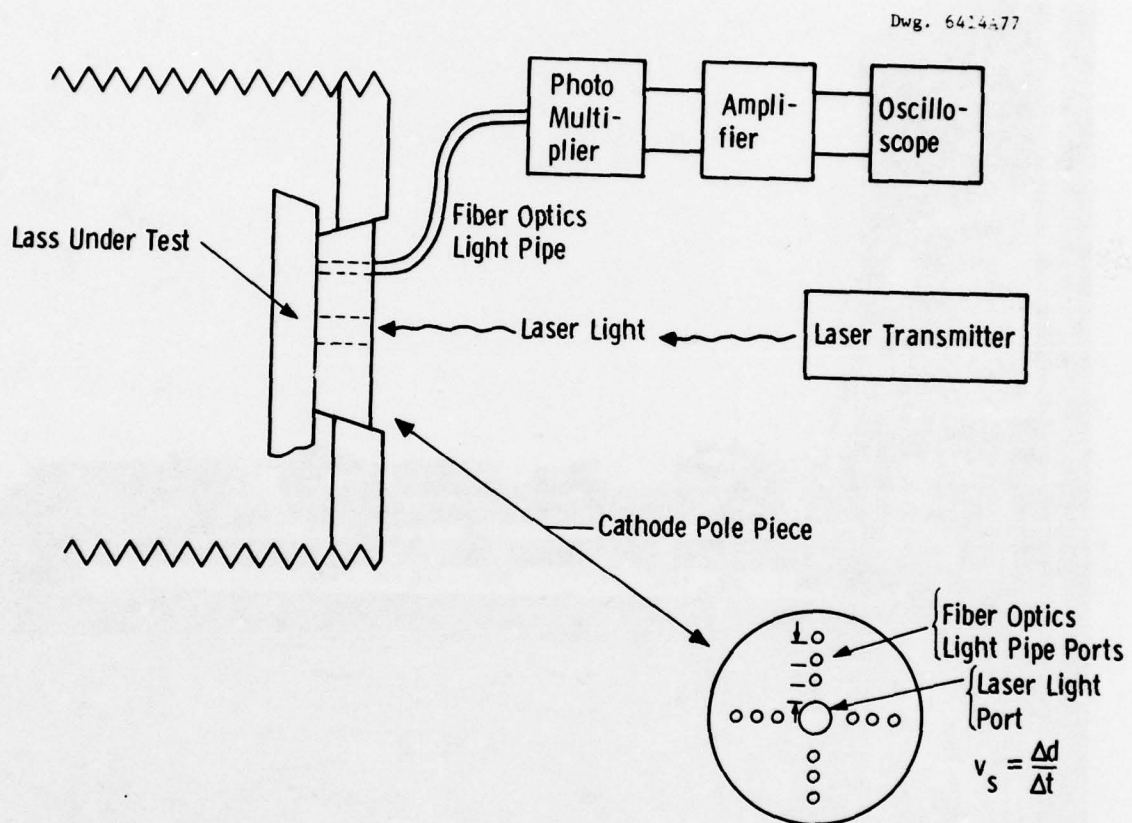


Figure 3.3-12. Schematic diagram of the photomultiplier tube plasma spreading measurement set-up.

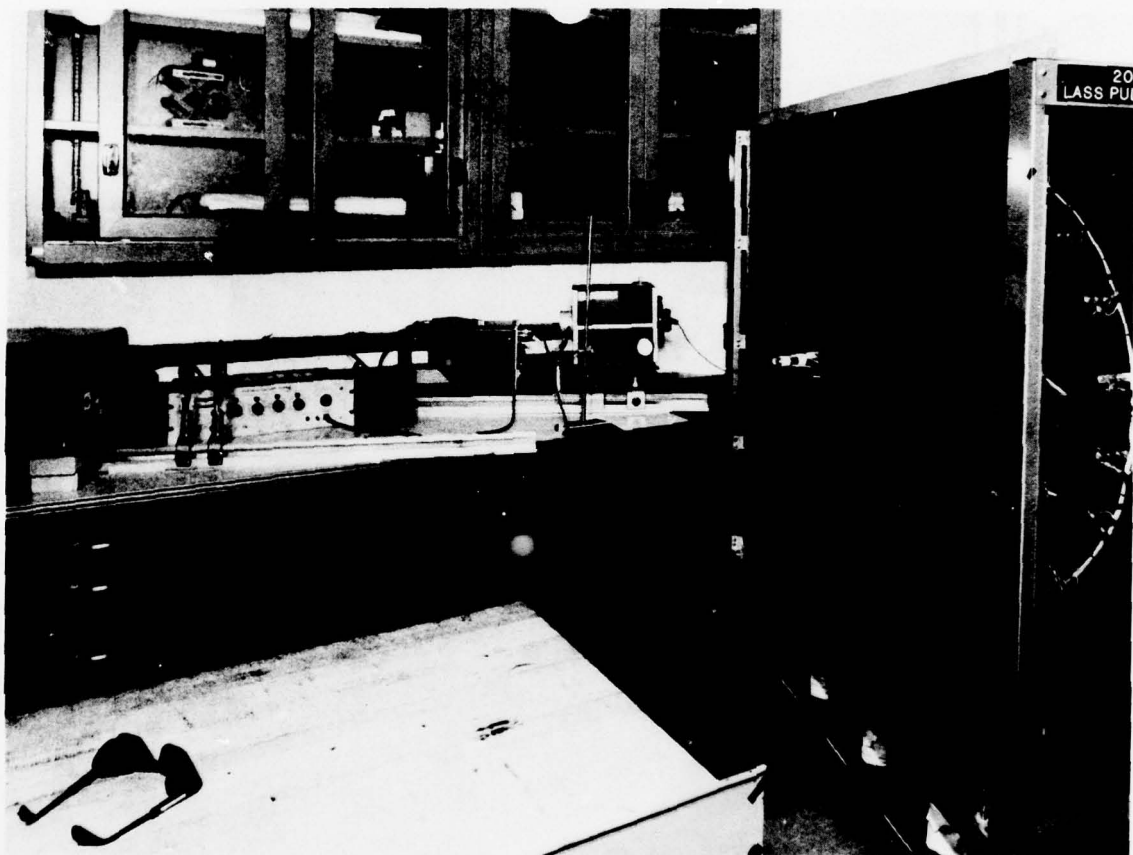


Figure 3.3-13. Photograph of set-up to measure spreading velocity under high current conditions. The laser head is at the extreme left of the picture, and the PFN unit is the large equipment partially shown at the right. The photomultiplier tube and its amplifiers are on the bench with the photomultiplier at the right edge of the bench.



Figure 3.3-14. Top view of LASS showing circular optical activation window in the center. Contact region removed in four radial strips for infrared observation of plasma spreading. Note device failure at metallization between window and observation strip.

activation window and the etched infrared observation strip is an electrical and thermal stress point. Not only is the current channeled through this contact area as the plasma spreads, but some reduction in heat sinking of the region also results.

As a result of the above problem, efforts were made, successfully, to improve the sensitivity of the photomultiplier system so that an adequate signal can be obtained from a 0.0127 cm (0.005") diameter hole in the metallization. This increased sensitivity was achieved by improving the signal to noise ratio of the photomultiplier tube by cooling it with dry ice and alcohol as described above, and increasing the gain of the amplifier. This method not only provides a smaller perturbation in the contact configuration, but also distributes the current and thermal stress region over a larger area.

Therefore, the second type of observation windows employed holes etched 0.0127 cm (0.005") in diameter on 0.0508 cm (0.020") centers over the entire cathode contact area of a device to permit the recombination radiation to escape from the device for observation. Again a fiber optic light pipe was inserted in holes in the cathode pressure contact electrode, and the other end was placed in intimate contact with the photomultiplier tube input. The light pipe is approximately 0.066 cm (0.026") in diameter so that regardless of where the hole is placed in the cathode contact pole piece, it will always line up with at least one of the observation windows in the contact. After a device had been tested and observations made, the locations of the observation windows which were aligned were noted and the distances were measured relative to the observation window used rather than the ports in the pressure electrode pole piece. See Figure 3.3-15.

To facilitate these infrared observations for analysis and correction of the computer model, electrodes with various patterns of small holes in the pole face were fabricated to permit the 0.050 cm (0.020") diameter fiber optic light pipe to be brought into contact with the silicon surface at various radii. Figure 3.3-16 is a photograph

Dwg. 6414A72

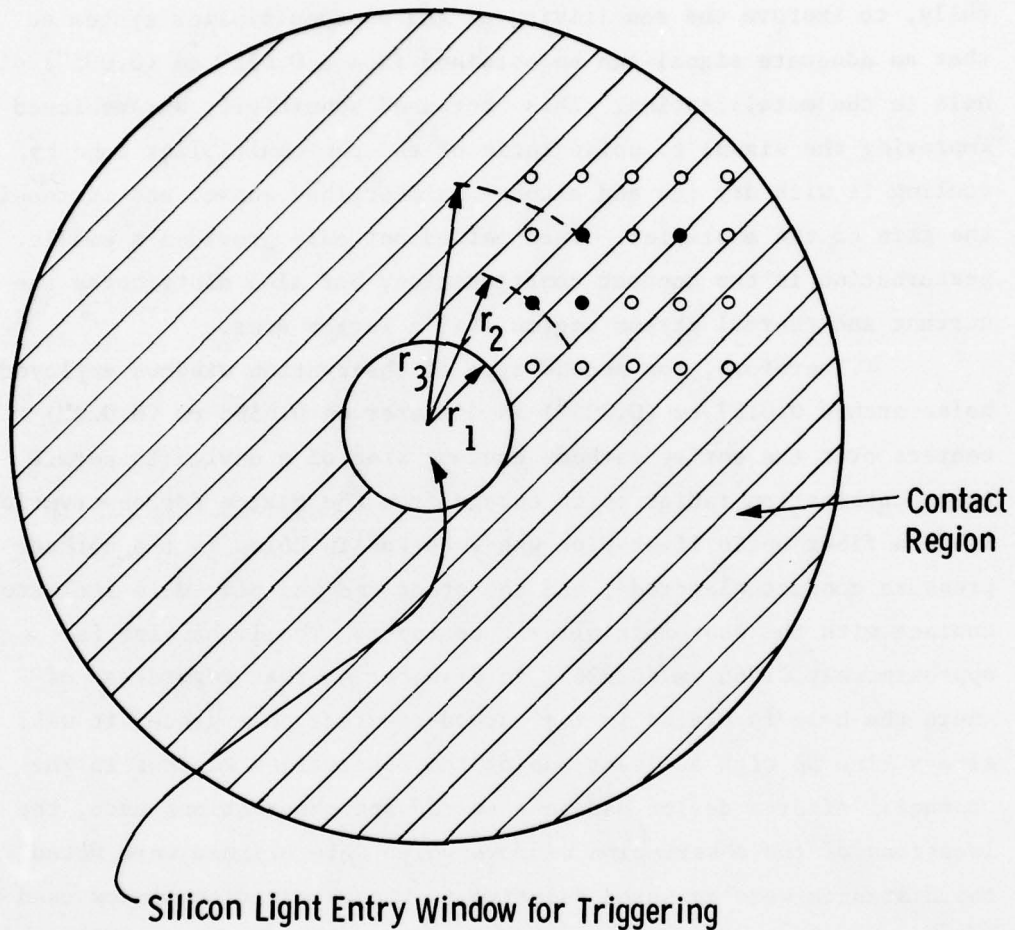


Figure 3.3-15. Plan view of cathode side of thyristor active element showing the central window for triggering and the grid of 0.0127 cm diameter infrared observation holes in the contact region. Darkened holes are examples of ones that aligned with pole piece ports and were used in data gathering.

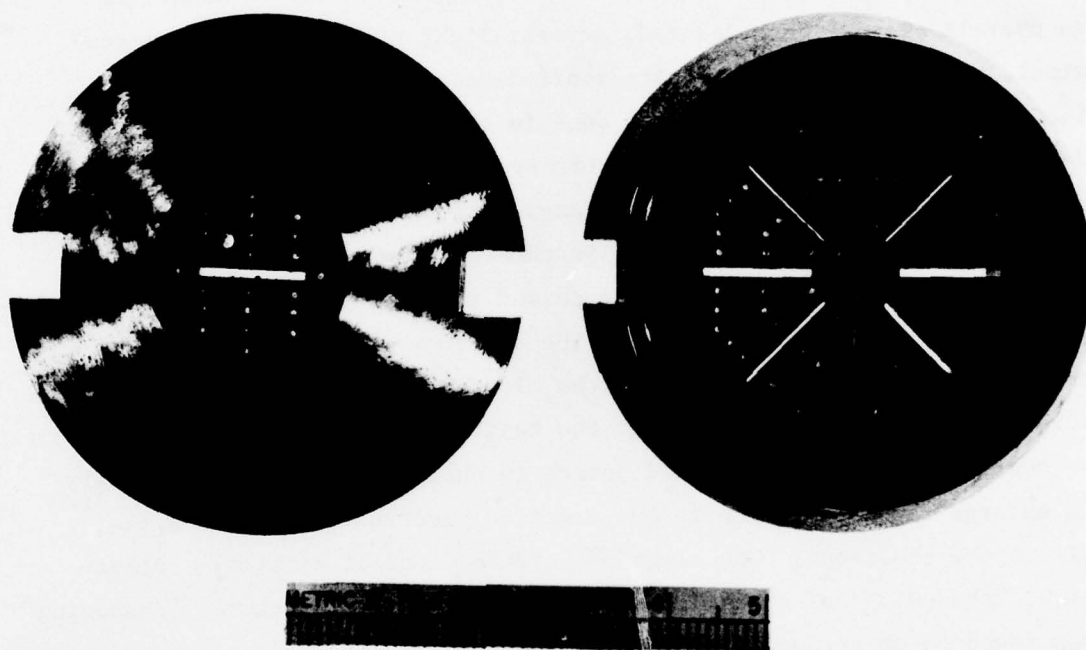


Figure 3.3-16. Photograph of cathode electrodes showing patterns of observation ports (small holes) for infrared recombination radiation using the photomultiplier (PM) technique. The left electrode shown is for 23 mm diameter active elements and the right one is for 50 mm diameter active elements.

showing the patterns fabricated for both the 23 mm and 50 mm diameter devices. Observation of spreading of the on region was achieved by coupling the output of the light pipe to the photomultiplier tube. The time from the laser pulse to an observation on the photomultiplier indicates the spreading velocity (to a given radius and consequently at a given current density). Not all of the holes were used simultaneously. One piece of light pipe was moved around to obtain average values. The new method does not permit the overall radial spread to be observed in a single observation, but a quantitative determination of the time to reach the on state at a given radius can be made. If an overall picture were desired, several light pipes could be inserted simultaneously and their outputs applied to the image converter and intensifier tubes. This was not done in the present work because all data available indicated very uniform spreading of the plasma.

In order to align the rectangular slots in the electrode to the rectangular aperture patterns in the device metallization, the device was aligned under a microscope and then mounted to the electrode with a removable silicone rubber. The silicone rubber was needed to hold the device in alignment with the electrode while the two parts were inserted as an assembly into the test system. Errors which occur in centering the pattern on the device in photoresist made it necessary to enlarge the indentation in the negative electrode to insure a flat fit to the electrode. The alignment of the slots is critical: otherwise, "shadowing" of the silicon by the electrode will occur. "Shadowing" was found to cause localized heating and burn-out in earlier experiments (See Section 3.4.3(b)).

It was found that the photomultiplier tube had to be masked so that no spurious light was received from the laser pulse. Otherwise, the amplifier of the photomultiplier was driven into saturation and did not recover in time to provide useful information.

The technique introduces an uncertainty in the time measurement since the observation hole(s) in the metallization will fall

somewhere within a fiber optics light pipe observation port but not at a predictable point. To determine the location of these holes, a clear lacquer was sprayed into the observation ports after testing of a given device was complete. Microscopic observation of the lacquer on the surface of the device after removal from the circuit was used to locate the relative position of the observation holes.

The spreading velocity is a function of the current density J and is measured as follows: The laser is fired. Sufficient laser light leaks through the optical system to cause a signal on the PM tube output which is observed on the oscilloscope trace. (The oscilloscope trace is synchronized to the laser pulse). This indicates time zero. At some later time another signal is observed on the oscilloscope when the on region has spread to the observation window opposite the light pipe. This is t_{r_n} . By placing the light pipe in the electrode at various radii, various t_{r_n} 's are obtained. The radius r_n used to obtain t_{r_n} is noted. Then

$$v_{s_{r_m, r_n}}(J_{r_m, r_n}) = \frac{\Delta r}{\Delta t} = \frac{r_n - r_m}{t_{r_n} - t_{r_m}} .$$

Referring to Figure 3.3-11 where the darkened points are assumed to be observation windows used in obtaining signals with the PM tube and light pipe,

$$\begin{aligned} v_{s_{r_2, r_3}}(J_{r_2, r_3}) &= \frac{r_3 - r_2}{t_{r_3} - t_{r_2}} \\ J_{r_2, r_3} &= \frac{\text{Ipulse (which is constant)}}{\text{Average On Area}} \\ &= \frac{\text{Ipulse}}{\pi(r_3^2 + r_2^2 - 2r_1^2)/2} . \end{aligned}$$

When working with rectangular illumination ports, the r_n becomes the distance of the observation windows from the axis of the illumination port. This is reasonable for windows near the port and near the center of the long dimension of the port, but constitutes a possible source of error in current density determinations.

Measurements of velocity using $t=0$ as an end point in Δt are not considered reliable because the initial on area is not well defined (believed for modeling purposes to be significantly larger than the illuminated area, but the scattering experiment of section 3.5.3.1 indicates otherwise) and it is impossible with present techniques to determine when the central illuminated region goes off during the initial spreading. It is assumed that after the first radius is reached by the plasma that only the area beneath the electrical contact is actually conducting. Then the on area is well defined for future spreading. It is also assumed that the plasma is spreading uniformly radially. This does appear to be the case at these current densities since v_s measurements on a single device are in good agreement made at different angular directions.

Spreading velocity (v_s) can in principle also be obtained by timing the difference between when the signal first appears in a given observation port and when the signal peaks in that port. (See Figure 3.3-17.) But so many arguable assumptions have to be made, and the numerical results are so inconsistent with all other known ways to determine v_s , that this approach was not pursued further.

It turned out that the photomultiplier technique to measure v_s was successful only with 23 mm diameter devices. As is discussed in Section 3.4.3, Device Under Test,

AD-A080 567

WESTINGHOUSE RESEARCH AND DEVELOPMENT CENTER PITTSBU--ETC F/G 9/1
OPTICALLY ACTIVATED SWITCH.(U)
APR 78 L R LOWRY

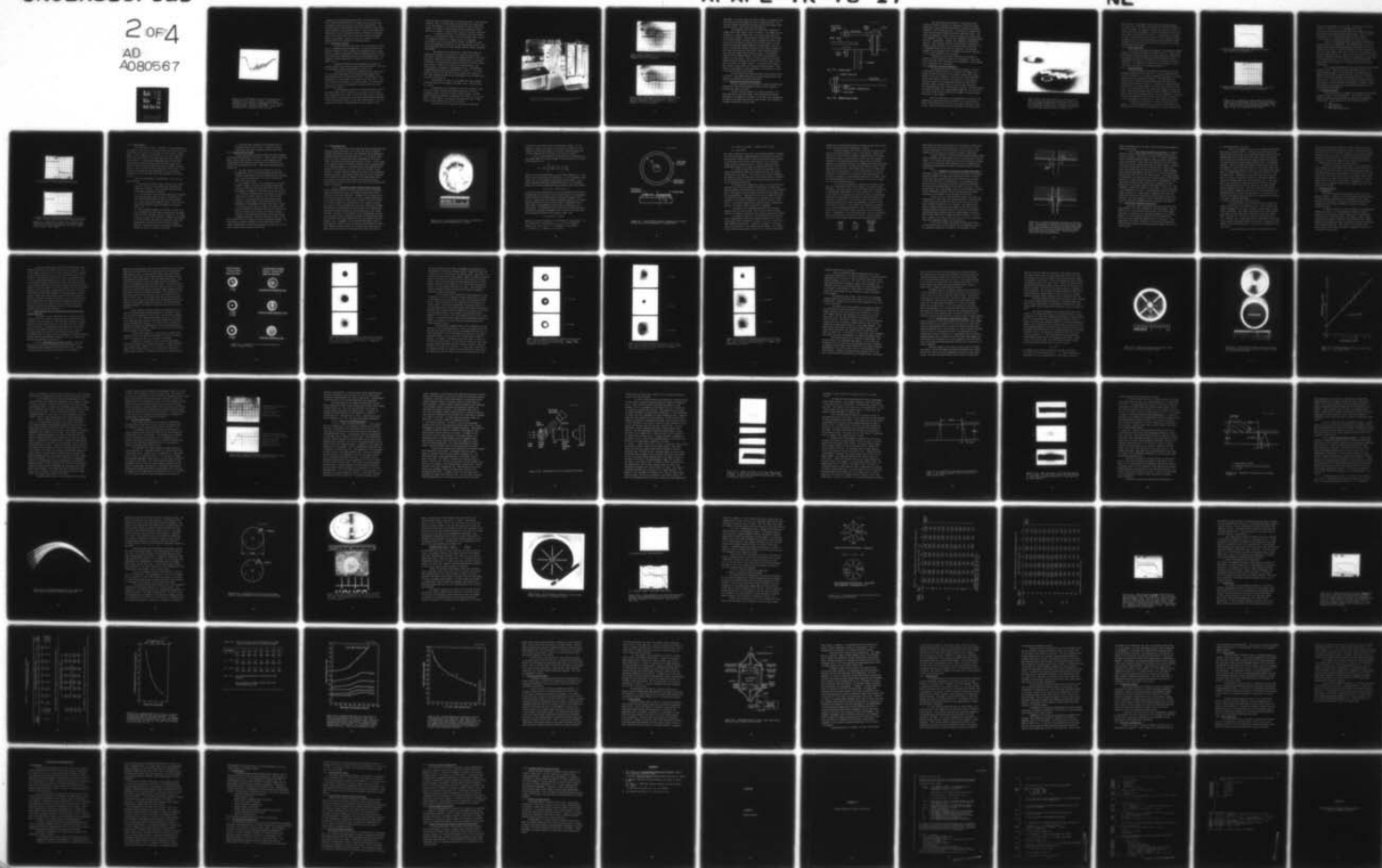
UNCLASSIFIED

AFAPL-TR-78-17

F33615-74-C-2029

NL

2 OF 4
AD
A080567



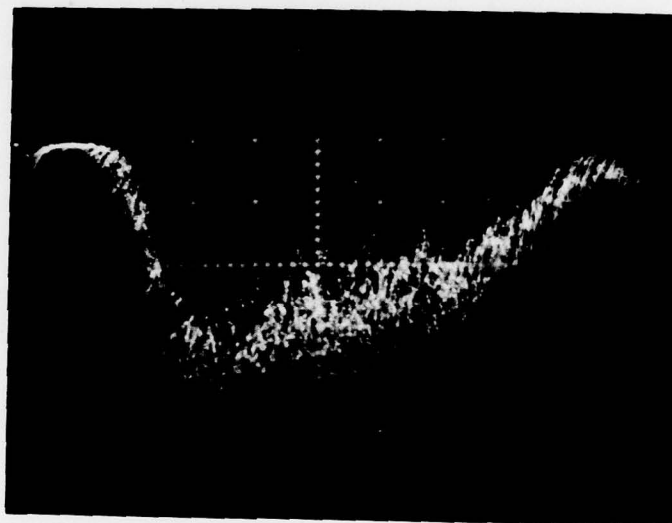


Figure 3.3-17. Photomultiplier signal from infrared port in thyristor cathode. Scales: Vertical - 1 mv/division; horizontal - 5 μ sec/division. Oscilloscope is exposure of 10 device pulses. Note laser feedthrough at $t = 0$. Device current was 5000 A. $dI/dt \approx 10,000$ A/ μ sec. Device was blocking 850 volts immediately prior to firing.

a problem with obtaining adequate electrical contact between the device cathode metallization and the cathode pole piece was solved by applying a heavy gold plating to the device metallization. The plating operation (approximately 0.005 cm or 0.002 mils thick) effectively covered the tiny observation holes. Since the spreading data achieved with the 23 mm diameter devices is believed to be representative of that which would have been obtained using 50 mm diameter devices, the attempt to measure v_g with this technique on 50 mm diameter devices was aborted and not pursued further.

3.3.3 Pulsed Power Supplies

Two basic circuits were used. The first supplies a current pulse of variable duration and amplitude. It was used to pulse the thyristor element in order to observe the spreading of the on region using the infrared recombination radiation plasma spreading technique. This technique is described in detail in the preceeding section. The equipment is shown schematically in Figure 3.3-8 and pictorially in Figure 3.3-11.

Devices with various diffusion geometries were anode to cathode pulsed in this system and light fired with the Nd^{3+} : YAG laser. The experimental results are described in Section 3.5.

The second test system was designed and built specifically for this project and consists of 40 pulse forming networks (PFN) placed radially about a single device holder. Each PFN has its own characteristic load resistor of 1.6 ohms and any number from 1 to 40 can be connected in parallel to the device holder. The device under test acts as a switch to discharge the connected PFN's into their matched load resistors.

The pulse forming networks are resonantly charged from the main power supply which is variable in four equal steps at nominal line voltages from 225 to 875V. At 875V the PFN's charge to approximately 1700 volts and with all forty pulse forming networks connected to the load the pulse current is just under 20,000 amperes. The first inductor in each pulse forming network has been removed from the

circuit in order to minimize the rise time of the pulse. The resulting capacitive input of the PFN leads to the overshoot and ringing seen in the oscillographs of the current waveforms of devices under test; however, the current is significantly faster and provides a severe time rate of change of current (di/dt) stress on the device under test.

A detailed description of the design of the pulse forming network, its charging power supply, and the associated logic circuits is contained in Appendix IV. Figure 3.3-18 is a photograph of the PFN as part of the overall test set-up. One bank of 20 PFN legs is disconnected and swung out to show construction details. Note the octifurcated fiber optic cable hanging from the central opening of the 20 PFN's.

Upon completion of construction, a high speed switch was simulated by placing a spring metal bar across the test position electrodes. Risetime was determined by charging 20 PFN's to 100 volts, physically closing the "switch" with an insulated probe to discharge the network, and observing the voltage drop across the 0.001Ω current monitor shunt. Figure 3.3-19 shows this voltage waveform. The pulse duration is, nominally, the designed 40 μsec . The amplitude is approximately 10% below the design value of 1250 A. It is interesting to note that the LASS device, when tested later, appears to have lower impedance because the current magnitude for the LASS device was low by only about 2%.

The risetime is shown in the expanded time base in Figure 3.3-20 and appears to be slightly less than 1 μsec . (Specification is 1 μsec .)

Measurements were performed with the system charged to 100 volts with a small external power supply because of a lack of a convenient switch to test the circuit at higher voltage. The PFN charging network was checked at transformer tap levels of 25, 50, and 100%. At 100% (2000 V), the resistor load connectors arced. These connectors were modified to correct the problem.

The electrical fault detection circuit was checked and

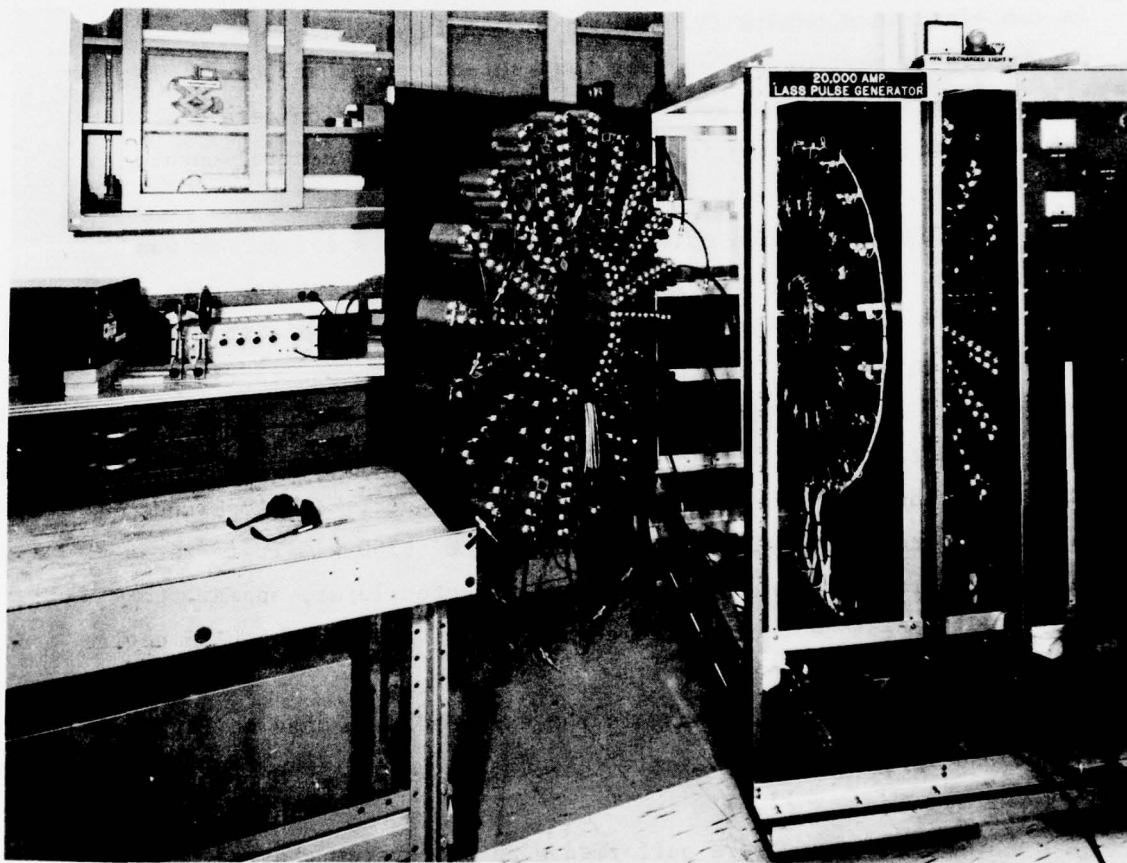


Figure 3.3-18. Photograph of high current test set-up with one bank of 20 PFN legs disconnected and exposed.

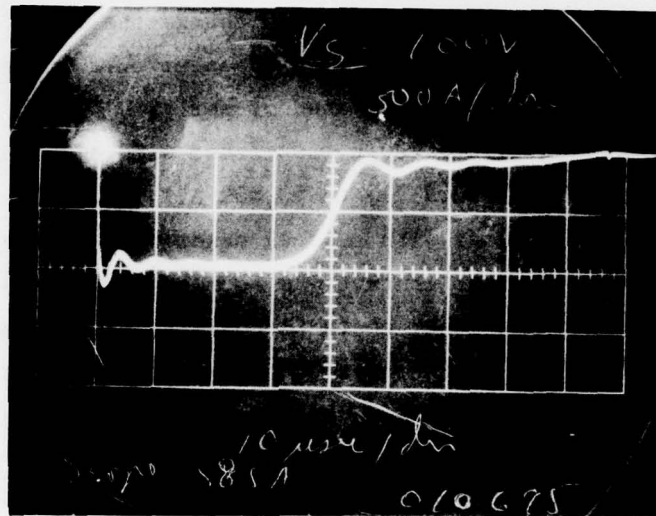


Figure 3.3-19. Pulse shape of test circuit PFN's. Scale: Vertical-500 A/division; horizontal - 10 μ sec/division. Baseline is at top of photograph.

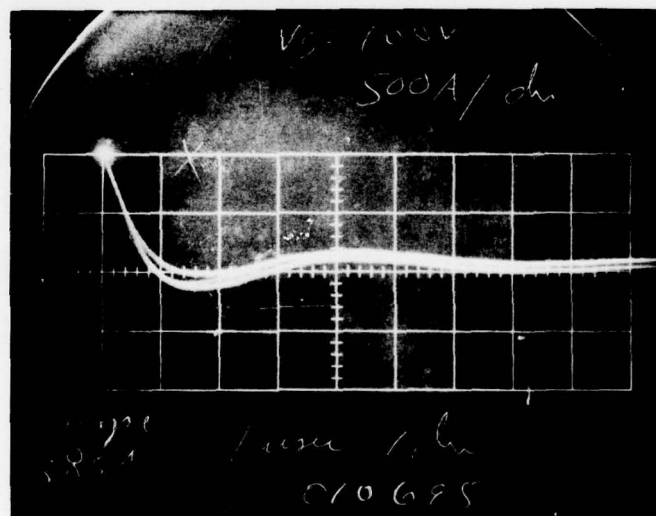


Figure 3.3-20. Pulse shape of test circuit PFN's switched with mechanical short (multiple exposure). Scales: Vertical - 500 A/division; horizontal - 1 μ sec/division. Baseline is at top of photograph.

calibrated. If a device under test fails (shorts), the charge circuit will overload when the command is given to charge the PFN's. This excessive current is detected and a high speed circuit breaker interrupts the supply. This circuit operated properly.

The completed test circuit was tested with a mechanical "hammer switch" (see Figure 3.3-21) to 10,000 A. The "hammer switch" consisted of a strip of brass with a steel point press fitted and riveted into the brass. This contact was screwed into one electrode of the device holder. The other contact consisted of a brass screw screwed into the opposite electrode of the device holder. A mylar insulating sheet was placed between the two electrodes. The brass strip is struck with a hammer, driving the point contact through the mylar into the head of the brass screw. This technique provides a very high-speed, high-current mechanical switch. At significant currents (a few thousand amperes), the contacts are destroyed in a single use of the switch. Cost of the point contact was excessive. Another system was designed (see Figure 3.3-22) which used an allen cone type screw as the point contact. This system did not appear to give as high a peak current as the press fit-riveted contact. This result was attributed to a high resistance of the switch as a result of the steel-to-brass screw threads.

The rise time of the system was about 1 μ sec and was tested to 10,000 A. This demonstrated that the pulse forming networks were capable of performing the required test tasks.

3.3.4 Attenuation of the Laser Light Energy.

Several techniques can be employed to reduce the light level entering the silicon and activating the device for the purpose of observing the effect on turn-on.

The most obvious technique is to reduce the power to the flash lamp pump in the laser cavity. This method has the decided disadvantage of changing the efficiency of the laser and, consequently, the shape of the light pulse used for light firing. This technique is considered undesirable for that reason.

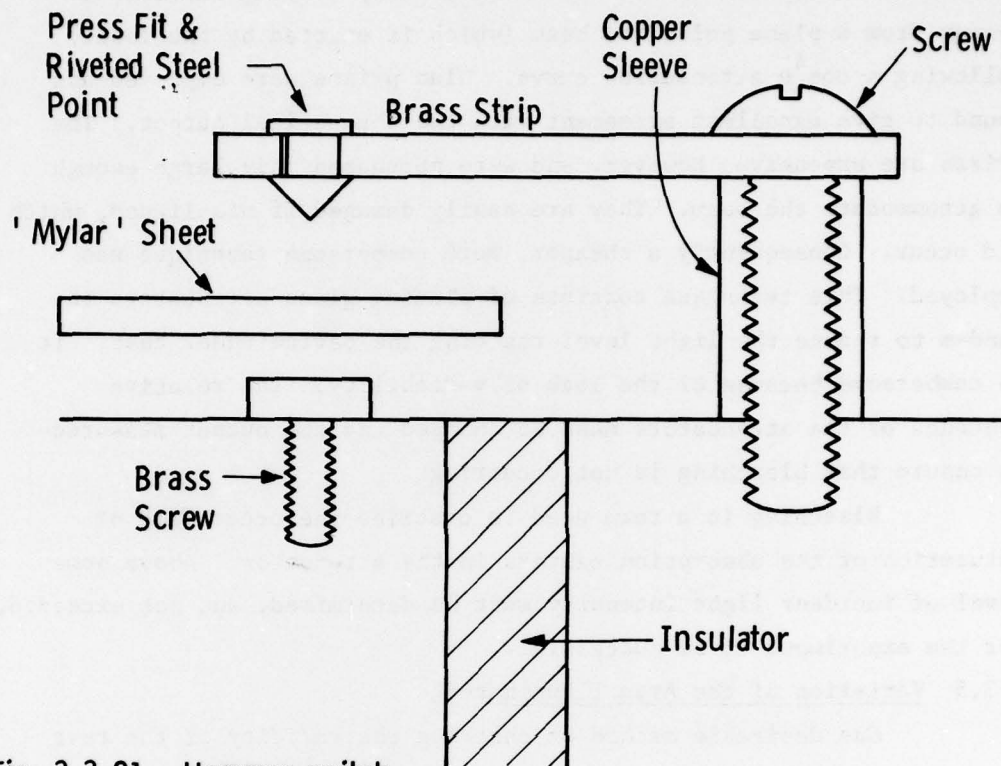


Fig. 3.3-21. Hammer switch

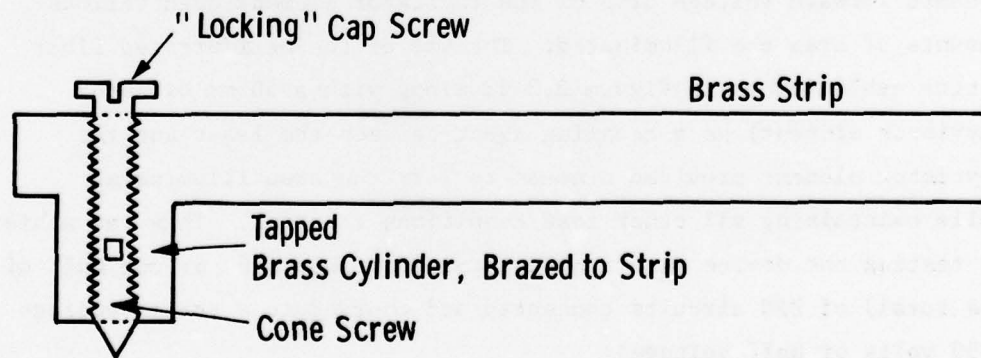


Fig. 3.3-22. Modified hammer switch

Two other methods were employed. Crossed glan prisms provide an excellent technique of continuously varying the output energy from a plane polarized beam (which is emitted by the laser) following a $\cos^4 \theta$ attenuation curve. Glan prisms were employed and found to give excellent agreement with the theoretical output. The prisms are expensive, however, and were purchased only large enough to accommodate the beam. They are easily damaged if misaligned, which did occur. Consequently a cheaper, more cumbersome technique was employed. This technique consists of placing glass attenuators in tandem to reduce the light level reaching the device under test. It is cumbersome because of the lack of variability. The relative sequence of the attenuators must be changed and the output measured to ensure that bleaching is not occurring.

Bleaching is a term used to describe the occurrence of saturation of the absorption centers in the attenuator. Above some level of incident light intensity must be determined, and not exceeded, for the experiment to be successful.

3.3.5 Variation of the Area Illuminated.

One desirable method of checking the validity of the test procedures and theoretical model is to observe the change in the dynamic forward voltage drop of the thyristor element when various amounts of area are illuminated. The use of the octifurcated fiber optics cable (shown in Figure 3.3-23 along with a 50 mm diameter thyristor element) as a coupling agent between the laser and the thyristor element provided a means to vary the area illuminated while maintaining all other test conditions constant. This was achieved by testing one device with a predetermined number (20, or one half of the total) of PFN circuits connected and charged to a preset voltage (850 volts or half voltage).

Thus the current was set at approximately one-fourth of the maximum value which was believed (correctly) to be a value that the device could withstand with only one of the eight input ports illuminated. Testing was started with all eight legs of the fiber optics

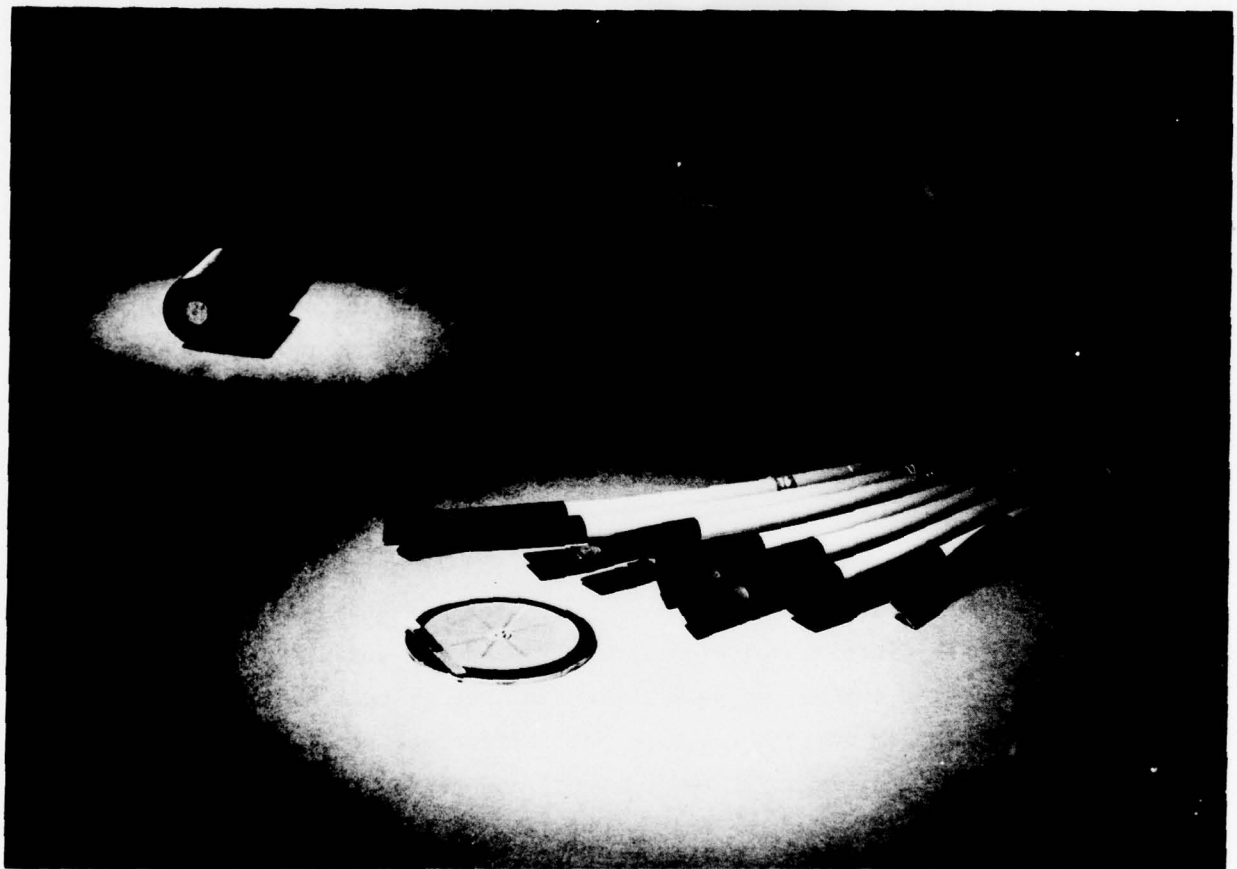


Figure 3.3-23. Fiber optic cable used in the high current tests. One end has circular cross-section; the fibers from this are randomly separated into 8 groups and each of these, at the other end, is formed into a rectangular cross-section. The circular device in the photo is a typical 50 mm diameter thyristor element showing the eight activation ports.

cable in place. Photographs of the current and voltage waveforms were taken; two of the cables were removed from the device holder and the test repeated. The sequence was repeated, removing two cables at a time, until only two remained. A final test was run using one fiber optic cable leg connected to the device. In this manner, the amount of light entering each leg of the fiber optic cable remained constant throughout the test; the current through the device remained constant throughout the test; but the current density increased as the number of connected legs decreased.

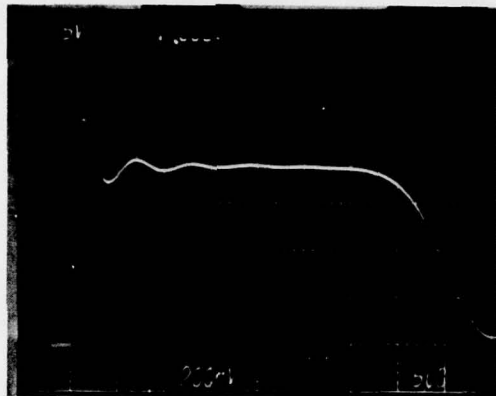
3.3.6 Current Monitoring.

The current was monitored by means of a non-inductive coaxial resistor of 0.001 ohm connected to the device test jig. Current waveform shape and resistance using the coaxial resistor as a monitor have been compared to those obtained using a Pearson Model 411 current transformer as a monitor on a single PFN in the parallel array of up to 40 PFN's. The comparison is shown in the oscillographs in Figure 3.3-24 and can be seen to be essentially identical.

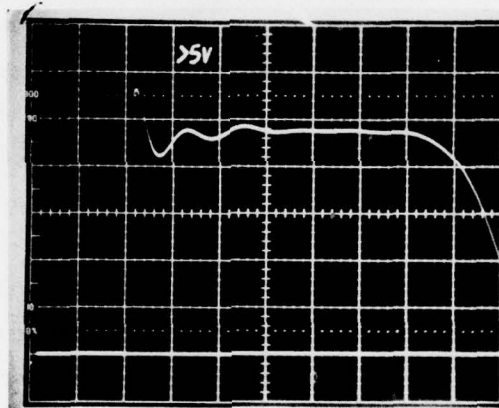
3.3.7 Voltage Monitoring.

Several problems are encountered in monitoring the dynamic voltage drop across the LASS under test. First, the voltage across the device changes by 2 to 3 orders of magnitude requiring a very large dynamic range of the monitoring equipment. The measurements of interest are the initial voltage transition and the forward drop across the device during the pulse. To achieve any reasonable degree of sensitivity, the voltage range on an oscilloscope should be of the order of 10 volts/division at the currents and voltages of the devices tested. The initial blocking voltage of 1000 to 2000 volts across the device drives the oscilloscope amplifier far into saturation, a condition from which the amplifier cannot recover rapidly enough to provide an accurate measurement of the dynamic "on" state forward voltage drop.

A circuit which overcomes this problem to some extent was devised. It allows the majority of the pulse to be monitored at high sensitivity but sacrifices any observation of the initial transition of



(a) 5000 A/cm division. Device 2G4. Indicates $\hat{I} = 24,000\text{A}$;
 $I_{\text{ave}} = 19,000\text{A}$; $dI/dt > 40,000\text{A}/\mu\text{sec}$.



(b) 100A/cm division (times 40 to compare with (a)). Device 2G6.
 Indicates $I = 22,600\text{A}$; $I_{\text{ave}} = 19,200$; $dI/dt > 40,000\text{A}/\mu\text{sec}$.

Figure 3.3-24. Comparison of current signal from 0.001 ohm resistor (a) and from Pearson model 411 current transformer (b). Test conditions were all PFN's connected and charged to 1700 volts. Current should be approximately 20,000 amperes. Time sweep is 5 μsec per cm division for both photos.

device from the blocking to the on state. The circuit is discussed in detail in Appendix II. It is fundamentally a clamp circuit which holds the oscilloscope input to the clamp voltage until the applied voltage drops below the clamp voltage. After an initial recovery time of the circuit (less than 1 μ sec) the voltage across the device is displayed accurately at a high sensitivity.

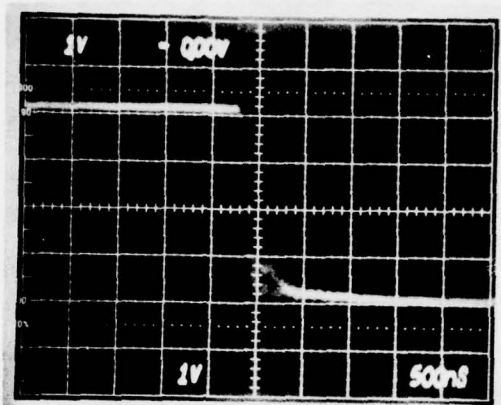
When one is working with large currents, the potential drop across contacts can be substantial. The device holder of the pulse forming network test circuit was modified to accept Kelvin probes to eliminate this problem. Each probe consisted of a fine tungsten wire which was spring loaded to make contact with one of the surfaces of the thyristor element under test. These in turn were connected to Tektronics matched, compensated, 100 times probes which applied the voltage signal to the differential input of the Tektronic type 6A13 differential input amplifier plug-in module of a Tektronic model 7844 dual beam oscilloscope.

For voltages greater than 400 volts, the clamp circuit described earlier was used. Figure 3.3-25 shows oscilloscope traces at two different gain settings of the oscilloscope. The difference in the apparent ringing shows how careful one must be with the instrumentation at the current, voltage, and switching time levels involved in this contract. In either case, the fall time of the voltage (90% to 10% points) is at most a few tens of nanoseconds. Attempts to measure fall time with faster sweep rate exceeded the writing speed of the scope/camera/film combination.

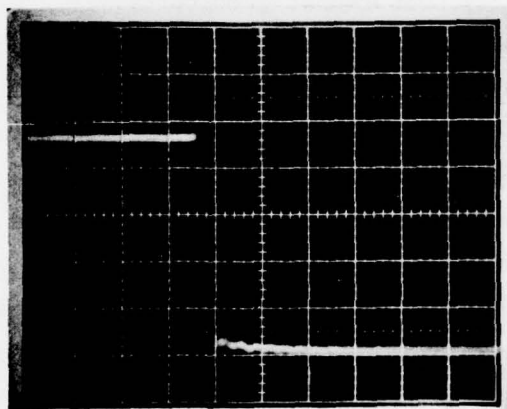
3.4 Problems Encountered.

Several problems with equipment and technique were encountered during the course of this investigation. The following sections describe the major problems and where appropriate the procedures to overcome them. These problems fall into four main categories:

1. Laser
2. Instrumentation
3. Device under test
4. Main power supply (pulser).



a) Oscilloscope at 1 V/cm X 100 differential probes



b) Oscilloscope at .5 V/cm Vernier calibrated to 1 V/cm X 100
Probes - Different range uses different input attenuators

Figure 3.3-25 Comparison of voltage turn-on waveforms with different oscilloscope range settings. Note greater ringing at edge of fast voltage transition (a) than in (b). Device 2 G-6 20 PFN's - 425 V - 2300 A

3.4.1 Laser Problems.

The laser posed a number of problems. Most significant was the tendency to emit one or a few pulses when first turned on that were appreciably less intense or weaker than the steady state or "good" pulses. Such a weaker pulse is referred to as a "soft" light drive. With a soft light drive to the device under test, device failure often resulted. A technique was implemented which involved hand shuttering the beam to the device under test with a laser light sensitive material (such as several thicknesses of Hadron footprint paper) to check if the laser were putting out a "good" pulse. Occasionally, this method was also catastrophic if one accidentally intercepted a part of the beam effectively allowing a "soft" drive to occur.

Other less catastrophic idiosyncrosies of the laser are described below.

- a. When using an external trigger, spurious laser output pulses are observed in switching between repetitive and single shot operation. These unwanted pulses interfere with orderly measurement procedures.
- b. At low repetition rate, the laser output drops radically after the main-power supply has been on 5 minutes or so. This effect occurs whether the laser is being operated (i.e. output pulses being emitted) or not. In our case the reduced energy pulses could cause damage to the system under test.
- c. With an external trigger, if the laser is turned on by first activating the high voltage, then throwing the toggle switch to "run", the laser will run. However, if the switch is thrown to single shot for about 20 seconds, then returned to the run position, the laser will rarely run unless the high voltage is switched off and the initial sequence repeated. This problem cannot be overcome by pushing the single shot button as stated in the manual.

- d. The power meter, intended to read average power in repetitive pulsing, did not work. Therefore all power measurements were made by using an external power meter.

3.4.2 Instrumentation Problems.

Several difficulties encountered during the test procedures have already been discussed in Section 3.3. These include the methods used to monitor LASS voltage and current, optical masking of the photomultiplier tube from stray laser light, and the necessity of cooling of the photomultiplier tube. Additional problems requiring mention are:

- a. The power supply and cathode follower unit for the photomultiplier tube infrared measurements required line isolation transformers to prevent feedthrough when the pulser test circuit was discharged by the laser activating the LASS in the test circuit.
- b. The electrode contact to the metallization of the LASS seemed to "wedge" on occasion and permitted feedthrough of the laser directly into the sensing fiber optics cable. The problem of "wedging" is discussed also in Section 3.4.3.
- c. In testing at maximum current and voltage, the oscilloscope had to be moved at least 10 feet from the 40 PFN pulser unit to prevent feedthrough when taking voltage readings. Certain ranges of the oscilloscope were more susceptible to feedthrough than others (See Figure 3.3-25).
- d. A special circuit had to be added to the logic control system to disable the shut-down safety circuit right at the time of the laser pulse firing of the device to prevent shutdown of the system when repetitive pulses were desired.

In general, whenever a system utilizes high current pulses with extremely fast rise, there are usually feedthrough problems. The system must be carefully grounded to avoid ground loops, and the readout equipment must be carefully positioned, shielded, and, in some cases, powered through isolation transformers.

3.4.3 Device Under Test.

Activating a switch such as the LASS under the high dI/dt and high peak current conditions of the pulser test circuit requires a uniformly distributed, large area, low resistance contact between the clamping electrode and the device under test. If the contact resistance is not low, excessive power may be dissipated in the device contact thus heating the device and causing it to fail. If the contact is not uniform, current will become localized causing increased stress in the localized regions. In the work reported many devices failed shorted in the pulser test circuit at lower than expected current densities. Failure analysis of these devices yield several mechanisms causing the failure: non-uniform contact and high lateral resistance at the surface of the device, shadowing of the unmetallized region by a portion of the fiber optics cable, and uncontrolled contact between the metal jacket of the fiber optics cable and the unmetallized region of the device.

3.4.3.1 Non-uniform contact and high lateral resistance.

A major problem encountered in device testing was that of obtaining a large area electrical contact to uniformly distribute the current under high current test conditions. Examination of the impression of the hard brass pressure electrode in the soft aluminum metallization of the device showed that contact was not made to the entire surface of the device because of non-parallelism of the component surfaces. As a result of this non-parallelism, electrical contact was sometimes remote from the illuminated port forcing current for a comparatively long lateral distance through the thin metallization of the cathode electrode. Because of the resistance of this metallization, and the large currents involved, appreciable voltage was developed and arcing occurred between the device metallization and the pressure electrode (Figure 3.4-1). Presumably, if the cathode metallization (which is metallurgically sintered to the silicon) were made sufficiently thick, even a remote electrical contact of relatively small area would not unduly stress the silicon by resistance heating since the lateral

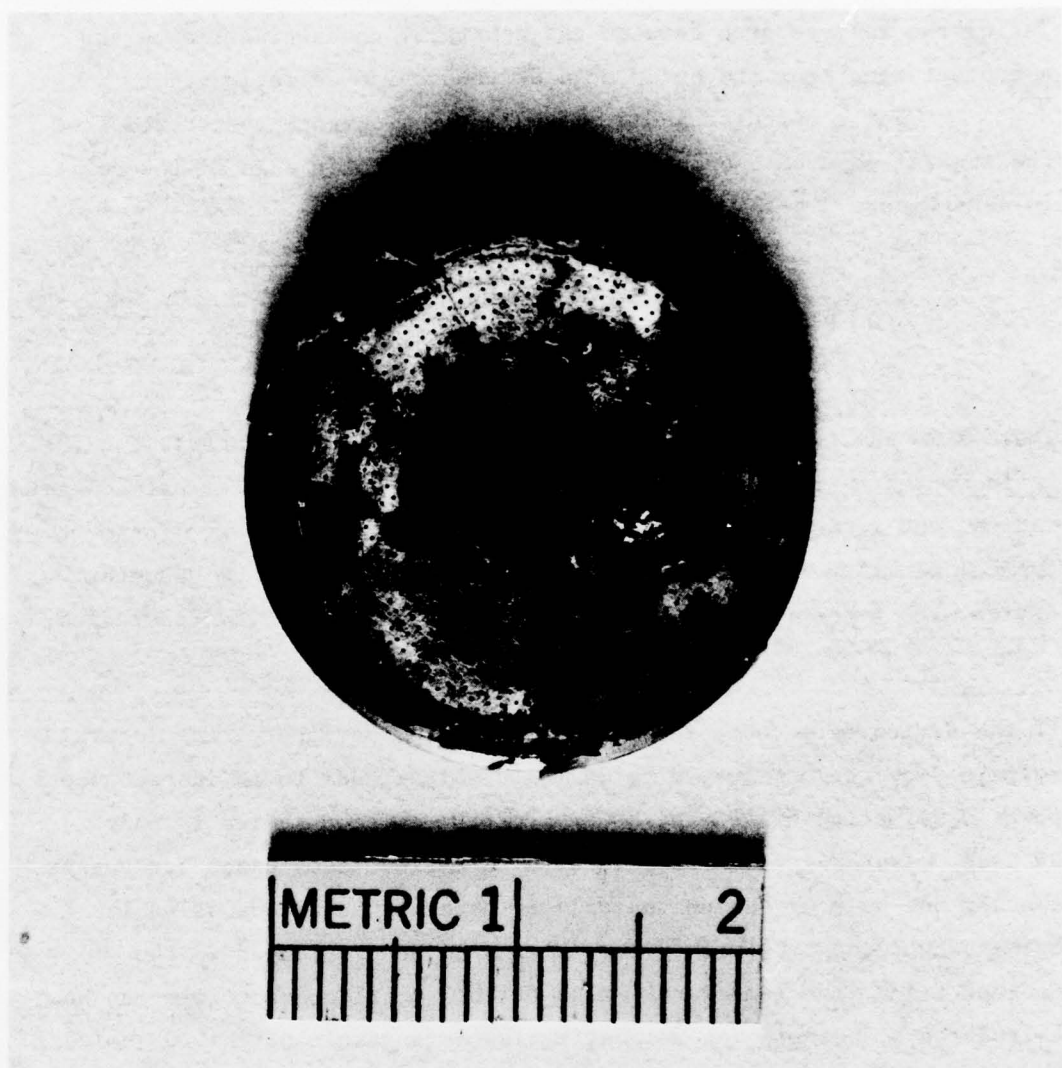


Figure 3.4-1. Failed device showing arcing in metallization well away from the illuminated port or window.

resistance of the contact would be considerably reduced. One can attempt to calculate the order of metal thickness required by calculating the voltage drop between the centrally conducting region and a contact ring near the outer edge of the device as follows:

For a circular geometry the lateral contact resistance from the central edge of the optical window to the outer edge of the device is (See Figure 3.4-2)

$$R = \int_{r_1}^{r_2} dR = \int_{r_1}^{r_2} \frac{\rho_s dr}{r 2\pi} = \frac{\rho_s}{2\pi} \left[\ln \frac{r_2}{r_1} \right]$$

where R is the total resistance, ρ_s is the sheet resistance (i.e., the ratio of the resistivity to the thickness), r_2 is the outermost contact radius, and r_1 is the radius of the central optical window. For a typical aluminum metallization 60,000 Å thick on a 2.54 cm diameter device with a central window opening approximately of 0.178 cm radius,

$$R \approx 1.2 \text{ m}\Omega \quad \text{where } r_2/r_1 = 6.$$

If the device were contacted only at the outer periphery, the lateral voltage drop at 20 KA would be 24 volts which leads to an instantaneous power dissipation of 480 kW; however, total pulse duration is only 40 μsec. Assuming that the lateral dissipation takes place for approximately one-half of the pulse (only an order of magnitude value is being sought), approximately 10 joules will be dissipated in the contact film. The temperature rise of this metal contact film can be calculated by assuming an adiabatic rise as a result of the 10 joules being dissipated uniformly in the contact volume. Then

$$\Delta T = Q/(\rho\pi(r_2^2 - r_1^2)tc)$$

where Q is the heat dissipated, ρ is the density of the material, c is the specific heat of the material, r_1 , r_2 , and t are defined in Figure 3.4-2. For $Q = 10 \text{ J}$, $\rho = 2.7 \text{ gm/cm}^3$, $c = 0.93 \text{ J/gm}^\circ\text{C}$, $r_1 = 0.178 \text{ cm}$, $r_2 = 1.068 \text{ cm}$, $t = 6 \times 10^{-4} \text{ cm}$

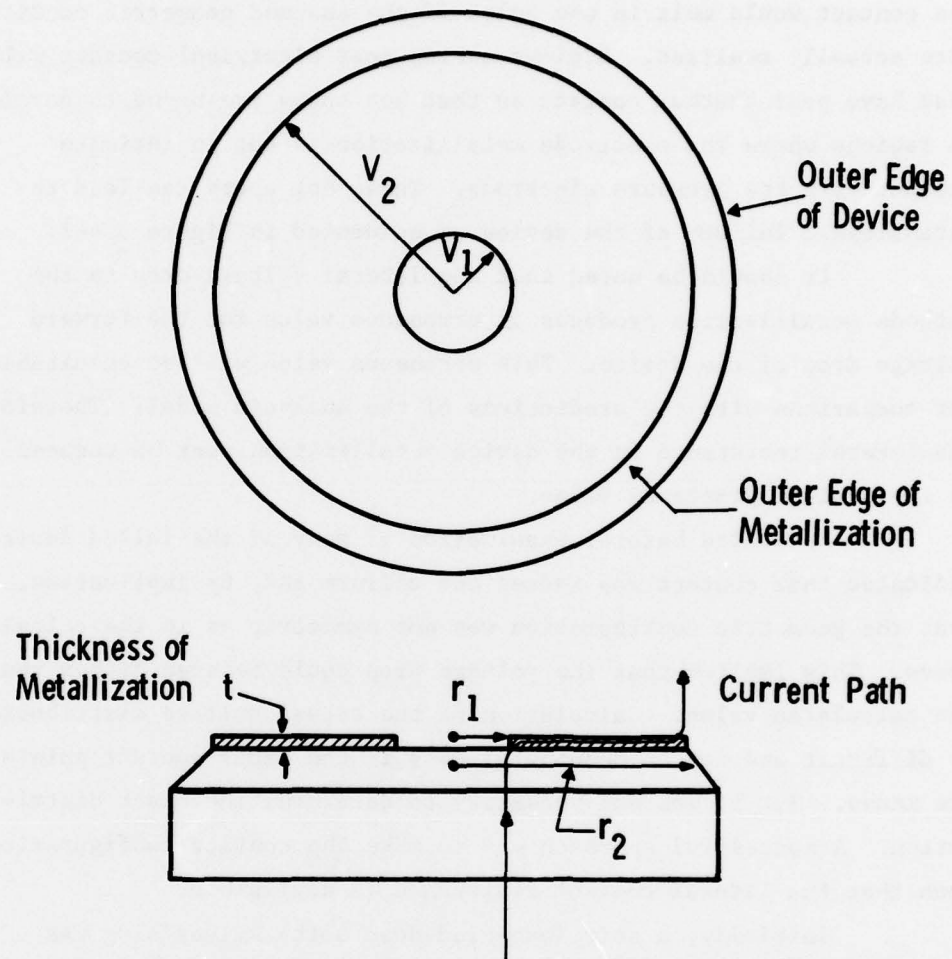


Figure 3.4-2. Sketch defining contact configuration for lateral voltage drop in the metallization of the LASS device.

$$\Delta T = 10 / (2.7 \times \pi (1.068^2 - 0.178^2) 6 \times 10^{-4} \times 0.93)$$

$$\Delta T = 2.0 \times 10^3 \text{ } ^\circ\text{C}.$$

The contact would melt in one pulse if the assumed geometric condition were actually realized. Regions making poor electrical contact will also have poor thermal contact so that hot spots are bound to develop in regions where the electrode metallization is not in intimate contact with the pressure electrode. These hot spots can lead to catastrophic failure of the device as evidenced in Figure 3.4-1.

It should be noted that the lateral voltage drop in the cathode metallization produces an erroneous value for the forward voltage drop of the device. This erroneous value will be unsuitable for comparison with the predictions of the analytic model. Therefore, the lateral resistance in the device metallization must be reduced to the minimum practical value.

As stated before, examination of many of the failed devices indicated that contact was indeed not uniform and, by implication, that the geometric configuration was not symmetric as in the calculation above. This implies that the voltage drop could be even higher than the calculated value. Calculation of the actual voltage distribution is difficult and can be meaningful only if the exact contact points are known. But it was not necessary to determine the exact distribution. A successful approach was to make the contact configuration such that the lateral contact resistance is negligible.

Initially, a soft (annealed dead soft) silver slug was inserted into the contact system. This slug did not deform satisfactorily in clamping, and devices still failed at high current levels.

By plating a metal on top of the metal contact to a thickness of approximately 10 times the original thickness, all lateral voltage drops would be reduced by a factor of 10 (to 2.4 volts in the above symmetric calculation). A value of 2.4 volts is of the same order as the accuracy of the forward drop measurement. The required plating thickness using gold was about 50 μm . Gold was successfully

plated onto the aluminum metallization and devices were tested to full voltage and current without degradation or failure.

Several techniques were tried to build up the contact thickness on the sintered aluminum contact on the cathode. Rather than describe all of the various techniques attempted (such as electroless nickel plus silver, or silver directly, etc.), the most successful technique of electroplating gold onto aluminum will be described. Although it has long been known that an aluminum-gold system eventually leads to the now historic and famous "purple plague problem" of early semiconductor device work, purple plague does not pose a problem for these short term experiments. If it is found necessary in eventual production of these devices to incorporate thick metallizations on the device electrodes, an aluminum-gold system must be avoided. There are other metallizations such as titanium-silver that are in common use in the semiconductor industry.

The gold plating employed a commercially available citrate gold bath (trade name Sel-Rex) which contains 1 troy ounce of gold per gallon. The bath is held at about 55°C which gives a plating rate of approximately 1000 Å/minute at a current density of 1.7 ma/cm². It was found that increasing the plating rate slowly in steps between 150 Å/minute to 1500 Å/minute resulted in a uniform gold plate with relatively good adherence. The aluminum surface of the device was cleaned by swabbing with acetone and immediately etching the aluminum surface for about 5 to 10 seconds in an aluminum etch solution (e.g., 25 parts concentrated phosphoric acid, 1 part concentrated nitric acid, 5 parts glacial acetic acid, and 4.5 parts de-ionized water). Subsequently, a quick de-ionized water rinse was used and the devices were immersed in the Sel-Rex solution. A typical plating run for two 50 mm diameter devices plated simultaneously would be

| <u>Current</u> | <u>Time</u> | <u>Approximate Thickness</u> |
|----------------|-------------|----------------------------------|
| 10 ma | 25 min | 3,750 |
| 20 ma | 55 min | 16,500 |
| 50 ma | 25 min | 18,750 |
| 100 ma | 210 min | 315,000 |
| | | 354,050 Å |

These times and currents were found to be not critical as long as the initial rate was slow and increased over a period of time. It was found (by measurement) that the thickness of the plating was quite predictable if the times and currents were added as shown above.

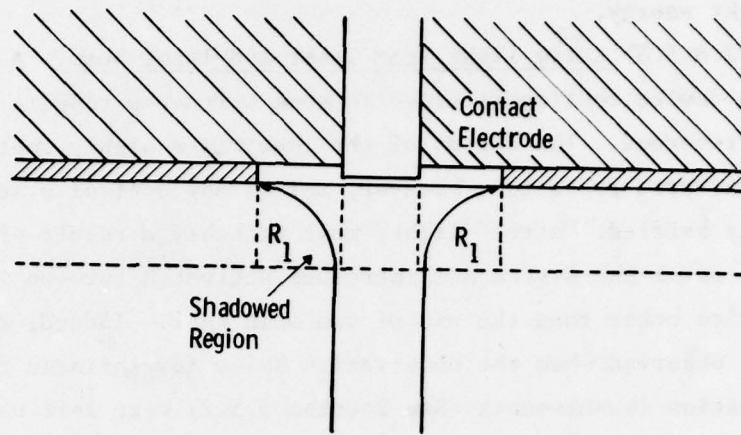
Another technique to overcome the non-uniform contact and high lateral resistance was applied when a device was mounted into the test holder. It was found that tightening the pressure electrode, allowing a settling or creep period (about 30 minutes), and retightening the mounting screws periodically provided an improved electrical contact to the device.

3.4.3.2 Shadowing of a portion of the light input window.

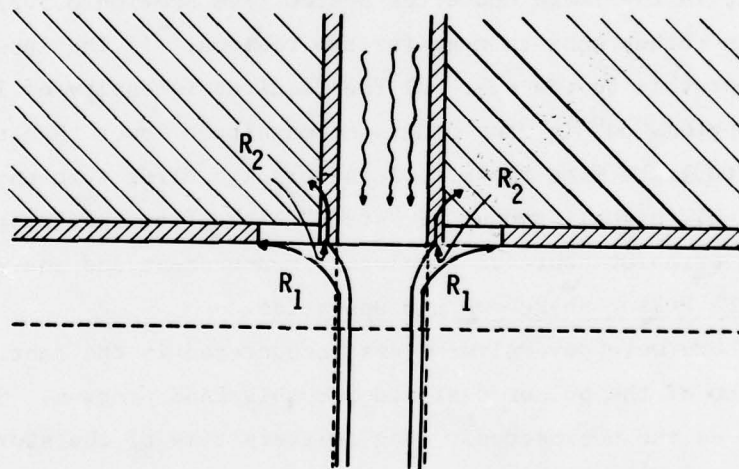
Referring to Figure 3.4-3a, it can be clearly seen that if the contact electrode "shadows" the light input window, there will be a region between the light activated region and the metallization (contact) to the silicon which will be unmodulated. As a consequence, this region will have a high lateral resistance causing an undesirable and unnecessary power dissipation in the device in turn-on. If the lateral drop in R_1 is high enough, arcing can occur between the silicon and the "shadowing" electrode (which is an equipotential surface) depending on the proximity of the electrode to the silicon.

Figure 3.4-3b is a cross-sectional sketch of the same configuration as a) except that the circular light pipe is jacketed with a metal sheath and is allowed to touch the silicon as well as the metal electrode through which it is inserted. Any potential drop across R_1 appears between the metal sheath and the silicon either causing arcing and subsequent melting of the silicon or providing a comparatively high resistance path for current between the silicon and the metal sheath on out through the metal electrode. It can be seen in Figures 3.5-17a and 3.5-17b that the silicon does indeed meet under these conditions leading to device failure.

If the optical light input window is always made smaller in all dimensions than the cross-section of the illuminating source, the unmodulated region will be avoided. The difference in size



a.



b

Figure 3.4-3. Sketches illustrating the effects of poor geometric and electrical configurations associated with the light input. (a) Shadowing of a portion of the input window caused by too small an entrance port through the pressure electrode (misalignment of electrode port/window would cause similar effect, but would not be symmetric). (b) Metal jacket of fiber optics cable touching silicon.

should be minimized since any light striking the metallized region is wasted light energy.

3.4.3.3 Stray light from laser and laser beam. A problem related to device testing resulted in some erroneous results being initially recorded. The output of the laser is a highly concentrated pulse of infrared radiation; however, unless any optical system is effectively baffled, "stray" light, most probably a result of reflections, can enter the system and introduce activated turn-on in regions of the device other than the aim of the main beam. Indeed, this result was observed when the observation holes for infrared recombination radiation measurements (See Section 3.5.2) were left uncovered when the laser was fired into the optical window. Stray light entered the observation ports and turned on the device locally in those regions giving rise to some erroneous spreading velocity measurements. The same effect was observed when devices were illuminated at an off normal angle in the image converter system (See Section 3.5.2). The oversight is rather easy to make for two reasons. 1) The laser light is not discernible to the eye. 2) The required intensity of light to trigger a region "on" is many orders of magnitude lower than that being used to light fire these devices for high dI/dt turn-on; consequently, only a small amount of "stray" light from the laser beam can lead to erroneous spreading velocity measurement and analysis.

3.4.4 40 PFN Pulser Shakedown and Operation.

There were several problems encountered in the fabrication and operation of the pulser designed for this LASS program. Some of these, such as the unexpectedly long delivery time of the storage capacitors, increased the cost and delayed completion of the pulser. However, only the operational problems will be discussed below. There were three operational problems worthy of discussion: noise sensitivity of the logic, operation of the safety shut-down when a thyristor device failed, and improper operation (false trips) of the safety circuit.

a. Noise sensitivity of the logic

Early in the shakedown of the pulser it demonstrated extreme sensitivity to spurious noise. In reality, the noise was generated when the PFN's of the pulser were discharged through the LASS. Various methods were used to isolate the control logic from the main pulser stack of PFN's such as maximizing the physical separation; modifying the interconnections by using twisted shielded pairs, or introducing inductive loops or isolation transformers; and using line isolation transformers to isolate the power supplies of the control logic. Each time that the problem seemed to be cured at a given voltage and current level, it appeared again as the test voltage and current were raised to higher levels. Unfortunately, this work required the use of the LASS, so it was not practical to quickly go to the design maximum current and voltage levels and solve the problem once. It was necessary to work up slowly as other problems such as device contacting were solved permitting the system to operate at the higher levels without catastrophic failure. The final solution to the problem was to completely disable the safety circuit just before, during, and immediately after the pulser discharge period. If the pulser is to be used in some manner where this feature is undesirable, the control logic must be modified accordingly.

b. Safety circuit operation after LASS failure

The present safety circuit senses the current through the thyristor shortly after the system has fired. Since the PFN's have already discharged by this time, no current is sensed until the next cycle is attempted. This control logic means that the main charging power supply is connected across the LASS device when the command SCR's are turned on. If the device failed on the previous pulse (i.e., shorted), then a large power pulse is dissipated in the shorted device causing considerable melting of the device. Consequently, any details of the true failure mode of the device are obliterated by this next pulse.

A circuit technique which could be incorporated into the

system to avoid this problem would be to add a thyristor circuit of high impedance which would momentarily impress a high voltage across the device just prior to the main charging cycle of the pulse forming networks and test for leakage. If sufficient leakage were detected indicating a shorted device, the system would shut down and avoid connecting the main power supply across an already "failed" device.

c. Improper timing of the safety circuit operation

During the shakedown of the pulser, it was found that the safety sensing circuit was sensing the thyristor device current too soon after the device was fired. This mistiming occurred because of the unanticipated delay, by the designer of the control logic, of the laser output pulse (~ 200 to $250 \mu\text{sec}$) after the master control logic trigger input to the laser was activated. This delay can be and was adjusted within the logic circuits (refer to Appendix IV). If the safety circuit is modified as suggested in paragraph (b) above, this timing must be checked.

3.5 Experimental Results.

3.5.1 Introduction.

This section describes the pertinent results of the test program in detail. In general, the major problems encountered during the test program are discussed in the preceeding section. Major differences in approaches or results are discussed in detail below ignoring the small, nuisance problems that plague any extensive experimental work.

It should be pointed out that the purpose of the experimental testing was twofold: (1) the development of empirical values of parameters for the analytic computer program; and (2) confirmation of the validity of the predictions of the computer program. These objectives were achieved. Empirical values required by the computer program were determined and used in the program to predict performance under different conditions. These results are contained in the papers by Davis and by Davis and Roberts in Appendix V and will not be repeated in this section.

All tests, unless specifically identified otherwise, were conducted using the active element or fusion of the thyristor. This active element, or device as it is often referred to herein, consists of the diffused silicon slice (23 or 50 mm in diameter and 1/4 to 1/2 mm thick) metallurgically bonded on one side to a molybdenum plate (1 to 1.5 mm thick and diameter equal to that of the silicon slice) for structural strength, and metallized on the other side with about 6.0 μ m thick of evaporated and sintered aluminum into which the various windows or ports are etched. This small element, about 5% of the total volume of the conventional packaged thyristor, does all of the work. The remainder of the volume consumed by the package makes electrical contact, removes heat, and otherwise protects the active element or device by providing a hermetic seal between it and the outside world. These functions are not required during a parametric study; and, in fact, interfere with the orderly process of generating good data. Therefore, research and development testing is performed whenever possible using only the active element.

3.5.2 Plasma Spreading Velocity Measurements Using Infrared Recombination Radiation

The purpose of these experiments was to determine how the conducting area of a thyristor changes with time during the turn-on transient. From these data, one can infer both the change in current density with time and the velocity of the plasma front as a function of current density. By coupling this information with other observables such as forward voltage drop versus time, etc., a check can be accomplished on the accuracy of the analytic computer model. The computer model can then be used with confidence to predict thyristor behavior under various operating conditions. The test circuits and techniques are described in Section 3.3.

3.5.2.1 Observations at low dI/dt and low J . The laser was set up in the infrared plasma spreading laboratory with the crossed glan prisms attenuator and beam directing prism. In order to obtain data for correlation to the model, it is desirable to

observe the turn-on spread as soon after the laser fires as is possible. Opening of the shutter before the laser pulse is over saturated the image converter tube. It was found that there was too much jitter between the laser firing and the image converter tube shutter firing when running the system slaved to the anode pulse power supply. This problem was corrected by slaving the image converter tube shutter pulse to a photodiode pick-up of the laser pulse. The earliest observation that could be made after the laser fired (t_o) was $t_o = 0.75 \mu\text{sec}$ which was the delay time from the photodiode output through the pulse generator to the shutter voltage power supply. The photodiode in the laser power monitor circuit was not used for this purpose as it was found to be too noisy. The thyristor under test was fired with the laser; a 100 μsec square wave current pulse of approximately 600 A was supplied by the standard pulse power supply for the infrared plasma spreading equipment. The dI/dt of this current source is less than 100A/ μsec .

Seven different cathode structures were examined with the laser and infrared plasma spreading apparatus to determine if there were any obvious advantages to any of them. The structures examined were the H, J, K, and R designs described in Section 3.2, the conventional amplifying gate structure, the inside-outside gate structure, and the snowflake gate structure. The latter three are commercially available structures, and demonstrated the normal spreading pattern observed in electrical gating. Figure 3.5-1 is a photo of the cathode side electrodes of these devices.

In the early testing, the J and R types of cathode design exhibited a much faster spread of the turned on area as a function of time (5 to 10 times as fast as an H design, for example).

Figures 3.5-2 through 3.5-5 are a series of photographs showing the spread of the "on" region with time. (Lighted observation holes indicate that a region is "on.") Figure 3.5-2 shows the "on" region of an H design device at 2, 10, and 40 μsec . (The shutter time is about 0.75 μsec .) The device was found to completely turn on

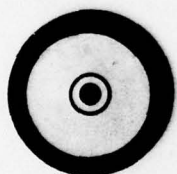
Special Designs
Showing Central
Optical Window



H-Type

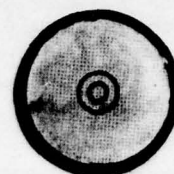


J-Type
R-Type



K-Type

Commerically Available
Designs - Central Gate
Metal Not Removed



Conventional Amplifying Gate

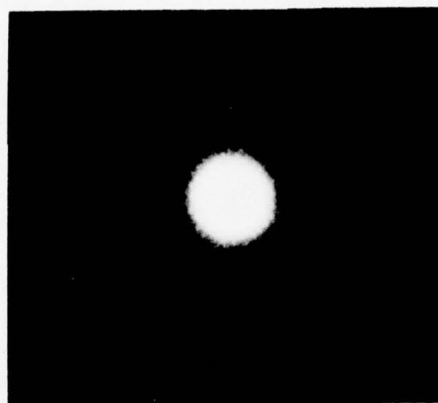


Inside-Outside Amplifying Gate

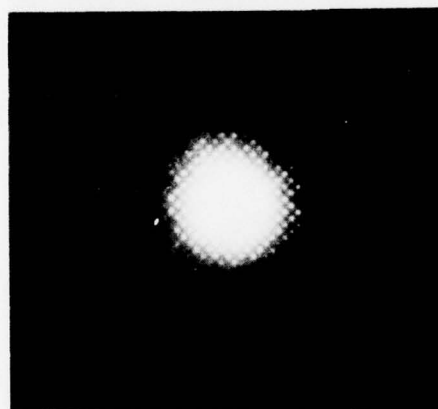


Snowflake Amplifying Gate

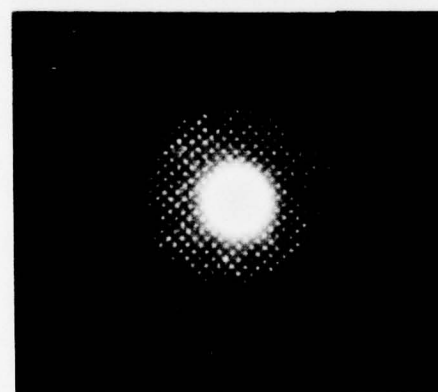
Figure 3.5-1. Cathode view of the structures examined for plasma spreading velocity.



$t = 2 \mu\text{sec}$



$t = 10 \mu\text{sec}$



$t = 40 \mu\text{sec}$

Figure 3.5-2. Infrared recombination radiation emission after Nd^{3+} : YAG laser turn-on of H-type emitter with $I_{\text{Anode}} = 600 \text{ A}$; pulse width $\approx 100 \mu\text{sec}$; shutter pulse width $\approx 2 \mu\text{sec}$; laser repetition rate = 50 pps.

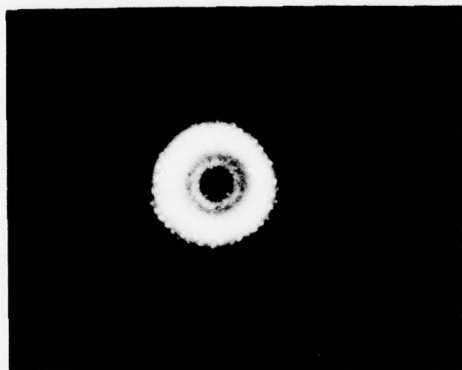
50 μ sec after the laser is fired. The spread is relatively slow in this design but the spread is highly uniform. Figure 3.5-3 shows the on region at 5, 10, and 40 μ sec of a K design device. This device is not on until about 100 μ sec have elapsed. Again, the spread is uniform. Figure 3.5-4 shows the on region at 5, 8, and 10 μ sec of a J design device. Here it was found that the entire device was on in 10 μ sec. Figure 3.5-5 shows the on region at 2, 4, and 5 μ sec of an R design device. Here the entire device is on in 5 μ sec. This difference in turn-on spreading indicates that the emitter design is extremely important in light fired turn-on.

It was observed that a reduction in laser energy by an order of magnitude (to 1.6 mJ) resulted in a large reduction in the spread of the turned on area as a function of time in the direction perpendicular to the plane formed by the laser beam and the normal to the silicon surface. Further work showed that if the laser beam were carefully apertured so that neither light scattered from the attenuator prism nor light straight from the flashlamp were incident on the infrared observation windows of the thyristor, the spreading velocity appeared to be the same for the J and R design as it was for the other designs. It appears that laser light entering through the observation windows was causing the device to exhibit an unrealistically fast plasma spreading velocity.

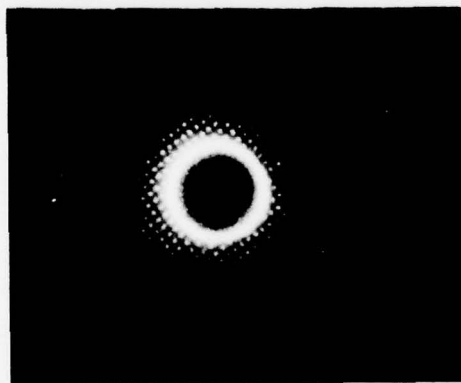
This observation suggested that a "bias illumination" could contribute to the spreading velocity. That is, if regions remote from the laser pulse optical entry port were illuminated with some level of light insufficient to turn on the device but sufficient to generate a significant number of excess carriers, spreading velocity might be enhanced. An attempt to accomplish this end was made on a device in the PFN test circuit system. It was found here again that laser light entering through observation apertures caused a decrease in the time required for a region to be turned on. If light from a flashlight or an incandescent lamp were shone onto the region while the laser light was apertured so that it could not reach the observation ports, the



$t = 5 \mu\text{sec}$



$t = 10 \mu\text{sec}$

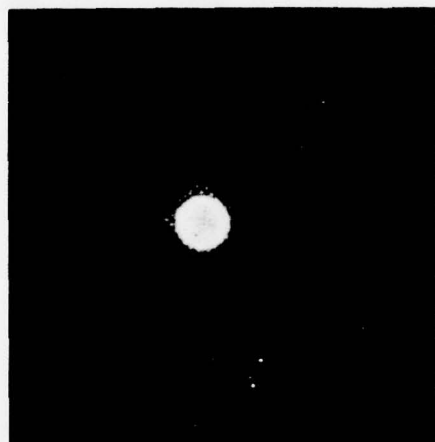


$t = 40 \mu\text{sec}$

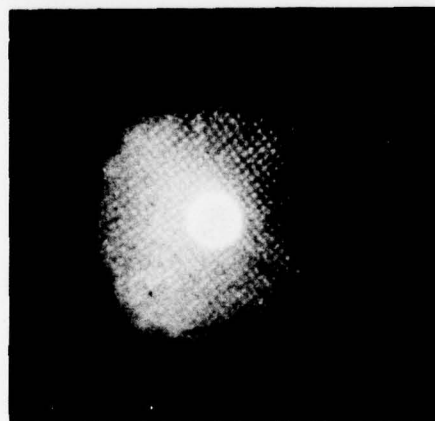
Figure 3.5-3. Infrared recombination radiation emission after Nd^{3+} : YAG laser turn-on of K-type emitter. $I_{\text{Anode}} = 600 \text{ A}$; pulse width $\approx 100 \mu\text{sec}$; shutter pulse width $\approx 2 \mu\text{sec}$; laser repetition rate = 50 pps.



$t = 5 \mu\text{sec}$



$t = 8 \mu\text{sec}$

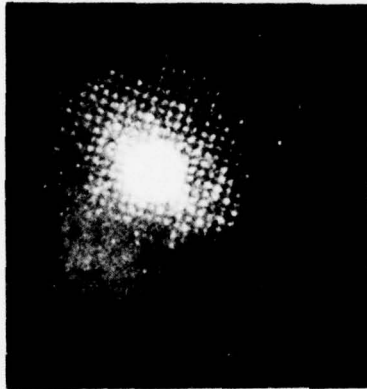


$t = 10 \mu\text{sec}$

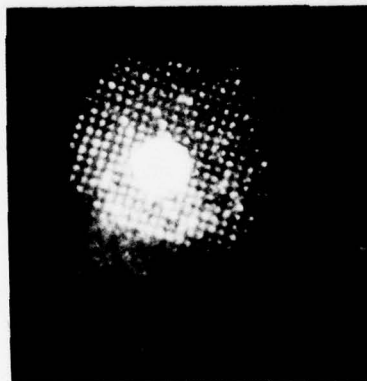
Figure 3.5-4. Infrared recombination radiation emission after Nd^{3+} : YAG laser turn-on of J-type emitter with $I_{\text{anode}} = 600 \text{ A}$; pulse width $\approx 100 \mu\text{sec}$; shutter pulse width $\approx 0.75 \mu\text{sec}$; laser repetition rate = 50 pps.



$t = 2 \mu\text{sec}$



$t = 4 \mu\text{sec}$



$t = 5 \mu\text{sec}$

Figure 3.5-5. Infrared recombination radiation emission after Nd^{3+} : YAG laser turn-on of R-type emitter with $I_{\text{Anode}} = 600 \text{ A}$; pulse width $\approx 100 \mu\text{sec}$; shutter pulse width $\approx 1.5 \mu\text{sec}$; laser repetition rate $= 40 \text{ pps}$.

spreading velocity was not enhanced.

That an incandescent lamp has negligible effect is not surprising. Sensitizing of the silicon should occur by creating carriers some depth into the structure, and this required light with a wavelength from about $1.0\text{ }\mu\text{m}$ to $1.1\text{ }\mu\text{m}$. Only a very tiny portion of the light emitted from an incandescent lamp has this wavelength, and therefore there was not a sufficient number of carriers generated to be noticable. Unfortunately a second source of intense light of about $1.06\text{ }\mu\text{m}$ wavelength was not available to further investigate this phenomenon.

Two questions came to mind. First, why is the spreading enhanced rather than the device being turned on at all of the observation ports? Second, why is the effect seen primarily in the J and R type of structure?

The answer to the first question can be argued as follows. The laser beam, in general, was about 0.5 cm in diameter and has a higher intensity at the center than at the periphery and, in fact, in the image converter tube experiments the laser was run in the TEM_{00} mode so that the light distribution is Gaussian about the axis of the beam. The central, intense, region of the beam activated a region about 0.5 cm diameter on Hadron footprint paper, and presumably was of appreciable intensity at even larger diameters. Thus regions away from the axis of the beam, although triggered, would still turn-on more slowly than regions near the center where the device is light fired. (See Section 2 on light fired versus triggered.) This effect would give the appearance of a faster spreading velocity.

The second question is not answered as convincingly. The K-type structure is an amplifying gate design. As such, when very strongly fired as with the laser, the amplifying structure introduces an impedance in the cathode circuit during the early stage of turn-on, and therefore can slow the initial turn-on of the cathode near the central region. However, this effect should disappear after a few μsec , and the entire device should be on in about $60\text{ }\mu\text{sec}$. The H-type

device turns on at about the speed expected by electrical gating-- why neither the H nor K types turn-on faster from light entering the infrared observation windows is not understood. The R-type design has a narrower N-base width than do the H or J units which were made in one process run and therefore have identical base widths. It is known from previous plasma spreading experiments that a narrower N-base tends to enhance plasma spreading velocity.

Spreading velocity, in general, should not be any faster in a light fired device than in the same electrically fired device structure if there are no light scattering effects present. This should be obvious since within less than 1 μ sec after firing a device cannot "know" whether it was initially turned on by a laser light pulse (typically <15 nanoseconds in duration) or an electrical trigger because all transient effects of the light pulse per se are over. After a microsecond or two in either the light fired or electrically gated case, the thyristor has a small area of conducting plasma that will spread at a rate dependant upon the internal structure of the thyristor, the electrical properties of silicon, and the current density.

3.5.2.2 Observations at high dI/dt and high J. These experiments incorporate the use of the high current high dI/dt pulse forming networks (which can be paralleled to 40) and the use of a fiber optics cable and photomultiplier tube to observe the infrared recombination radiation emission from the silicon device in order to measure spreading velocity for use in the analytical model. The experimental set-up is described in detail in Section 3.3. Observations with the infrared imaging equipment were not made using the high power pulse-forming networks because it was impractical to focus through the tiny observation holes in the massive pressure electrode required for the high levels of current conducted.

Thyristor elements were tested at various levels of voltage and current. Several electrodes and infrared observation port configurations were used in the tests depending on the type of device being tested. The laser was fired directly into the device in some tests,

while in others the laser was fired into a fiber optics cable and the opposite end (or ends in the multifurcated types) of the fiber optics cable was placed in intimate contact with the optical window (or windows) in the silicon. It will be restated here that two types of windows were used in testing a device. One was the window or port used for introducing laser light into the silicon for the purpose of firing the device. The other was the window, which is preferably as small as possible, used to permit infrared recombination radiation to escape through the cathode surface in order to observe the plasma spreading (forward current conduction area) in the device with time.

Successful observations were made on devices 23 mm in diameter with various contact-window configurations. Although attempts were made to obtain similar data on 50 mm diameter devices at very high current levels, these attempts were unsuccessful as will be explained later.

The initial experiments were performed using radial slots etched in the cathode metallization of the thyristor device as shown in Figure 3.5-6. This slot configuration was chosen to ease the alignment of the observation holes in the pressure electrode (refer to Figure 3.3-18) with the observation windows in the device metallization. However, this configuration had a serious problem with device failure and an improved design was fabricated using an overall pattern of 0.127 mm diameter observation holes in the cathode metallization as described in Section 3.3.2.2. The pattern of observation holes can be seen clearly in Figure 3.5-7. Using this method data were obtained on 23 mm diameter devices fired at 7500 amperes peak current. Figure 3.5-8 is a plot of the data. The relationship between spreading velocity and current density appears to be of the form

$$v_s = B_o J_o^{C_o}$$

A straight line fit to the log-log plot in Figure 3.5-8 gives $B_o = 9.84 \times 10^{-3} \mu\text{m-cm}^2/\mu\text{sec-A}$ and $C_o = 1.1$. Yamasaki obtained an equivalent C_o of 0.37 corresponding to a much slower increase in

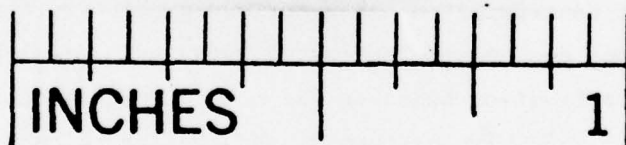


Figure 3.5-6. Twenty-three mm diameter thyristor element with slots as infrared observation windows.

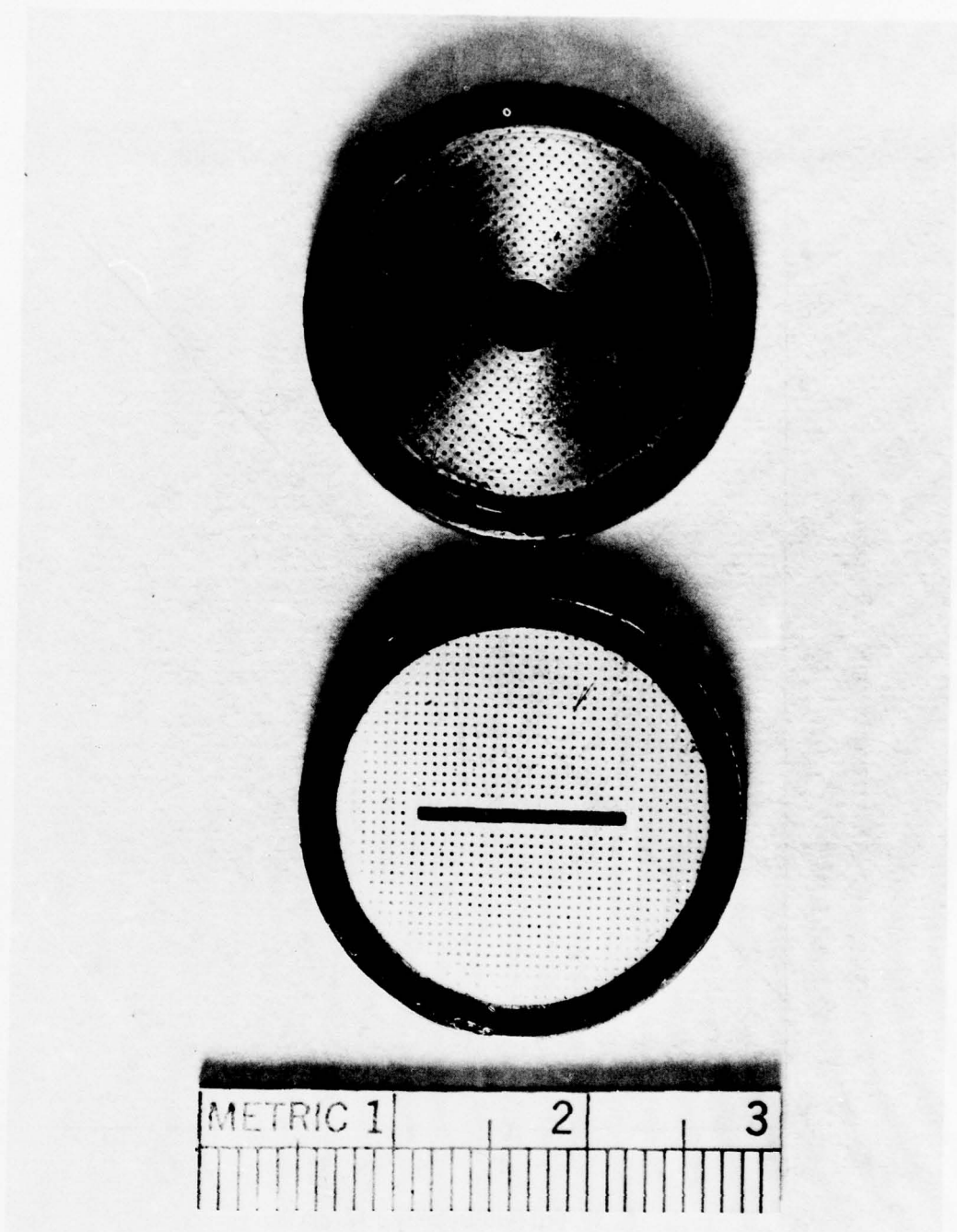


Figure 3.5-7. Twenty-three mm diameter LASS devices showing the overall pattern of 0.0127 mm diameter observation windows in the cathode metallization.

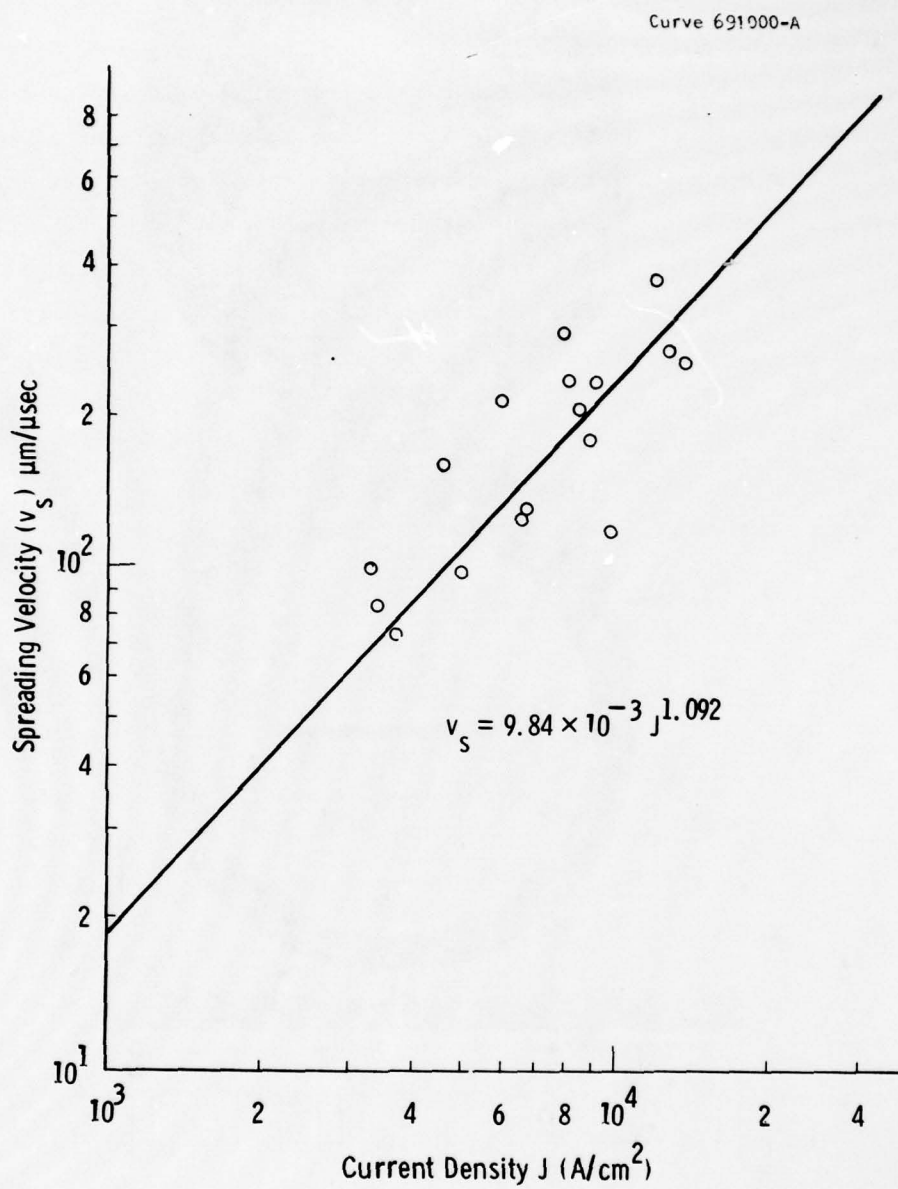


Figure 3.5-8. Plasma spreading velocity (v_s) versus current density (J). Peak current 7500 A.

v_s as J is increased; he did not report a value for B_0 . These constants were used in the computer model data correlation discussed in Section 2.2.

This relationship of the plasma spreading velocity to the current density is of considerable importance to the designer of devices that are to operate at very high current densities for long (several microseconds) pulses. It means that considerably more area of a device will be turned-on than would be indicated from Yamasaki's data at lower current density values. This in turn means that smaller or fewer illumination ports, or less light, or a lower conducting loss can be traded to achieve a near optimum design for a given application.

There are several sources of error in these measurements. First, it has been observed and reported for earlier, low dI/dt , low current infrared plasma spreading studies that the central triggering region radiates infrared for a short time during turn-on indicating that a plasma is present and that this region is conducting immediately after conduction is initiated. The infrared from this region is subsequently observed to extinguish indicating that this area is no longer conducting, or is conducting at a very low current density. Consequently, the assumed area of conduction from which the current density (J) is derived is only approximate. This is the most significant source of error. Second, the initially turned on area is not confined to the window area as some scattering takes place. This is now known to be so small as to approach insignificance during the initial turn-on, but may provide a biasing effect to increase the plasma spreading velocity, which would be important in pulses longer than one microsecond. Third, the "on" region does not necessarily spread in a uniform manner and since observations are being made at discrete points, the actual conduction area could be in error from the inferred circular or linear (depending upon the shape of the illumination port) geometry. More observation ports would clarify this point, but at a sacrifice in contact electrode area which is significant at the high current densities found here.

Spreading velocity data were not obtained at the very high

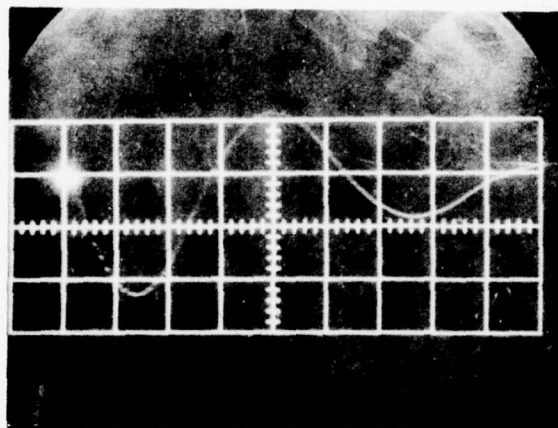
values of anode current achieved when 50 mm diameter devices were fired at 1700 V at dI/dt values in excess of 40,000 A/ μ sec. The reason for this was that considerably more device area was illuminated when the large devices were fired so that the peak current densities in the 50 mm diameter devices were comparable to those of the 23 mm diameter devices. There was also the experimental problem of the heavy gold plating, which was necessary to obtain adequate electrical contact (see Section 3.4.3.1) between the device cathode and the associated pressure plate, closing the observation holes in the metal contact. It did not seem to be worth the cost of overcoming this problem when no improvement in understanding of the device physics was expected.

3.5.3 Electrical Measurements.

This section reports all of the electrical measurements performed under contract except those required for equipment check-out (Section 3.3) and plasma spreading velocity (Section 3.5.2).

A preliminary test was performed with a LASS mounted in a coaxial capacitor power supply and fired with the laser because the 40 PFN pulser was not yet available. The experiment was performed using a J-type device (see Section 3.2 for a description of the device), and provided interesting data on the reverse blocking capability of this LASS device immediately after it had sustained a high dI/dt and high current density pulse.

The discharge of a coaxial capacitor through a bilateral switch gives rise to a sinusoidal waveform, the system merely being a series LCR circuit. Figure 3.5-9 is a comparison of a LASS firing in the circuit at a repetition rate of 2 pps to that of a "hammer switch" single discharge of the circuit. In both cases the capacitor was charged to 500 volts. This test provided some measure of the uniformity of turn-on since the voltage reverses across the switch when the current passes through zero. The dynamic voltage was not measured since Kelvin probes were not incorporated into the system. An analysis of the "hammer switch" waveform shows that $L = 25 \times 10^{-9}$ h, $C = 1 \mu f$ and $R = 0.047 \Omega$ (L and R will depend on the switch but

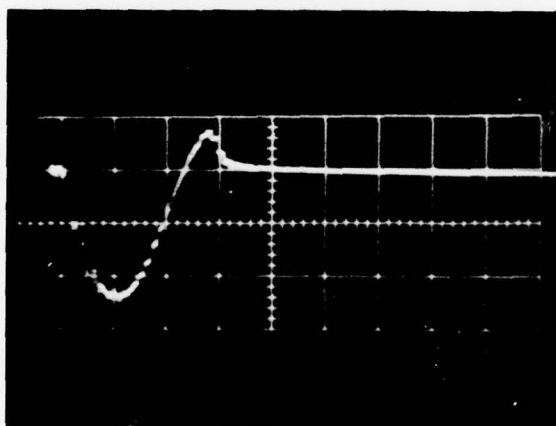


"Hammer Switch" Closing on 1.0 μ f
coaxial capacitor

$V_{\text{capacitor}} = 500$ volts

Vertical = 1000 A/cm

Horizontal = 0.20 μ sec/cm



Laser Light Activated Thyristor
closing on 1.0 μ f coaxial capacitor

$V_{\text{capacitor}} = 500$ volts

Vertical = 1000 A/cm

Horizontal = 0.20 μ sec/cm

Repetition Rate = 2 pps

Figure 3.5-9. Comparison of mechanical "hammer switch" to laser light activated thyristor in coaxial capacitor circuit.

should not vary greatly). Then the reverse voltage appearing across the device immediately after the device has been in heavy forward conduction is approximately 750 volts (V_c and LdI/dt). Conventionally fired thyristors will be destroyed under these test conditions.

The peak current in the figure was about 2400 A and the device supported (blocked) reverse voltage about 200 nsec after passing through current zero. Also note that the dI/dt for the LASS is actually greater than that of the hammer switch. The device was operated as high as 800 volts on the capacitor at a dI/dt of 25,000 A/ μ sec at a repetition rate of 2 pps. Considering the small area illuminated ($< 0.1 \text{ cm}^2$), this was an impressive performance.

3.5.3.1 Tests on 23 mm diameter devices.

3.5.3.1.1 Light scattering experiments. A brief experiment was performed early in the program to qualitatively determine the extent of spreading of the laser beam inside the silicon. The laser beam was directed onto a device which had not been alloyed to a molybdenum anode contact. The beam entry angle was approximately 75° off normal on the cathode side of the chip. The infrared image converter tube was focussed on the back (anode) of the chip and the emerging pattern observed. The size of the emerging pattern was compared to that of the impinging pattern. Comparison in this manner is qualitative for two reasons. First, a photosensitive paper was used to measure the incident beam size. The sensitivity is not necessarily the same as that of the image converter tube. Second, the emerging pattern will have a size dependent on how well the image converter tube is focussed on the back of the slice. The pattern size was minimized consistent with focus and appeared to be nearly 10 times the size of the incident pattern. This seems to be an unreasonably large increase so a second experiment was performed with improved accuracy and with special attention to the sensitivity of the light detecting media. For if the laser beam does in fact spread out considerably as it passes through the silicon, it would have important implications for device operation. The optical spreading could be

used to advantage to cause carriers to be generated under metal contacts, giving a low resistance, low loss path for flow of the switched current. In addition, the correct optical path should be incorporated into the computer modelling effort to accurately reflect the true nature of device operation. Possible sources of beam spreading include scattering at the incident surface, scattering from internal structures, and reflection from internal surfaces. This experiment shows there is very little scattering, whether from the surface or internal structure, while multiple reflections can be observed if the laser beam is incident at an angle to the wafer. The laser light distribution inside the wafer can be accurately computed by geometrical optics.

a. Experimental procedure. In order to look for beam spreading, several silicon wafers were prepared with metal masks on one surface. Photographs of the mask define the reference dimension. This dimension is checked, and system operation confirmed, by photographing laser light emerging from the aperture in the mask. The sample is then placed with the laser light incident on the masked surface, and photographs made of the light emerging from the unmasked surface. Beam spreading from any source will cause this image to be larger than the reference dimension. With careful measurements of image sizes, a semi-quantitative limit of beam spreading can be stated.

Several silicon samples were prepared with evaporated aluminum masks deposited on one surface. The masked surface was either lapped or polished, while the other surface was lapped only. The metal mask defines a sharp edged aperture, in this case a stripe about 625 μm wide. The sample is placed in the laser beam path as shown in Figure 3.5-10. The lens is positioned to form an image of the rear face of the sample on the infrared image converter tube. Initial focusing is done with illumination from a lamp shining upon the rear surface, and checked by looking for sharp surface detail in the transmitted laser light. A camera is placed on the optical axis to photograph the image on the converter tube. With the sample carefully aligned perpendicular to the optical axis, sharp focus can be main-

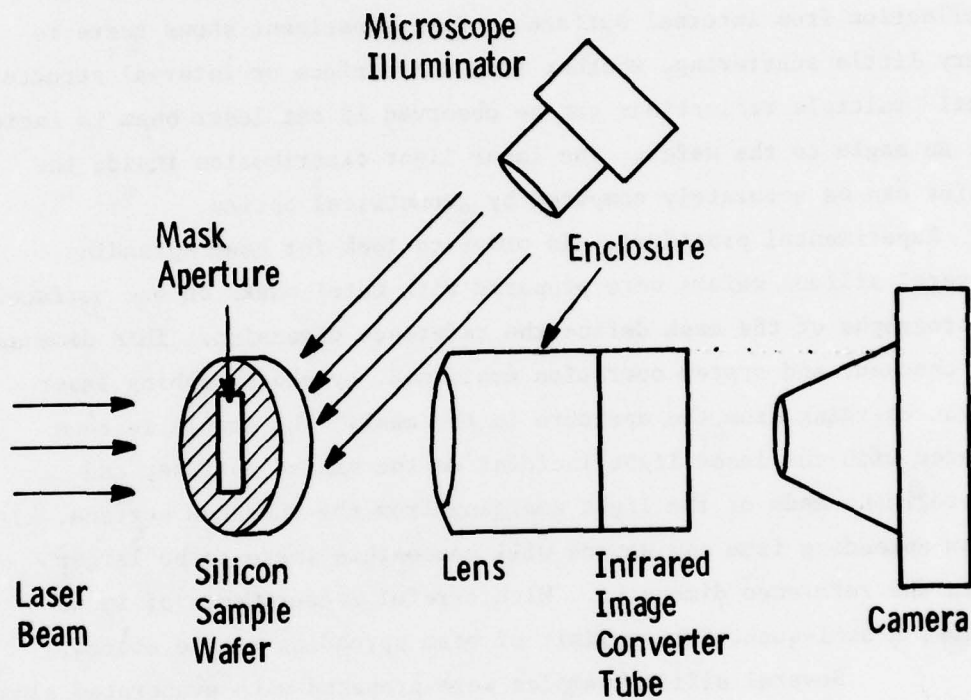


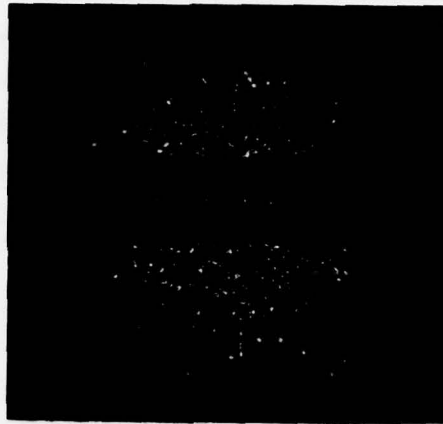
Figure 3.5-10. Experimental setup for studying beam spreading

tained across the image plane, subject to the inevitable distortion caused by the image converter.

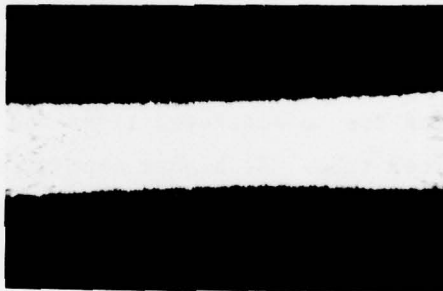
In order to obtain accurate size comparisons, precautions must be taken against changes in apparent image size caused by illumination level. Image converter tubes are generally susceptible to image blooming, that is, enlargement of the image size if the incident optical intensity saturates the converter. This possibility was avoided by taking photographs at several laser intensities. In this experiment, the image sizes were independent of laser illumination level. Apparent image size also depends on the film exposure. In fast Polaroid film needed to photograph the relatively dim image in the infrared converter, the film latitude is very limited. Unless the image intensity is very uniform, the apparent size will depend on exposure time. For each measurement, several exposures were taken to ensure against this problem. The underexposed photo showed very sharp images, proving that there was no fogging due to scattered light and no blooming of the image on the converter tube. At higher exposures, enlargement of the image is seen in certain cases explained below, as relatively dim portions of the image begin to register on the film.

b. Results Figure 3.5-11 shows a series of photographs taken with the laser beam at normal incidence to the sample surface. The lapped surface with the metal mask is shown under illumination from the microscope lamp in Figure 3.5-11a. The sharp detail of surface asperities shows that the image is well focused in the center of the field of view, but becomes blurred and distorted by the image converter at the edges of the field. All measurements of image size are made in the center of the field of view. In Figure 3.5-11b, the sample is in the same position, with the mask surface facing the camera, with illumination provided from the back side by the laser. This image is overexposed deliberately to show there is no image spreading. For Figure 3.5-11c, the sample was flipped over so that the masked surface faced the laser. Without any adjustment of the optical system, the focus of the unmasked surface was sharp, implying that the magnification

a.



b.



c.



Figure 3.5-11. Images from sample 1, with laser beam at normal incidence. a) Mask aperture illuminated by lamp. Masked face is lapped. b) Laser light emerging from mask aperture. c) Laser light emerging from rear face.

for Figure 3.5-11c was exactly the same as that for 3.5-11a and 3.5-11b.

The image sizes were measured directly from the photographs using vernier calipers. The reference dimension, taken from Figures 3.5-11a and 3.5-11b, is 0.495 inches. The image size on Figure 3.5-11c was 0.505. Both Figures 3.5-11b and 3.5-11c are examples from a series of photos taken with different exposure times. In each series, the image size was independent of exposure time.

Since the measurement precision is only about 10 mils in determining the size of the image, it can be said that the beam spreading is barely observable in this sample. Some estimate on the upper limits of spreading can be obtained from the sample dimensions as shown in Figure 3.5-12. The mask aperture was 625 μm , the beam spreading was two percent or less, giving about 6 μm displacement of the edges of the image. The sample was 330 μm thick, giving a scattering angle θ of one degree or less. This shows that the total amount of scattering, even in a sample with a lapped surface, is small.

Another series of photographs was made with the laser beam striking the surface of another sample at about 60° angle of incidence measured from the normal to the surface. This second silicon sample had a polished surface on which the aluminum mask was formed, and a lapped surface on the back. The reference photo of light emerging from the mask aperture is shown in Figure 3.5-13a. Although the photo is deliberately overexposed, the image remains sharp with no trace of image blooming. The image width measured with vernier calipers is 0.495 inches. Figure 3.5-13b shows a view of the light emerging from the back surface of the sample. At this moderate exposure level, the image width is 0.495. Figure 3.5-13c differs from 3.5-13b only in increased exposure, but the image now shows a ragged edge that extends in places to 0.565 inches wide. The extra width is due to a relatively weak light signal on the right side of the image which is too dim to register on the film at the reduced exposure of Figure 3.5-13b. The ragged edge is caused by the shadow of a residue inadvertently deposited

Dwg. 6415A19

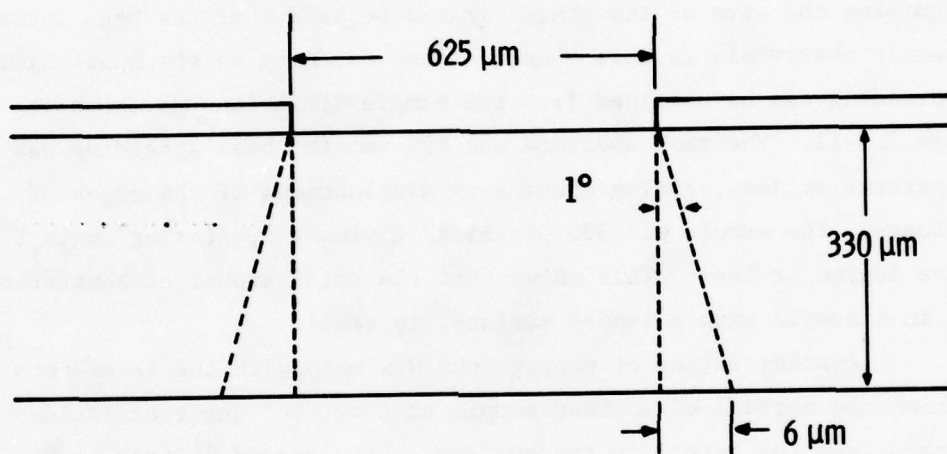


Figure 3.5-12. Dimensions of mask aperture and thickness of sample 1. Very little spreading of beam is observed as it passes through sample.

a.



b.



c.



Figure 3.5-13. Images from sample 2 with laser beam incident 60° from normal. a) Laser light emerging from mask apertures b) Laser light emerging from rear face c) Same view as b), but longer exposure

in the mask aperture during handling the sample.

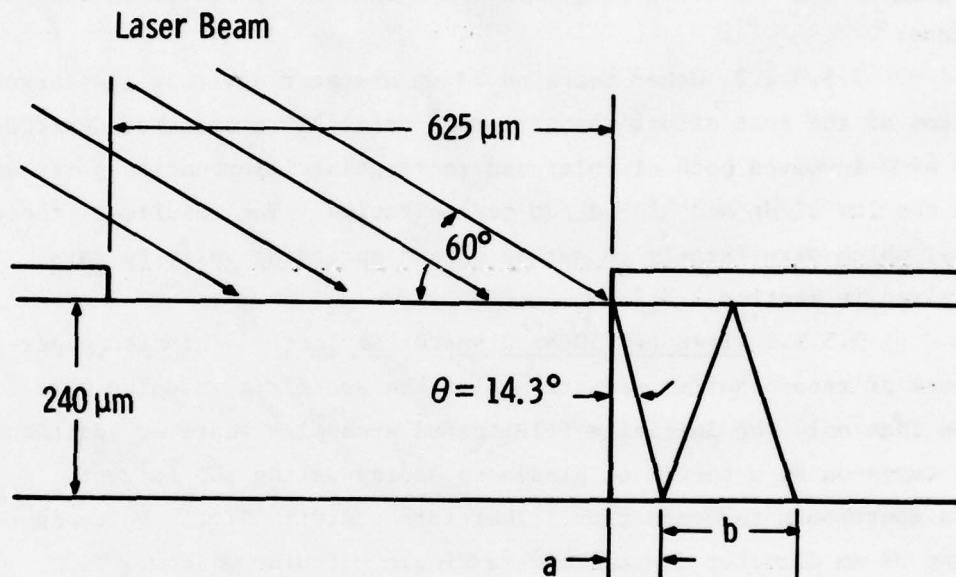
It has been noted above that the image width does not change with exposure when the laser is at normal incidence to the sample (Figure 3.5-11c). The increased width of Figure 3.5-13c can be explained by multiple reflections inside the sample as shown in Figure 3.5-14. The refraction condition at the surface for a ray incident at 60° onto silicon of index 3.5 gives an internal angle θ of 14.3° . The thickness of Sample 2 was $240\text{ }\mu\text{m}$, giving an edge displacement, b , of $122\text{ }\mu\text{m}$, or about 20 percent widening of the image width of the $625\text{ }\mu\text{m}$ mask aperture. The image spreading observed in Figure 3.5-13 is about 15 percent, which is adequate agreement with model considering the limitations of this technique. Similar results have also been obtained on a sample with a lapped surface.

c. Conclusion. Contrary to the preliminary results, very little scattering takes place as the laser beam passes through the silicon device structure. This verifies that there are no internal structures which might cause unforeseen scattering. This also indicates that the lapped surface does not cause substantial scattering. Because of the non-linear characteristics of the film used to record the images, complete quantitative data was not obtained. Judging by the film images, only a very small fraction of the incident light is lost through scattering. This means that the optical path of laser light in the device can be adequately described by a simple idealized model and ordinary geometric optics.

Multiple reflections are observed inside the silicon wafer when the laser beam is incident at an angle to the surface of the wafer. The ray trajectories of the reflected light can be predicted by geometric optics, but the intensity of the reflected beam cannot be predicted because of uncertainties in the absorption constant of the silicon and the reflectivities of the faces. By proper device design it will be possible to utilize internal reflections to increase device performance.

Further work could include quantitative measurements of

Dwg. 6415A16



a = displacement of image

b = widening of image by multiple reflections

$b = 2 t \tan \theta$

Figure 3.5-14. Dimensions of mask aperture and thickness of sample 2.

light distribution by substituting a mechanically scanned fiber-coupled detector for the image converter and camera of the present system. With reliable quantitative data it should be possible to measure the material absorption length and the reflectivities of the surfaces. These parameters would be useful for optimizing device design. Using masks with smaller apertures would allow more accurate measurement of total scattering, and it would be interesting to investigate how the scattering could be increased by modifying surface texture.

3.5.3.1.2 Other tests on 23 mm diameter devices. A large portion of the test effort was performed using 23 mm diameter devices. This work involved both circular and rectangular illumination ports and both the low dI/dt and high dI/dt test circuits. The results of these tests, which were largely to gather plasma spreading velocity data, are given in Section 3.5.2.

3.5.3.2 Tests on 50 mm diameter devices. Infrared observations of recombination radiation plus the scattering studies have shown that only the initially illuminated area plus whatever additional area turns-on as a result of plasma spreading during the current pulse contribute to conduction. Therefore there is little value in firing 50 mm diameter devices with a single circular window. To demonstrate the feasibility of multiple firing points in a single optically triggered thyristor, six "windows" were opened in the metal contact of each of several 50 mm diameter silicon thyristors. These windows were illuminated simultaneously by firing the laser beam pulse into the single end of a multifurcated fiber optics light pipe which branched into six legs of equal cross section (Figure 3.5-15), each section being approximately 0.032 cm^2 . The fiber optics branches were in direct contact and alignment with the optical windows in the silicon.

Two window sizes were used. The first size had an area of 0.13 cm^2 , i.e., considerably larger than the fiber optics cross section. The second size window was 0.0013 cm^2 , i.e., considerably

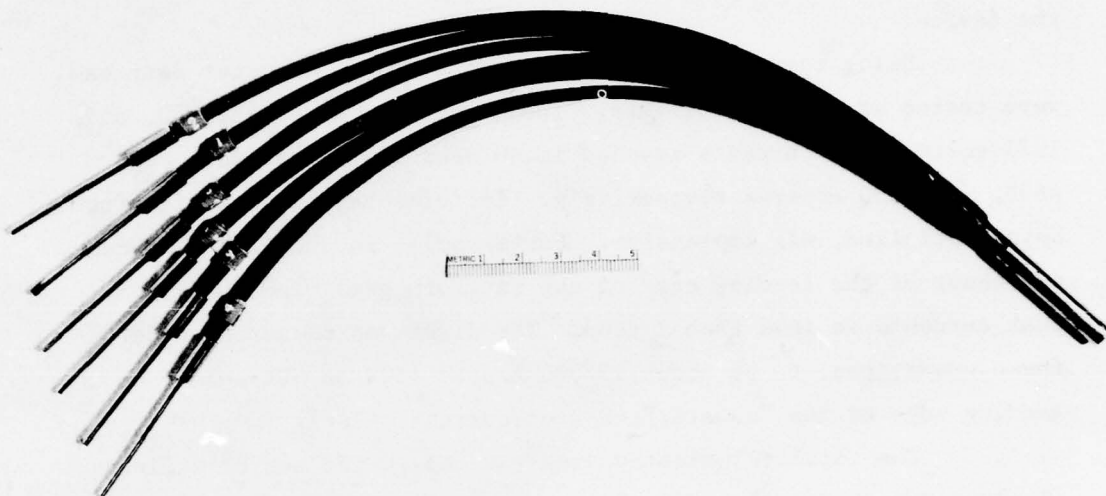


Figure 3.5-15. One-to-hexifurcated fiber optics cable used to show initial feasibility of multiple firing points.

smaller than the fiber optics cross section (See Figure 3.5-16). The latter case proved to be the most effective. Catastrophic failure resulted after a short time in the large window configuration. The pattern of the fiber optics cable metal outer case "burned" into the silicon surface because of localized conduction through the light pipe case to the cathode pole piece. (Figure 3.5-17.) It has been found, in general, that any time the optical window is "shadowed" by a contact to the cathode pole piece (including the cathode pole piece itself), conduction of the locally turned-on region through the high contact resistance of silicon to pole piece results in localized melting of the silicon and eventual catastrophic failure of the device.

Using the smaller optical windows, 50 mm diameter devices were tested at various voltages. These voltages were 425, 850, and 1275 volts. The currents reached in 40 μ sec PFN pulses were 2300, 4600, and 7000 amperes respectively. Performance, although far from being optimized, was impressive. For example, in the 1275-volt case, overshoot of the leading edge of the waveform gave rise to 8000 A peak currents in less than 1 μ sec. The dI/dt was measured, under these conditions, to be about 13,000 A/ μ sec (10% to 90% points on the leading edge of the "square," 40 μ sec current pulse).

The total illuminated area was only 0.008 cm^2 of silicon (i.e., 6 X 0.0013 cm^2). The illumination of each of the six bundles was not optimized for laser light uniformity; however, it was shown by this work that high current levels and high dI/dt can be achieved by illuminating a multiplicity of small distributed windows.

The computer program model predicted that a thin rectangular illumination port would be superior to a circular pattern. This prediction is not surprising since such a configuration maximizes the periphery relative to the total illuminated area. To obtain a practical maximum value of periphery on available 50 mm diameter devices and simultaneously the ability to vary the amount of illuminated area (and associated periphery), a design was established incorporating

Dwg. 6414A73

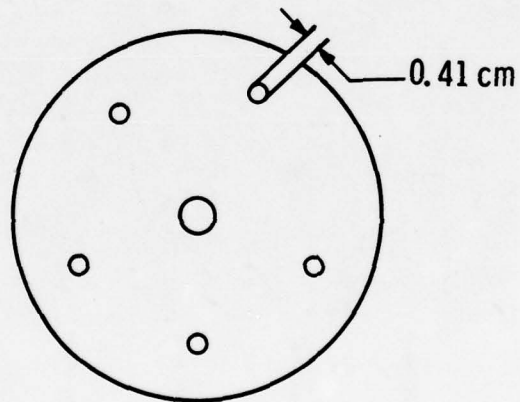
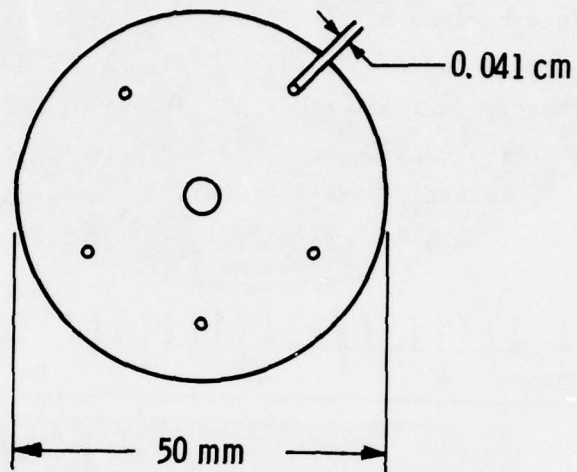


Figure 3.5-16. Illumination ports used with 50 mm diameter devices in initial feasibility tests of multiple point firing.

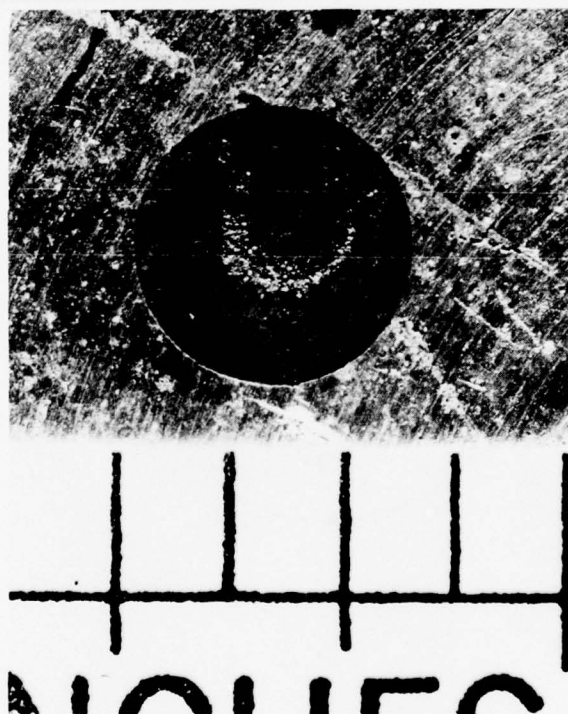
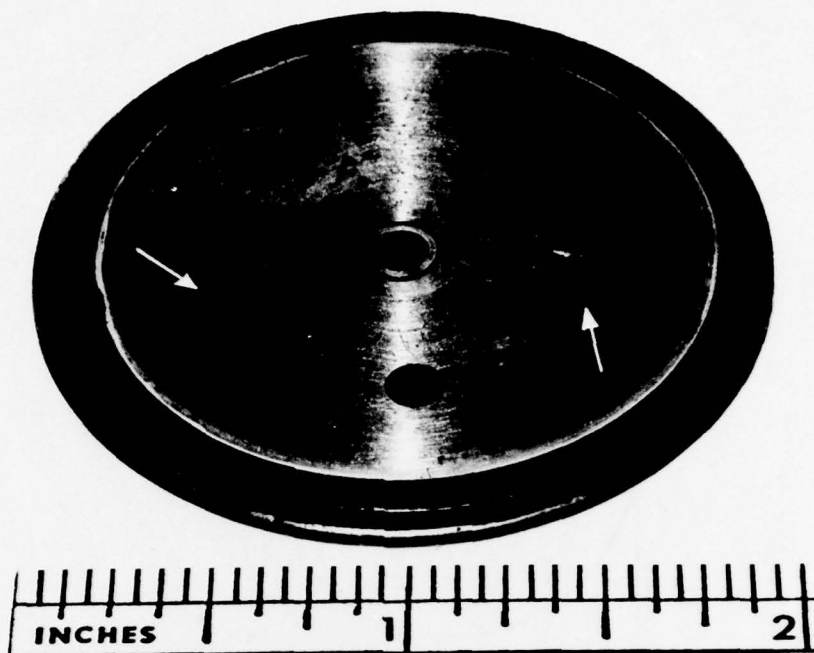


Figure 3.5-17. Device with pattern of fiber optics cable metal outer case burned into illumination port. (a) View of overall device. (b) Enlargement of one of the window areas showing the molten material.

eight rectangular ports aligned radially about the center of the cathode surface similar to the spokes of a wheel. The modified device is shown in Figure 3.5-18. The area of each port is 0.064 cm^2 . Special electrodes (Figure 3.3-18) were fabricated, and an eight leg multifurcated fiber optics cable (Figure 3.3-25) with rectangular cross-sections at one end and a random distribution of the fibers in a single disk pattern at the other end was designed and fabricated. This configuration permitted the use of from one to eight light inputs to the device with essentially the same light intensity available at each rectangular entrance port. A measurement of the transmission of the fiber optics cable provided the following data:

| | | |
|----------------------------------|---|---------|
| measured light input to cable | - | 80 mJ |
| measured light output - each leg | - | 7-10 mJ |

The indications were that the light output was very uniform from leg to leg. The spread in values of the output indicates the estimated value--the instrumentation available at the time was not accurate at levels below 10 mJ. Taking the lower value, 7 mJ, indicates that the transmission efficiency of 1/2 meter long cable, including coupling losses, is at least 70%. Recently announced improvements in materials for fiber optics cables should increase the efficiency.

Using the eight-port 50 mm diameter device and associated laser, electrodes, fiber optics cable, and the specially constructed pulse forming network, the current waveform of Figure 3.5-19 was obtained. This shows a peak current of 24,000 A, with the flat region in the pulse somewhat above 19,000 A. The dI/dt (2000 A to 18,000 A) is 30,000 A/ μsec , with an initial dI/dt greater than 40,000 A/ μsec . These data showed that one set of the technical goals of the contract are attainable.

An attempt to measure the initial rate of voltage decrease as the switch turns on shows that the LASS is "on" in about 20 nsec. The trace on the oscilloscope film was extremely faint, and attempts to intensify it by repeated pulses were unsuccessful because the jitter in the system is of the same order of magnitude as the voltage

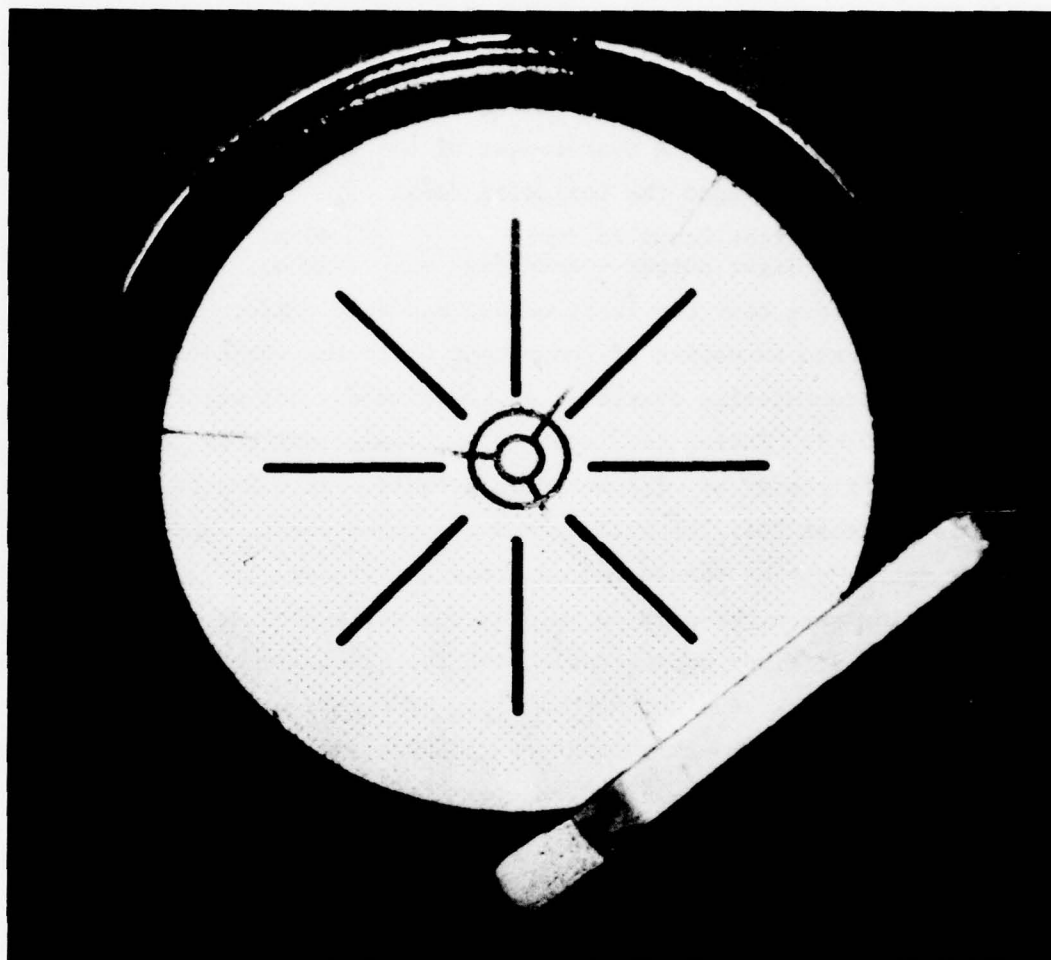
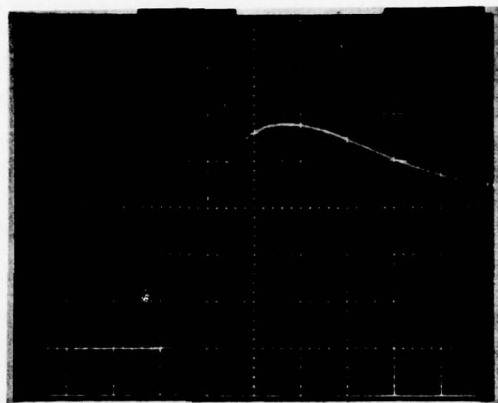
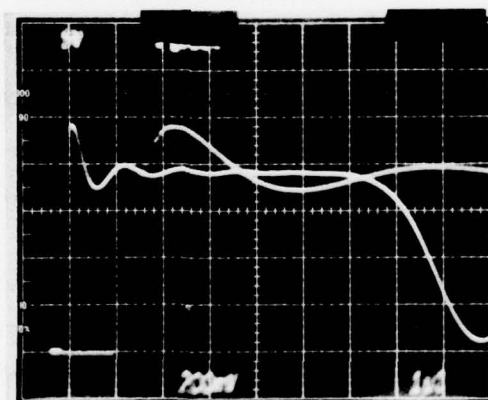


Figure 3.5-18. Fifty mm diameter semiconductor switch element showing radial pattern of rectangular windows.



(a) Horizontal scale 500 nsec/division



(b) Horizontal scales 1 μ sec and 5 μ sec/division

Figure 3.5-19. Current waveform for 40 paralleled pulse forming networks, 1700 V, 5000 A/division, device G4, 50 mm diameter with eight rectangular ports illuminated. Repetition rate about 1 pps.

fall time. However, by eye the faint trace can be followed until the voltage starts to fall, and can then be found again about 30 nsec later during the fluctuations of the voltage. Traces at slower sweep rates are brighter, but only indicate that the fall time is less than 100 nsec.

3.5.3.2.1 Voltage-current data. Voltage current data were taken extensively on 50 mm diameter devices. The primary purpose of these data were to supply parameter values to the analytic computer program and to verify the predictions of that program. The data were taken with the first inductor removed from each PFN to cause overshoot of the current waveform. This approach increases the dI/dt that each device must withstand, and also results in a higher initial peak current. Illumination ports were opened in the devices as shown in Figure 3.5-18 and as dimensioned in Figure 3.5-20 which also shows the port dimensions of the contact electrode.

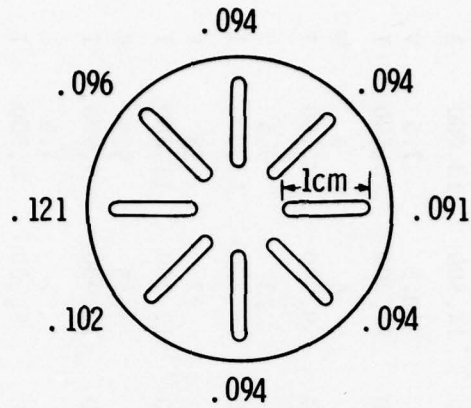
Because these data were primarily obtained for use with the analytic computer program, no additional interpretation will be done. A reduction of some of the data is presented in Tables 3.5-1 and 3.5-2 to ease the task of the casual reader; the serious investigator will want to refer to the prints of the oscillograms presented in the various figures and in the appendix.

3.5.3.2.2 Effect of varying the light input.

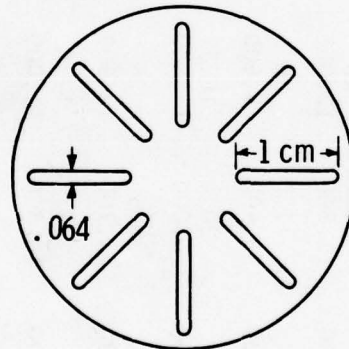
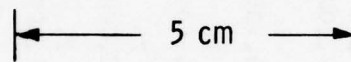
a) Effect of varying the area illuminated.

One useful piece of information for the theoretical model is how the forward voltage drop of the LASS changes with current density. By using the octifurcated fiber optics cable and removing one or two branches of the cable at a time from the device electrode, the area illuminated can be progressively reduced while the light intensity (J/cm^2) and the current conducted remain constant. Then the resulting forward voltage drop can be determined at any time during the pulse as a function of the current density if proper allowance is made for plasma spreading. This technique is described in Section 3.3.5.

Figure 3.5-21 shows traces of the device current when illuminated using one branch and two branches of the fiber optics cable.



Contact Electrode Port Dimensions - as Measured



Device Metallization Port Dimensions. Area of Each Port is 0.064 cm^2 . All Dimensions in cm.

Figure 3.5-20. Illumination ports in 50 mm diameter devices for voltage-current measurements.

Table 3.5-1. Voltage-Current Data for 50 mm Diameter Thyristor 2G4

| Supply Voltage | No. of PFN's | Time after Start of Pulse - μ sec | | | | | | | | V(Volts) | I(Amps) |
|----------------|--------------|---------------------------------------|--------|--------|--------|--------|--------|--------|--|----------|---------|
| | | 5 | 10 | 15 | 20 | 25 | 30 | 35 | | | |
| 1700 | 40 | 40 | 30 | 24 | 21 | 19 | 17 | 11.5 | | | |
| | * | 18,000 | 17,600 | 18,000 | 19,000 | 19,000 | 18,000 | 16,000 | | | |
| | 40 | 26 | 18 | 16.5 | 16.5 | 15.5 | 14 | 9 | | V | |
| | * | 19,800 | 18,600 | 19,100 | 19,200 | 19,000 | 18,900 | 17,200 | | I | |
| | 35 | 23.5 | 16.5 | 14 | 14 | 13.5 | 12 | 8 | | V | |
| | *** | 17,500 | 16,400 | 16,800 | 16,900 | 16,700 | 16,600 | 16,000 | | I | |
| | 30 | 25 | 17 | 14.5 | 14 | 13 | 11.5 | 8 | | V | |
| | * | 15,000 | 14,200 | 14,600 | 14,800 | 14,600 | 14,500 | 13,000 | | I | |
| | 25 | 15 | 15 | 13 | 13 | 12 | 10.5 | 7.5 | | V | |
| | | 11,600 | 11,800 | 12,000 | 12,100 | 12,000 | 11,900 | 10,500 | | I | |
| 1275 | 20 | 10 | 7 | 6 | 7 | 6.5 | 6 | 3 | | V | |
| | ** | 10,000 | 9,400 | 9,600 | 9,700 | 9,600 | 9,500 | 8,500 | | I | |
| | 40 | 30 | 20 | 16.5 | 16 | 14.5 | 13 | 9.5 | | V | |
| | * | 14,600 | 14,000 | 14,300 | 14,400 | 14,300 | 14,200 | 13,000 | | I | |
| | 35 | 38 | 28.5 | 26 | 25 | 23.5 | 22 | 18 | | V | |
| | * | 13,200 | 12,700 | 12,900 | 13,000 | 12,900 | 12,800 | 11,800 | | I | |
| | 30 | 19 | 13 | 11.5 | 11 | 9.5 | 8.5 | 5.5 | | V | |
| | * | 11,200 | 10,800 | 11,000 | 11,100 | 11,000 | 11,000 | 9,900 | | I | |
| | 25 | 14 | 10 | 9 | 8.5 | 8 | 7 | 4.5 | | V | |
| | *** | 9,600 | 9,200 | 9,400 | 9,400 | 9,400 | 9,100 | 8,500 | | I | |
| | 20 | 14 | 9.5 | 8.5 | 8 | 7 | 6.5 | 4.5 | | V | |
| | | 7,200 | 7,100 | 7,300 | 7,300 | 7,300 | 7,200 | 6,600 | | I | |
| | 11 | 7 | 6 | 6 | 5.5 | 5.5 | 5 | 4 | | V | |
| | | 3,800 | 3,800 | 3,800 | 3,800 | 3,800 | 3,800 | 3,400 | | I | |

* First values for V and I are at 6 μ sec

** First values for V and I are at 6.5 μ sec

*** First values for V and I are at 7 μ sec

Table 3.5-2. Voltage-Current Data for 50 mm Diameter Thyristor 2G6

| Supply Voltage | No. of PFN's | Time after Start of Pulse - μ sec | | | | | | | V(Volts) | I(Amps) |
|----------------|--------------|---------------------------------------|--------|--------|--------|--------|--------|--------|----------|---------|
| | | 5 | 10 | 15 | 20 | 25 | 30 | 35 | | |
| 1700 | 35 | 12 | 13 | 12 | 11 | 9.5 | 9 | 4 | | |
| | | 15,200 | 15,400 | 15,700 | 15,800 | 15,800 | 15,700 | 14,000 | | |
| | 30 | 18 | 16.5 | 14 | 12.5 | 11 | 10 | 6 | | |
| | | 12,800 | 13,400 | 13,500 | 13,600 | 13,600 | 13,500 | 12,100 | | |
| | 25 | 17 | 15 | 12 | 10.5 | 9.5 | 8 | 5.5 | | |
| | | 11,200 | 11,300 | 11,500 | 11,600 | 11,500 | 11,400 | 10,200 | | |
| | 20 | 15 | 12.5 | 11 | 10 | 9 | 8 | 6 | | |
| | | 8,800 | 9,000 | 9,500 | 9,000 | 9,000 | 9,000 | 8,500 | | |
| | 40 | 25 | 20 | 17 | 15.5 | 14 | 12.5 | 9 | | |
| | | 13,200 | 13,400 | 13,600 | 13,600 | 13,600 | 13,500 | 12,400 | | |
| 1275 | 35 | 25 | 19 | 17 | 14 | 14 | 13 | 9 | | |
| | | 12,200 | 12,100 | 12,000 | 12,400 | 12,400 | 12,200 | 11,400 | | |
| | 30 | 13 | 12.5 | 11 | 9.5 | 9 | 8 | 6 | | |
| | | 10,200 | 10,300 | 10,600 | 10,600 | 10,600 | 10,400 | 9,800 | | |
| | 25 | 15 | 12.5 | 11.5 | 10 | 9.5 | 9 | 6.5 | | |
| | * | 8,800 | 8,400 | 8,500 | 8,600 | 8,550 | 8,500 | 7,900 | | |
| | 20 | 10 | 9 | 8.5 | 8 | 7.5 | 7 | 5 | | |
| | * | 7,200 | 6,900 | 7,000 | 7,200 | 7,100 | 7,100 | 6,600 | | |
| | 40 | 22 | 17 | 14 | 12 | 11 | 10 | 8.5 | | |
| | | 9,100 | 9,200 | 9,200 | 9,200 | 9,200 | 9,200 | 8,300 | | |
| 850 | 39 | 9 | 8 | 7.5 | 7 | 6.5 | 6 | 5 | | |
| | * | 4,600 | 4,400 | 4,500 | 4,500 | 4,500 | 4,400 | 4,000 | | |
| | 20 | 8 | 7 | 7.5 | 7 | 6.5 | 6 | 5 | | |
| | * | 2,350 | 2,300 | 2,350 | 2,300 | 2,300 | 2,300 | 2,100 | | |
| | 20 | 5 | 6 | 5 | 5 | 4 | 4 | 4- | | |
| | | 2,100 | 2,100 | 2,100 | 2,200 | 2,100 | 2,100 | 1,900 | | |

* First values for V and I are at 6 μ sec

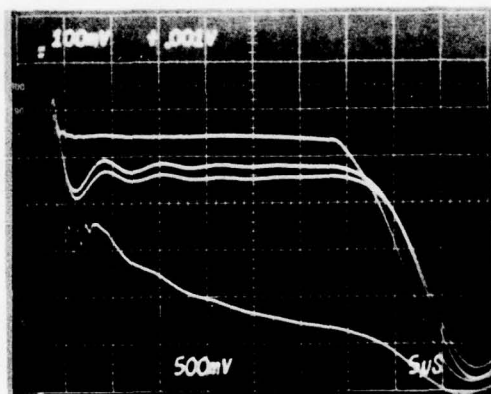


Figure 3.5-21. Multiple exposure current waveform using one and two branches of the fiber optics cable. Ignore the uppermost and lowermost traces. The lower of the two central traces shows the current for the case of the single branch. Current zero is at the bottom line of the graticule. Scale is 1000 A/cm vertical, 5 μ sec/cm horizontal. Device was 50 mm diameter, # 1. Conditions were 20 PFN's charged to 850 V. Light output level believed to be 7-10 mJ/branch.

The current is about 10% below the expected value when only one branch is used, indicating that the device is introducing appreciable impedance into the circuit. But when two branches are used, the current level (4800 A at 20 μ sec) is essentially that obtained in other tests with all eight branches used. It was concluded that useful data could be obtained using two or more branches.

The original data are shown in Figure 3.5-22 and a reduction of these data is contained in Table 3.5-3 and Figure 3.5-23. A check experiment was performed to determine if non-uniformities in the LASS might be a significant factor in the previous data. This experiment was performed using four branches of the fiber optics cable but inserting them into different illumination ports of the LASS. As can be seen in Table 3.5-4, the differences are within the expected range of experimental error, and it was concluded that the performance of the LASS device was independent of which ports were illuminated.

b) Effect of attenuation of the light level.

The effect of attenuating the level of laser light that reaches the LASS element is shown in Figure 3.5-24. Oscillograms are contained in Appendix VI. As expected, the effect of light attenuation is most noticeable early in the pulse. Figure 3.5-25 is an expanded scale measurement during the first 10 μ sec of the pulse at the highest level of attenuation practical with the filters available. These data are of interest for the analytic computer program, and will not be discussed further.

3.5.4 Extended Work.

As a result of the information derived in part from this contract, Westinghouse was able to cooperate with the Lawrence Livermore Laboratories (LLL) of the Energy Research and Development Administration in the fabrication and testing of special LASS devices. LLL has a special expertise in very fast rise, high peak current, short pulse circuits and instrumentation as a result of their weapons work. A firm conclusion reached from the work done for the USAF contract was that the di/dt was circuit limited and that much



Figure 3.5-22. Multiple exposure oscillogram of voltage waveforms for area variation by changing the number of branches of the fiber optics cable used. From the top, sequence of traces is current waveform (2 branches), and voltage waveforms for 2, 4, 6, and 8 branches. Vertical scale is 10 V/cm, horizontal 5 μ sec/cm. Device was 50 mm diameter, ± 1 . Conditions were 20 PFN's charged to 850 V. Light output level believed to be 7-10 mJ/branch.

Table 3.5-3. Forward Voltage Drop (V_F) as a Function of Initially Illuminated Area

| No. of Branches | | Time after Start of Pulse - μsec | | | | | | | | | $J @$ 2 μsec A/cm ² |
|--------------------|--------------------|---|------|------|------|------|------|------|------|------|---|
| | | 2 | 5 | 7 | 12 | 17 | 22 | 27 | 32 | 37 | |
| | I (A) | 5000 | 4800 | 4900 | 4900 | 4800 | 4800 | 4800 | 4750 | 3900 | |
| 8 | V _F (V) | 6 | 11.5 | 10 | 9 | 8 | 7.5 | 6.5 | 6 | 3.5 | 9.8 x 10 ³ |
| 6 | V _F (V) | 10 | 13.5 | 11.5 | 10 | 8.5 | 7.5 | 6.5 | 6 | 3.5 | 1.3 x 10 ⁴ |
| 4 | V _F (V) | 17.5 | 20 | 18.5 | 15 | 12 | 10.5 | 9.5 | 8 | 5.5 | 2 x 10 ⁴ |
| 2 | V _F (V) | 35 | 36 | 32 | 25 | 20 | 17 | 15 | 13 | 8 | 3.9 x 10 ⁴ |

Test Conditions: 20 PFN's charged to 850 volts, 50 mm diameter device #1

| | | Time after Start of Pulse - μsec | | | | | | | | | |
|---|-----------|---|------------------------------|------|------|------|------|------|--|--|--|
| | | 6 | 10 | 15 | 20 | 25 | 30 | 35 | | | |
| 8 | I (A) | 9600 | 9200 | 9600 | 9500 | 9500 | 9400 | 8000 | | | |
| | V_F (V) | 18 | 14 | 12 | 11 | 9.5 | 8.5 | 6 | | | |
| 6 | I (A) | 9000 | 9000 | 9000 | 9500 | 9500 | 9000 | 7800 | | | |
| | V_F (V) | | Voltage Data Not Taken | | | | | | | | |
| 5 | I (A) | 8800 | 8800 | 9000 | 9000 | 9000 | 8800 | 8000 | | | |
| | V_F (V) | 32 | 25 | 21 | 18 | 16 | 14 | 11 | | | |
| 4 | I (A) | 8400 | 8600 | 8800 | 9000 | 9000 | 9000 | 7800 | | | |
| | V_F (V) | 40.5 | 31 | 24.5 | 21 | 19 | 17 | 12 | | | |

Test Conditions: 40 PFN's charged to 850 volts, 50 mm diameter device 2G6

Curve 691065-A

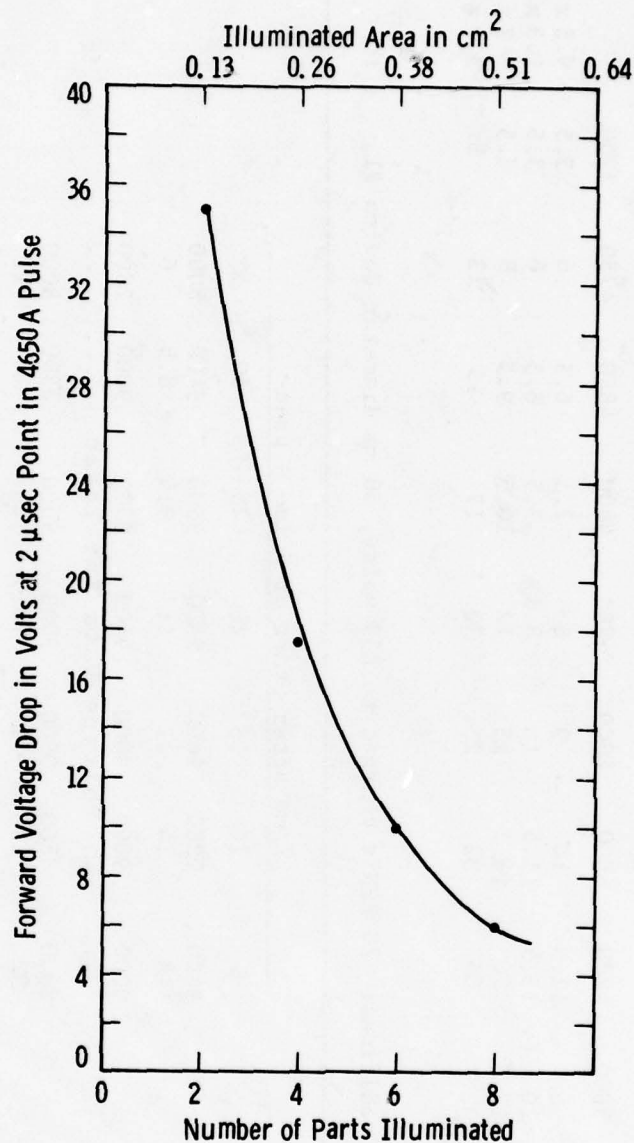


Figure 3.5-23. Forward voltage drop at 2 μ sec as a function of initially illuminated area. Test conditions: 20 PFN's charged to 850 volts, 50 mm diameter device #1. Area changed by removing legs of fiber optics cable. Light level believed to be 7-10 mJ per leg. Data fits a straight line on semilog plot with a slope of -1.25.

Table 3.5-4. Effect of Varying the Ports, Taken Four at a Time,
Keeping the Fiber Optic Cable Branches Constant

| Port Numbers | | | 6 | 10 | 15 | 20 | 25 | 30 | 35 |
|--------------|-----|---|------|------|------|------|------|------|------|
| 1-3 | 5-7 | $V_F(V)$ | 38 | 29 | 24 | 21 | 18 | 16 | 12 |
| | | $I(A)$ | 8800 | 8800 | 8900 | 9000 | 9000 | 8900 | 7600 |
| 1-4 | 5-8 | $V_F(V)$ | 41 | 32 | 30 | 23 | 20 | 18 | 13 |
| | | $I(A)$ | 8800 | 8800 | 8800 | 8900 | 8900 | 8800 | 7700 |
| 2-4 | 6-8 | $V_F(V)$ | 40.5 | 31 | 24.5 | 21 | 19 | 17 | 12 |
| | | $I(A)$ | 8400 | 8600 | 8800 | 9000 | 9000 | 9000 | 7800 |
| 8-1 | 2-3 | was corresponding sequence of fiber optics cable branches | | | | | | | |

Test conditions: 40 PFN's charged to 850 volts
50 mm diameter device 2G6

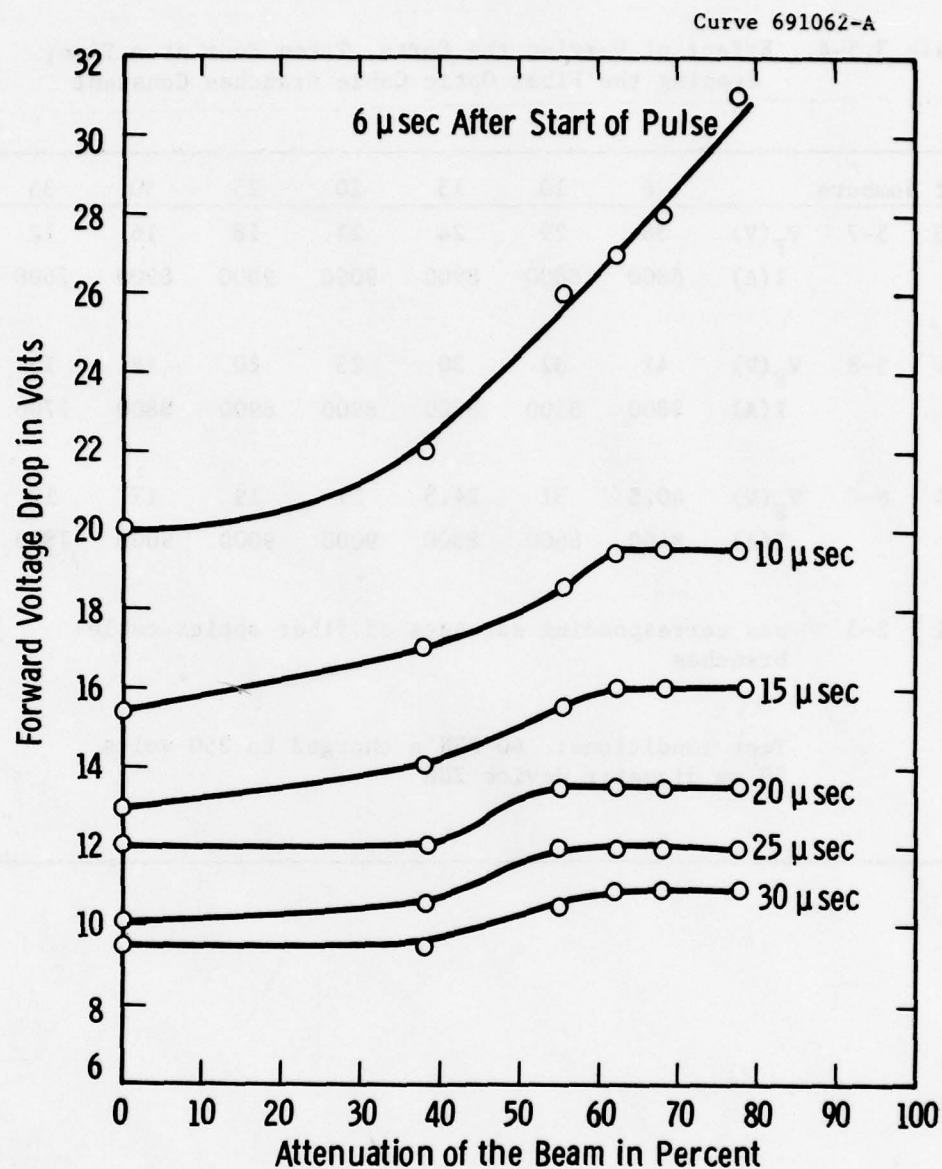


Figure 3.5-24. Forward voltage drop at various times as a function of attenuation of the laser beam. Beam input at zero attenuation believed to be 80 mJ per pulse. Device 2G6, using all 8 fiber optics cable branches. Blocking voltage instrumentation clamped at about 45 volts maximum to provide expanded scale at low voltages. Test conditions, 40 PFN's charged to 850 volts. Pulse current approximately 9300 A.

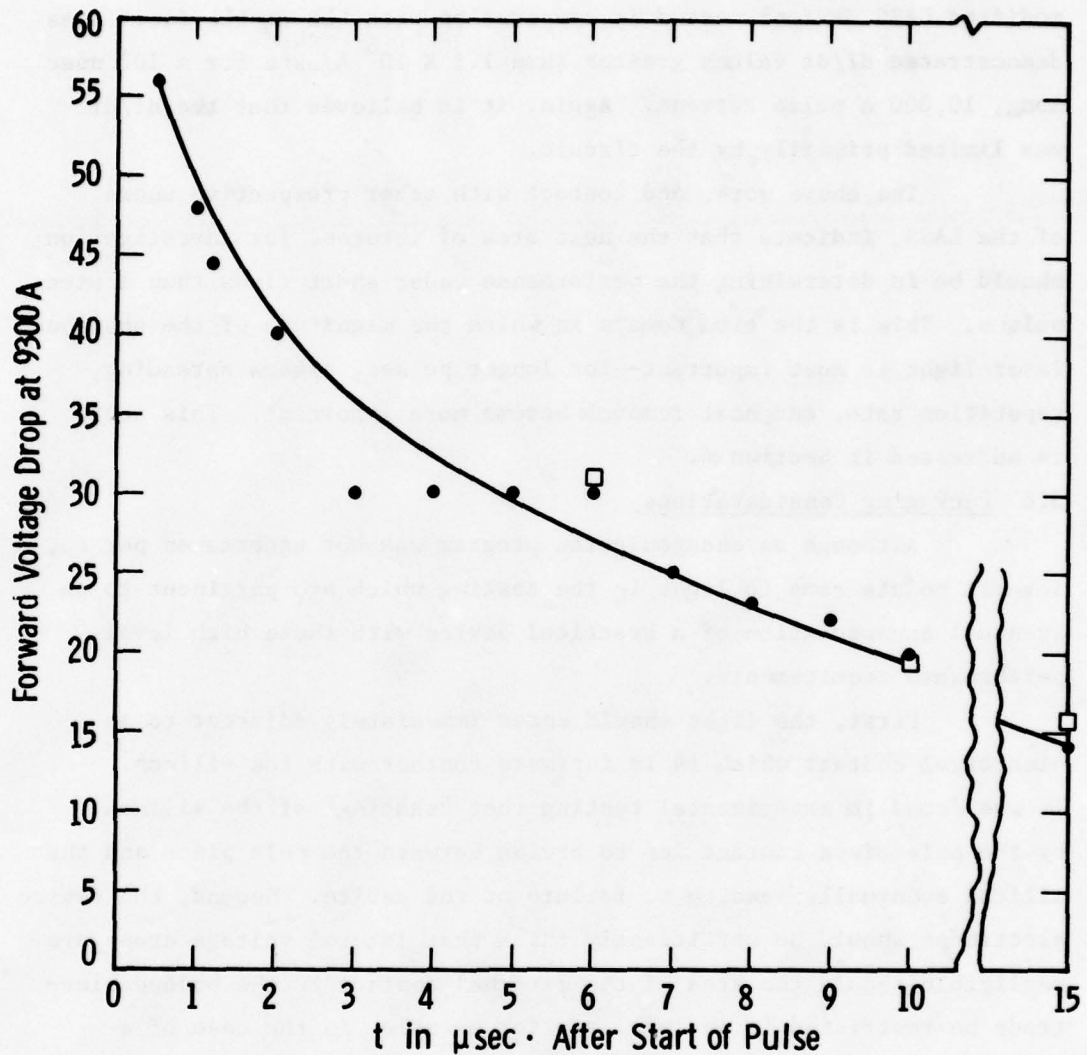


Figure 3.5-25. Forward voltage drop as function of time for 77.3% attenuation of the laser beam. Beam input at zero attenuation believed to be 80 mJ per pulse. Device 2G6, using all 8 fiber optics cable branches. Voltage probes direct (no clamping) with 50 V/cm deflection on oscilloscope. Data points \square are from previous figure and show good agreement between voltage measurement techniques.

higher dI/dt values could be achieved if adequate circuits were available. This was well beyond the scope of the USAF contract. However, modified LASS devices tested in cooperation with LLL at LLL facilities demonstrated dI/dt values greater than 1.1×10^6 A/ μ sec for a 100 nsec long, 10,000 A pulse current. Again, it is believed that the dI/dt was limited primarily by the circuit.

The above work, and contact with other prospective users of the LASS, indicate that the next area of interest for investigation should be in determining the performance under short (less than 1 μ sec) pulses. This is the time domain in which the magnitude of the absorbed laser light is most important--for longer pulses, plasma spreading, repetition rate, and heat removal become more important. This topic is addressed in Section 4.

3.6 Packaging Considerations.

Although an encapsulation program was not undertaken per se, several points came to light in the testing which are pertinent to an eventual encapsulation of a practical device with these high level performance requirements.

First, the light should enter immediately adjacent to an electrical contact which is in intimate contact with the silicon. It was found in experimental testing that "shading" of the silicon by the pole piece contact led to arcing between the pole piece and the silicon eventually leading to failure of the device. Second, the device electrodes should be sufficiently thick that lateral voltage drops are negligible should the area of the external contact to the bonded electrode be restricted in any way, as, for example, in the case of a pressure contact with a large surface area which is cocked relative to the surface of the bonded contact. This problem was encountered in the test holder and was significantly reduced by electroplating gold on top of the aluminum contact to ensure an effective large area electrical contact to the silicon. Third, if some sort of reusable light pipe or fiber optics cable is to be used to introduce the light into the silicon a method should be devised for readily repolishing

the optical surface in the event that a device failure damages the optical finish on the light pipe. Fourth, the fiber optics cable, if used to introduce the light into the silicon, should not have a metal jacket which can make uncontrolled electrical contact between the device surface and the electrode.

It seems unlikely that the LASS will be used as a single, large current, low voltage ($\sim 2\text{kV}$) device. Probably a plurality of LASS elements will be connected in series to form a high current, high voltage switch. As such, it seems futile to expend energy designing a package for a single device. Rather the approach should be to integrate the active elements of several LASS units with their optical coupling, heat removal means, electrical contact, and such equalizing components as are required. Presumably all of these elements would be contained within one hermetically sealed, low inductance package with only electrical, optical, and fluid (for cooling) connections to the outside world. For very high dI/dt , very low jitter applications, it may be necessary to integrate the switch packaging with the rest of the circuit.

The packaging of the LASS is a complex problem which in general cannot be accomplished independently of the application circuit. The following is a brief description of the switch design problem with a conceptual switch design (Figure 3.6-1) to illustrate the approach.

3.6.1 Optical Design.

The LASS requires light to turn-on. The initial conducting area turned-on is only slightly larger than the directly illuminated region (port). The current density in the device, and therefore the conducting voltage drop and power dissipated, is reduced as the illuminated area is increased. Therefore, it is desirable to illuminate the entire surface of the device to keep the current density as low as possible. This will also tend to reduce the inductance of the switch. However, electrical contact must be made to the device. It has been found experimentally that the current should not have to travel laterally along the surface of the device without a substantial

156

metal contact. Therefore, it is desirable that the surface of the device be nearly completely covered by a metallization. This is incompatible with the desire to illuminate the entire surface.

There are ways to resolve this incompatibility. One compromise is to provide a number of small diameter holes in the metallization to permit the illumination of small regions with close contact metal. Another approach is to configure the window into one or more rectangular slits. The latter approach has been demonstrated to work at current densities up to at least $15,000 \text{ A/cm}^2$.

Getting the light from the laser to the surface of the silicon also needs attention. Two approaches have been tried experimentally and both have advantages and disadvantages. The first approach is to pass the laser beam through dielectrically coated beam splitters that divide the beam energy equally among the switch elements. This technique has been demonstrated for up to 10 elements in series, and in principle could be extended to an unlimited number of elements. This technique is very advantageous -- indeed, it is almost mandatory -- when it is desired to work with polarized light. By using light polarized with the electric vector in the plane of incidence at the silicon and entering the silicon at Brewster's angle, the reflected light is zero and all of the light in the beam enters the silicon. However, the amount of polarized light available from a laser is always less than that available unpolarized, and specific designs must be investigated to determine which approach is the most advantageous. The disadvantages of the beam splitter approach are that the beam splitters must be carefully aligned and maintained in alignment, and the laser beam is exposed if the laser is not integral with the switch assembly. The problem of alignment could be partially overcome by the arrangement shown in Figure 3.6-1 where the beam splitters are mounted onto the heat sinks which are integral with the silicon active elements. Alignment is thus a matter of precise machining of two of the heat sink surfaces.

A second approach is to transmit the light from the laser

to the silicon by means of a fiber optics cable, one end of which is branched (multifurcated) with one branch going to each silicon element. This method encloses the laser beam for essentially its entire length, divides the laser light energy equally among the switch elements, and is fairly easy to align. Operation at energy levels comparable to those contemplated in this program were demonstrated with a one-to-octifurcated cable in the present USAF program. The disadvantages of the fiber optics cable approach are that there is some loss in light collection from the laser because of the non-conducting interstices surrounding each fiber of the bundle, there is some absorption (0.04 to 1.0 dB/m of cable length) of light in the cable, and it is not practical to work with polarized light.

3.6.2 Thermal Design.

The thermal design of the switch must be carefully coordinated with the performance requirements of the switch and with the other elements of the design task -- especially the optical design. Because a semiconductor switch is not a perfect switch, i.e., it does not have infinite resistance when "open" and zero resistance when "closed", heat is dissipated in the switch. Except in unusual circumstances, the heat generated while blocking voltage is small compared to that generated during conduction. The higher the peak current density is while conducting, the higher the dissipation will be. The emphasis must be on configurations to minimize the amount of heat generated and to remove the heat which is generated.

To lower the heat generated within the switch element, the conducting area of the element must be increased in order to reduce the current density. This, however, has practical limitations imposed by the optical design problem previously discussed and by the light required of the laser. For, as the illuminated area increases, the radiation energy (J/pulse) required from the laser increases in direct proportion. These are the primary constraints on the size of the illuminated area and this area will normally be sized to the minimum that will provide either the peak conducting voltage drop allowed or

the maximum peak temperature allowed.

Another source of heat generated in the active element is the lateral conduction of current across the surface of the device, and this situation occurs under two conditions. The first condition occurs because uniform contact to the edge of the metallization window is extremely difficult to achieve. This phenomenon forces the current to pass along the surface from the edge of the conducting region of the active element to the points where contact is made to the metal electrode. If this path has a high resistance, intense heat can be generated locally and catastrophic device failure will result from melting of the silicon. An approach that appears to have been successful in solving this problem is to increase the thickness of the metallization layer by a factor of 10. More work is required in this area to relate the thickness of metallization required to the current pulse (peak current, pulse width) and electrode configuration.

The second known problem of localized heat generation occurs when the optical window is in partial shadow for any reason. This corresponds to an especially bad case of the high resistance problem, for at least a portion of the current from the window will cross the non-illuminated region to get to an electrical contact point of the metal electrode. The non-illuminated region will have a high surface resistance resulting in intense local heating and catastrophic device failure. This problem can be avoided by careful design that avoids shadowing of the window region.

To summarize, the electrical metallization and optical window design must be carefully considered for their effects on heat generation at the surface of the active element.

Assuming that the design has appropriately considered these problems, there remains the problem of removing the heat from the immediate sinks to the environment. One approach with variations is shown in Figure 3.6-1. If the rate of heat generation is low enough, the heat can be removed by fluid conduction/convection between the sinks for each element and the wall of the switch case. Fins or tubes

for coolant can be attached to the case to aid transfer from the case to the environment. By using pressurized nitrogen, sulfur hexafluoride, or transformer oil inside the case, substantial heat transfer rates can be obtained by this means. The pressurized gas also improves the quality of the electrical insulation within the switch. This will be necessary to withstand the rather high voltage stand-off capabilities desired. Alternatively, the coolant/insulating medium can be circulated in the case, through an external heat exchanger, pump, purifier and back into the case to remove the heat. Large quantities of heat can be removed by this means with only a modest rise in the temperature of the element heat sinks; but, if a liquid coolant is used, care must be taken to avoid trapping any gas pockets or corona conditions may result leading to ultimate switch failure. Any fluid medium must be chemically and optically compatible with the means chosen for the introduction of the laser light to the silicon.

3.6.3 Equalization Design.

When switch elements are connected in series, provisions must be made for the small differences in various performance parameters. Experiments conducted on the USN supported program N00039-71-C-0028 indicate that the only equalization circuit required for the LASS consists of resistors in parallel with each active element to swamp out the differences in leakage current when the switch is in the "off" state. Each of these resistors will dissipate several watts to several tens of watts, and since ideally they would be incorporated within the switch case, their heat load must be added to that of the active elements for the total thermal system heat removal.

In addition, the resistors must have a configuration compatible with the shape of the switch case and the active elements, and they must be made from or coated with a material that is compatible with the fluid medium at the temperatures contemplated.

3.6.4 Inductance Considerations.

Figure 3.6-1 shows a coaxial arrangement that should aid in maintaining low inductance. Proper design of the illuminated area can

help to minimize the self-inductance. This area will require considerable analysis and iteration of various designs to arrive at an "acceptable" design approach.

3.6.5 Switch Package.

There are several problems that must be addressed during the design of the switch package. If the switch package were self-contained with the laser, laser power supplies, and control circuits integrated with the switch proper, such an arrangement would be likely to produce the minimum size and weight for the switch system. But, such an arrangement may not integrate well with the rest of the equipment involved in the application. For maintenance purposes, it may be desirable to have the output laser rod with its associated pumping lamp(s) (the only system component expected to require maintenance) located in an easily accessible area with the laser beam directed to the switch proper by mirrors or fiber optics cable.

The materials in the switch must be compatible with the fluid used for internal insulation/cooling over the anticipated operating and storage temperature range. If the light is transmitted to the silicon elements by mirrors, the optical properties of the fluid must be suitable so that there is not excessive absorption or distortion of the laser beam.

A coaxial design, similar in concept to the crude version shown in Figure 3.6-1 will be desirable to keep the inductance low. This may cause problems interconnecting the switch with the other components of the application. Although the resistive component and attenuation should be very low when conducting, the switch element should match the characteristic impedance of the interconnecting transmission lines to avoid undesirable reflections and losses.

3.6.6 Laser Light Source.

The laser light source is certainly critical from the standpoint of its importance to the LASS concept. There is also a very important question in the switch design that involves the laser; Where should the laser and its power supplies and controls be located?

Because of the physical size of the laser head and the power supplies, preliminary thinking is that a switch system should consist of two major components -- the switch proper, and a separate package containing the ancilliary components (laser, laser power supply and controls, and coolant pump and heat exchanger, if needed). This point must be discussed with the switch users to determine the best system configuration.

One component of the laser that must be considered carefully is the pumping lamp. This is the only component in the contemplated switch system that has a limited life associated with it. For this reason, it should be easily replaceable. For some applications, it may be desirable to use a multiple lamp arrangement to provide longer periods between scheduled maintenance and backup in case of failure. Under normal conditions, the period between scheduled lamp changes (routine maintenance) could exceed 600 hours or 10^{10} laser pulses, depending upon the mode of operation.

One of the most expensive components of the laser light source is the Q-switch and its control. A possible approach to improve the cost is the Frustrated Total Internal Reflection Acoustoptic Q-Switch (FTIR A-0). It is comparatively low in cost, even in small quantities, with promise of lower cost if produced in quantity. The laser pulse width produced with present designs is 15 to 20 nsec compared to the 10 to 15 nsec available from Pockels cells. Q-switch efficiency of about 90% has been obtained with a 1 cm diameter beam.

4.0 CONCLUSIONS AND RECOMMENDATIONS

4.1 Conclusions.

The specific performance goals of the contract were attained: current pulses of 40 μsec , 20,000 A peak, with a rise of 20,000 A/ μsec , at a repetition rate of 1 pulse per second were obtained on a number of occasions for durations exceeding 10 seconds. An analytic model was developed and coded in FORTRAN; the model faithfully predicts the forward voltage drop in the device. The model also predicts the temperature rise in the device; this value was confirmed experimentally to the extent that the model predicts device failure in the test fixture from excessive temperature after a number of pulses, and otherwise successful devices failed in this mode.

It is evident from the experimental work that the dI/dt limit of the LASS was not reached even at greater than 40,000 A/ μsec because, in the extended work reported, dI/dt values in excess of 10^6 A/ μsec were obtained. Obviously the circuit configuration is of more importance in determining the current rise time than is the LASS device. This is reasonable when one considers the configuration of the LASS: a very short (approximately 2 mm) current path length with a comparatively large (order of square centimeters) conducting area. It may be that, for circuits designed to operate at current rises in excess of 10^6 A/ μsec , special attention should be given to the configuration of the conducting area of the LASS so as to further reduce the device inductance.

A specific conclusion obtained from the experimental program is that the plasma spreading velocity is significantly higher at very high current densities ($>10,000$ A/cm²) than it is at the lower values of current density where measurements have previously been made.

Additional conclusions can be drawn from the analytical and experimental tasks as follows:

- a. As expected, the thermal design of the LASS device and its immediate environment is very important. Considerable heat is generated in a very localized region in the LASS during the current

pulse, and this heat must be removed effectively if the LASS is to survive repeated pulses. For pulses longer than a few microseconds, plasma spreading is an important consideration in increasing the electrical conduction area of the LASS. This is fortunate because, for these longer pulses, the major contribution to the heat buildup occurs during the pulse conduction rather than during the turn-on transient.

b. The electrical contact, especially at the cathode of the LASS, is crucial to the long life of the device. The experimental work clearly demonstrated that if, for any reason, the current must pass through a comparatively high resistance path, excessive heat will be generated in a very localized region. Since poor electrical contact also implies poor thermal contact, device failure is certain to follow very quickly. In the present program this problem was overcome by gold plating the cathode metallization to a thickness of about 50 μm . A superior metallurgical combination can be readily obtained when starting with a new device design.

c. The introduction of the light into the silicon wafer is an important design consideration for three reasons: (1) as much silicon as possible should be illuminated to reduce the subsequent electrical losses; (2) all of the area in an illuminated port or window must be illuminated in order to avoid a high resistance region leading to the failure mode described in (b) above; and (3) the laser light should be used as efficiently as possible to fire the LASS because it is relatively expensive in both initial cost for equipment and in energy conversion from the primary energy source. Thus the optical design must consider not only the direct introduction of the light into the silicon wafer, but also all of the other ramifications of collecting, transmitting, and dividing the light from the laser output into the silicon wafer. This program demonstrated the technical feasibility of using fiber optics cable to collect, transmit, and distribute equally the light from one laser to a plurality of illuminated regions.

These regions could obviously be all on one LASS element, as in the present case, or on various elements.

4.2 Recommendations.

A research program normally generates more questions than it can answer within its time and funding limitations. This program was normal in this respect. The program greatly increased the level of understanding how a LASS works and where its physical limits are, but much remains to be done before sufficient technology is available to design and fabricate a LASS system for operational use. Completion of the following tasks is recommended for a future research and development program. The items are not necessarily listed in the order of importance:

- Determine minimum light requirements
- Improve analytic model
- Explore means of coupling light into silicon
- Improve heat removal technique
- Develop improved instrumentation
- Measure dynamic forward drop
- Design, fabricate and evaluate a complete switch system
- Increase thyristor blocking voltage
- Create true ON-OFF switch

The following paragraphs elaborate upon each of these tasks.

4.2.1 Determine Light Requirements.

By combining very short (~ 100 nsec) current pulses with calorimetric techniques it should be possible to obtain an empirical relationship between the level of the light drive and the turn-on losses. The information so obtained would be the most important fundamental knowledge now missing. For a major question remaining on the LASS concept is how much laser light is needed for a given set of requirements. The theoretical analysis of Section 2.3.2 only sets upper limits. The present experimental program was unable to answer this question satisfactorily for two reasons: (1) the instrumentation to measure the

forward voltage drop was blinded during the time when the effect of changing the level of the light should be most significant ($< 1 \mu\text{sec}$); and (2) most of the thermal effects of the pulse were caused by the long (40 μsec) pulse length.

4.2.2 Improve Analytic Model.

The analytic model should continue to be improved by the addition of the information from 4.2.1 above and by the expansion of the scope of the device parameters considered by the model; e.g., the profile of the carrier density generated by the light trigger and how the carrier density changes spatially and temporally during the current pulse. Such improvements would help increase the effectiveness and versatility of the model and reduce the need for detailed experiments during switch system design.

4.2.3 Explore Means of Coupling Light into Silicon.

Because of the apparent importance of illuminating as large an area of the silicon as practical, preferably under a good electrical contact, means should be investigated to better distribute the light within the silicon. The investigation should include such obvious approaches as varying the surface finish of the window region and the possible use of optical waveguides as well as the use of beam splitters to introduce the light at Brewster's angle and other possibilities that may arise during the investigation. The use of the information generated by this investigation, coupled with the improved analytic model, would be expected to reduce significantly the light drive requirements and also to reduce the failure of devices because of poor electrical contact near the illuminated region.

4.2.4 Improve Heat Removal Technique.

The ultimate cause of the failures of the LASS devices is excessive heat. For this reason an investigation of means to improve the electrical and thermal contact between the device anode and cathode and the adjacent heat sink electrodes is in order. Coupled with this should be an analytical and experimental study to quantitatively determine the heat generated, the temperatures reached in the silicon, and the improvements in performance obtained by various approaches. This information should be iteritively incorporated into the improved analytic model of 4.2.2 above.

4.2.5 Develop Improved Instrumentation.

At present there is no known, reasonably priced instrumentation available to measure accurately a voltage in the range of 20-50 volts immediately after ($< 1 \mu\text{sec}$) the instrument is exposed to the forward blocking voltage (> 1000 volts) of the LASS device. It would seem that a combination of compensated attenuators, very fast gates, sample and hold units, and analog to digital converters coupled with a microprocessor could be arranged to determine a limited number of points accurately within a one-to-two microsecond test time. Conversion and readout, onto an oscilloscope or printed on a teletype or similar machine, could occur within a few seconds of the actual test. The ability to measure the transient forward drop while the LASS device was turning on would be a significant step in verifying or correcting the analytic model; and it would thus aid the device designer to evaluate the effect of changing other design parameters. This parameter is also of importance to the ultimate user because it determines the effective efficiency of the switch.

4.2.6 Measure Dynamic Forward Drop.

Once the instrumentation to measure the transient V_F (as described in (e) above) is available, an analytic and experimental study should be undertaken to measure V_F under a variety of LASS device designs and operating conditions. The primary purpose of this study is to supply information to improve the analytic model and to perform a sufficient number of controlled experiments to verify the predictions of the model.

4.2.7 Design, Fabricate, and Evaluate a Complete Switch System.

It would be appropriate, once the basic information discussed above were available, to design a complete light activated silicon switch system of modest rating, perhaps 10 kA peak current and 10 kV blocking voltage, to force careful examination of all of the interfaces between the electrical, thermal, and optical components of the system. Fabrication and evaluation of a limited number of such switches would demonstrate that the technology then exists for the operational use of the LASS system.

4.2.8 Increase Thyristor Blocking Voltage.

Because the LASS presently has limited voltage capability (a few kV) in each unit, it must be connected in series for high voltage applications. Although this is advantageous in covering a wide range of voltage systems (the LASS is, in effect, modular, and only the packaging of varying quantities of devices need be changed for various voltage requirements), for very high voltage systems this may become cumbersome. Therefore, a study to determine how the blocking voltage of each element could be raised significantly would be appropriate. There are several possible approaches that such a study could consider, but these details are beyond the scope of this document.

4.2.9 Create True ON-OFF Switch.

The present LASS is a "turn-on" device only: some external construction in the overall circuit, such as a pulse forming network, is required to reduce the current to near zero value so that the LASS can turn-off. It would be desirable, and it seems possible, to have a LASS that would turn-off as well as turn-on. A study of the various approaches to obtaining a true "switch" that is activated optically would be likely to lead to one or more such devices.

Accomplishment of the above tasks will require several years. There are already indications that various military and civil (isotope separation and advanced fusion power experiments) programs will require the LASS to meet their objectives in the early to mid 1980's. Unless development is pursued promptly, the LASS will not be available when needed.

REFERENCES

1. F.E. Gentry, et al, Semiconductor Controlled Rectifiers; Prentice-Hall, Englewood Cliffs, NJ (1964).
A. Blichter, Thyristor Physics; Springer-Verlag, New York, NY (1976).
2. H. Yamasaki, IEEE Trans. Electron Devices, Vol. ED-22, pp. 65-69 (1975).
H.J. Ruhl, Jr., IEEE Trans. Electron Devices, Vol. ED-17, pp.478-484 (1966).
I. Somos and D.E. Piccone, loc. cit., pp. 680-687.
3. D.E. Lencioni, APL 25, No. 1, 1 July 74, pp. 15-17.

APPENDICES

APPENDIX I

COMPUTER LISTINGS

APPENDIX I-1

Thermal Program for Infinite Silicon Slab

```

1-10)
C      PROGRAM WRITTEN JUNE 1974
C
C      CALCULATE THE DECAY IN THE THERMAL DIFFERENCE BETWEEN POINTS IN THE
C      SILICON SLICE AND THE AMBIENT. INFINITE HORIZONTAL SLAB ASSUMED.
C
C      DEFINITIONS ARE AS FOLLOWS
C
C      DLTA      IS A DUMMY DLTA USED IN THE CALCULATION OF THE
C      DLTA(I)    WHICH ARE THE DLTA'S OF THE THERMAL
C                  CALCULATION. DLTA(I) = N(I)* X.
C
C      H        = COEFFICIENT OF HEAT TRANSFER ACROSS FACE OF SLICE
C
C      K        = COEFFICIENT OF HEAT TRANSFER OF THE SILICON
C
C      X        = 1/2 THE THICKNESS OF THE SILICON
C
C      THETA(I) = THE CALCULATED VALUE OF THE TEMPERATURE AT A GIVEN
C                  TIME AND PLACE. IT IS CALCULATED FOR 20 VALUES OF
C                  TIME. REFER TO STEP
C
C      THETAZ    = THE INITIAL VALUE OF THE TEMPERATURE DIFFERENCE
C                  BETWEEN THE CENTER OF THE SLICE AND THE AMBIENT
C
C      ALPHA    = THERMAL DIFFUSIVITY OF SILICON
C
C      T        = TIME IN MICROSECONDS
C
C      FX       = F(DLTA(I)) IN THE SUCCESSIVE LIMITS APPROXIMATION
C
C      U        = THE NUMBER OF COMBINATIONS OF H,K, X, AND ALPHA
C
C      F        = THE NUMBER OF COMBINATIONS OF EKS AND THETAZ
C
C      EKS      = THE DISTANCE FROM THE MIDPLANE TO THE POINT WHERE
C                  THE TEMPERATURE IS BEING CALCULATED.
C
C      A(I)     = THE COEFFICIENTS OF THE EXPANSION OF THETA(I)
C
C      U(I)     = THE EXPONENT ASSOCIATED WITH THE TIME OF DECAY
C
C
C      THE PROGRAM IS SELF CHECKING TO PREVENT LOOPING IN THE CALCULATION
C      OF THE DLTA(I). FLAGS ARE PRINTED IF CERTAIN CRITERIA ARE NOT MET.
C      THE PROGRAM ATTEMPTS ALL OF THE DLTA(I) FOR EACH SET OF H,K, AND X.
C      BUT WILL NOT TRY TO CALCULATE THE A(I), U(I), OR THE THETA(I) FOR
C      THOSE VALUES FOR WHICH THE DLTA(I) ARE UNSUCCESSFUL.
C
C
C      INPUT DATA AS FOLLOWS
C
C      H, K, X, AND ALPHA IN FORMAT 4F10.5
C
C      EKS, THETAZ IN FORMAT 2F10.5
C
C      NEW VALUES OF EKS AND THETAZ UNTIL ALL DESIRED FOR THIS SET
C      OF H, K, L, AND ALPHA
C
C      0.0 AND 0.0 IN FORMAT 2F10.5
C
C      NEW VALUES OF H, K, L, AND ALPHA
C
C      EKS, THETAZ, ETC.
C
C      REPEAT SEQUENCE UNTIL ALL DATA IS ENTERED.
C
C      LAST EKS AND THETAZ VALUE ENTERED IS TO BE 0.0 AND 0.0
C
C      -5. , U. , 0. , 0. IN 4F10.5 WILL CAUSE PROGRAM TO TERMINATE
C
C      DIMENSION DLTA(75),A(75),U(75)
C      REAL H,K,X,DLTAA,DLTA,A,U,ALPHA,THETAZ,THETAU,THETA,EKS

```

0
0

DAT

```

0103:      INTEGER I,M, R,R,T
C
C
C
C      READ AND STORE ALL OF THE VALUES OF H,K,X, AND ALPHA
C
0104:      10 READ 1100, H,K,X,ALPHA
0105:      IF ( H .LT. 0.0 .AND.
1          K .EQ. 0.0 .AND.
2          X .EQ. 0.0 .AND.
3          ALPHA .EQ. 0.0 ) STOP
C
C
C      MAIN DO LOOP THAT CALCULATES AND PRINTS ALL OF THE DESIRED VALUES
C      OF THETA(X,T) AND THE INPUT PARAMETERS.
C
C
C      SET COUNTER TO PREVENT MEANINGLESS CALCULATION OF THETA IF THE
C      DELTA'S DO NOT CONVERGE
C
0106:      H = U
C
C      CALCULATE THE DELTA(I) FOR THE GIVEN VALUES OF H,K, AND X
0107:      DO 175 I = 1,50
C
C      SET UP THE COUNTER FOR THE NUMBER OF ITERATIONS
0110:      R = 0
C
C      SET THE VALUES OF THE UPPER AND LOWER LIMITS FOR EACH VALUE OF I
C
0111:      DLOWR = ( 1 - 1 ) * 3.1415927 + 1.0E-4
0112:      DUPR = ( 2 * 1 - 1 ) * 1.5707963 - 1.0E-4
C      START WITH THE MIDPOINT
0113:      20 DELTAA = ( DUPR + DLOWR ) / 2
C
C      IF THE DIFFERENCE IN LIMITS IS NEGLIGIBLE, GO TO NEXT I
0114:      IF ( ABS ( DUPR - DLOWR ) .LT. 1.0E-5 ) GO TO 125
C
C      CALCULATE THE VALUE OF FX
C
0115:      FX = ( (K * DELTAA ) / ( H * X ) ) - (COS(DELTAA)/SIN(DELTAA))
C
C      ADVANCE THE ITEATION COUNTER. STOP IF 50
0116:      R = R + 1
0117:      IF ( R .EQ. 51 ) GO TO 505
C
C      IF FX NEAR ZERO, GO TO NEXT I
0120:      IF ( ABS (FX) .LT. 1.0E-5 ) GO TO 125
C

```

DATE

```

C      DETERMINE WHICH LIMIT TO REPLACE BY DLTA AND DO IT
C
0121:      IF (FA) 40,125,25
0122:      25      DUPR = DLTA
0123:      GO TO 20
0124:      40      DLOWR = DLTA
0125:      GO TO 20
0126:      505     PRINT 2000, 1,DLTA, R
C
C      ADVANCE COUNTER FOR FAILURE TO CONVERGE
0127:      B = B + 1
0130:      125     DLTA(I) = DLTA
0131:      175     CONTINUE
C      IF THERE HAS BEEN NON-CONVERGENCE, GO TO THE NEXT VALUE OF X*H/K
C
0132:      IF ( B .GT. 0 ) GO TO 10
C
C      CALCULATE THE A(I) AND U(I)
0133:      DO 150 I=1,50
0134:      A(I) = ( SIN(DLTA(I)) ) / ( ( SIN(DLTA(I)) ) * ( COS(DLTA(I)) ) +
          1      DLTA(I) )
0135:      U(I) = ( (DLTA(I) **2) * ALPHA ) / ( X**2 )
0136:      150     CONTINUE
C
C      PRINT HEADINGS AND THE J, DLTA(J),A(I) AND U(I) FOR THE GIVEN
C      VALUES OF H, K, X, AND ALPHA
0137:      PRINT 2100, H,K,X,ALPHA
0140:      PRINT 2200
0141:      PRINT 2250, ( 1, DLTA(I), A(I), U(I), I =1,50 )
C
C      READ THE SPACIAL COORDINATE EKS AND THE MIDPLANE TEMP RISE THETAZ
C
0142:      80 READ 1100, EKS,THETAZ
0143:      IF ( EKS .EQ. 0.0 .AND. THETAZ .EQ. 0. ) GO TO 10
0144:      T = 1
0145:      N = 1
0146:      PRINT 2300, EKS, THETAZ
0147:      PRINT 2400
C
C      CALCULATE THE TEMPERATURE RISE FOR EACH VALUE OF TIME FOR THE
C      GIVEN SPATIAL POSITION
C
0150:      DO 100 N=1,20
0151:      THETA = 0
0152:      DO 90 I =1,50
0153:      UA = U(I) * T*(1.0E-6)
0154:      IF (UA .GE. 80.) GO TO 90
0155:      IF ( UA .GE. 68. .AND. A(I) .LT. 1.E-8 ) GO TO 90
0156:      THETAD = 2. * THETAZ * A(I) * (EXP( -( U(I) * T *
          1      1.0E-6 ))) * COS(DLTA(I) * EKS / A )
0157:      THETA = THETA + THETAD
0160:      IF ( ABS ( THETAD ) /THETA .LT. 1.E-4 ) GO TO 95
0161:      90      CONTINUE
0162:      95      PRINT 2450 ,T, THETA

```


DATE

```

C
C      DETERMINE NEXT INCREMENT FOR T AND CONTINUE UNTIL 20 VALUES HAVE
C      BEEN CALCULATED.
C
0163:      IF (M=2) 600, 610, 620
0164: 600      T = 2 * T
0165:      M = M + 1
0166:      GO TO 100
0167: 610      T = 2.5 * T
0170:      M = M + 1
0171:      GO TO 100
0172: 620      T = 2 * T
0173:      M = 1
0174: 100      CONTINUE
0175:      GO TO 80

C
C
C
C
C
C
C
C
C
0176: 1100 FORMAT ( 4F10.5)
0177: 2000 FORMAT ( ' DELTA FAILS TO CONVERGE FOR I=',I3,' DELTA=',F10.5,
1          ' R=',I3 )
0200: 2100 FORMAT (1H0.5X,' H=',1PE12.5,' , K=',1PE12.5,' , X=',1PE12.5,
1          ' , ALPHA=',1PE12.5 //)
0201: 2200 FORMAT ( 12X,' I', 8X,' DELTA(I) ',10X,' A(I) ',10X,' U(I) ' / )
0202: 2250 FORMAT ( 10X,I3,3E18.5)
0203: 2300 FORMAT (1H0.5X,' EKS=',1PE12.5, ' THETAZ =',1PE12.5 // )
0204: 2400 FORMAT ( 10X,' T',8X,' THETA(T)' / )
0205: 2450 FORMAT ( 10X,I7, F14.5)
0206:      END

```

3 THE SYMBOL 'N' OCCURS ONLY ONCE IN THE PROGRAM.

THIS PAGE IS BEST QUALITY PRINTING
 FROM GARY F. HARRIS, JR.

APPENDIX I-2

Thermal Program for Composite Material Infinite
Lateral Extent Repetition Pulses

AD-A080 567

WESTINGHOUSE RESEARCH AND DEVELOPMENT CENTER PITTSBU--ETC F/G 9/1
OPTICALLY ACTIVATED SWITCH.(U)
APR 78 L R LOWRY

UNCLASSIFIED

AFAPL-TR-78-17

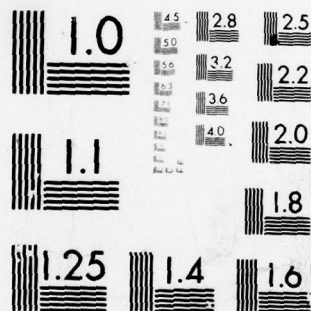
F33615-74-C-2029

NL

3 OF 4

AD
A080567





MICROCOPY RESOLUTION TEST CHART
NATIONAL BUREAU OF STANDARDS-1963-A

01/74-1109:19 (,0)

RAM

SET CODE(1) 000726; DATA(0) 151367; BLANK COMMON(2) 000000

REFERENCES (BLOCK, NAME)

INTRS

ICRS

SCRS

NRCDs

NPRTS

IN

OS

XP

STOPS

ASSIGNMENT (BLOCK, TYPE, RELATIVE LOCATION, NAME)

| | | | | | | |
|--------------|--------|---------------|--------|---------------|--------|---------------|
| 50710 1001F | 0001 | 000141 101L | 0000 | 150713 1012F | 0000 | 150715 1021F |
| 50743 1041F | 0000 | 150747 1051F | 0000 | 150750 1061F | 0000 | 150762 1071F |
| 51013 1091F | 0000 | 151113 1100 | 0000 | 151117 1126 | 0000 | 151130 1230 |
| 00345 125L | 0000 | 151140 1310 | 0000 | 151154 1470 | 0000 | 151162 1516 |
| 51177 1646 | 0000 | 151203 1700 | 0001 | 000271 20L | 0000 | 151214 2000 |
| 51030 2011F | 0000 | 151043 2021F | 0000 | 151046 2031F | 0000 | 151062 2041F |
| 00114 2106 | 0001 | 000132 2176 | 0000 | 151224 2270 | 0000 | 151230 2316 |
| 00156 2406 | 0000 | 151237 2420 | 0000 | 151245 2570 | 0001 | 000231 2776 |
| 51262 3010 | 0000 | 151272 3100 | 0001 | 000247 3136 | 0001 | 000703 3251 |
| 00333 35L | 0001 | 000355 3516 | 0000 | 151302 3570 | 0001 | 000674 360L |
| 51317 3740 | 0001 | 000431 3776 | 0001 | 000677 400L | 0001 | 000512 4046 |
| 51322 4470 | 0001 | 000336 505L | 0001 | 000722 600L | 0000 R | 005154 A |
| 50475 B | 0000 R | 004057 DIA | 0000 R | 004164 DLOWR | 0000 R | 004170 DLTA |
| 04165 DUPER | 0000 R | 004167 FX | 0000 R | 004126 H | 0000 R | 000045 HI |
| 50444 IDENT | 0000 R | 000137 INPTS | 0000 I | 150706 J | 0000 I | 150663 JERRY |
| 04102 KA | 0000 R | 000012 KA1 | 0000 I | 150677 KB | 0000 I | 150676 KC |
| 50462 MAT | 0000 R | 004070 MATL | 0000 R | 000001 MATRIL | 0000 I | 000000 MAX |
| 50447 N1 | 0000 I | 150701 N2 | 0000 I | 150655 N3 | 0000 I | 150656 N4 |
| 50202 N6 | 0000 I | 150657 PERIOD | 0000 I | 150650 PL | 0000 I | 150654 POINTH |
| 04114 RHO | 0000 R | 000034 RH01 | 0000 R | 004140 SPHT | 0000 R | 000023 SPHT1 |
| 07124 THETA2 | 0000 R | 007125 THETA1 | 0000 R | 047775 THETA2 | 0000 R | 150445 THETA1 |
| 50652 T1 | 0000 I | 150653 TT | 0000 R | 006140 U | 0000 R | 150707 UA |
| 00126 X | | | | | | |

- C PROGRAM WRITTEN AUGUST, 1974
- C CALCULATES INSTANTANEOUS TEMPERATURE AT MIDPOINT OF SILICON SLICE
- C AND ON EACH SIDE OF EACH INTERFACE OF FUSION
- C ASSUMES CATHODE - ANODE SINK SYMMETRY
- C DEFINITIONS ARE AS FOLLOWS
- C ΔT_{AA} = A DUMMY ΔT_{AA} USED IN THE CALCULATION OF THE

```

C      DLTA(I)      = WHICH ARE THE DLTA'S OF THE THERMAL CALCULATION.
C      HIL(I+1)    = COEFFICIENT OF HEAT TRANSFER BETWEEN SLICE I AND
C                      SLICE I+1
C      K(I)         = COEFFICIENT OF THERMAL CONDUCTIVITY OF SLICE (I)
C      X(I)         = THICKNESS OF THE SLICE (I)
C      THETA(T)     = THE CALCULATED VALUE OF THE TEMPERATURE AT A GIVEN
C                      TIME AND PLACE.
C      THETAZ       = THE INITIAL VALUE OF THE TEMPERATURE DIFFERENCE
C                      BETWEEN THE CENTER OF THE SLICE AND THE AMBIENT
C
C
C      ALPHA(I)     = THERMAL DIFFUSIVITY OF SILICON
C      T            = TIME IN MICROSECONDS
C      FA           = F(DLTA) IN THE BINARY LIMITS APPROXIMATION USED TO
C                      CALCULATE THE DLTA(I).
C      EKS(I)       = EFFECTIVE THICKNESS OF THE SLICE UNDER IMMEDIATE
C                      CONSIDERATION. EKS(I) = X/2. ALL OTHER EKS(I)=X(I)
C      A(I)         = THE COEFFICIENTS OF THE EXPRESSION THETA(I)
C      U(I)         = THE EXPONENT ASSOCIATED WITH THE TIME OF DECAY

```

```

C THE PROGRAM IS SELF CHECKING TO PREVENT LOOPING IN THE CALCULATION
C OF THE DLTA(I). FLAGS ARE PRINTED IF CERTAIN CRITERIA ARE
C NOT MET. THE PROGRAM ATTEMPTS ALL OF THE DLTA(I) FOR EACH
--C SET OF H, K, AND X, BUT WILL NOT TRY TO CALCULATE THE A(I),U(I),
C OR THE THETA(I) FOR THOSE VALUES FOR WHICH THE DLTA(I)
C ARE UNSUCCESSFUL. THE PROGRAM THEN TERMINATES.

```

C INPUT DATA AS FOLLOWS

THIS PAGE IS BEST QUALITY PRACTICE

DATE

```

C
C
C
C
C
REAL MATRIL(9),KAI(9),SPHTI(9),RHOI(9),HI(9), NCRMNT(40),X(9) 1010
REAL INPTS(2000),DIA(9),MATL(10),KA(10),RHO(10),H(10),SPHT(10) 1012
REAL ALPHA(10),DLOWR,DUPER,DLTAA,FX,DLTA(10,50),A(10,50) 1014
REAL U(10,50),THETAZ,THETA1(10,2500),THETA2(10,2500),THETD1,THETD2 1016
INTEGER NI,PL,PPS,TI,TT,POINTV,N3,N4,PERIOD,N5,ULIM,MAT,JERRY 1020
INTEGER IDENT(9),B,KC,KB,T,MAX,N2,N6,KD 1022
C READ AND STORE ALL OF THE MATERIALS PARAMETERS 1030
READ 1001 (MATRIL(I),IDENT(I),KAI(I),SPHT(I),RHO(I),H(I),I=1,9) 1040
READ 1012 (NCRMNT(I),I=1,40) 1050
READ 1051 (NI,PL,PPS,TI,TT,POINTV ) 1060
N2 = TI * 1000. / T1 1070
N6 = POINTV / T1 1075
C CALCULATE THE INCREMENTAL TEMPERATURE IN THE SILICON CRYSTAL 1080
C DUE TO THE CONDUCTING PULSE 1081
PERIOD = 1.E6 / PPS 2000
N3 = PL / T1 2010
N4 = PERIOD / T1 2020
N5 = 1 2030
PRINT 1001 (MATRIL(I),IDENT(I),KAI(I),SPHT(I),RHO(I),H(I),I=1,9) 2031
PRINT 1012 (NCRMNT(I),I=1,40) 2031
PRINT 2051 (NI,PL,PPS,TI,TT,POINTV ) 2031
PRINT 2031 (N2,N6,PERIOD,N3,N4 ) 2031
DO 101 K = 1, N4 2050
INPTS(K) = 0. 2055
IF (K.GT. N3 ) GO TO 101 2070
ULIM = N5 + T1 = 1 2080
DO 111 J = N5, ULIM 2090
INPTS(K) = NCRMNT(J) + INPTS(K) 2100
111 CONTINUE 2110
N5 = N5 + T1 2120
101 CONTINUE 2130
PRINT 1012 (INPTS(K),K=1,N4) 2140
PRINT 1031 2170
C INPUT THE MATERIALS IN ORDER FROM THE CENTER OUT. ASSIGN PROPER 2180
C VALUES TO THE PARAMETERS AND CALCULATE THE ALPHA'S AND XI. 2190
DO 131 MAT = 1, NI 2200
READ 1021 (JERRY, X(MAT), DIA(MAT)) 2210
MATL(MAT) = MATRIL (JERRY) 2220
KA(MAT) = KAI(JERRY) 2230
RHO(MAT) = RHOI(JERRY) 2240
H(MAT) = HI(JERRY) 2250
SPHT(MAT) = SPHTI(JERRY) 2260
IF (MAT.EQ. 1 ) X = X / 2 2270
ALPHA(MAT) = KA(MAT) / ( RHO(MAT) * SPHT(MAT) ) 2280
PRINT 1041 (MATL(MAT),KA(MAT),RHO(MAT),H(MAT),SPHT(MAT),X(MAT), 2290
MAT,JERRY,DIA(MAT),ALPHA(MAT) ) 2291
131 CONTINUE 2300
C CALCULATE THE DLTA'S, A'S, AND THE U'S 2310
C SET COUNTER TO PREVENT MEANINGLESS CALCULATION IF COVERGENCE PROBLEM 2320
B=0 2330
DO 200 MAT= 1,NI 2340

```


| | DAT |
|---|------|
| PRINT 1071, H(MAT), KA(MAT), X(MAT), ALPHA(MAT), MATL(MAT) | 2350 |
| PRJNT 1081 | 2360 |
| DO 175 J = 1, 50 | 2370 |
| DLOWR = (J - 1) * 3.1415927 + 1.0E-4 | 2380 |
| DUPER = (2 * J - 1) * 1.5707963 - 1.0E-4 | 2390 |
| 20 DLTA = (DUPER + DLOWR) / 2 | 2400 |
| IF (ABS (DUPER - DLOWR) .LT. 1.0E-5) GO TO 125 | 2410 |
| FX = ((KA(MAT) * DLTA) / (H(MAT) * X(MAT))) - | 2420 |
| 1 (COS(DLTA) / SIN(DLTA)) | 2421 |
| IF (J .EQ. 51) GO TO 505 | 2430 |
| IF (ABS (FX) .LT. 1.0E-5) GO TO 125 | 2440 |
| IF (FX) 35, 125, 25 | 2450 |
| 25 DUPER = DLTA | 2460 |
| GO TO 20 | 2470 |
| 35 DLOWR = DLTA | 2480 |
| GO TO 20 | 2490 |
| 505 PRINT 2001, J, DLTA | 2500 |
| B = B + 1 | 2510 |
| 125 DLTA(MAT,J) = DLTA | 2520 |
| 175 CONTINUE | 2530 |
| IF (B .GT. 0) GO TO 600 | 2540 |
| DO 150 J = 1, 50 | 2550 |
| A(MAT,J) = (SIN(DLTA(MAT,J))) / ((SIN(DLTA(MAT,J))) * (COS(DLTA(MAT,J))) + DLTA(MAT,J)) | 2560 |
| 1 U(MAT,J) = (((DLTA(MAT,J)) ** 2) * ALPHA(MAT)) / (X ** 2) | 2570 |
| 150 CONTINUE | 2580 |
| PRINT 1091 (J, DLTA(MAT,J), A(MAT,J), U(MAT,J), J = 1, 50) | 2590 |
| 200 CONTINUE | 2600 |
| KD = 0 | 2700 |
| KC = 0 | 2720 |
| PRINT 2011 | 2770 |
| DO 300 K = 1, N2 | 2780 |
| KB = K - 1 | 2790 |
| KC = KC + 1 | 2800 |
| KD = KD + 1 | 2820 |
| T = T1 + K | 2840 |
| DO 325 MAT = 1, N1 | 2860 |
| MAX = MAT - 1 | 2880 |
| IF (K .EQ. 1 .AND. MAT .EQ. 1) THETAZ = 20.46 | 2900 |
| IF (K .EQ. 1 .AND. MAT .GT. 1) THETAZ = 0 | 2920 |
| IF (K .GT. 1 .AND. KD .NE. N4 .AND. MAT .EQ. 1) THETAZ = | 2930 |
| 1 THETA1(KB) | 2931 |
| IF (KD .EQ. N4 .AND. MAT .EQ. 1) THETAZ = THETA1(1, KB) + 20.46 | 2940 |
| IF (K .GT. 1 .AND. MAT .GT. 1) THETAZ = THETA2(MAX, KB) | 2960 |
| THETA1(MAT, K) = 0 | 2980 |
| THETA2(MAT, K) = 0 | 3000 |
| DO 350 J = 1, 30 | 3020 |
| UA = U(J) * T1 * 1.E-6 | 3030 |
| IF (UA .GE. 80.) GO TO 360 | 3032 |
| IF (UA .GE. 68. .AND. A(J) .LT. 1.E-8) GO TO 360 | 3034 |
| THETD1 = 2. * THETAZ * A(MAT, J) * EXP(-(U(MAT, J) * T1 * 1.E-6 | 3040 |
| 1)) | 3051 |
| THETA1(MAT, K) = THETA1(MAT, K) + THETD1 | 3060 |
| THETD2 = THETD1 * COS(DLTA(MAT, J)) | 3080 |
| THETA2(MAT, K) = THETA2(MAT, K) + THETD2 | 3100 |
| 350 CONTINUE | 3120 |

| | | |
|------|---|------|
| 360 | CONTINUE | 3125 |
| | IF (KC .EQ. N6) GO TO 400 | 3130 |
| | GO TO 325 | 3132 |
| 400 | PRINT 2021 (T, THETA1 (MAT, K1), THETA2 (MAT, K1), MATL (MAT)) | 3134 |
| 325 | CONTINUE | 3140 |
| | IF (KD .EQ. N4) KD = 0 | 3140 |
| | IF (KC .EQ. N6) KC = 0 | 3170 |
| | GO TO 300 | 3180 |
| 300 | CONTINUE | 3260 |
| 1001 | FORMAT (A5, 15, 4F10.5) | |
| 1012 | FORMAT (8F10.5) | |
| 1021 | FORMAT (15, 2F10.5) | |
| 1031 | FORMAT (/ MATL, 5X, KA, 6X, RHO, 7X, H, 6X, SPHT, 8X, X, L 10X, MAT, 5X, JERRY, DIA, 6X, ALPHA) | |
| 1041 | FORMAT (A5, 5F10.5, 2110, 2F10.5) | |
| 1051 | FORMAT (615) | |
| 1061 | FORMAT (' CALCULATED VALUES OF TEMPERATURE PULSE FOR ONE PERIOD') | |
| 1071 | FORMAT (11H1, 3X, H, F7.4, KA, F7.4, X, F7.4, ALPHA, F7.4, I MATL IS, A5 /) | |
| 1081 | FORMAT (12X, J, 8X, DLTA (J), 10X, A (J), 10X, U (J) /) | |
| 1091 | FORMAT (10X, 13, 3E18.5) | |
| 2001 | FORMAT (' DLTA FAILS TO CONVERGE FOR J=, 13, DLTA=, F10.5 -) | |
| 2011 | FORMAT (11H1, 5X, T, 12X, THETA1, 5X, THETA2, MATERIAL) | |
| 2021 | FORMAT (110, 2F14.5, A7) | |
| 2031 | FORMAT (3X, N2, 17, N6, 15, PERIOD=, 116, N3, 15, L N4, 15) | 2031 |
| 2041 | FORMAT (3X, THETAZ=, F10.6, THETA1=, F10.6, THETA2=, F10.6) | |
| 2051 | FORMAT (5X, N1, 13, PL, 13, PPS, 14, T1, 15, T2, I 15, POINTV=, 15) | |
| 400 | STOP | |
| | END | 3280 |

COMPILATION: NO DIAGNOSTICS.

THIS PAGE IS NOT QUALITY PRINTED
FROM GSA Form 44-481

0AT

N1= 5 PL= 40 PPS= 500 IT= 50 POINTV= 500
 N2= 100 N6= 1 PERIOD= 2000 N3= 0 N4= 4
 .00000 .00000 .00000

| MATL | KA | RHO | M | SPHT | X | MAT | JERRY DIA | ALPHA |
|------|---------|----------|----------|---------|---------|-----|-----------|---------|
| SI | 1.25000 | 2.32260 | 20.00000 | .71130 | .02540 | 1 | 1 5.00000 | .75436 |
| PS | .83500 | 2.32260 | 20.00000 | .71130 | .10160 | 2 | 8 5.00000 | .50391 |
| MO | 1.78000 | 19.35000 | 20.00000 | .13390 | .25400 | 3 | 5 5.00000 | .49700 |
| BE | 2.18000 | 1.85000 | 20.00000 | 1.82420 | .12700 | 4 | 3 5.00000 | .64597 |
| CU | 3.98000 | 8.92000 | 20.00000 | .38490 | 1.00000 | 5 | 7 5.00000 | 1.15923 |

| T | THETA1 | THETA2 | MATERIAL |
|------|----------|----------|----------|
| 500 | 17.58145 | 14.54185 | SI |
| 500 | .000000 | .000000 | PS |
| 500 | .000000 | .000000 | WO |
| 500 | .000000 | .000000 | BE |
| 500 | .000000 | .000000 | CU |
| 1000 | 15.10789 | 12.49593 | SI |
| 1000 | 10.49033 | 4.45423 | PS |
| 1000 | .000000 | .000000 | WO |
| 1000 | .000000 | .000000 | BE |
| 1000 | .000000 | .000000 | CU |
| 1500 | 12.98234 | 10.73786 | SI |
| 1500 | 9.01443 | 3.82756 | PS |
| 1500 | 2.56336 | .97946 | WO |
| 1500 | .000000 | .000000 | BE |
| 1500 | .000000 | .000000 | CU |
| 2000 | 28.73729 | 23.76898 | SI |
| 2000 | 7.74618 | 3.28905 | PS |
| 2000 | 2.20272 | .84166 | WO |
| 2000 | .73296 | .45134 | BE |
| 2000 | .000000 | .000000 | CU |
| 2500 | 24.69420 | 20.42489 | SI |
| 2500 | 17.14668 | 7.28054 | PS |
| 2500 | 1.89281 | .72324 | WO |
| 2500 | .62984 | .38784 | BE |
| 2500 | .11845 | .02998 | CU |
| 3000 | 21.21994 | 17.55128 | SI |
| 3000 | 14.73429 | 6.25623 | PS |
| 3000 | 4.18987 | 1.60095 | WO |
| 3000 | .54123 | .33328 | BE |
| 3000 | .10178 | .02576 | CU |
| 3500 | 18.23447 | 15.08197 | SI |
| 3500 | 12.66130 | 5.37603 | PS |
| 3500 | 3.60039 | 1.37571 | WO |
| 3500 | 1.19805 | .73773 | BE |
| 3500 | .08246 | .02214 | CU |
| 4000 | 33.25049 | 27.50191 | SI |
| 4000 | 10.87996 | 4.61967 | PS |
| 4000 | 3.09385 | 1.18216 | WO |
| 4000 | 1.02949 | .63394 | BE |
| 4000 | .19360 | .04901 | CU |
| 4500 | 26.57243 | 23.63263 | SI |
| 4500 | 19.63957 | 8.42395 | PS |
| 4500 | 2.65857 | 1.01584 | WO |
| 4500 | .88465 | .54475 | BE |
| 4500 | .16637 | .04211 | CU |
| 5000 | 24.55253 | 20.30772 | SI |
| 5000 | 17.04832 | 7.23877 | PS |
| 5000 | 4.84789 | 1.85238 | WO |
| 5000 | .76019 | .46811 | BE |
| 5000 | .14296 | .03619 | CU |
| 5500 | 21.09820 | 17.45060 | SI |
| 5500 | 14.64976 | 6.22034 | PS |
| 5500 | 4.16583 | 1.59177 | WO |
| 5500 | 1.38620 | .85359 | BE |
| 5500 | .12285 | .03110 | CU |

| | | | |
|-------|----------|----------|----|
| 6000 | 35.71132 | 29.53729 | SI |
| 6000 | 12.58867 | 5.34519 | PS |
| 6000 | 3.57974 | 1.36782 | WO |
| 6000 | 1.19117 | .73350 | BE |
| 6000 | .22401 | .05670 | CU |
| 6500 | 30.68704 | 25.38125 | SI |
| 6500 | 21.30788 | 9.04739 | PS |
| 6500 | 3.07610 | 1.17538 | WO |
| 6500 | 1.02359 | .63030 | BE |
| 6500 | .19249 | .04873 | CU |
| 7000 | 26.36964 | 21.81067 | SI |
| 7000 | 18.31004 | 7.77950 | PS |
| 7000 | 5.20667 | 1.98947 | WO |
| 7000 | .87958 | .54162 | BE |
| 7000 | .16541 | .04187 | CU |
| 7500 | 22.65965 | 18.74209 | SI |
| 7500 | 15.73397 | 6.68070 | PS |
| 7500 | 4.47414 | 1.70957 | WO |
| 7500 | 1.48879 | .91676 | BE |
| 7500 | .14214 | .03598 | CU |
| 8000 | 37.05309 | 30.64709 | SI |
| 8000 | 13.52034 | 5.74078 | PS |
| 8000 | 3.84467 | 1.46905 | WO |
| 8000 | 1.27933 | .78278 | BE |
| 8000 | .24059 | .06090 | CU |
| 8500 | 31.84003 | 26.33530 | SI |
| 8500 | 22.10847 | 9.38733 | PS |
| 8500 | 3.30376 | 1.26237 | WO |
| 8500 | 1.09934 | .67695 | BE |
| 8500 | .20674 | .05233 | CU |
| 9000 | 27.36041 | 22.63015 | SI |
| 9000 | 18.99800 | 8.06661 | PS |
| 9000 | 5.40230 | 2.06422 | WO |
| 9000 | .94467 | .58171 | BE |
| 9000 | .17765 | .04497 | CU |
| 9500 | 23.51104 | 19.44628 | SI |
| 9500 | 16.32514 | 6.93171 | PS |
| 9500 | 4.64225 | 1.77380 | WO |
| 9500 | 1.54473 | .95121 | BE |
| 9500 | .15266 | .03864 | CU |
| 10000 | 37.78469 | 31.25220 | SI |
| 10000 | 14.02833 | 5.95648 | PS |
| 10000 | 3.98912 | 1.52425 | WO |
| 10000 | 1.32740 | .81738 | BE |
| 10000 | .24963 | .06319 | CU |
| 10500 | 32.46870 | 26.85528 | SI |
| 10500 | 22.54499 | 9.57268 | PS |
| 10500 | 3.42789 | 1.30980 | WO |
| 10500 | 1.14065 | .70238 | BE |
| 10500 | .21451 | .05430 | CU |
| 11000 | 27.90063 | 23.07698 | SI |
| 11000 | 19.37311 | 8.22588 | PS |
| 11000 | 5.50897 | 2.10498 | WO |
| 11000 | .98017 | .60356 | BE |
| 11000 | .18433 | .04666 | CU |
| 11500 | 23.97525 | 19.83024 | SI |

| | | | |
|-------|----------|----------|----|
| 11500 | 16.64748 | 7.06857 | PS |
| 11500 | 4.73391 | 1.80883 | WO |
| 11500 | 1.57523 | .96999 | BE |
| 11500 | .15840 | .04010 | CU |
| 12000 | 38.18359 | 31.58214 | SI |
| 12000 | 14.30532 | 6.07408 | PS |
| 12000 | 4.06789 | 1.55434 | WO |
| 12000 | 1.35361 | .83352 | BE |
| 12000 | .25456 | .06444 | CU |
| 12500 | 32.81149 | 27.13880 | SI |
| 12500 | 22.78301 | 9.67374 | PS |
| 12500 | 3.49557 | 1.33566 | WO |
| 12500 | 1.16317 | .71625 | BE |
| 12500 | .21874 | .05537 | CU |
| 13000 | 28.19519 | 23.32061 | SI |
| 13000 | 19.57763 | 8.31273 | PS |
| 13000 | 5.56713 | 2.12720 | WO |
| 13000 | .99952 | .61548 | BE |
| 13000 | .18797 | .04758 | CU |
| 13500 | 24.22837 | 20.03960 | SI |
| 13500 | 16.82323 | 7.14320 | PS |
| 13500 | 4.78388 | 1.82792 | WO |
| 13500 | 1.59186 | .98023 | BE |
| 13500 | .16152 | .04089 | CU |
| 14000 | 38.40110 | 31.76204 | SI |
| 14000 | 14.45634 | 6.13821 | PS |
| 14000 | 4.11083 | 1.57075 | WO |
| 14000 | 1.36790 | .84232 | BE |
| 14000 | .25725 | .06512 | CU |
| 14500 | 32.94839 | 27.29339 | SI |
| 14500 | 22.91279 | 9.72884 | PS |
| 14500 | 3.53247 | 1.34976 | WO |
| 14500 | 1.17545 | .72381 | BE |
| 14500 | .22105 | .05596 | CU |
| 15000 | 28.35580 | 23.45345 | SI |
| 15000 | 14.68915 | 8.36008 | PS |
| 15000 | 5.59884 | 2.13932 | WO |
| 15000 | 1.01007 | .62198 | BE |
| 15000 | .18995 | .04808 | CU |
| 15500 | 24.36638 | 20.15375 | SI |
| 15500 | 16.91906 | 7.18389 | PS |
| 15500 | 4.81113 | 1.83834 | WO |
| 15500 | 1.60093 | .98581 | BE |
| 15500 | .16323 | .04132 | CU |
| 16000 | 38.51969 | 31.86013 | SI |
| 16000 | 14.53869 | 6.17318 | PS |
| 16000 | 4.13425 | 1.57970 | WO |
| 16000 | 1.37569 | .84712 | BE |
| 16000 | .25871 | .06549 | CU |
| 16500 | 33.10030 | 27.37769 | SI |
| 16500 | 22.98355 | 9.75889 | PS |
| 16500 | 3.55259 | 1.35745 | WO |
| 16500 | 1.18214 | .72794 | BE |
| 16500 | .22231 | .05627 | CU |
| 17000 | 28.44337 | 23.52588 | SI |
| 17000 | 19.74996 | 8.38590 | PS |

| | | | |
|-------|----------|----------|----|
| 17000 | 5.61613 | 2.14593 | WO |
| 17000 | 1.01583 | .62552 | BE |
| 17000 | .19103 | .04836 | CU |
| 17500 | 24.44163 | 20.21599 | SI |
| 17500 | 16.97131 | 7.20607 | PS |
| 17500 | 9.82592 | 1.84401 | WO |
| 17500 | 1.60587 | .98886 | BE |
| 17500 | .16416 | .04155 | CU |
| 18000 | 38.58435 | 31.91362 | SI |
| 18000 | 14.58359 | 6.19224 | PS |
| 18000 | 4.14702 | 1.58458 | WO |
| 18000 | 1.37994 | .84974 | BE |
| 18000 | .25951 | .06569 | CU |
| 18500 | 33.15587 | 27.42365 | SI |
| 18500 | 23.02213 | 9.77527 | PS |
| 18500 | 3.56357 | 1.36164 | WO |
| 18500 | 1.18579 | .73018 | BE |
| 18500 | .22300 | .05645 | CU |
| 19000 | 28.49112 | 23.56537 | SI |
| 19000 | 19.78312 | 8.39997 | PS |
| 19000 | 5.62556 | 2.14953 | WO |
| 19000 | 1.01896 | .62745 | BE |
| 19000 | .19162 | .04851 | CU |
| 19500 | 24.48266 | 20.24993 | SI |
| 19500 | 16.99980 | 7.21817 | PS |
| 19500 | 4.63409 | 1.84711 | WO |
| 19500 | 1.60857 | .99052 | BE |
| 19500 | .16466 | .04168 | CU |
| 20000 | 38.61961 | 31.94278 | SI |
| 20000 | 14.60807 | 6.20263 | PS |
| 20000 | 4.15398 | 1.58724 | WO |
| 20000 | 1.38226 | .85116 | BE |
| 20000 | .25995 | .06580 | CU |
| 20500 | 33.18616 | 27.44870 | SI |
| 20500 | 23.04317 | 9.78420 | PS |
| 20500 | 3.56955 | 1.36393 | WO |
| 20500 | 1.18779 | .73141 | BE |
| 20500 | .22337 | .05654 | CU |
| 21000 | 28.51715 | 23.58691 | SI |
| 21000 | 19.80119 | 8.40765 | PS |
| 21000 | 5.63070 | 2.15149 | WO |
| 21000 | 1.02067 | .62851 | BE |
| 21000 | .19195 | .04859 | CU |
| 21500 | 24.50503 | 20.26843 | SI |
| 21500 | 17.01533 | 7.22477 | PS |
| 21500 | 4.83851 | 1.84880 | WO |
| 21500 | 1.61004 | .99142 | BE |
| 21500 | .16424 | .04175 | CU |
| 22000 | 38.63884 | 31.95868 | SI |
| 22000 | 14.62142 | 6.20830 | PS |
| 22000 | 4.15777 | 1.58869 | WO |
| 22000 | 1.38352 | .85194 | BE |
| 22000 | .26018 | .06586 | CU |
| 22500 | 33.20268 | 27.46237 | SI |
| 22500 | 23.05464 | 9.78907 | PS |
| 22500 | 3.57281 | 1.36517 | WO |

| | | | |
|-------|----------|----------|----|
| 22500 | 1.18887 | .73208 | BE |
| 22500 | .22358 | .05660 | CU |
| 23000 | 28.53135 | 23.59865 | SI |
| 23000 | 19.81105 | 8.41184 | PS |
| 23000 | 5.63350 | 2.15257 | WO |
| 23000 | 1.02161 | .62908 | BE |
| 23000 | .19212 | .04863 | CU |
| 23500 | 24.51723 | 20.27852 | SI |
| 23500 | 17.02380 | 7.22836 | PS |
| 23500 | 4.84092 | 1.84972 | WO |
| 23500 | 1.61084 | .99192 | BE |
| 23500 | .16509 | .04179 | CU |
| 24000 | 38.64932 | 31.96735 | SI |
| 24000 | 14.62870 | 6.21139 | PS |
| 24000 | 4.15984 | 1.58948 | WO |
| 24000 | 1.38421 | .85236 | BE |
| 24000 | .26031 | .06589 | CU |
| 24500 | 33.21169 | 27.46982 | SI |
| 24500 | 23.06090 | 9.79173 | PS |
| 24500 | 3.57459 | 1.36585 | WO |
| 24500 | 1.18946 | .73244 | BE |
| 24500 | .22369 | .05662 | CU |
| 25000 | 28.53909 | 23.60505 | SI |
| 25000 | 19.81642 | 8.41412 | PS |
| 25000 | 5.63503 | 2.15315 | WO |
| 25000 | 1.02212 | .62939 | BE |
| 25000 | .19222 | .04866 | CU |
| 25500 | 24.52388 | 20.28402 | SI |
| 25500 | 17.02842 | 7.23032 | PS |
| 25500 | 4.84223 | 1.85022 | WO |
| 25500 | 1.61128 | .99219 | BE |
| 25500 | .16517 | .04181 | CU |
| 26000 | 38.65504 | 31.97208 | SI |
| 26000 | 14.63267 | 6.21308 | PS |
| 26000 | 4.16097 | 1.58991 | WO |
| 26000 | 1.38458 | .85259 | BE |
| 26000 | .26038 | .06591 | CU |
| 26500 | 33.21660 | 27.47388 | SI |
| 26500 | 23.06431 | 9.79318 | PS |
| 26500 | 3.57556 | 1.36622 | WO |
| 26500 | 1.18978 | .73264 | BE |
| 26500 | .22375 | .05664 | CU |
| 27000 | 28.54331 | 23.60854 | SI |
| 27000 | 19.81936 | 8.41536 | PS |
| 27000 | 5.63587 | 2.15347 | WO |
| 27000 | 1.02239 | .62957 | BE |
| 27000 | .19227 | .04867 | CU |
| 27500 | 24.52751 | 20.28702 | SI |
| 27500 | 17.03094 | 7.23139 | PS |
| 27500 | 4.84295 | 1.85049 | WO |
| 27500 | 1.61152 | .99233 | BE |
| 27500 | .16522 | .04182 | CU |
| 28000 | 38.65815 | 31.97466 | SI |
| 28000 | 14.63483 | 6.21400 | PS |
| 28000 | 4.16159 | 1.59014 | WO |
| 28000 | 1.38479 | .85272 | BE |

| | | | |
|-------|----------|----------|----|
| 28000 | .26042 | .06592 | CU |
| 28500 | 33.21948 | 27.47610 | SI |
| 28500 | 23.06617 | 9.79397 | PS |
| 28500 | 3.57609 | 1.36643 | WO |
| 28500 | 1.18996 | .73275 | BE |
| 28500 | .22378 | .05665 | CU |
| 29000 | 28.54561 | 23.61044 | SI |
| 29000 | 19.82095 | 8.41604 | PS |
| 29000 | 5.63632 | 2.15364 | WO |
| 29000 | 1.02254 | .62966 | BE |
| 29000 | .19230 | .04868 | CU |
| 29500 | 24.52949 | 20.28866 | SI |
| 29500 | 17.03231 | 7.23198 | PS |
| 29500 | 4.84334 | 1.85064 | WO |
| 29500 | 1.61165 | .99241 | BE |
| 29500 | .16524 | .04183 | CU |
| 30000 | 38.65985 | 31.97606 | SI |
| 30000 | 14.63601 | 6.21450 | PS |
| 30000 | 4.16192 | 1.59027 | WO |
| 30000 | 1.38490 | .85279 | BE |
| 30000 | .26044 | .06593 | CU |
| 30500 | 33.22074 | 27.47730 | SI |
| 30500 | 23.06718 | 9.79440 | PS |
| 30500 | 3.57638 | 1.36654 | WO |
| 30500 | 1.19006 | .73281 | BE |
| 30500 | .22380 | .05665 | CU |
| 31000 | 28.54687 | 23.61148 | SI |
| 31000 | 19.82182 | 8.41641 | PS |
| 31000 | 5.63657 | 2.15374 | WO |
| 31000 | 1.02263 | .62971 | BE |
| 31000 | .19231 | .04868 | CU |
| 31500 | 24.53057 | 20.28955 | SI |
| 31500 | 17.03306 | 7.23229 | PS |
| 31500 | 4.84355 | 1.85072 | WO |
| 31500 | 1.61172 | .99246 | BE |
| 31500 | .16526 | .04183 | CU |
| 32000 | 38.66078 | 31.97683 | SI |
| 32000 | 14.63666 | 6.21477 | PS |
| 32000 | 4.16210 | 1.59034 | WO |
| 32000 | 1.38496 | .85283 | BE |
| 32000 | .26045 | .06593 | CU |
| 32500 | 33.22154 | 27.47796 | SI |
| 32500 | 23.06773 | 9.79463 | PS |
| 32500 | 3.57653 | 1.36660 | WO |
| 32500 | 1.19011 | .73284 | BE |
| 32500 | .22381 | .05665 | CU |
| 33000 | 28.54755 | 23.61205 | SI |
| 33000 | 19.82230 | 8.41661 | PS |
| 33000 | 5.63670 | 2.15379 | WO |
| 33000 | 1.02267 | .62974 | BE |
| 33000 | .19232 | .04868 | CU |
| 33500 | 24.53115 | 20.29003 | SI |
| 33500 | 17.03347 | 7.23247 | PS |
| 33500 | 4.84367 | 1.85077 | WO |
| 33500 | 1.61175 | .99248 | BE |
| 33500 | .16526 | .04183 | CU |

| | | | |
|-------|----------|----------|----|
| 34000 | 38.66128 | 31.97725 | SI |
| 34000 | 14.63701 | 6.21492 | PS |
| 34000 | 4.16220 | 1.59038 | WO |
| 34000 | 1.38499 | .85285 | BE |
| 34000 | .26046 | .06593 | CU |
| 34500 | 33.22197 | 27.47832 | SI |
| 34500 | 23.06803 | 9.79476 | PS |
| 34500 | 3.57662 | 1.36663 | WO |
| 34500 | 1.19014 | .73286 | BE |
| 34500 | .22382 | .05666 | CU |
| 35000 | 28.54792 | 23.61236 | SI |
| 35000 | 19.82256 | 8.41672 | PS |
| 35000 | 5.63678 | 2.15382 | WO |
| 35000 | 1.02270 | .62975 | BE |
| 35000 | .19233 | .04868 | CU |
| 35500 | 24.53147 | 20.29030 | SI |
| 35500 | 17.03369 | 7.23256 | PS |
| 35500 | 4.84373 | 1.85079 | WO |
| 35500 | 1.61178 | .99249 | BE |
| 35500 | .16527 | .04184 | CU |
| 36000 | 38.66156 | 31.97747 | SI |
| 36000 | 14.63720 | 6.21500 | PS |
| 36000 | 4.16226 | 1.59040 | WO |
| 36000 | 1.38501 | .85286 | BE |
| 36000 | .26046 | .06593 | CU |
| 36500 | 33.22221 | 27.47852 | SI |
| 36500 | 23.06820 | 9.79483 | PS |
| 36500 | 3.57666 | 1.36665 | WO |
| 36500 | 1.19015 | .73287 | BE |
| 36500 | .22382 | .05666 | CU |
| 37000 | 28.54813 | 23.61252 | SI |
| 37000 | 19.82270 | 8.41678 | PS |
| 37000 | 5.63682 | 2.15383 | WO |
| 37000 | 1.02271 | .62976 | BE |
| 37000 | .19233 | .04869 | CU |
| 37500 | 24.53165 | 20.29044 | SI |
| 37500 | 17.03381 | 7.23261 | PS |
| 37500 | 4.84376 | 1.85081 | WO |
| 37500 | 1.61179 | .99250 | BE |
| 37500 | .16527 | .04184 | CU |
| 38000 | 38.66171 | 31.97760 | SI |
| 38000 | 14.63730 | 6.21505 | PS |
| 38000 | 4.16229 | 1.59041 | WO |
| 38000 | 1.38502 | .85286 | BE |
| 38000 | .26047 | .06593 | CU |
| 38500 | 33.22233 | 27.47862 | SI |
| 38500 | 23.06829 | 9.79487 | PS |
| 38500 | 3.57669 | 1.36666 | WO |
| 38500 | 1.19016 | .73287 | BE |
| 38500 | .22382 | .05666 | CU |
| 39000 | 28.54824 | 23.61262 | SI |
| 39000 | 19.82278 | 8.41681 | PS |
| 39000 | 5.63684 | 2.15384 | WO |
| 39000 | 1.02272 | .62976 | BE |
| 39000 | .19233 | .04869 | CU |
| 39500 | 24.53174 | 20.29052 | SI |

| | | | |
|-------|----------|----------|----|
| 39500 | 17.03388 | 7.23264 | PS |
| 39500 | 4.84378 | 1.85081 | W0 |
| 39500 | 1.61179 | .99251 | BE |
| 39500 | .16527 | .04184 | CU |
| 40000 | 38.66179 | 31.97767 | SI |
| 40000 | 14.63736 | 6.21507 | PS |
| 40000 | 4.16230 | 1.59042 | W0 |
| 40000 | 1.38503 | .85287 | BE |
| 40000 | .26047 | .06593 | CU |
| 40500 | 33.22241 | 27.47868 | SI |
| 40500 | 23.06834 | 9.79489 | PS |
| 40500 | 3.57670 | 1.36666 | W0 |
| 40500 | 1.19017 | .73288 | BE |
| 40500 | .22382 | .05666 | CU |
| 41000 | 28.54830 | 23.61267 | SI |
| 41000 | 19.82282 | 8.41683 | PS |
| 41000 | 5.63685 | 2.15384 | W0 |
| 41000 | 1.02272 | .62977 | BE |
| 41000 | .19233 | .04869 | CU |
| 41500 | 24.53180 | 20.29057 | SI |
| 41500 | 17.03392 | 7.23266 | PS |
| 41500 | 4.84379 | 1.85082 | W0 |
| 41500 | 1.61180 | .99251 | BE |
| 41500 | .16527 | .04184 | CU |
| 42000 | 38.66183 | 31.97770 | SI |
| 42000 | 14.63739 | 6.21508 | PS |
| 42000 | 4.16231 | 1.59042 | W0 |
| 42000 | 1.38503 | .85287 | BE |
| 42000 | .26047 | .06593 | CU |
| 42500 | 33.22244 | 27.47871 | SI |
| 42500 | 23.06836 | 9.79490 | PS |
| 42500 | 3.57671 | 1.36666 | W0 |
| 42500 | 1.19017 | .73288 | BE |
| 42500 | .22382 | .05666 | CU |
| 43000 | 28.54833 | 23.61269 | SI |
| 43000 | 19.82284 | 8.41684 | PS |
| 43000 | 5.63686 | 2.15385 | W0 |
| 43000 | 1.02272 | .62977 | BE |
| 43000 | .19233 | .04869 | CU |
| 43500 | 24.53182 | 20.29059 | SI |
| 43500 | 17.03394 | 7.23266 | PS |
| 43500 | 4.84380 | 1.85082 | W0 |
| 43500 | 1.61180 | .99251 | BE |
| 43500 | .16527 | .04184 | CU |
| 44000 | 38.66186 | 31.97772 | SI |
| 44000 | 14.63741 | 6.21509 | PS |
| 44000 | 4.16232 | 1.59042 | W0 |
| 44000 | 1.38503 | .85287 | BE |
| 44000 | .26047 | .06593 | CU |
| 44500 | 33.22247 | 27.47873 | SI |
| 44500 | 23.06838 | 9.79491 | PS |
| 44500 | 3.57672 | 1.36667 | W0 |
| 44500 | 1.19017 | .73288 | BE |
| 44500 | .22382 | .05666 | CU |
| 45000 | 28.54835 | 23.61271 | SI |
| 45000 | 19.82285 | 8.41685 | PS |

| | | | |
|-------|----------|----------|----|
| 45000 | 5.63686 | 2.15385 | WU |
| 45000 | 1.02272 | .62977 | BE |
| 45000 | .19233 | .04869 | CU |
| 45500 | 24.53184 | 20.29060 | SI |
| 45500 | 17.03395 | 7.23267 | PS |
| 45500 | 4.84380 | 1.85082 | WU |
| 45500 | 1.61180 | .99251 | BE |
| 45500 | .16527 | .04184 | CU |
| 46000 | 38.66187 | 31.97773 | SI |
| 46000 | 14.63742 | 6.21509 | PS |
| 46000 | 4.16232 | 1.59043 | WU |
| 46000 | 1.38503 | .85287 | BE |
| 46000 | .26047 | .06593 | CU |
| 46500 | 33.22248 | 27.47874 | SI |
| 46500 | 23.06839 | 9.79491 | PS |
| 46500 | 3.57672 | 1.36667 | WU |
| 46500 | 1.19017 | .73288 | BE |
| 46500 | .22382 | .05666 | CU |
| 47000 | 28.54836 | 23.61272 | SI |
| 47000 | 19.82286 | 8.41685 | PS |
| 47000 | 5.63686 | 2.15385 | WU |
| 47000 | 1.02272 | .62977 | BE |
| 47000 | .19233 | .04869 | CU |
| 47500 | 24.53185 | 20.29061 | SI |
| 47500 | 17.03395 | 7.23267 | PS |
| 47500 | 4.84380 | 1.85082 | WU |
| 47500 | 1.61180 | .99251 | BE |
| 47500 | .16527 | .04184 | CU |
| 48000 | 38.66188 | 31.97774 | SI |
| 48000 | 14.63742 | 6.21510 | PS |
| 48000 | 4.16232 | 1.59043 | WU |
| 48000 | 1.38503 | .85287 | BE |
| 48000 | .26047 | .06593 | CU |
| 48500 | 33.22248 | 27.47875 | SI |
| 48500 | 23.06839 | 9.79491 | PS |
| 48500 | 3.57672 | 1.36667 | WU |
| 48500 | 1.19017 | .73288 | BE |
| 48500 | .22382 | .05666 | CU |
| 49000 | 28.54836 | 23.61272 | SI |
| 49000 | 19.82286 | 8.41685 | PS |
| 49000 | 5.63686 | 2.15385 | WU |
| 49000 | 1.02272 | .62977 | BE |
| 49000 | .19233 | .04869 | CU |
| 49500 | 24.53185 | 20.29061 | SI |
| 49500 | 17.03396 | 7.23267 | PS |
| 49500 | 4.84381 | 1.85082 | WU |
| 49500 | 1.61180 | .99251 | BE |
| 49500 | .16527 | .04184 | CU |
| 50000 | 38.66188 | 31.97774 | SI |
| 50000 | 14.63742 | 6.21510 | PS |
| 50000 | 4.16232 | 1.59043 | WU |
| 50000 | 1.38503 | .85287 | BE |
| 50000 | .26047 | .06593 | CU |

APPENDIX II

VOLTAGE CLAMPING CIRCUIT

When the thyristor is in the blocking state, a potential of the order of 2000 volts is impressed across it; shortly after the thyristor is fired, the potential across it is a few volts or a few tens of volts. The voltage as a function of time is a very important parameter in thyristor design and application. An oscilloscope is used to provide a voltage versus time trace.

The Tektronic oscilloscope specifications state that the recovery time of the instrument when heavily saturated is of the order of 1 μ sec. It has been found in the present work that attempts to read voltage after the oscilloscope amplifiers have been overdriven results in a d-c offset in the reading for the entire 40 μ sec pulse.

In addition, above 600 volts across the device under test, either a clamping circuit or an attenuator must be used to prevent damage to the oscilloscope probes. Higher voltage probes are available but do not have a sufficient frequency response for readings on the high speed transients encountered in this test program.

This problem was discussed extensively over a period of several years with representatives of high technology instrumentation manufacturers such as Tektronics, Hewlett-Packard, Biomation, and Nicollette. None have been able to recommend an effective piece of equipment or approach for a reasonable cost.

The approach taken to partially resolve this dilemma was to design and fabricate a voltage clamping circuit as shown schematically in Figure II-1. The clamping circuit is to the right of the vertical dashed line. The portion of the schematic to the left of the dashed line indicates how the voltage clamping circuit is connected to the device under test and the relationships with the pertinent parts of the rest of the test circuit.

The Kelvin probe connections across the device are connected to the clamping circuit and to the oscilloscope through differential probes to observe the voltage decay across the device. The oscillo-

Dwg. 6415A21

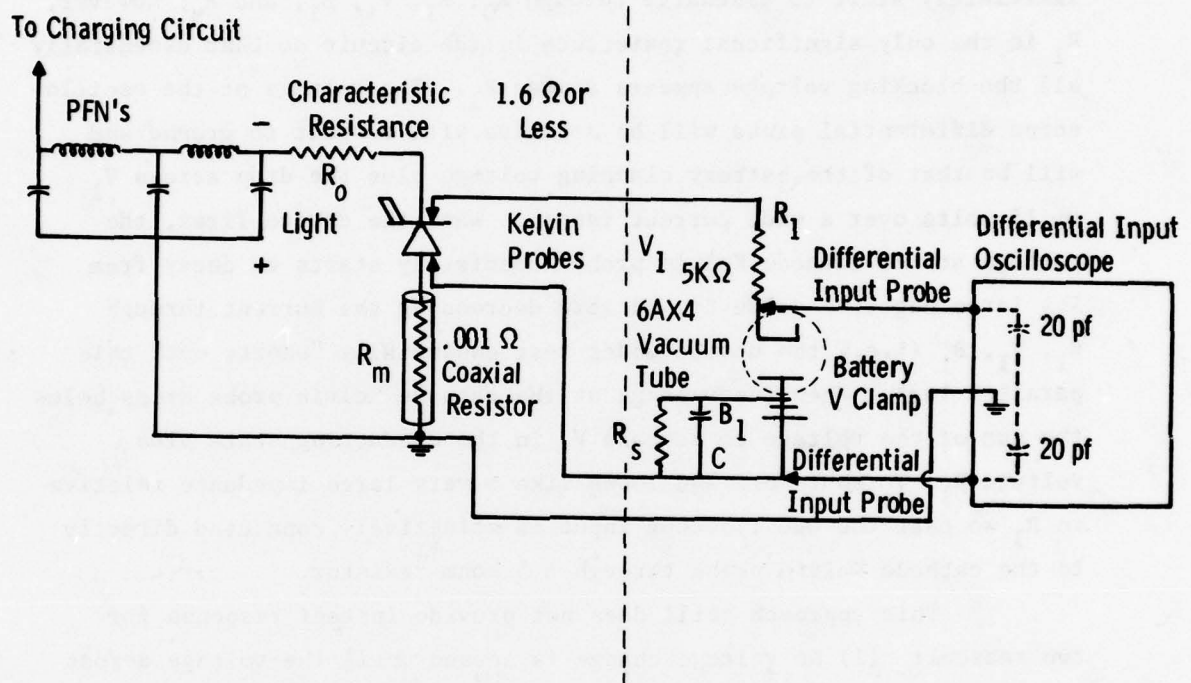


Figure II-1. Schematic diagram of voltage clamping circuit.

scope is grounded to the coaxial resistor ground which is ground for the entire system. The differential probes are tied common at the probe ends of their respective coaxial cables as recommended by the instruction manual for the Tektronix model 7A13 differential comparator.

The sequence of events is as follows: The pulse forming networks (PFN's) are charged to the voltage to be blocked (up to 2000 volts) which is sustained by the device under test. The PFN's immediately start to discharge through R_0 , R_1 , V_1 , B_1 , and R_M ; however, R_1 is the only significant resistance in the circuit so that essentially all the blocking voltage appears across R_1 . The voltage at the oscilloscope differential probe will be negative with respect to ground and will be that of the battery clamping voltage plus the drop across V_1 (~ 15 volts over a wide current range). When the device fires, the voltage at the cathode Kelvin probe immediately starts to decay from its large negative value toward zero decreasing the current through R_1 , V_1 , B_1 (i.e., the device under test essentially "shorts out" this parallel leg). When the voltage at the cathode Kelvin probe drops below the sum of the voltage to sustain V_1 in the conducting state plus voltage B_1 , V_1 shuts off and looks like a very large impedance relative to R_1 so that the oscilloscope input is effectively connected directly to the cathode Kelvin probe through a 5 kohm resistor.

This approach still does not provide instant response for two reasons: (1) No voltage change is sensed until the voltage across the device under test is low enough that the tube ceases to conduct. This requires the major part of the fall time of the voltage transient and is believed to be of the order of 50 nsec. (2) The tube capacitance (and all of the distributed stray capacitance of the comparatively long (~ 1 meter) sensing leads of the clamp circuit) must discharge through the 5 kohm resistor. This requires about 20 nsec per pf to be within 2% of the true voltage value, and although the tube interelectrode capacitance is small (5 to 8 pf), that of the rest of the circuit is not. The total capacitance may well be several hundred pf, leading to delays of the order of a few microseconds. The voltage traces

taken with the clamp circuit are so noisy for the first 5 μ sec that the operation of the clamp circuit in this time frame at the full operational voltage is difficult to determine.

The technique described above successfully provides for accurate voltage readings within a few microseconds of the transient by preventing saturation of the oscilloscope amplifiers. It also protects the oscillograph probes by limiting the input signal voltage to a preselected value. Battery voltages of 45 and 90 volts were used in the present program. The battery can be replaced by a variable power supply so that the clamping level is adjustable. This has the advantage of permitting one to experimentally determine the earliest time at which a voltage value can be determined with confidence. Varying the clamping voltage should not vary the voltage reading for times greater than that required for the recovery time of the circuit. The shortest time for which the voltage value is unchanged as the clamping voltage is varied is thus the earliest reliable reading.

The problem still has not been solved of accurately measuring a small voltage immediately after a very large voltage is impressed on the sensing circuit. A redesign of the thyristor mounting technique and of the Kelvin probes and associated leads to the oscilloscope could improve the present situation somewhat. If such a redesign permitted the use of the oscilloscope in the single end mode, rather than a differential mode, the oscilloscope response would be improved. However, it is not believed that the oscilloscope response is a limitation at present if amplifier saturation is avoided.

APPENDIX III

PURCHASE SPECIFICATIONS FOR 100 mJ, 50 Hz Q-SWITCHED LASER

1. SCOPE

1.1 This specification describes the desired performance of a Q-switched Nd:YAG laser operating at 1.06 μm with an output of 100 mJ at a repetition rate of 50 Hz. The vendor is asked to respond with a state of the art system, the performance of which can be demonstrated by completed equipment. When the equipment does not fulfill a particular requirement listed below, the vendor is required to specifically say so and list his own specifications. Only minor changes in present systems should be undertaken to fulfill the requirements. No major development work should be considered.

1.2 Design features that may improve the operational capability or reduce the cost of the facility are requested and should be noted in the quotation.

2. EQUIPMENT

All equipment, such as laser head, power supply, cooling system and interconnecting hoses and cables necessary for generating a laser beam with the characteristics described in Section 4 will be provided by the vendor. The following points are specially noted:

2.1 Output Energy Monitor, such as a photodiode, which continuously samples the output energy. The monitor shall provide an output which can be displayed on an oscilloscope or as an added option (separately priced) on a panel meter.

2.2 PFN Voltage. A display of the pulse forming network (PFN) charge voltage.

2.3 A Pulse Counter for monitoring total number of laser output pulses.

2.4 An internal clock which provides several discrete repetition rates between 1 and 50 Hz or continuously variable between 0 and 50 Hz. Specify rates if discrete.

2.5 A terminal for externally triggering the laser in the range from 1 Hz to 50 Hz. Specify trigger voltage, rise time, and impedance requirements.

2.6 If power supply does not automatically maintain laser energy output with changing repetition rate and component aging, an external control allows the operator to do so. When repetition rate is changed without adjusting pump energy, specify expected variation in laser output energy over the range of 1 to 50 Hz.

2.7 An aperture (or other means) in the laser resonator for adjusting the laser to TEM₀₀ output. Vendor shall state energy output obtainable (which is expected to be less than the 0.1 joule specified for multi-mode operation).

2.8 A He-Ne laser beam aligned with the optical axis of the YAG laser output beam. Preferred source of He-Ne beam is located inside the laser head, but can be located externally with adequate optics provided to introduce the He-Ne beam coaxial to the YAG laser beam. Price quote either or both of the above approaches.

2.9 Instruction Manual to include the following as a minimum:

- 2.9.1 Complete schematic diagrams of all circuits
- 2.9.2 Mounting and cabinet dimensions
- 2.9.3 Laser specifications
- 2.9.4 Alignment procedure
- 2.9.5 Flash lamp replacement procedure
- 2.9.6 Block diagrams and general description of circuit functions and operation

3. CONFIGURATION AND SIZE

3.1 It is anticipated that the He-Ne laser and the YAG laser be one unit, which by an umbilical cord is connected to the power supply cabinet and cooling system.

3.2 The umbilical cord should be of a length consistent with sound engineering, but not less than 8 ft.

3.3 The laser head should be of a sound design capable of fulfilling the specifications in Section 4 in a laboratory environment without the need for special vibration damped tables or frequent realignment.

3.4 All optical components must be shielded by dust-tight enclosures to protect optical surfaces against contamination.

3.5 A control cabinet on which is mounted all control switches, knobs, selectors, pushbuttons, panel meters, indicator lights, warning lights.

3.6 The control cabinet should have a large, clearly visible, red "panic" button for closing down the laser and discharge all circuits of significant voltage or current.

3.7 The control cabinet should be mounted on wheels or rollers.

3.8 An outline drawing of the equipment showing mounting holes, dimensions, etc., will be provided by vendor at least one month before delivery of system.

4. LASER SPECIFICATIONS

4.1 Output wavelength 1.06 μm .

4.2 Output energy at all repetition rates between 1 Hz and 50 Hz must be 100 mJ per pulse or more.

4.3 Maximum energy variation between pulses over a period of 5 min, after a 2-min warm-up period, should be 5%.

4.4 Output should be Q-switched with all energy in a single pulse of typically 20 nsec halfwidth or shorter. Any additional pulses emitted by the laser (i.e., as a result of Q-switch ringing) must have a total energy of less than 1 mJ.

4.5 Time between output pulses from the laser shall be $\leq \pm 2 \mu\text{sec}$ variation, once the nominal repetition rate is established.

4.6 The output of the laser shall be polarized with the \vec{E} -vector in the vertical plane.

4.7 Beam Divergence. Vendor shall specify beam divergence, beam diameter, and beam stability. Vendor shall also specify how these parameters are to be measured, including equipment to be used and the geometry and spacing of components.

4.8 All optical components shall be guaranteed for one year or 10^6 laser pulses, whichever comes first. All other components shall be guaranteed for one year. Any exceptions shall be specified by the vendor and the expected life shall be stated.

4.9 The cooling system must be dimensioned to permit continuous operation of the laser within the specifications outlined in this section.

4.10 Construction of the laser head shall facilitate change of the lamp. Realignment feature must be specified and not unduly complicated. It is preferred that no alignment be necessary.

4.11 Power Input. 60 Hz, 3-phase, WYE, 208-volt preferred. 60 Hz, 1-phase 120-volt acceptable.

4.12 Cooling System. Vendor shall specify options available and price. Buyer has available recirculating water for use with heat exchanger.

5. SAFETY FEATURES

5.1 Interlock for preventing accidental access of lethal voltages and currents.

5.2 Warning light outlet which is energized when laser power supply is turned on, in addition to a warning light on power supply.

5.3 Interlocks to protect laser head and electronics from damage caused by operator error or equipment failure, i.e., coolant flow and/or temperature interlocks.

6. ACCEPTANCE TESTS

6.1 Acceptance tests and equipment demonstration will be conducted on the Total Laser System at the vendor's plant as follows:

6.1.1 The vendor shall notify the purchaser at least one week prior to completion of the facility and/or scheduled start of acceptance tests.

6.1.2 The vendor shall set up and perform all necessary demonstrations within his plant with his people to prove that the equipment meets this specification.

6.1.3 The vendor shall make available all necessary equipment over and above that being tested which is necessary to perform the final acceptance tests.

6.1.4 The equipment shall be demonstrated actually lasing under the conditions expressed in ¶4.1 to 4.5 for 5 min at each of the repetition rates to be specified.

6.2 The output energy of 100 mJ or more shall be demonstrated by use of a reliable thermal pulse energy calorimeter and/or a thermal average power meter.

6.3 The pulse shape and stability of the laser shall be demonstrated on an oscilloscope. Rise time on detector-oscilloscope combination shall be 10 nsec or better. This demonstration shall be in accordance with Section 4.3.

6.4 Demonstration of the beam divergence shall be in accordance with the specifications outlined in the vendor's quote.

APPENDIX IV

PULSED POWER SUPPLY TEST CIRCUIT

IV-1. Introduction.

The needs of the Light Activated Switch Test System were to generate a test pulse of 20,000 ampere peak, with 40 μ sec duration. It was decided to produce this pulse both at voltage levels of 1600 volts and the 2000 volt level. The rise time of the current pulse was to be at least 20,000 amperes/ μ sec.

It was considered advantageous to also test initially at reduced voltage levels, and capability was provided to test at 500 and 1000 volts. As a cost consideration only discrete voltage adjustability was provided.

Pulse rate considerations of the test system were initially determined by the available pulse rate of the laser, the available power in the vicinity of the test system, and the ability to cool the test switch. Power to the test facility was limited to 30 kilowatts thus limiting maximum pulse rate to 40 Hz at full voltage and current. Some consideration was given to running the test switch to higher pulse rates at reduced voltage level, but these schemes were still limited by the available power in the test facility and the fixed current capacity of the test system main transformer and wiring; i.e., no trade-off existed such as running increased current and reduced voltage to maintain the input power constant. The primary considerations of input source power and fixed current capability thus determined the maximum test pulse rate which was 40 Hz.

IV-2. Pulse Generation Techniques.

The one microsecond risetime of the required 20,000 A test pulse is not excessive; however, the high energy storage requirements of the pulse (800 J), and the relatively low voltage of 2000 V, required a circuit arrangement which has inherent pulse width determination techniques, allowed means for pulse current measurement, and also means for laser access to the switch. The pulse width requirements

were best satisfied with pulse forming networks (PFN's) for which the test device could switch-on, and a current pulse would be produced of the required pulse-width by proper PFN loading without external switching elements.

The pulse risetime, device current measurement, and laser access to the switch were satisfied by arranging 40 discrete pulse forming networks concentrically and in parallel about a central device mounting jig which included a high response coaxial current sensing resistor. The device mounting jig is shown in Figure IV-1. The current measuring resistor is shown as item (9), and is fundamentally coaxial in character. This is threaded into a device mounting pedestal (1) upon which the test device (13) is mounted. The concentric pulse forming networks are connected to flange (12), and cover plate (8). Pressure is applied to the test device with pole piece (6), which is locked in place with threaded plug (7). A hole through the pole piece and access plug allow laser illumination of the thyristor surface. Final pressure on the test device is provided by insulated screws (16) which force the cover plate to apply pressure to the pole piece. The mounting pedestal is enclosed in a coaxial brass can (4 & 11), and the total assembly is securely mounted to a vertical plane mounting board through the use of mounting flange (14). The radial PFN's and test device mounting jig are shown in Figure IV-2 and Figure IV-3.

IV-3. Power Circuit

The energy needs of the test pulser are as follows:

1) 1600 V system -- Forty pulse forming networks to be charged to 1600 volts. Each network has 12.5 μf of capacitance, and the total storage capacitance is 500 μf . The total energy storage is then:

$$W = 1/2 CE^2 = 640 \text{ J.}$$

2) 2000 V system -- Thirty-two pulse forming networks are to be charged to 2000 volts. Each network has 12.5 μf of capacitance, and the total storage capacitance is 400 μf . The total energy storage is then:

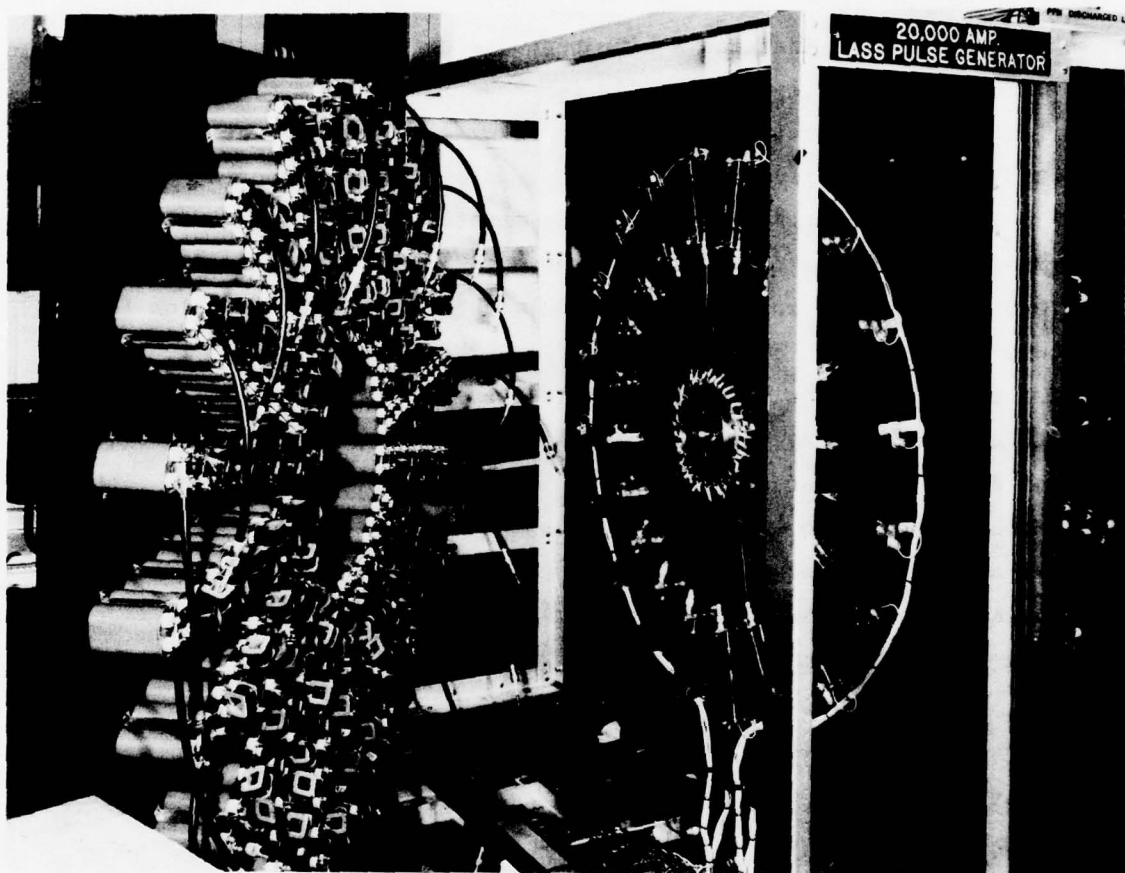


Figure IV-2. View of assembled pulser showing 20 of 40 PFN's arranged in a radial manner with their associated load resistors arranged radially about the thyristor test holder in right center of the photo.

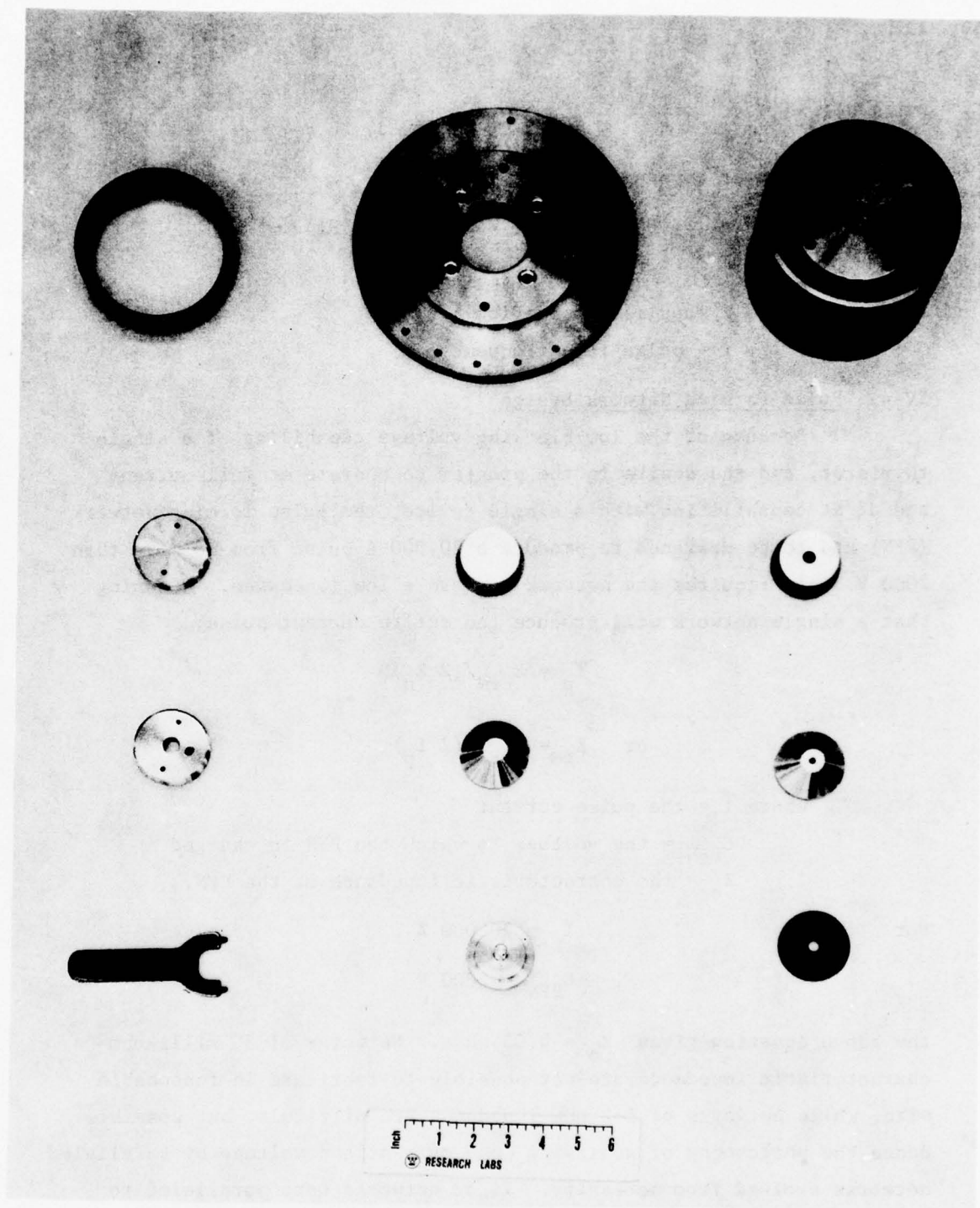


Figure IV-3. Test device mounting jig component parts.

$$W = 1/2 CE^2 = 800 \text{ J.}$$

The maximum power consumption rate is then:

$$P = W/T = Wf = (800 \text{ J})(40 \text{ Hz})$$

$$P = 32 \text{ kW}$$

where T = pulse rate period

f = pulse rate frequency

IV-4. Pulse Forming Network Design

Because of the low blocking voltage capability of a single thyristor, and the desire in the program to operate at full current and dI/dt capabilities with a single device, the pulse forming network (PFN) had to be designed to produce a 20,000 A pulse from no more than 2000 V. This requires the network to have a low impedance. Assuming that a single network will produce the entire current pulse:

$$I_p = E_{PFN} / (2 Z_o)$$

$$\text{or } Z_o = E_{PFN} / (2 I_p)$$

where I_p = the pulse current

E_{PFN} = the voltage to which the PFN is charged

Z_o = the characteristic impedance of the PFN.

For

$$I_p = 20,000 \text{ A}$$

$$E_{PFN} = 2000 \text{ V}$$

the above equation gives $Z_o = 0.05$ ohms. Networks of 50 milli-ohm characteristic impedance are not possible to fabricate in reasonable size, while networks of 1-2 ohm impedance are difficult, but possible. Hence the philosophy of achieving load current and voltage by paralleled networks evolved from necessity. If 32 networks were paralleled to achieve 20,000 amperes, then each network would supply a current of:

$$I_{pn} = \frac{20,000}{32} = 625 \text{ A.}$$

The characteristic impedance of each network would then be:

$$Z_{on} = \frac{E_{pn}}{2 I_{pn}} = \frac{2000 \text{ V}}{2 \times 625 \text{ A}} = 1.6 \text{ ohms.}$$

The scheme of current waveform fabrication is then to parallel 32 networks, each loaded with its equivalent characteristic impedance, Z_{on} . A symbolic network and resistive load impedance is shown in Figure IV-4. To achieve 20,000 A at 1600 V, forty parallel networks such as shown in Figure IV-4 are required. In this case, each network supplies 500 A.

The main pulse generator power circuit is shown in Figure IV-5. The 1.6 ohm PFN's are shown in this drawing as PFN's 1-40. For 2000 V operation, 8 PFN's are disconnected by quick disconnect convectors. Each PFN is charged through individual charging rectifiers, and is discharged through individual load resistors, R 1 to R 40. The load current of each PFN is summed in the test device, whose anode is near ground potential. All pulse forming networks are resonantly charged through the action of charging choke #187 and command charge switch's T 507.

DC power is supplied to the charging switch from a three phase full wave rectifier system using two 15 KVA three phase rectifiers connected in series. The three phase full wave rectifiers provide a very low ripple (about 6%) at 360 Hz in the dc output. Thus a high voltage filter capacitor is not required in the power supply to charge the pulse forming networks. Taps on the power supply isolation transformers (not shown) allow change of the output voltage at 25, 50, 75, or 100% of rated output. The power supply isolation transformers are connected to the ac three phase line through two breakers. The first is a high speed, shunt trip breaker which is quickly opened in event of device failure. The second breaker, closed after the shunt trip breaker, removes some series resistance from the three phase line which is initially present to limit to a safe level the inrush current to the main power transformers. In the event of a fault in the main rectifier, PFN, or test device, the main breaker is opened with a logic signal which activates a solid state relay to apply power to the

Dwg. 6415A15

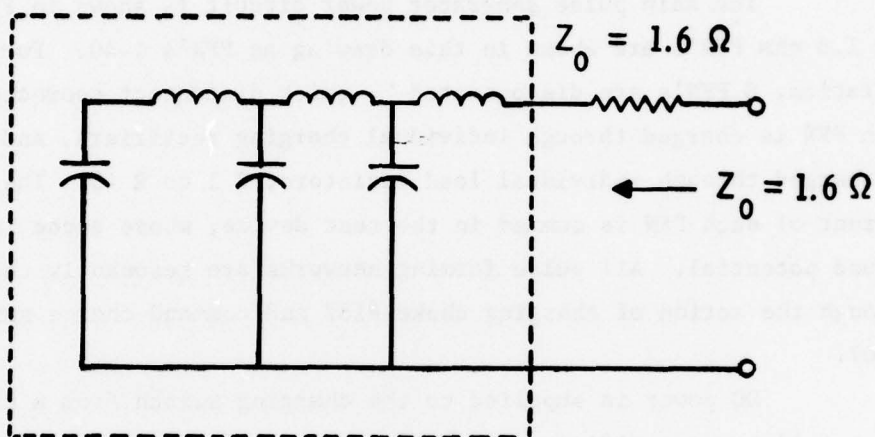


Figure IV-4. Symbolic PFN network and resistive load impedance.

shunt trip of the main breaker.

The sequence of events to obtain an output pulse from the pulser test circuit is as follows: Power is applied to the main rectifiers. The charging of the PFN's is initiated by triggering the T 507 charging switch. The charging action is resonant, and after the 1/2 sine wave charging current ends, the charging switch is self commutated. After a suitable waiting time for recovery of the charging switch, the logic system generates a trigger to fire the laser. The laser apparatus has an internal delay of about 12 μ sec after the logic signal occurs before the laser fires, triggering the device under test, and discharging the PFN's. Each PFN is loaded with its own characteristic impedance of 1.6 ohms, causing the PFN discharge to produce a rectangular, 40 μ sec current pulse of 625 A when the PFN voltage is 2000 V. If 32 PFN's are used, then the summation will produce the required 20,000 A peak current.

Should the test device fail, such that after failure the succeeding charging pulse is short circuited, there will be charging current through the shorted device at a time other than the specified charging period. This irregular event charging current will also pass through sense rectifiers R404007's, and cause an output voltage at the output of sense amplifier 741 P. This voltage will be transferred to the logic network and cause the main breaker to trip and indicate a fault condition. Once the fault or failure is corrected, normal operation will be restored.

IV-5. Pulser Timing Unit

The pulser timing unit produces a clock pulse at a predetermined pulse rate which originates from:

- 1) a free running oscillator (VFO)
- 2) pulse rate division of the line frequency.

Understanding of the following discussion will be aided by referring to Figure IV-6.

IV-5.1. VFO.

The variable frequency free running oscillator consists of

three cascaded 748 amplifiers, plus an output emitter follower for current amplification. The initial 748 amplifier is a simple relaxation oscillator, provided with a frequency range selection switch and a fine frequency adjust. These controls set the time constant of the relaxation oscillator. The following 748 amplifiers provide pulse shaping and amplification to produce a symmetrical square wave at the emitter follower output. A light emitting diode is provided in a feedback path to give visible indication of the selected pulse rate.

IV-5.2. Fine Origin Clock

A second clock signal originates from the line 60 Hz power signal and is developed by first forming a 120 Hz line clocked signal in mono-stable stage N-1. Stage N-1 is directly triggered from the full wave rectified line. Output from N-1 feeds two cascaded decade counters. The output of counters N2 and N3 are binary 4 bit signals which are converted to decimal indications by decoder units N4 and N5.

As an example, consider that it is desired to divide the input line clock signal by sixty. Then the units switch of decoder N4 is turned to zero, and the tens switch of decoder N5 is turned to six. When counters N2 and N3 count to the 60 level, outputs will appear simultaneously at decoder outputs zero of N4 and six of N5. These two outputs will be sensed by pins 13 and 1 of NAND gate N7. This will cause output at pin 13 of N7 which will cause a set signal to be formed at pin 10 of N7. The remaining two NAND gates of N7 form a bistable, and a low signal on pin 10 of this bistable will cause pin 8 to rise high, yielding a reset signal to the decade counters, and a signal which is fed to an output monostable as the clock pulse. Hence the decoder switch selectors will set the line frequency divisor, which in the example caused two output counts for every 120 input pulses. The range of line clock divisor is one-nine-nine.

Decoder outputs are inverted by hex inverter stage N6, which also provides amplifier drive of the reset signal. Two hex inverters of N6 are paralleled to provide drive into a light emitting diode, such that visible indication of the line synched clock is seen at the front

panel of the timing unit.

A selector switch selects either V_{FO} source, or discrete twice line frequency divided by N signal as input to a pulse shaping monostable. The output clock pulse (Cp) then is sent to the run timer control system.

IV-5.3. Run Timer and Control Logic

Inasmuch as the Run Timer is the most complex portion of the control circuitry, it will be described from the block diagram of Figure IV-7. The clock pulse (Cp) is the main input into the Run Timer and Control Logic System. The Run Timer uses the line as origin of the reference signal which determines running time. Line sync is shaped into a pulse by Pulse Shaper H-1. The output signal (Cpp) is a standard logic level signal of one millisecond duration. The signal Cp then drives a divide by 60 stage (H 17, 18, 19) to give a 1 Hz reference signal suitable for clocking purposes. The 1 Hz signal drives a preset timer which may be used to set the desired running time. Running time is selected by three controls which determine the running period in seconds, 10 seconds, and minutes. The maximum running time is 9 minutes 59 seconds.

The run time is begun by a front panel control called timer start. This enables a synchronizing bistable such that with the occurrence of the next clock pulse (Cp), the clock pulse will be allowed to pass. The clock pulse in turn causes the main enable bistable H-6 to change state, and this allows passage of the clock pulse (Cp) to the output pulse shaper H-14, as well as release of input pulse shaper H-1, allowing the 60 Hz timer reference signal to pass into the divide by 60 circuit. The timer will run and count one-second pulses for a duration determined by the setting of the desired run time. After passage of the desired run time, the input synchronizing and enable bistables are reset, shutting off passage of the clock pulse (Cp) and run timer reference (Cpp). Hence clock pulse (Cp) will pass to the output for the prescribed time, and all timing will be synchronized with the clock pulse. No timing can begin without the clock pulse,

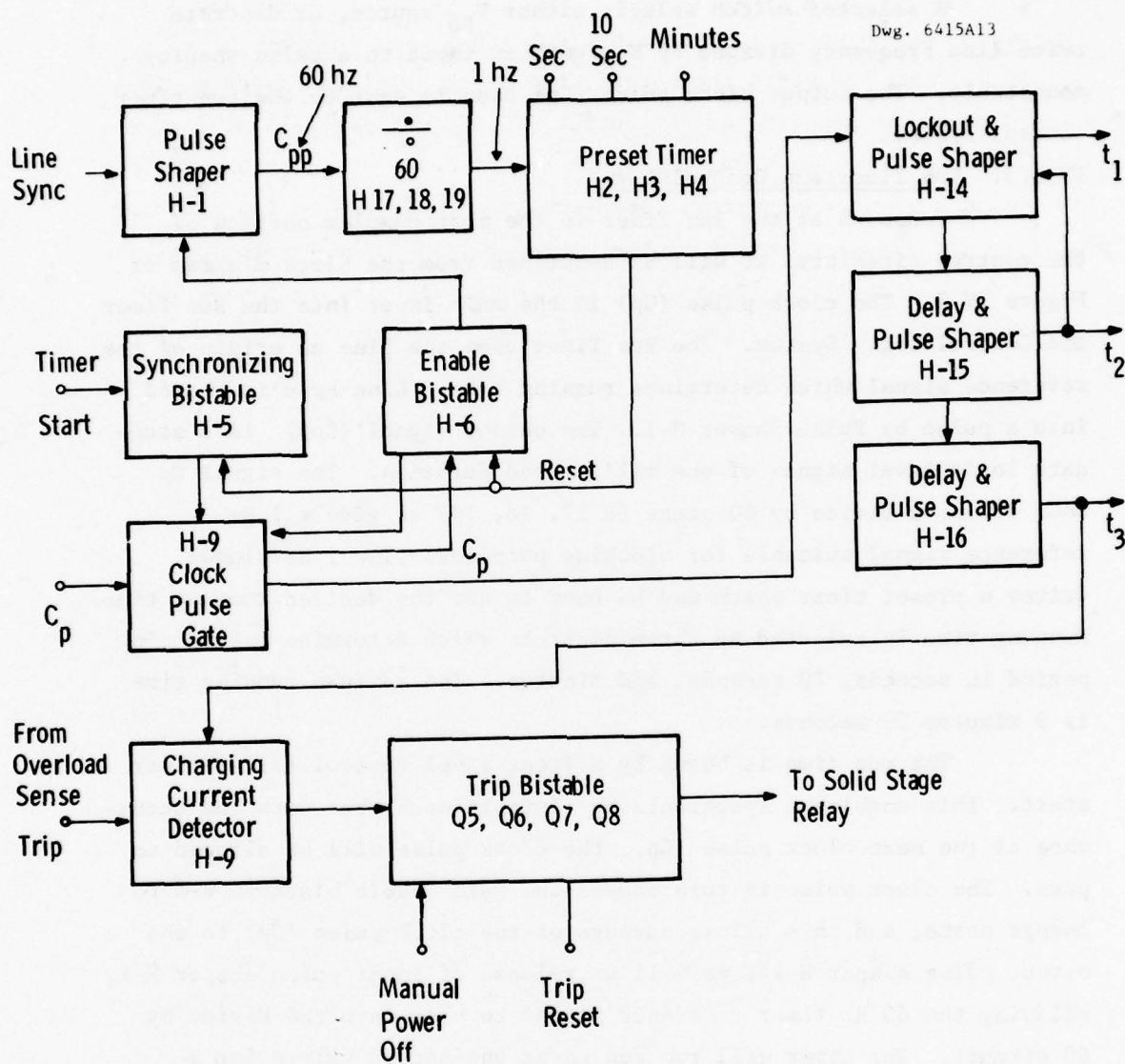


Figure IV-7. Run timer and control logic system block diagram.

and no run time interval will begin at mid-clock pulse interval or thereabouts. All time intervals will be identical to every other time interval because all are synched to the main clock (Cp).

When passed to the output, the clock pulse is shaped to its final form. This appears at the output of pulse shaper H-14 at time t_1 . The timing sequence is shown in Figure IV-8. Pulse t_1 is passed to the output through appropriate isolation techniques and begins a firing cycle by initiating charging of the many parallel pulse forming networks. A period of 24 msec is allowed for PFN charging; therefore the period between firing pulses can be no shorter than this value. Because of other time requirements, the repetitive cycle is limited to 25 msec, corresponding to a 40 Hz repetition rate. This is in keeping with the maximum power available from the line at the tester location.

Charging trigger t_1 is suitably delayed 24 msec and again shaped as pulse t_2 . Pulse t_2 will cause firing of the laser.

Trigger t_2 is suitably delayed 250 μ sec to form pulse t_3 . During the normal charging interval, PFN charging current will flow from the main supply to PFN networks from time t_1 to time t_2 , but at no other period in normal operation. If charging current should occur at some other time, such as during trigger time t_3 , it could only indicate failure of the test device to hold-off charging voltage. Trigger pulse t_3 is used to check for charge current at an unspecified moment. If such occurs, a trip bistable will change state, causing activation of a solid state relay, and in turn activation of the high speed breaker which disconnects the main high power input. Front panel controls of the control logic console may activate the trip bistable manually, as well as providing the reset function.

With the occurrence of laser trigger t_2 , laser firing occurs some 12 μ sec afterward. With firing of the test switch, some interference was experienced with the logic due to the high dI/dt and high dv/dt caused by the quick response of the test switch. An effective deterrent to false triggering was to initiate a shut down pulse at trigger time t_2 , such that for a period of 400 μ sec after t_2 a false

signal may not trigger pulse shaper H-14. For this period, bonafide triggers do not occur and interference signals have been great. A lockout signal is initiated at trigger time t_2 such that a false clock pulse may not trigger the input pulse shaper H-14.

The state of the run timer is indicated by a front panel light. When the timer is activated, the light will be on, indicating charge and fire triggers are being produced.

IV-5.4. Logic Isolation

All connections of electrical signals to the run timer and logic control are made through light-isolator diode-photo-transistors. The two signals which contact the environment outside the run timer are triggers 1 and 2. Refer to Figure IV-9.

Signals are simply coupled out of the run timer by photo isolators. In the logic isolators, triggers 1 and 2 are branched and their power amplified, yielding triggers which are transformer coupled out of the logic isolator to trigger the charging network thyristors and a trigger to fire the laser. Other triggers at the same times are made available by transformer isolation for general purpose sync.

Besides triggers, the signal indicating the occurrence of charging current is also coupled by a light isolator into the control logic module. As a consequence of this isolation system, reasonable performance free from interference effects were experienced by the test logic system.

IV-6. Assembly and Checkout

Assembly of the pulse forming network test circuit was completed mid-March, 1975. Figures IV-10 through IV-17 show various views during and after assembly was complete. The system performance was checked as described in Section 3.3.3 and found to perform as desired.

Figure IV-10 is a photograph of all of the major components of the PFN test circuit. The power supply transformers can be seen in the lower left, the rack of control logic at the right, and the main frame with the PFN circuits in the background.

Figure IV-11 is an edge view of the pulse forming networks.

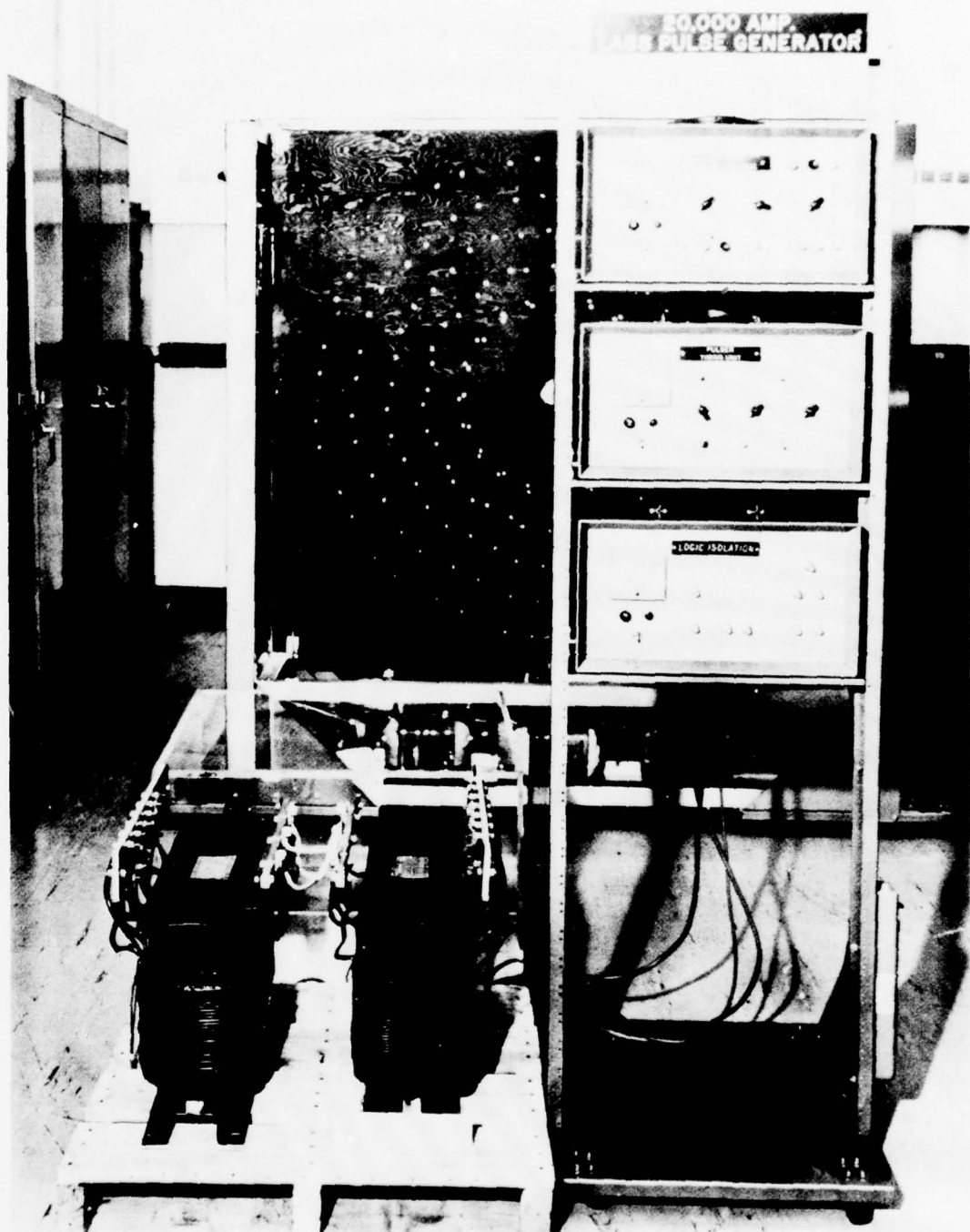


Figure IV-10. Major components of the PFN pulser test circuit. Logic control (on right, power transformers (foreground lower left), and PFN stack (background).

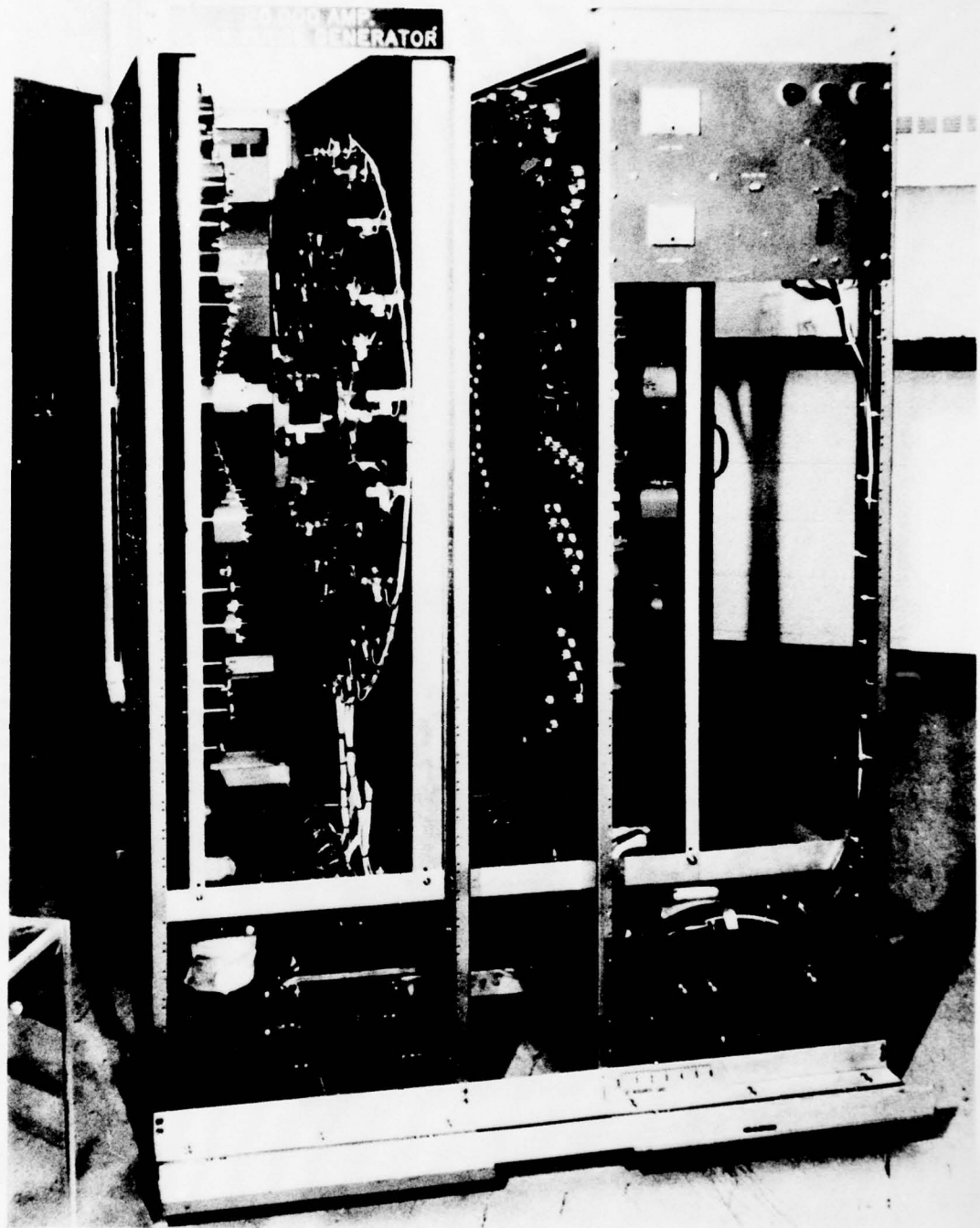


Figure IV-11. Pulsar test circuit: side view of PFN stack.

The main power breaker and charge current and voltage meters are located at the upper right.

Figure IV-12 shows the left panel swung out on its mounting hanger exposing one-half (20) of the pulse forming networks on the left (which were not complete at the time of the photograph) and one-half of the load resistors on the right arranged in a circle about the test device holder in the center on the right.

Figure IV-13 is the same as Figure IV-12 except that the right side has been folded out. Note that the inductors have been mounted on the capacitors on this side. Also note that the coaxial connector on the coaxial shunt monitoring resistor is exposed on this side of the test device holder in the center on the left.

Figure IV-14 shows a side view of the completed PFN stack. The cables connecting each PFN with its load resistor can be seen clearly, as can the bifurcated fiber optics cable used to conduct the laser beam into the device under test.

Figures IV-15 and IV-16 show close-up views of the side and front, respectively, of the device holder or test jig. The fiber optics cable was removed before Figure IV-16 was taken to avoid hiding the details of the device holder.

The charging network for the PFN is shown in Figure IV-17. This network is mounted in the frame of the PFN stack but under the assembly of the 40 PFN's.

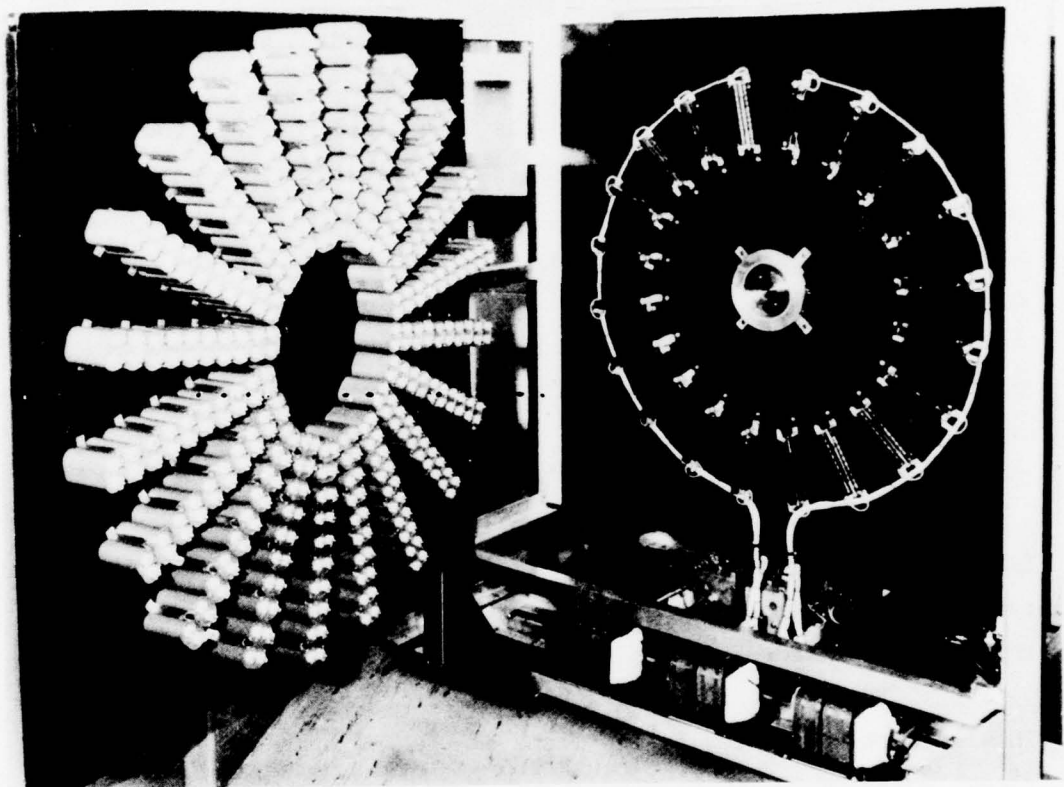


Figure IV-12. Pulser test circuit: PFN stack capacitor bank and load resistors prior to completion. Device under test mounts in fixture located in the center of the load resistor network.

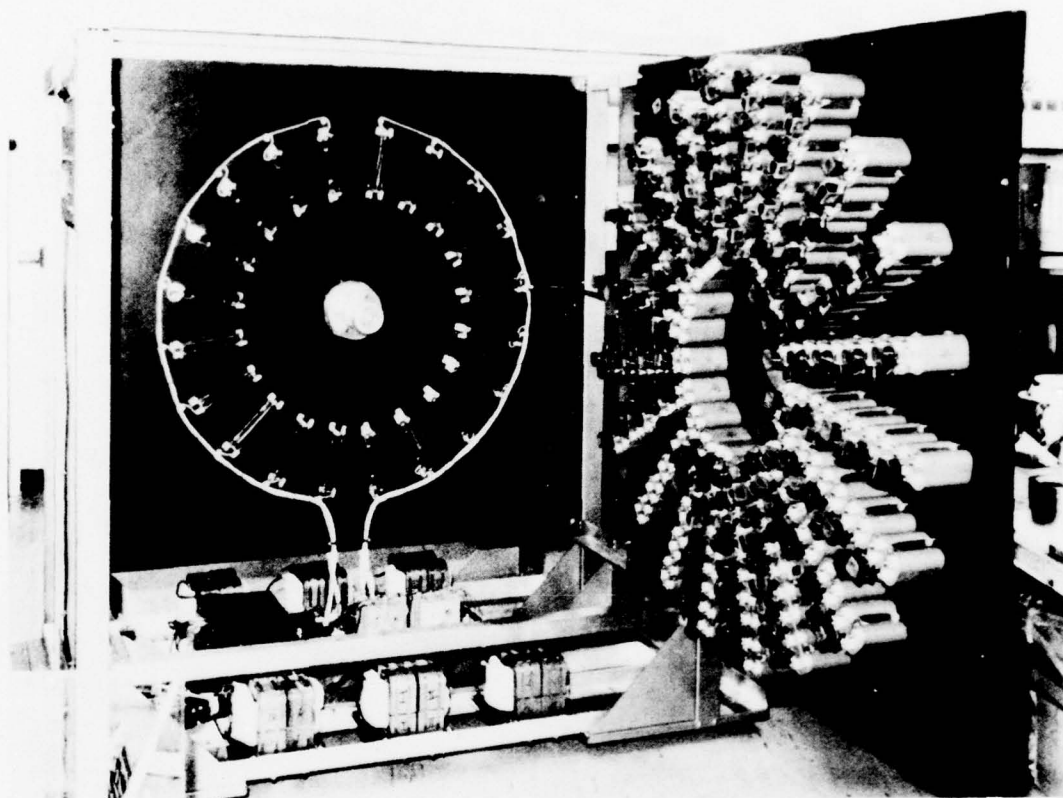


Figure IV-13. Pulser test circuit: PFN stack-capacitor bank with inductors mounted and load resistors. Current monitor coaxial shunt is located in the center of the load resistor network.

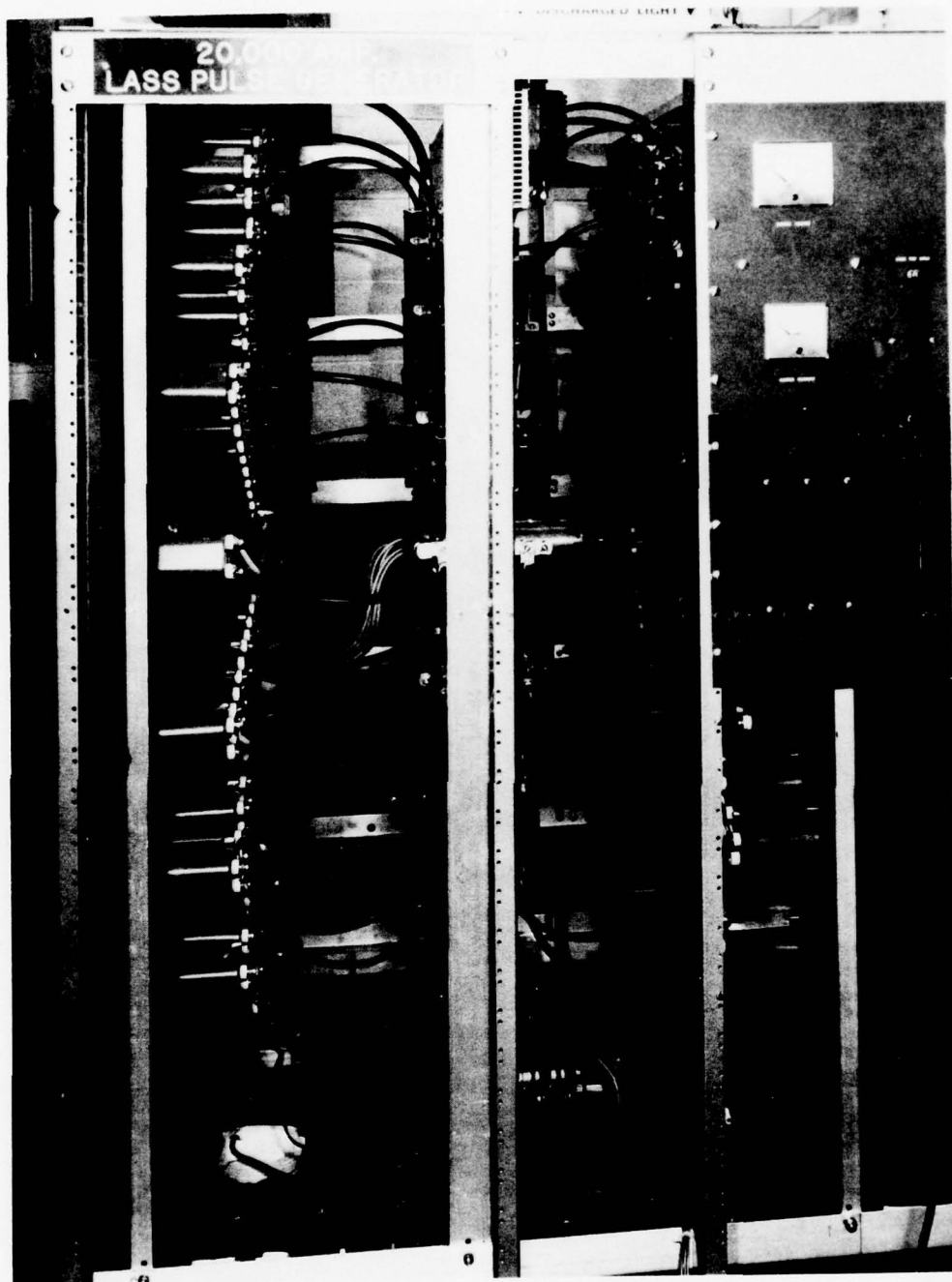


Figure IV-14. Pulser test circuit: PFN stack, side view, completed unit.

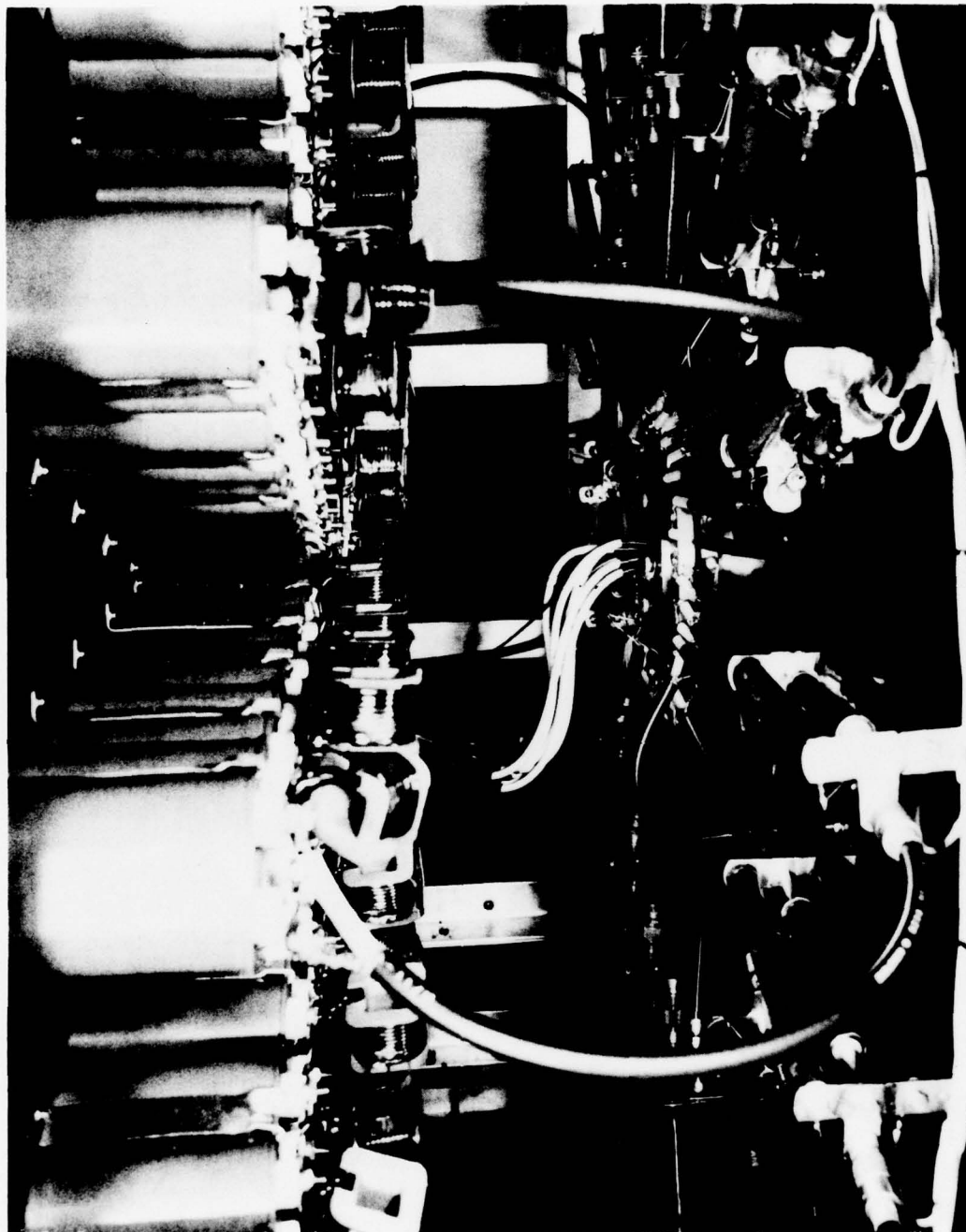


Figure IV-15. Pulser test circuit: PFN stack assembled showing close-up of device holder, side view. Note fiber optics cable to conduct the laser beam into the device fixture.



Figure IV-16. Pulser test circuit: PFN stack assembled showing close-up of device holder, front view.

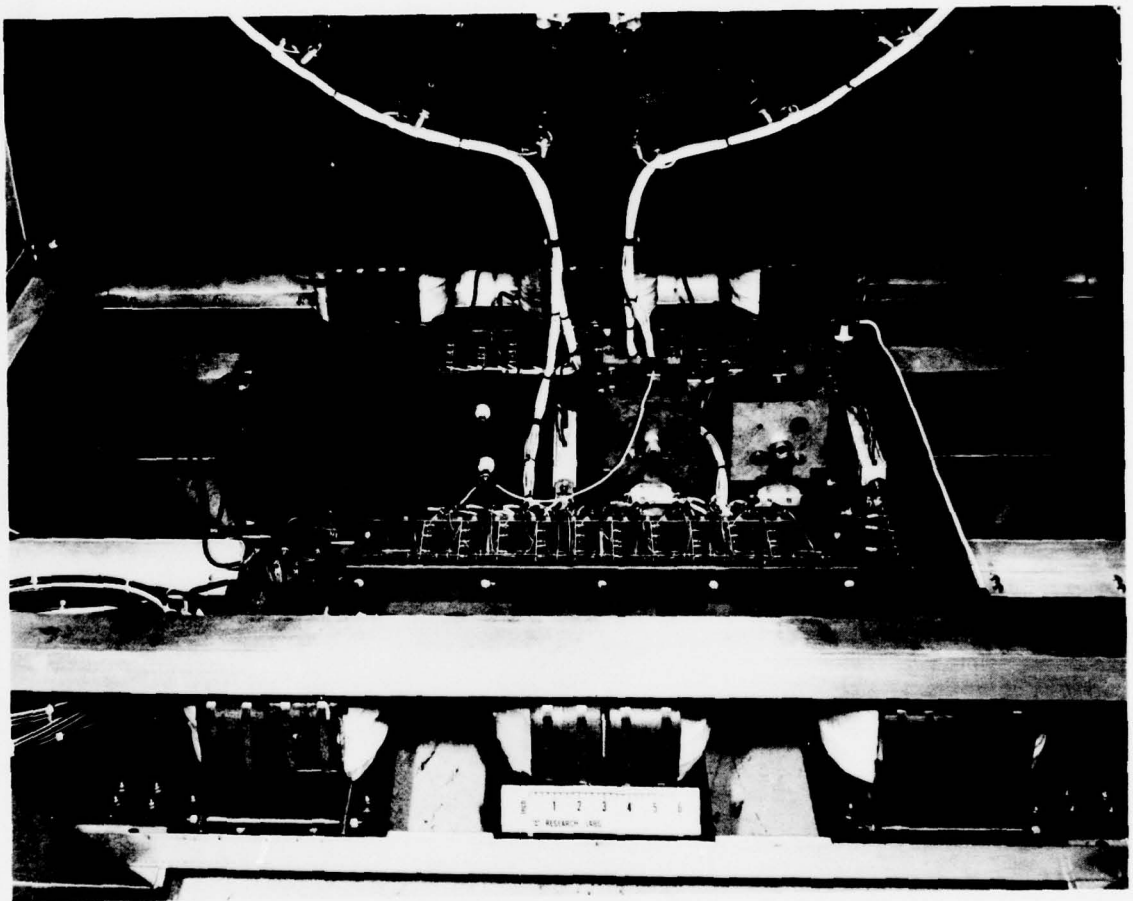


Figure IV-17. Pulser test circuit: charging network for the PFN stack.

APPENDIX V

PAPERS PUBLISHED RELATED TO THIS CONTRACT

APPENDIX V-1

Paper Given at Power Electronics Specialists' Conference-1976

ULTRA FAST, HIGH-POWER LASER-ACTIVATED SWITCHES

J. R. Davis and J. S. Roberts

Westinghouse Research Laboratories

Pittsburgh, Pennsylvania 15235

ABSTRACT

Laser fired semiconductor switches have been operated reliably at multi-megawatt power levels with nanosecond rise-times. Pulse currents up to 10,000 amperes and durations from 50 nanoseconds to 40 microseconds were obtained from storage lines charged as high as 1300 volts. In this paper data obtained from several experiments are compared to calculated results from a theoretical computer model. The analysis, reported previously (1), has been extended to include the effects of the initial carrier dynamics during turn-on.

INTRODUCTION

Light-activated semiconductor switches [LASS] can be turned on many orders of magnitude more rapidly than conventional electrically triggered devices. Conventional devices depend on comparatively slow drift and diffusion mechanisms to establish and to spread the conduction plasma throughout the device. With light-activation, the conduction plasma is produced by a spatially distributed laser illumination. By choosing a suitable combination of light wavelength, pulse energy and illumination geometry, a large area of conduction is established in a time corresponding to a combination of the transit time of the light through the device [~ 1 picosecond] and the duration of the light pulse [a few picoseconds to several nanoseconds]. Once the plasma is established, current conduction begins within a dielectric relaxation time [~ 1 picosecond]. The rate of current rise experimentally observed depends almost entirely on the inductance of the external circuit; the intrinsic inductance of the device is only a few picohenries. The maximum power level is limited primarily by the device's ability to dissipate thermal energy, typically less than 200 watts/cm² in the steady-state. By reducing conduction times and using low-duty cycles, laser-fired devices have been operated reliably and repetitively, switching more than 50 megawatts/cm² with current densities above 50,000 amps/cm². This is a power level of considerable interest in the areas of ultra-high power microwave generation and energy compression for fusion reactors, laser systems and so on.

Thermal effects are relatively unimportant for pulses shorter than a few microseconds and low repetition rates, but long pulses [10 to 100 microseconds] produce not only high temperature rise but considerable anisotropy in temperature and current distribution. In this case the operating limits must be derated below the values indicated above.

These considerations and experimental data have been used to extend a previously reported analysis (1) and an improved analytic model for the device operation has been developed. The analysis includes the effects of initial carrier dynamics, displacement current, the temperature dependent voltage-current-density characteristics and conduction area spreading. A three-dimensional time dependent heat flow analysis was carried out using a finite-element program to provide closed form heat-flow approximations which could be implemented in the device model.

EXPERIMENTAL

Two different sets of experiments were performed using similar equipment systems. The long-pulse [40 microsecond] studies were conducted at the Westinghouse Research Laboratories, while the short-pulse [50 nanosecond] work was conducted jointly with Westinghouse at the Lawrence Livermore Laboratory (2).

The two systems are essentially as illustrated in Fig. 1, not shown, but included, are oscilloscopes and meters to measure the various operating parameters and waveforms.

The Westinghouse system used as a storage element an array of up to 40 parallel networks which can be charged to 2000 volts and deliver a 20,000 ampere pulse with a rise-time below 1 microsecond. An IR apparatus was used to measure conduction area spreading by observing recombination radiation. The equipment consisted of a time-resolved image tube apparatus (3) or an SI photo-multiplier and a fiber-optic imaging array. The voltage transient was measured directly across the silicon wafer and current was measured using a .001 ohm sampling resistor.

In the Livermore experiments (2), the storage

element was a parallel array of up to 12, 1.25 ohm strip transmission lines. With a charging voltage of 1300 volts up to 9800 ampere pulses were produced with a duration of 50 nanoseconds and rise-times from 3 to 12 nanoseconds. IR spreading measurements were not made. The device voltage and current were calculated from measurements of the transmission line impedance and the transient line voltage.

In both cases, Q-switched Nd doped YAG [1.06 μ] lasers were used. Energy density at the device window was 10 to 20 mJ/cm² with a pulse duration of 5 to 10 nanoseconds. The light generated carrier density was approximately 10¹⁸/cm².

ANALYTIC MODEL

The device structure, shown in Fig. 2, locates and defines the various functional regions used in the analysis and in the computer model. The computer model, which is described in some detail in (1), is based on an iterative algorithm, which determines for each element of a time grid, how the current is spatially distributed in the device. The driving function is defined as the device current versus time function and the voltage drop across the device is calculated for each time point, from the current and temperature distributions. The analysis takes into account the temperature dependent voltage-current characteristics of the finite elements making up the spacial grid. The energy dissipated in each element is integrated in time and determines the local temperature rise as a function of time and the location of the element. The time constant for significant heat-flow is about 400 microseconds and the device is essentially adiabatic during the conduction pulse. Virtually all heat transfer occurs during the non-conduction interval. The incremental conduction area due to spreading is calculated at each time interval, from the current density at the outer edge of the conduction region.

The model has been extended and now includes a simplified two-dimensional, finite-element heat flow calculation which operates during both the conducting and non-conducting intervals.

The following additional mechanisms have been included.

Carrier Generation and Heating By The Light Pulse

The laser pulse produces a temperature rise, ΔT , given by:

$$\Delta T = E / [1.83 \times X] \quad (1)$$

E = Absorbed light energy in Joules/cm²
 X = Silicon thickness in cm.

The carrier concentration, n_0 , assuming uniform generation is:

$$n_0 = E / [h\nu \times 1.6 \times 10^{-19}] \quad (2)$$

$h\nu$ = Photon energy in eV = 1.17 eV [Nd YAG].

These equations are satisfactory up to approx-

imately 1 Joule/cm² which produces a temperature rise of 10°C and a carrier concentration of 10²⁰/cm³. Above this level, free carrier absorption begins to dominate, the generated carrier concentration ceases to increase linearly, and heating increases more rapidly as the absorption localizes near the surface.

Div. 6353A84

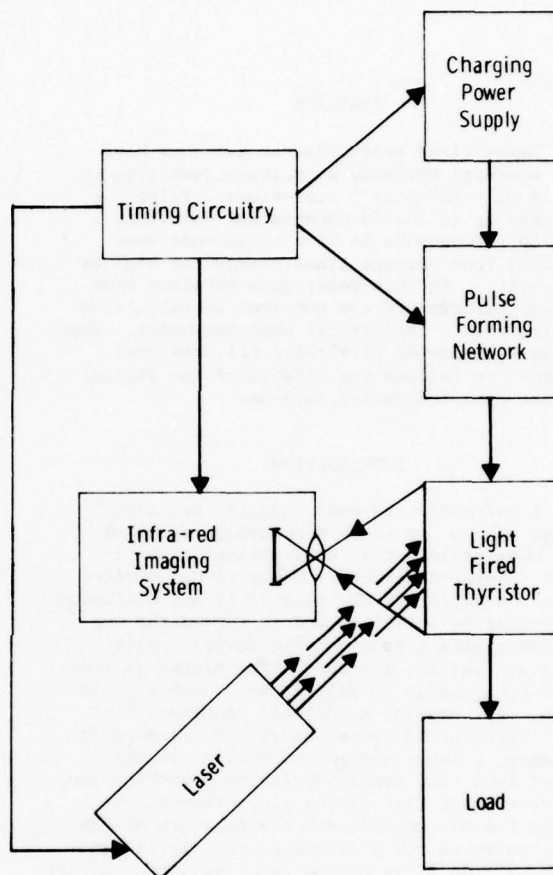


Fig. 1 - Block diagram of the experimental system

Relaxation of The Light Generated Plasma During Turn-on

The light injected plasma typically has a density from 10¹⁸ to 10²⁰/cm³. At this level carrier-carrier [Auger] recombination is dominant and carrier mobilities are determined by carrier-carrier scattering. The initial carrier concentration, n_0 , will decay to a steady-state level as:

$$n(t) = n_0 \exp[t(1/\tau_A + 1/\tau_0)], \quad (3)$$

where the Auger lifetime τ_A is given by (4-7);

$$\begin{aligned}\tau_A &= 1/[C_n n^2(t)] \\ C_n &= 2 \times 10^{-31} \text{ cm}^6/\text{sec} \\ \tau_0 &= \text{low-level base region lifetime.}\end{aligned}\quad (4)$$

A light generated carrier density in the base of $10^{20}/\text{cm}^3$ will decay, very rapidly at first, then slowing; reaching $10^{19}/\text{cm}^3$ in 30 ns and $\sim 2 \times 10^{18}/\text{cm}^3$ in 500 ns.

$$\begin{aligned}\text{For Silicon } A_{12} &= 8.05 \times 10^{14} \\ C_{12} &= 8 \times 10^8 \\ \mu_0 &= \text{low level mobility} \\ T &= \text{temperature, } ^\circ\text{K}\end{aligned}$$

The mobilities are small at high carrier levels [the electron mobility = $\sim 40 \text{ cm}^2/\text{voltsec}$ for $n(t) = 10^{19}/\text{cm}^3$], none the less, the voltage drop is reduced for short, fast rising pulses.

Doc. 6353AB3

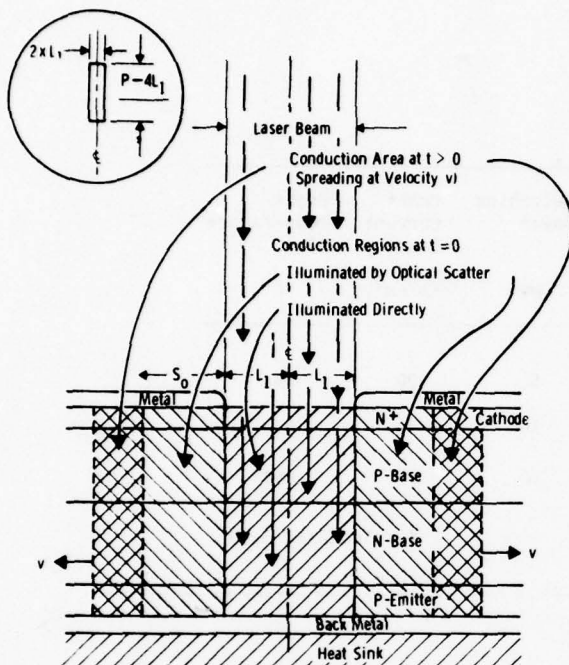


Fig. 2 - Device geometry

Numerical calculations using the modified model of Choo (1, 8-10) for a current density of $50,000 \text{ A}/\text{cm}^2$ give $\sim 4 \times 10^{18}$ for the average steady-state base carrier concentration. The Auger decay from eqs.(3) and (4) reaches this level in 190 ns [$\tau_0 = 2 \mu\text{s}$, $n_0 = 10^{20}/\text{cm}^3$]. Carrier injection will sustain the carrier concentrations near the emitter boundaries at $\sim 10^{20}/\text{cm}^3$. Therefore, with pulses shorter than 190 ns the voltage-current characteristic is determined largely by this process. At these extreme levels, current-voltage behavior is dominantly ohmic and the voltage, as a function of time in the decay regime, can be approximated using Ohm's Law and including carrier-carrier scattering (11,12).

$$V(t) = J \times X/[n(t)q\mu(n(t))] \quad (5)$$

$$\mu = [1/\mu_{12} + 1/\mu_0]^{-1} \quad (6)$$

$$\mu_{12} = A_{12} T^{3/2} / [n(t) \ln(1 + C_{12} T^2 / n^{2/3}(t))] \quad (7)$$

RESULTS

There are four experimentally observable variables which can be compared to the calculations: conduction area, current, temperature and voltage. Of these, the first two are used as input data and the third has not been successfully measured, leaving the transient voltage.

Table I is a summary of three cases for which data are presented in Figs. 3 through 11. The first two cases correspond to the experiments mentioned earlier, while the third case is the predicted result of extending the pulse duration of case II from 50 ns to 10 μs .

The data are presented as three figures for each case. Figs. 3, 6 and 9 are isometric plots of the calculated current density as a function of time and distance. The distance being measured from the centerline of the window (see Fig. 2), perpendicularly along the surface of the device.

Figs. 4, 7 and 10 are plots of the temperature rise with the other coordinates the same as for the current density figures.

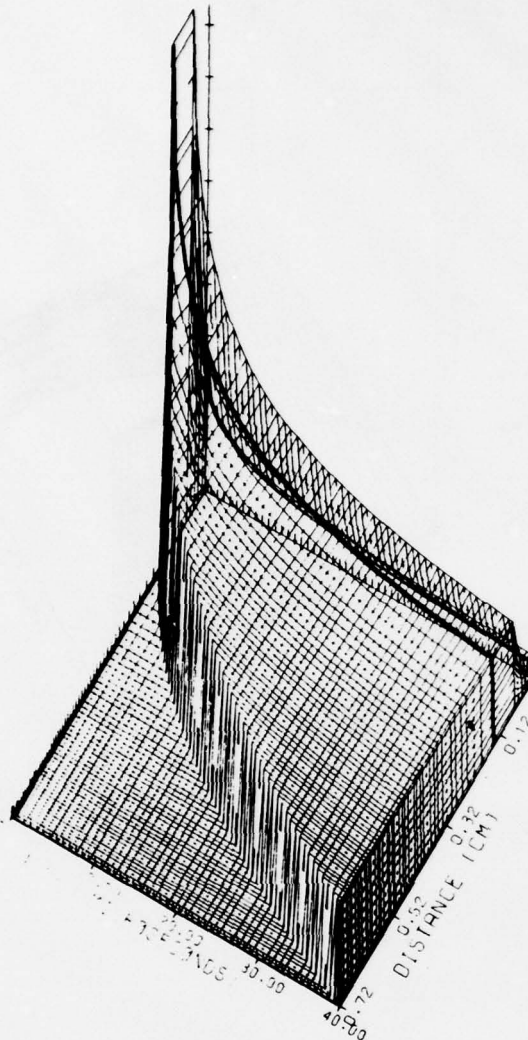
Figs. 5, 8 and 11 plot the calculated voltage and the driving current waveforms. Figs. 5 and 8 include the measured voltage and current data points for comparison with the calculated curves. The uppermost curves are current data.

Notice in Fig. 9, the shift of current density to the cooler, outer regions of the device; a consequence of the fact that at high currents the voltage drop increases with temperature.

TABLE I
Summary of Data

| | Pulse Current | Line Voltage | Pulse Duration | Rise Time | dI/dt | Switching Power | Peak* Current Density | Peak* Temperature Rise |
|------|------------------|-----------------|-------------------|--------------|-------------|--------------------|-----------------------------|------------------------------|
| | KA | KV | μ s | μ s | KA/ μ s | MW | KA/cm ² | °C |
| I | 5 | 1 | 40 | .316 | 16 | 5 | 20 | 68 |
| II | 9.8 | 1.3 | .05 | .012 | 750 | 10 | 56 | 6 |
| III* | 9.8 | 1.3 | 10 | .012 | 750 | 10 | 56 | 360 |

* Calculated data



17: 3 169/76
OPTAC-173/JMDAVIS

1500 VOLT LIGHT FIRED THYRISTOR
PERIETER, P0=0.00CM SLIT WIDTH, L1=-1.00CM OPTICAL SPREAD, S0=0.0750CM
PULSE LENGTH, L0= 40.00US FREQ, F0= 1.00MHZ RISE/FALL, R1= .313US
PEAK CURRENT, I0= 5.000AMPS DI/DT, K0= 16.000AMPS/US
THICKNESS, X0=.05CM BASE WIDTH, B1=.0250CM INIT TEMP, T0=300DEG/K
SHEFT HMO, H0= 2.000HMS/SQUARE HEAT CAPACITY, K1=1.38J/DEGCM³
SPREADING CONSTANTS, B0= .01 C0=1.099 VELOCITY LIMIT, V0=500U/US
IV CONSTANTS, C4= .75 C5=-5.89E-04 D4=1.774E-03 D5=1.5390E-11
SEG-2 V3=15.00 K3= 1.41
SEG-3 V4=30.00 K4= 1.12
SEG-4 V5=42.00 K5= 1.04

Fig. 3-Current density profiles versus time for case I. Distance is measured from the center of the window. Current density is reduced in the window region because it lacks contact metallization. Conduction area spreading is seen as the diagonal "wall" in the foreground. Current density reaches a maximum of 20KA in 313ns, then diminishes, as the area expands, to about 4KA at the end of the current pulse.

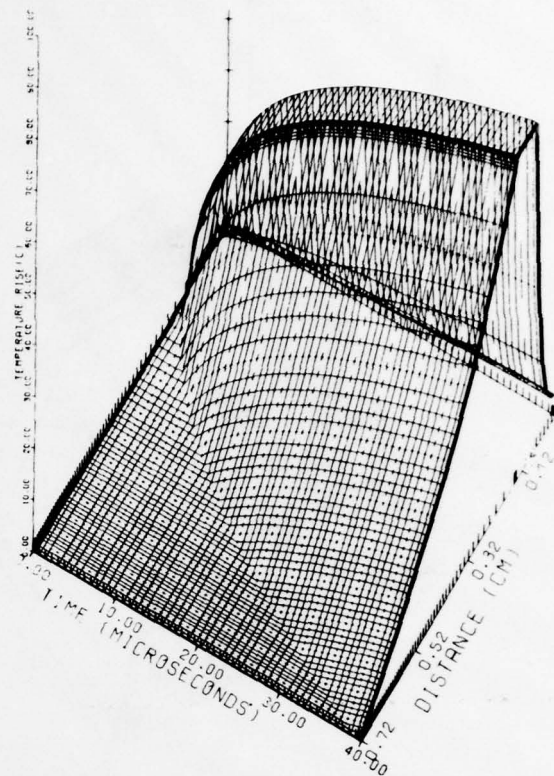


Fig. 4-Temperature profiles versus time for case I. The region turned on by optical scatter, defined in Fig. 2, is treated as a single element in the space grid and is seen as the flat peak in the plot.

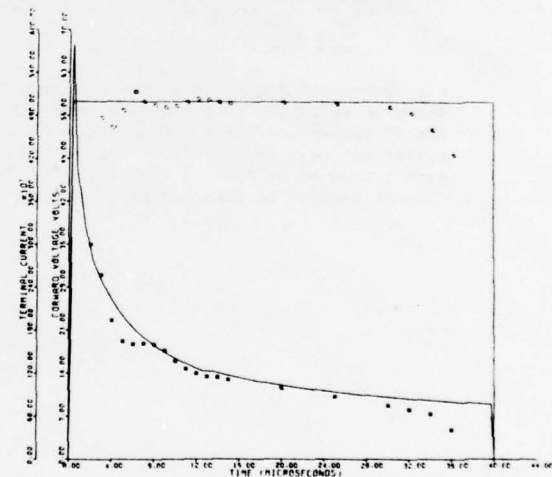
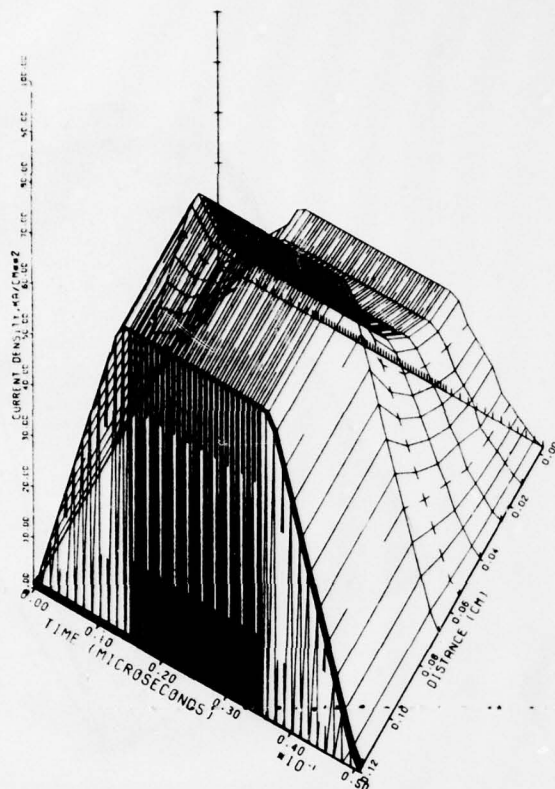


Fig. 5-The calculated voltage and the driving current waveforms along with the experimental data. The current data are at the top of the figure.



16155 16V/76
OPTAC-173/JHDAVIS

1500 VOLT LIGHT PIPED THYRISTOR
PERIMETER, P0=1.83CM SLIT WIDTH, L1=1.40CM OPTICAL SPREAD, S0=0.0500CM
PULSE LENGTH, L0=0.05US PNEW, P0=1.00HZ RISE/FALL, R1=0.013US
PEAK CURRENT, I0=9.800AMPS DI/DT, K0=750.000AMPS/US
THICKNESS, A0=0.05CM BASE WIDTH, B1=0.0500CM INIT TEMP, T0=300DEG/K
SHEET RHO, R0=2.000HMS/SQUARE HEAT CAPACIT, K1=1.78J/DEG*CM**3
SPREADING CONSTANTS, B0=0.01 CO=1.092 VELOCITY LIMIT, V0=5000/US
IV CONSTANTS, C4=0.75 C5=5.79E-04 D4=1.654E-03 D5=1.519UE-11
SEG-2 V3=15.00 K3=1.41
SEG-3 V4=30.00 K4=1.12
SEG-4 V5=40.00 K5=1.04

Fig. 6-Current density profiles for case II. There is virtually no conduction spreading during the 50 nanosecond pulse. Conduction remains almost entirely in the window region and the region turned on by optical scatter. The peak current density is 56KA/cm² at 12 nanoseconds.

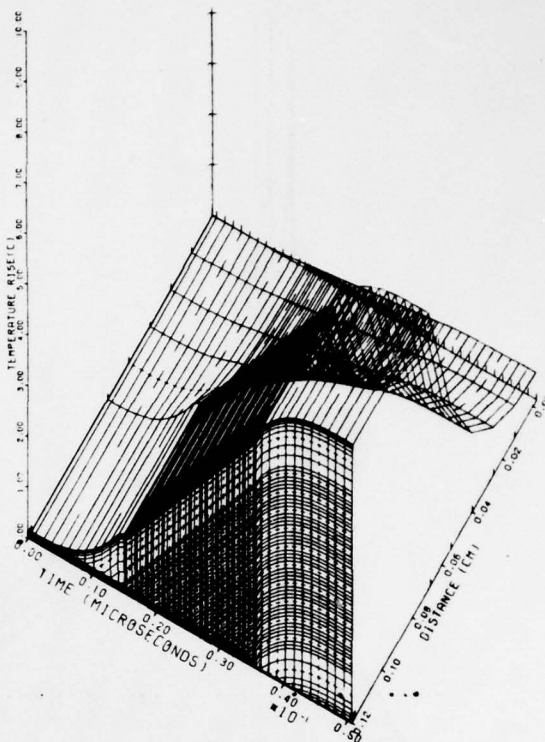


Fig. 7-Temperature profiles for case II. The energy dissipation varies with J^2 , resulting in the initial parabolic temperature rise. The maximum temperature rise is less than 6°C.

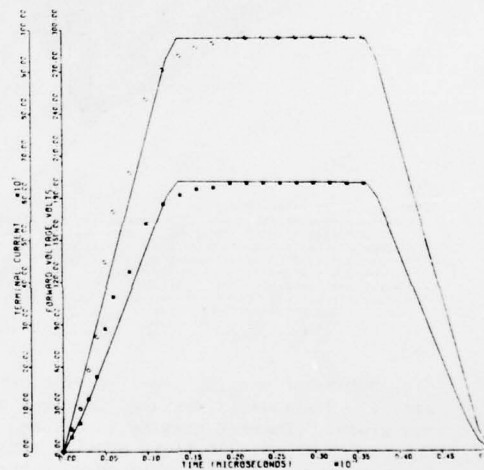
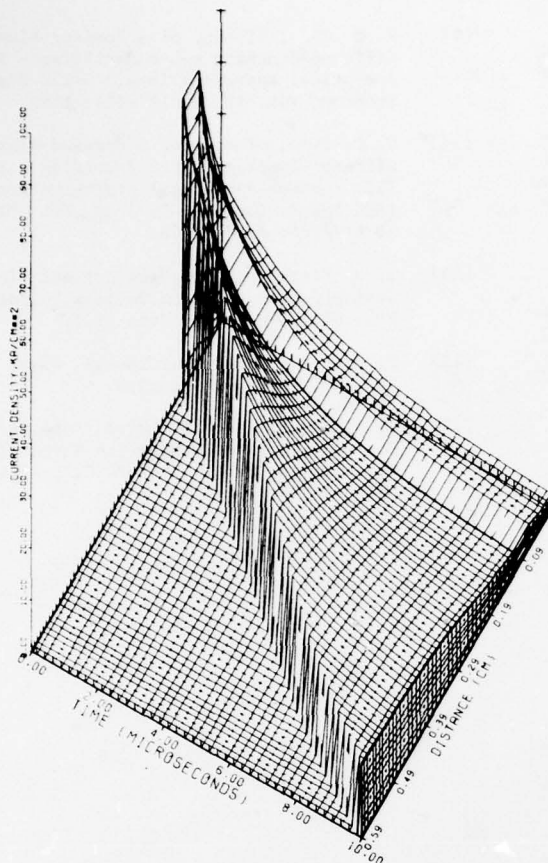


Fig. 8-The calculated voltage and the driving current waveforms for case II, along with the experimental data.



15154 174/76
OPTAC-188/JRDAVIS

1500 VOLT LIGHT FIXED THYRISTOR
PERIMETER, P0=1.83CM SLIT WIDTH, L1=1.40CM OPTICAL SPREAD, S0=0.0500CM
PULSELENGTH, L0= 10.00US FREQ, F0= 1.00HZ RISE/FALL, H1= .013US
PEAK CURRENT, I0= 9.800A/DI/DI, K0=750.000A/US
THICKNESS, X0=.05CM BASE WIDTH, B1=.0250CM INIT TEMP, T0=300DEG/K
SHEET RHO, R0= 2.000HMS/SQARE HEAT CAPACITY, K1=1.38J/DEG*CM^3
SPREADING CONSTANTS, B0= .01 C0=1.092 VELOCITY LIMIT, V0=500U/US
IV CONSTANTS, C4= .75 C5=5.79E-04 D4=1.654E-03 D5=1.5390E-11
SEG-2 V3=15.00 K3= 1.41
SEG-3 V4=30.00 K4= 1.12
SEG-4 V5=42.00 K5= 1.04

Fig. 9-Current density profiles for case III. This simulation was the same as case II, except that the pulse length was increased to 10 microseconds. Conduction spreading is evident. A large temperature difference between the center and the edge results in a shift of current to the cooler edges of the device.

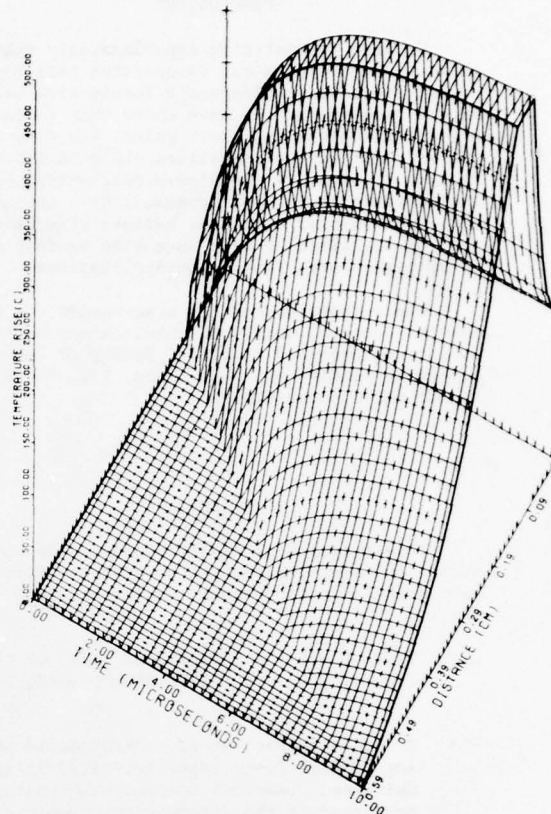


Fig. 10-Temperature profiles for case III. The predicted rise for this 10 microsecond pulse reaches $\sim 350^{\circ}\text{C}$. It is likely a device operated with these conditions would become thermally unstable and be destroyed.

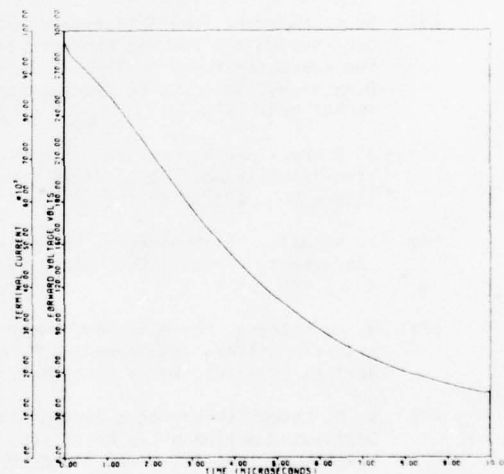


Fig. 11-The calculated voltage and current waveforms for case III.

CONCLUSIONS

We have demonstrated experimentally that the light fired switches can be operated reliably and repetitively at multimegawatt levels with nanosecond rise-times. We have shown that thermal effects are small for short pulse, low duty cycle operation at current densities above $50,000 \text{ A/cm}^2$. We have developed a computer model, which predicts device behavior in good agreement with the available experimental data. We believe this device will be successfully used in a wide variety of ultra-high power, fast pulse applications.

The authors gratefully acknowledge the experimental results, useful discussions and editorial assistance provided by O.S.F. Zucker of Lawrence Livermore Laboratory, L.R. Lowry, P.L. Hower, R.J. Fiedor and E. Adams-Davis

REFERENCES

This research partially supported by United States Air Force, Aeronautical Systems Division, Aero Propulsion Laboratory, Contract F33615-74-C-2029.

- (1) J. R. Davis, "A Theoretical Model of Light-Fired Thyristors," IEEE PESC Record, 309-311; 1975.
- (2) O. S. F. Zucker, et al., "Nanosecond Switching of High Power Laser Activated Silicon Switches," Lawrence Livermore Laboratories, presented at the International Topical Conference on Electron Beam Research and Technology, Albuquerque, N.M., sponsored by Sandia Laboratories; 2 November 1975.
- (3) H. Yamasaki, IEEE Trans. Electron Devices, VOL. ED-22, pp 65-69; 1975.
- (4) N. G. Nilsson, "The Influence of Auger Recombination on the Forward Characteristics of Semiconductor Power Devices at High Current Densities," Solid State Electronics, VOL. 16, pp 681-688; 1973.
- (5) J. D. Beck and R. Conradt, "Auger-Rekombination in Silizium," Solid State Communications, VOL. 13, pp 93-95; 1973.
- (6) R. N. Hall, "Recombination Processes in Semiconductors," Proc. IEEE, Part B Suppl., No. 17, p 106; 1959.
- (7) N. G. Nilsson, "Band-to-Band Auger Recombination in Silicon and Germanium," Physica Scripta (Sweden), to be published.
- (8) S. C. Choo, "Theory of a Forward-Biased Diffused-Junction p-L-n Rectifier - Part I: Exact Numerical Solutions," IEEE Trans. Electron Devices, VOL. ED-19, pp 954-966; August 1972.
- (9) S. C. Choo, "Theory of a Forward-Biased Diffused-Junction p-L-n Rectifier - Part II: Analytical Approximations," Solid State Electronics, VOL. 16, pp 197-211; 1973.
- (10) S. C. Choo, "Theory of a Forward-Biased Diffused-Junction p-L-n Rectifier - Part III: Further Analytical Approximations," IEEE Trans. Electron Devices, VOL. ED-20, pp 418-426; April 1973.
- (11) N. H. Fletcher, "The High Current Limit of Semiconductor Junction Devices," Proc. IRE, VOL. 45, pp 862-872; June 1957.
- (12) P. P. Debye and E. M. Conwell, Phys. Rev., VOL. 93, pp 692- ; 1954.
- (13) A. A. Jaecklin and M. Leitz, "Analysis of a Power Semiconductor Near Its Threshold of Destruction," Proc. 1974 PESC, pp 134-139; 1974.

APPENDIX V-2

Paper Given at Power Electronics Specialist Conference - 1975

A THEORETICAL MODEL OF LIGHT-FIRED THYRISTORS*

J. R. Davis

Westinghouse Research Laboratories
Pittsburgh, Pennsylvania 15235

ABSTRACT

A computer model of light-fired thyristors has been developed which calculates device voltage and the spatial distributions of current and temperature as functions of time throughout multiple pulse chains.

INTRODUCTION

A light-fired thyristor, as distinguished from a light-triggered device, is fully turned on within the illuminated region during the light pulse. The light pulse, typically produced by a Q-switched laser, provides sufficient energy to generate carrier concentrations throughout the illuminated part of the base regions of the same order of magnitude or greater than those which occur in the device in the normal on-state. This turn-on process is therefore free of the usual transit time delays and is capable of switching extremely large values of dI/dt . The magnitude of dI/dt and the amplitude of the pulse currents which are possible, depend on various device and operating parameters: the area and perimeter of the illuminated region; the shape, duration and duty cycle of the pulse; the initial temperature and the temperature-dependent voltage-current characteristic of the device; the conduction area spreading behavior; and the heat transmission and heat capacities of the device and its mounting assembly.

The analytic model is constructed of several separate elements. The first element is a determination of the voltage-current characteristic as a function of temperature for the high current densities experienced by these devices. A piecewise model is obtained experimentally for individual devices.

The next element is a calculation of the current distribution in the uncontacted region through which the laser beam enters the device. This provides an effective area of conduction at $t = 0$ and which remains turned on throughout the pulse.

Then a formulation of the conduction area spreading is obtained based on experimental time-dependent infrared measurements.

The next part is a calculation of the current and temperature distributions and the forward voltage drop as functions of time. These quantities are interdependent and are determined by a computer iteration technique.

Finally, a separate computer program is employed to solve the three dimensional, time-dependent heat-flow problem and obtain the temperature distributions during multiple pulse sequences.

The context of the following analysis is the experimental system shown in Figure 1 which consists of a pulse-forming-network supplying energy to a load through the laser-fired thyristor. The device geometry is shown in Figure 2. Light from the laser enters the rectangular window in the cathode metallization, generating a high concentration electron-hole plasma, which extends throughout the volume under the window area and by optical scattering into regions adjoining the window.

The analysis given here is based on this rectangular window geometry but provides essentially the same results as those obtained using a circular window as normally used on the experimental devices. In addition, the present version of the model is usable only for short pulses, since we assume adiabatic conditions and consider that all heat flow occurs during the interval of zero current between pulses.

VOLTAGE-CURRENT CHARACTERISTIC

At high current densities, the voltage-current behavior of power devices becomes increasingly dependent on carrier-carrier processes. Fletcher (6) and Dannhauser (7) examined the influence of carrier-carrier scattering and Nilsson (1,4) analyzed the effect of Auger recombination. These results have been combined along with lattice-scattering according to Debye and Conwell (17) in the numerical model of Choo (12-14). The calculated voltage-current characteristic agrees well with experimental pulse measurements up to 5000 or 6000 A/cm². Jaeklin (9,10) and Burtscher (5), using similar methods, obtained essentially the same results. A

* Research partially supported by United States Air Force, Aeronautical Systems Division, Aero Propulsion Laboratory, Contract #F33615-74-C-2029.

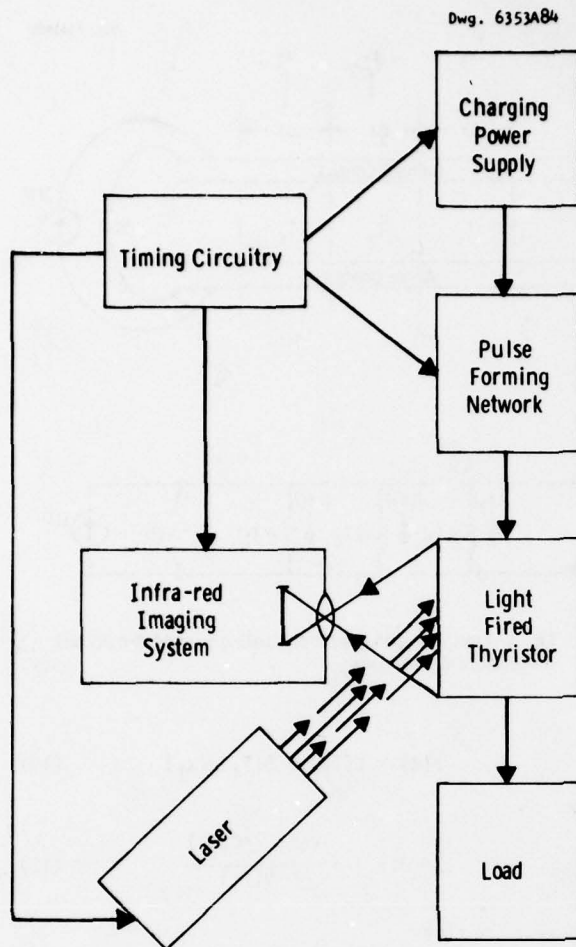


Fig. 1—Block diagram of the experimental system

significant feature of these results is that the voltage-current curve, above approximately 200 A/cm², can be closely approximated by a linear expression:

$$V = C_i(T) + D_i(T)J \quad (1)$$

where V = forward-voltage, volts
 J = current density, A/cm²
 T = temperature, °K.

At higher currents, above about 5000 A/cm², the theory diverges from experimental data. For the purposes of the present computer model, a three-segment piecewise linearization of the measured data is used. For example, a least-squares-regression of data taken for an experimental device having a total base width of 240 μm provided the following three-segment fit.

$$\begin{aligned} C_1 &= 1.25 - 9.19 \times 10^{-4} T \\ D_1 &= 8.378 \times 10^{-4} + 6.794 \times 10^{-12} T^3 \text{ for segment 1,} \\ C_2 &= -.21 + 1.195 \times 10^{-3} T \\ D_2 &= 1.089 \times 10^{-3} + 8.832 \times 10^{-12} T^3 \text{ for segment 2,} \\ C_3 &= -4.527 - 1.685 \times 10^{-3} T \\ D_3 &= 1.535 \times 10^{-3} + 1.245 \times 10^{-11} T^3 \text{ for segment 3.} \end{aligned}$$

CURRENT CONDUCTION IN THE WINDOW

The pulse-forming network, acting as a current source, will cause current to flow immediately in the region illuminated by the laser. It is assumed that as the current flow begins, the light generated carrier profile will relax to a quasi-steady-state profile in a negligible period of time (sub-microsecond). In any case, the dynamics of this carrier redistribution are not included in the present model.

Referring to Figure 2, the current is approximately one-dimensional and vertical in the combined base-regions and horizontal in the diffused cathode-region. The resulting non-uniform current distribution can be determined from the equivalent circuit shown in Figure 3.

$$i(x) = \int_0^x J(x) dx \quad (2)$$

or equivalently,

$$\frac{di(x)}{dx} = J(x). \quad (3)$$

Dwg. 6353AB3

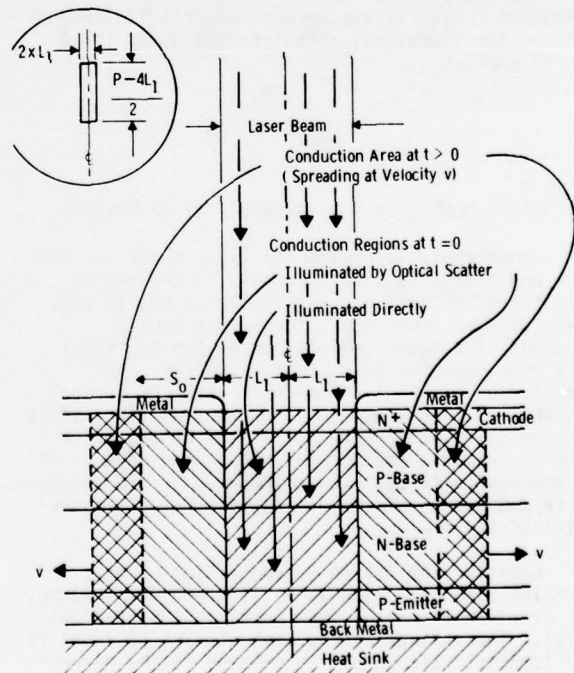


Fig. 2—Device geometry

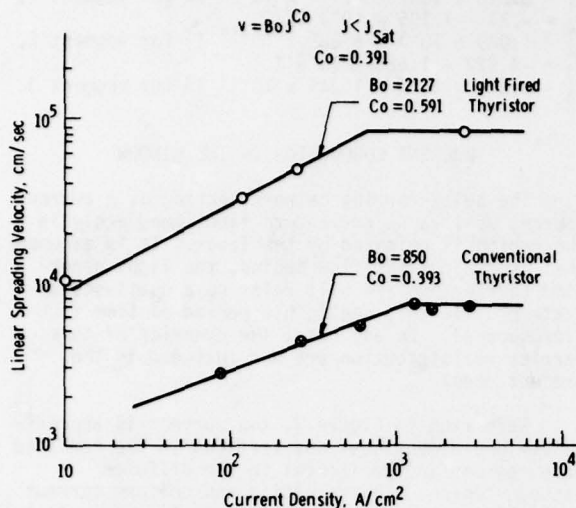


Fig. 4—Spreading velocity data for a light fired thyristor compared to a conventional device (The two devices are not of the same design)

has been observed only with certain device structures -- others exhibit velocities similar to those of conventionally operated devices. At present, no satisfactory explanation is available and investigation is still underway.

For the purposes of the computer model, the spreading constants are determined empirically and used in the functional relationships given in 1) and 2) above.

CURRENT DENSITY AND TEMPERATURE DISTRIBUTIONS

Immediately following the laser pulse, current flow and energy dissipation begin in the region illuminated directly or indirectly by the laser. Then, as time progresses, the active region expands. The outer regions, being turned on for less time, receive less energy, and therefore experience less temperature rise than the central regions. Although the total current at any instant in time is fixed by characteristics of the pulse-forming-network, the current within the device will be non-uniformly distributed because of the temperature dependence of the voltage-current characteristic of the device.

Consider the device as consisting of many parallel elements, each at a different temperature, T_i , or as in Figure 5, many parallel admittances, $g(T_i)$. The voltage across each element is equal to the terminal voltage and is related to the current density in that element as:

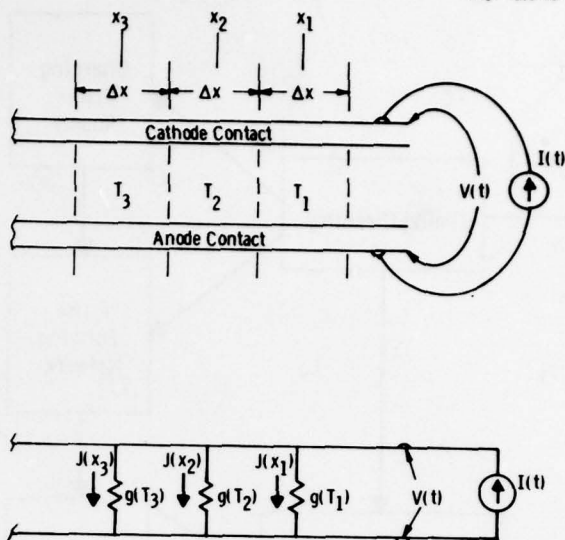


Fig. 5—Electrical analogue for calculating current-density and temperature distributions

$$V(t) = C(T_i) + D(T_i)J(x_i) \quad (14)$$

or

$$J(x_i) = \frac{V(t) - C(T_i)}{D(T_i)} \quad (15)$$

where t = time

T_i = temperature of i th element

x_i = x coordinate of i th element.

The integral of $J(x_i)$ over all conducting elements is the total current, $I(t)$.

$$I(t) = \int_{x_0}^{x_n} J(x_i) dx = V(t) \int_{x_0}^{x_n} \frac{dx}{D(T_i)} - \int_{x_0}^{x_n} \frac{C(T_i)}{D(T_i)} dx. \quad (16)$$

The voltage-current Equation (1) can be rewritten

$$J(x) = (V(x) - C_i)/D_i \quad (4)$$

Also from the figure:

$$dV(x) = i(x)\rho_s dx \quad (5)$$

which implies:

$$\frac{d^2V(x)}{dx^2} = \frac{di(x)}{dx} \rho_s \quad (6)$$

Combining Equations (3), (4) and (6) gives:

$$\frac{d^2V(x)}{dx^2} = \rho_s (V(x) - C_i)/D_i \quad (7)$$

The width of the window is small, and we assume the region is isothermal, so that C_i and D_i are constant with respect to x . The general solution for Equation (7) is:

$$V(x) = K_1 \exp(Ax) + K_2 \exp(-Ax) + C_i \quad (8)$$

where

$$A = \sqrt{\rho_s/D_i} \quad (9)$$

The solutions become, for the voltage:

$$V(x) = \frac{A(V_0 - C_i)}{\rho_s \cosh(AL)} \sinh(Ax) \quad (10)$$

and for the current density:

$$J(x) = \frac{I_0 A}{\sinh(AL)} \cosh(Ax) \quad (11)$$

It is convenient for the computer model to define an effective conduction width, W_0 , for the window region such that:

$$J_0 W_0 \equiv W_0 J(x) \Big|_x = L = \int_0^L J(x) dx = I_0 \quad (12)$$

Then, from Equations (11) and (12) we have:

$$W_0 = \{\tanh(AL)\}/A \quad (13)$$

This permits treating the conduction in the unmetallized region as if it were a metallized region W_0 wide and carrying a uniform current density, J_0 .

CONDUCTION SPREADING

The spreading of the conduction area during the turn-on of conventional thyristors has been studied by numerous investigators (18-22). The results of these and other studies provide the following general conclusions:

1) The linear-spreading-velocity is related to the current density as:

$$V = BJ^C \text{ for } J < J_{sat} \\ (\text{typically about } 1000 \text{ A/cm}^2).$$

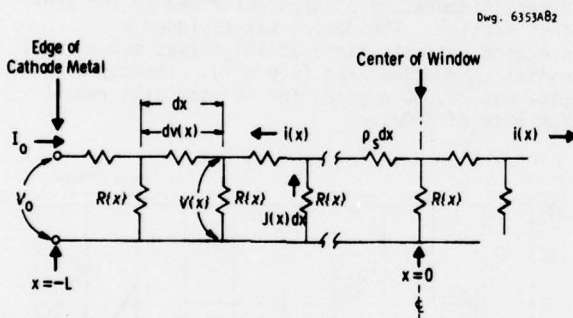
2) For current densities above J_{sat} , the velocity saturates with:

$$V_{sat} = 0.5 \times 10^3 \text{ to } 20 \times 10^3 \text{ cm/sec.}$$

3) The constants B , C , J_{sat} and V_{sat} are strongly dependent upon the device-design parameters, particularly the base widths and lifetimes, and the shunt and cathode geometries.

4) The velocity shows no significant temperature dependence.

In recent experiments, we have examined the spreading behavior of laser-fired devices using a gated infrared imaging system. Although the statements above remain qualitatively true, we have observed, in some devices, much higher velocities than are found with electrically triggered devices. The high velocity behavior shown in Figure 4 is based on limited experimental data and should be considered tentative. This high velocity behavior



ρ_s = Sheet Resistance of Diffused Cathode Layer ($2 \Omega/\square$)

V_0 = Potential Between Cathode and Anode Contacts

I_0 = Total Current Flowing in the Window Region

$R(x)$ = Effective Resistance of the Thyristor Element

$R(x) = C_i/J(x) + D_i$ (see Eq. (1))

Fig. 3—Equivalent circuit of the window region

The boundary conditions are:

$$\begin{aligned} i(x) \Big|_{x=0} &= 0, \\ i(x) \Big|_{x=L} &= I_0, \\ V(x) \Big|_{x=L} &= V_0. \end{aligned} \quad (9)$$

The terminal current $I(t)$ is known so that the terminal voltage $V(t)$ can be determined from:

$$V(t) = \frac{I(t) + \int_{x_0}^{x_n} \frac{C(T_i)}{D(T_i)} dx}{\int_{x_0}^{x_n} \frac{dx}{D(T_i)}} \quad (17)$$

If time is incremented by Δt and $I(t)$ becomes $I(t + \Delta t)$, the energy dissipated in the i th element is:

$$\Delta E(x_i) = J(x_i)V(t + \Delta t)\Delta t \quad (18)$$

where $V(t + \Delta t)$ is given by Equation (17) and $J(x_i)$ by Equation (15).

The temperature rise for the element:

$$\Delta T_i = \Delta E(x_i) / (\text{element volume} \times \text{heat capacity}). \quad (19)$$

As is indicated by the results of the heat-flow calculations in the next section, there is negligible heat loss during the pulse interval; i.e., the device is adiabatic and the element temperature:

$$T_i' = T_i + \Delta T_i \quad (20)$$

This implies a different distribution of $J(x_i)$ and a different T_i . These can be determined by iterating Equations (17) through (20) with T_i' replacing T_i , except in Equation (20) which defines the new T_i' . This self-consistent procedure is continued until a fixed configuration is obtained for

$$T_i' \equiv T_i'(t + \Delta t),$$

$$J(x_i) \equiv J(x_i, t + \Delta t),$$

and

$$V(t + \Delta t).$$

$T_i(t + \Delta t)$ is then set equal to T_i' . Time is incremented and the process repeated.

Over and above the mathematical stability of the algorithm, the device is inherently stable thermally. The device voltage, in the high current domain, has a positive temperature coefficient which tends to increase the current density in the cooler regions and decrease it in the hotter ones.

A computer program was written using this algorithm and including the results of the spreading and window conduction calculations. The program input consists of the various geometric, material and electrical properties of the device, as well as the initial temperature profile and

parameters of the current pulse. The output data are, as functions of time, the current density and temperature profiles, $J(x,t)$ and $T(x,t)$, and the voltage drop $V(t)$. Since this computation assumes adiabaticity, questions remain concerning the effects of heat-flow.

TRANSIENT HEAT-FLOW

The analysis of heat-flow in the device and its heat-sink structure utilizes a large Westinghouse proprietary, finite-element computer program. The input for this program consists of the structure geometry, materials and material properties, a mesh defining the elements and nodes to be used in the analysis, the temperature boundary conditions and the time-dependent heat input.

The device hypothesized in these examples is a 5-cm diameter fusion of silicon, molybdenum and copper with respective thicknesses of 0.05 cm, 0.15 cm and 1.0 cm. The heat-sink is single-sided and attached to the copper.

The initial temperature profile and the time-dependent energy input were obtained from the current/temperature program described in the previous section. The device was assigned a spreading-velocity limit of 10^4 cm/sec and a small initial conduction area (1.0 cm^2). The current pulse was 20,000 amperes for 40 μsec at a repetition rate of 500/sec.

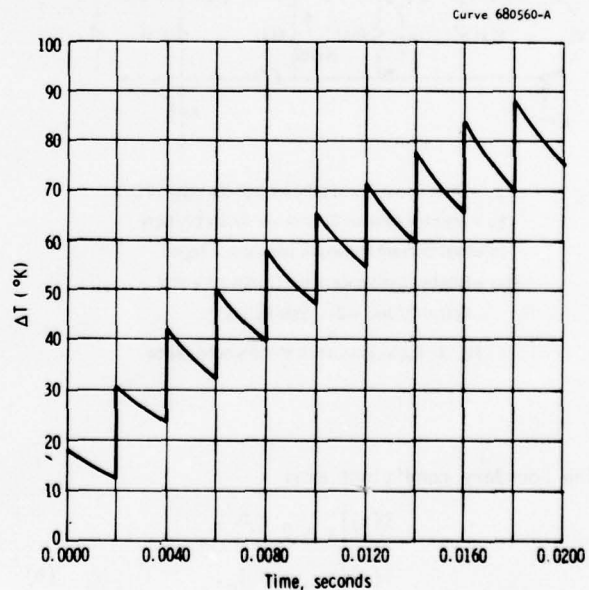


Fig. 6 - Center element temperature for a single sided heat sink. Pulse length = 40 μs , $f = 500 \text{ Hz}$, $I = 2 \times 10^4 \text{ amps}$, 10 pulses

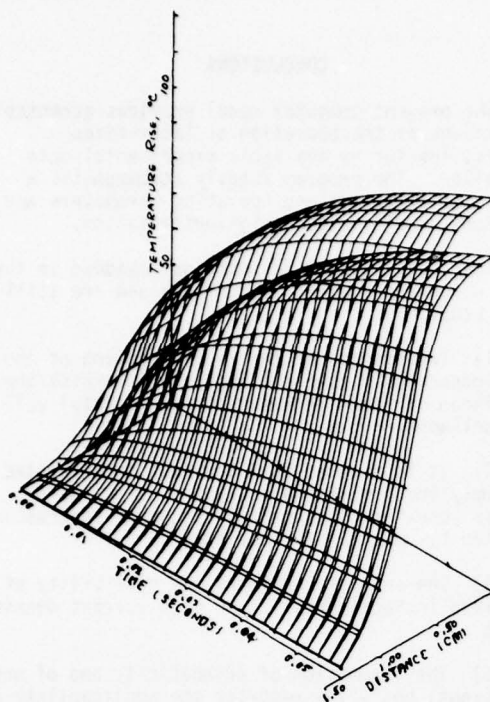


Fig. 7 - Temperature profiles as function of time for a sequence of 30 pulses. The upper surface is generated by the temperatures at the end of each pulse and the lower by those at the beginning of each pulse.

The output data consist of the temperatures as functions of time for each element and node of the mesh (over 400 of them in this case). Figure 6 shows the calculated temperature rise at the center of the device for a sequence of ten pulses. Figure 7 shows the temperatures as functions of time and distance for a thirty pulse sequence. The upper surface is generated by the temperatures at the end of each pulse and the lower surface by the temperatures at the beginning of the pulses.

These data and others generated by this analysis provide two important conclusions: (a) the heat-flow in the silicon is essentially one-dimensional for several hundred milliseconds; and (b) the temperature decay of the heated parts of the device can be closely approximated with the exponential function:

$$T(t) = T_0 \exp(A_2 t^{A_1}), \quad (21)$$

where t = μsec measured from the end of a pulse and for data in Figure 6:

$$A_1 = 0.81$$

$$A_2 = -1.0314 \times 10^{-3}$$

Incorporating these results in the current/temperature program allows this program to simulate multi-pulse performance. This is highly advantageous, since the cost and time per run for the current/temperature program are small fractions of those for the finite-element heat-flow program. In the following data it is assumed that the device is adiabatic during each pulse and that one-dimensional heat-flow following each pulse determines the starting temperature profile for the next pulse.

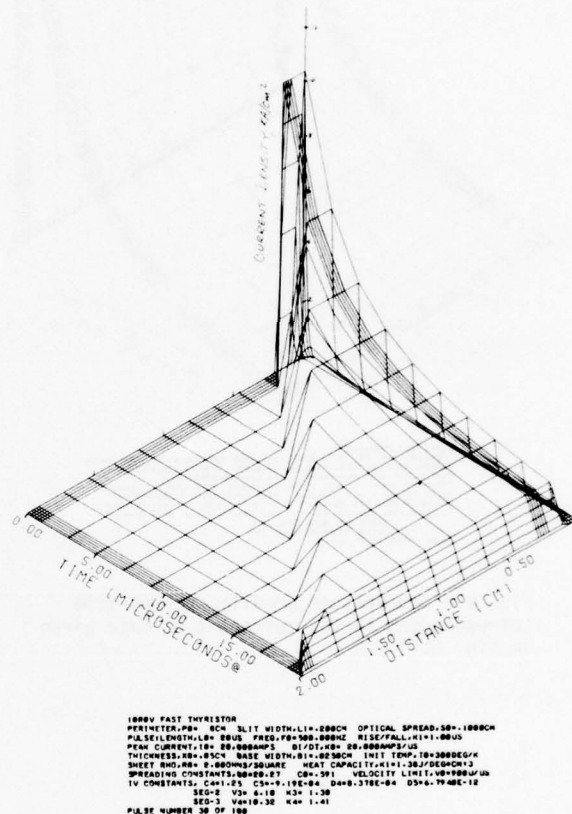


Fig. 8 - Current-density profiles as a function of time during the thirtieth pulse of a sequence of one hundred pulses. These data are for a fast spreading device.

Figure 8 is a three-dimensional plot of $J(x,t)$, the current-density profile versus time, with time measured from the beginning of the thirtieth pulse of a sequence and distance measured from center of the silicon wafer. These data apply to a fast-spreading device with the design and operating parameters given in the figure. Figure 9 illustrates the corresponding temperature versus time behavior. Figure 10 gives the voltage versus time data for the same pulse.

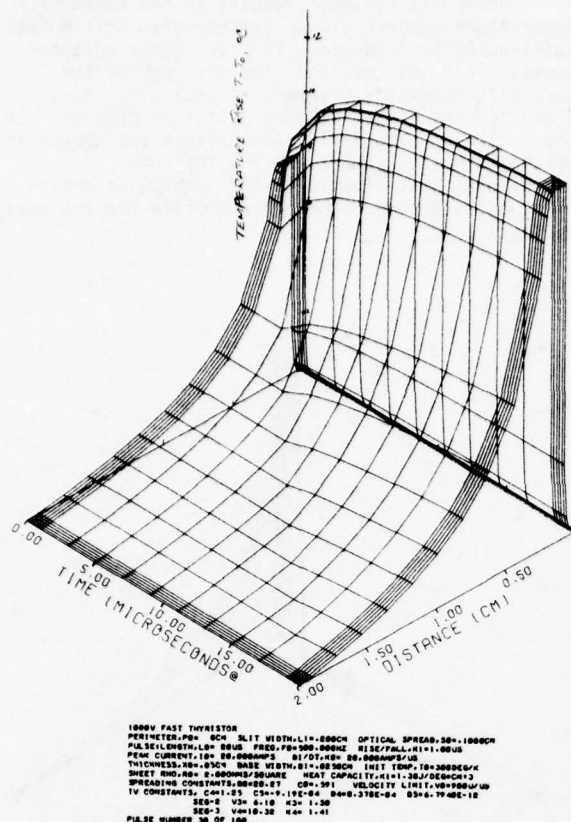


Fig. 9 - Temperature profiles versus time corresponding to the current-time data given in fig. 8.

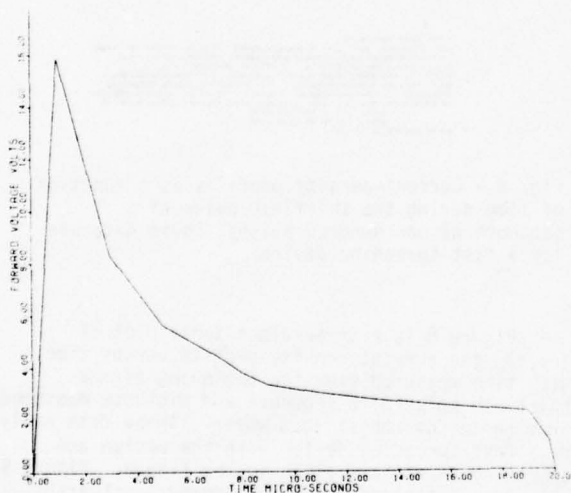


Fig. 10 - Voltage as a function of time corresponding to data of figs. 8 and 9.

CONCLUSIONS

The present computer model provides acceptable predictions of the operation of laser-fired devices, insofar as available experimental data will allow. The program readily accommodates a wide range of device and operating parameters and, therefore, facilitates design optimization.

There are several assumptions imbedded in the model which are subject to question and are still under study.

- 1) The effects of the redistribution of the light-generated plasma are neglected, despite the likelihood of their influence on the initial voltage collapse.
- 2) It is assumed that the heat is generated uniformly throughout the thickness of the wafer. This is somewhat optimistic in light of the results reported by Jaecklin (9) and others.
- 3) The analysis neglects the possibility of localized instabilities in the high current density plasma.
- 4) The assumption of adiabaticity and of one-dimensional heat-flow restrict the applicability of the program to short pulses and limited repetitions.

Work on this model is continuing in these areas as is the experimental program with which the analysis is correlated. Additional results will be reported at a later date.

The author gratefully acknowledges the useful discussions and experimental results provided by J. S. Roberts, L. R. Lowry, M. H. Hanes and R. J. Fiedor.

REFERENCES

1. N. G. Nilsson, "The Influence of Auger Recombination on the Forward Characteristics of Semiconductor Power Devices at High Current Densities," *Solid State Electronics*, Vol. 16, pp. 681-688 (1973).
2. J. D. Beck and R. Conradt, "Auger-Recombination in Silicon," *Solid State Communications*, Vol. 13, pp. 93-95 (1973).
3. R. N. Hall, "Recombination Processes in Semiconductors," *Proc. IEEE*, Part B Suppl., No. 17, p. 106 (1959).
4. N. G. Nilsson, "Band-to-Band Auger Recombination in Silicon and Germanium," *Physica Scripta* (Sweden), to be published.

5. J. Burtscher et al., "Recombination in Thyristors and Rectifiers," *Solid State Electronics*, Vol. 15, pp. 35-64 (1975).
6. N. H. Fletcher, "The High Current Limit of Semiconductor Junction Devices," *Proc. IRE*, Vol. 45, pp. 862-872 (June 1957).
7. F. Dannhauser, "The Dependence of the Carrier Mobilities in Silicon on the Free Carrier Concentration - I," to be published.
8. D. Silber and M. J. Robertson, "Thermal Effects on the Forward Characteristics of Silicon pin Diodes at High Pulse Currents," *Solid State Electronics*, Vol. 16, pp. 1337-1346 (December 1973).
9. A. A. Jaecklin and A. Marek, "Instantaneous Temperature Profiles Inside Semiconductor Power Devices: Part I," *IEEE Trans. Electron Devices*, Vol. ED-21, pp. 50-53 (January 1974).
10. A. Marek, A. A. Jaecklin and J. Cornu, "Instantaneous Temperature Profiles Inside Semiconductor Power Devices: Part II," *IEEE Trans. Electron Devices*, Vol. ED-21, pp. 54-60 (January 1974).
11. A. A. Jaecklin and M. Leitz, "Analysis of a Power Semiconductor Near Its Threshold of Destruction," *Proc. 1974 Power Electronics Specialists Conference*, pp. 134-139 (1974).
12. S. C. Choo, "Theory of a Forward-Biased Diffused-Junction p-L-n Rectifier - Part I: Exact Numerical Solutions," *IEEE Trans. Electron Devices*, Vol. ED-19, pp. 954-966 (August 1972).
13. S. C. Choo, "Theory of a Forward-Biased Diffused-Junction p-L-n Rectifier - Part II: Analytical Approximations," *Solid State Electronics*, Vol. 16, pp. 197-211 (1973).
14. S. C. Choo, "Theory of a Forward-Biased Diffused-Junction p-L-n Rectifier - Part III: Further Analytical Approximations," *IEEE Trans. Electron Devices*, Vol. ED-20, pp. 418-426 (April 1973).
15. J. Cornu and M. Lietz, "Numerical Investigation of the Thyristor Forward Characteristic," *IEEE Trans. Electron Devices*, Vol. ED-19, pp. 975-981 (August 1972).
16. I. Somos and D. E. Piccone, "Plasma Spread in High-Power Thyristors Under Dynamic and Static Conditions," *IEEE Trans. Electron Devices*, Vol. ED-17, pp. 680-687 (September 1970).
17. P. P. Debye and E. M. Conwell, *Phys. Rev.*, vol. 93, pp. 692- (1954).
18. W. H. Dodson and R. L. Longini, *IEEE Trans. Electron Devices*, Vol. ED-13, No. 5 (1966).
19. W. H. Dodson and R. L. Longini, *IEEE Trans. Electron Devices*, Vol. ED-13, No. 7 (1966).
20. H. J. Ruhl, Jr., *IEEE Trans. Electron Devices*, Vol. ED-17, pp. 478-484 (1966).
21. V. P. Voss, *Proc. VDE Meeting*, pp. 251-262 (1973).
22. H. Yamasaki, *IEEE Trans. Electron Devices*, Vol. ED-22, pp. 65-69 (1975).

APPENDIX V-3

Paper Given at National Aerospace and Electronics Conference - 1977

LIGHT ACTIVATED SEMICONDUCTOR SWITCHES

L. R. Lowry
D. J. Page

Westinghouse Research and Development Center
Pittsburgh, PA 15235

ABSTRACT

Recent advances in the emerging technology of light activated semiconductor switches (LASS) are described and the performance of two examples of LASS devices is discussed. The first example is a power thyristor with overall performance comparable to that of an electrically gated power thyristor, but with the advantages that light triggering brings such as electrical isolation between the control and power circuits and lower susceptibility to electrical noise. The second example describes a new kind of switch with extremely fast turn-on to high currents. This new switch is expected to bring the proven reliability of semiconductor devices to high power pulse switching systems. Turn-on rates of current rise in excess of 10^{12} A/sec have been demonstrated, and peak currents of 20,000 A for 40 μ sec at a low duty cycle have been obtained. Limitations and future possibilities of the technology are discussed and some numerical details are illustrated.

INTRODUCTION

We want to describe a new, emerging technology that we believe will be very useful in future power electronic systems. Aerospace electronics tends to lead in the application of new technologies but in this case a major impetus has also come from electric utilities and from fusion power generation. The new technology is the direct triggering of power semiconductors by light. Two examples, with very different parameters of operation, will be given to illustrate the range of operation possible. Even though neither example exactly fits present aerospace needs, perhaps examination of them will help suggest a possible solution to an existing or contemplated problem. The major accepted advantages of the light activated semiconductor switch (LASS) are: electrical isolation of the control circuit from the power circuit; very fast turn-on; simultaneity of turn on of related units; reduction of cushioning components when units are series connected; and insensitivity to electrical noise. In addition, there are certain other advantages such as lower cabling weight for fiber optic cable compared to copper.

It may be of interest to note that others have also reported on studies using light to turn-on power semiconductors. Grekov⁽¹⁾ in Russia has performed a theoretical study and has also reported results using small chips of silicon and in Europe, other workers⁽²⁾ have reported on a complete thyristor also achieving turn-on performance comparable to that obtained from electrically gated devices.

The LASS has been produced in two forms: (1) slow turn-on for phase control circuits and (2) ultra-fast turn-on for high energy pulsed power circuits. Many of the advantages are achieved in both cases, but some are specific to one or the other.

Before one can understand the advantages and limitations of the LASS, one must understand how a conventional, electrically triggered thyristor turns-on.

PRINCIPLES OF THYRISTOR TURN-ON

Figure 1 illustrates schematically a conventional pnpn or thyristor structure. Assume that the device is off and that the anode is biased positive with respect to the cathode electrode, reverse biasing the central p-n junction and creating a depletion region around it. The path of the electrical gate signal is as indicated from the central gate electrode to the cathode electrode.

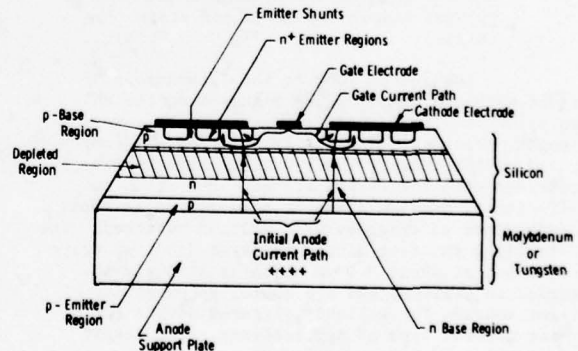


Fig. 1 Schematic cross-section of a conventional thyristor.

When the gate current is large enough, the p-n⁺ junction will be forward biased and electrons will be injected into the p-base at the inside edge of the cathode where some of them will diffuse towards the depleted region and then will be carried by drift across it. Their arrival at the anode p-n junction causes the injection of holes into the n-base; these holes then drift to the upper p-region where they in turn cause more electrons to be injected. The net result will be double injection of charge into the base regions and the voltage across the depletion region will collapse. Turn-on has now begun and anode current is established at the inside edge of the cathode as shown in Figure 1. This overall operation has been a rather slow process, of the order of one half to two microseconds, depending upon various device and circuit parameters. The "on" region will spread laterally at about 40 μm per μsec and, in order not to cause damage by excessive current density, the anode current must be limited by the external circuit until substantial spreading of the "on" region has taken place. When the turn-on process is completed, a plasma of electrons and holes exists in the base regions of the device with a density distribution as shown by the upper curves in Figure 2.

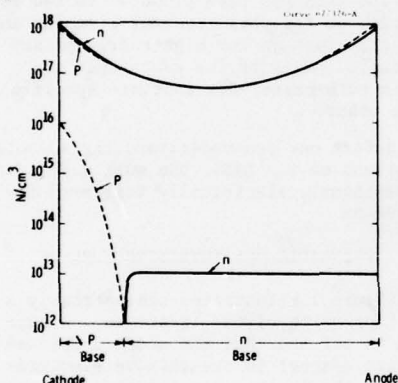


Fig. 2 Electron and hole distribution in a thyristor in the conducting state (upper curves) and in the unbiased state (low curves).

Now let us look at the interaction of light with silicon. Figure 3 shows how the absorption of light in silicon varies with wavelength. Three available light sources are indicated on the curve. Their output characteristics, combined with the very different absorption coefficients, provide dramatic differences in their performance as triggers with silicon switches. The GaAs light emitting diode and laser diode generate radiation at about 0.9 μm which is strongly absorbed in silicon, and are useful as potential light sources for a light triggered device for phase control type of applications. The deeply penetrating Nd:YAG radiation at 1.06 μm is useful to achieve very fast turn-on of thyristors as will be shown in a subsequent section.

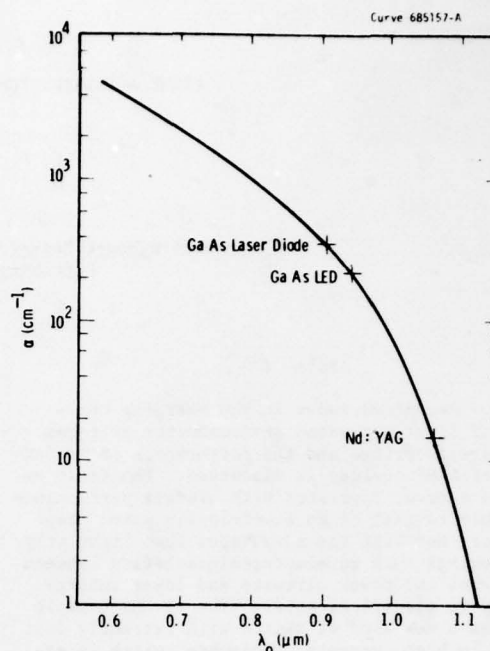


Fig. 3 Absorption coefficient, α , of silicon as a function of wavelength of light.

PHASE CONTROL SWITCHES

If we shine radiation of about 0.9 μm wavelength onto a sensitized region of silicon as shown in Figure 4, electron-hole pairs are created in a shallow region of the device because of the large absorption coefficient at this wavelength. The carriers so created act just as though they got there from an electrical gate signal -- the electrons in the upper p-base diffuse towards the depletion region and the electrons (holes) in the depletion region drift towards the anode (cathode) causing additional hole (electron) injection as described before. The net result is that the thyristor turns-on much as if it had been gated on electrically, and it turns-on with about the same speed.

Just as a minimum electrical gate signal is required to turn-on a conventional thyristor, so is a minimum light signal required for a light fired thyristor. Our studies indicated that about 0.3 μJ per pulse would provide adequate drive to assure consistent performance comparable to an electrically gated thyristor. The search for an inexpensive, reliable light source of adequate power ended with the selection of the laser diode as the best all around choice. Although light

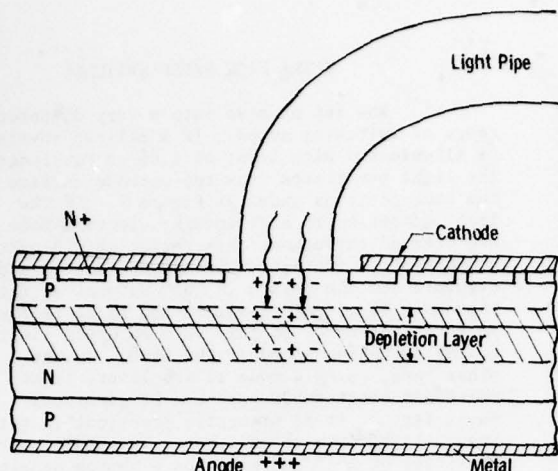


Fig. 4 Schematic cross-sectional view of a light activated thyristor.

emitting diodes have an advantage in cost, their comparatively low power output plus their very wide angular distribution of light adds to insufficient light collected by and delivered through a suitable fiber optic cable as shown in Figure 5. In fact, the laser diode-fiber optic cable combination shown in the figure provides barely enough overdrive for comfort when one considers the derating necessary to allow for aging. Techniques developed recently promise significantly better light collection and distribution efficiencies.

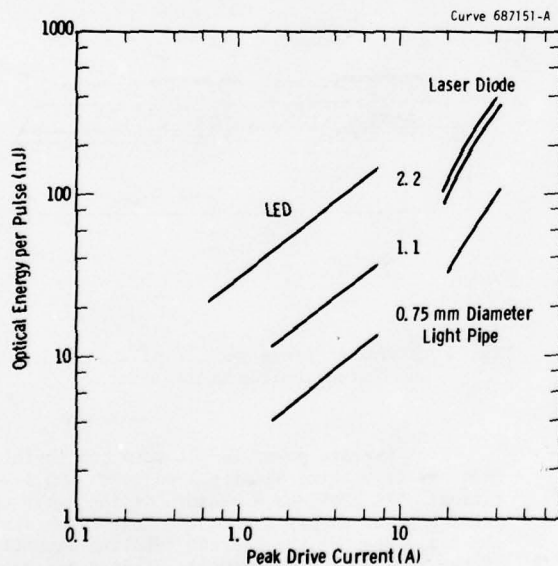


Fig. 5 Variation in the optical energy measured at the receiving end of light pipes as a function of the light source and current drive.

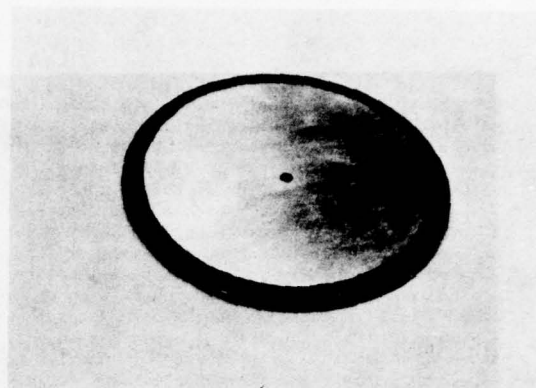


Fig. 6 Photograph of a phase control light activated semiconductor switch element.

The completed active element is shown in Figure 6. Note the light sensitive region identified by the small, dark circular region in the center of the unit. This unit is 5 cm in diameter.

The turn-on delay time of this device is displayed in Figure 7 as a function of the incident trigger light energy. From this figure, it is evident that delay times of less than one microsecond can be achieved with reasonable (about 300 nJ/pulse) light trigger pulses.

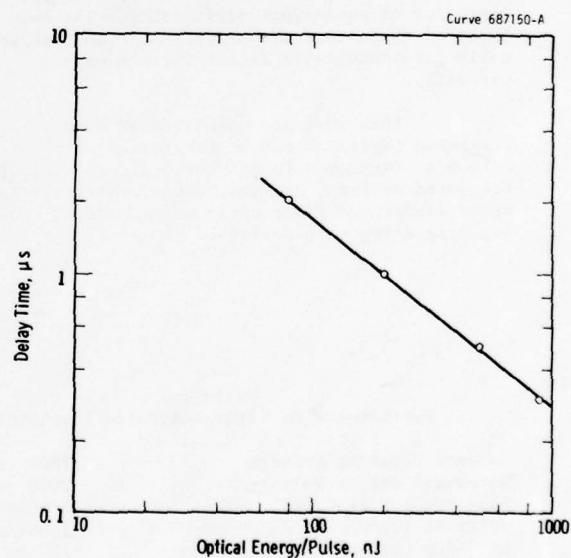


Fig. 7 Variation of the delay time for a light activated semiconductor switch as a function of the optical triggering energy.

ULTRA HIGH SPEED SWITCHES

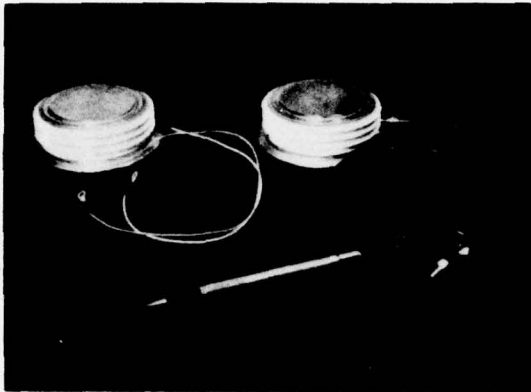


Fig. 8 Photograph of two completed thyristors, the one on the left is conventional, with electrical gate leads. The one on the right has the same performance, but is triggered on by an optical signal.

The performance of the device is summarized in Table 1. The values in this table compare very favorably with those of commercially available, electrically fired units. A photograph of the packaged light triggered thyristor is shown in Figure 8 along with an electrically triggered thyristor of equivalent performance. The two types of thyristors are electrically and mechanically interchangeable except for the gating circuits.

This work has demonstrated that a light triggered thyristor can be fabricated with performance comparable to conventional, electrically triggered devices; and that commercially available laser diodes and fiber optic cables are suitable for triggering such devices.

Table 1
Performance of Light-Activated Thyristor

| | |
|---------------------------------|-------------|
| Forward Blocking Voltage | 2000 volts |
| Reverse Blocking Voltage | 2000 volts |
| Forward Drop at 1300A | 2.0 volts |
| dV/dt at 125°C | >1000V/μsec |
| Latching Current | <100 ma |
| Holding Current | ~15 ma |
| Optical Energy to Trigger | 35 nJ |
| Optical Energy for Good Turn-on | 300 nJ |
| Delay Time | <1 μsec |
| Turn-on Time | <3.5 μsec |

Now let us move into a very different range of switching speed. If a silicon thyristor is illuminated with light of $1.06 \mu\text{m}$ wavelength, the light penetrates from the cathode surface to the back plate as shown in Figure 9. If the light intensity is high enough, electron-hole pairs are created throughout this region at a density comparable to that shown in the upper curves of Figure 2 and the device is "on" as soon as this happens. The light traverses the slice thickness in about one psec, so this sets an upper limit to the switching speed of the LASS. On the other hand, using a mode locked laser, light pulses as short as 20 psec can be generated. This is as fast as it is presently practical to get enough light into the silicon. To obtain carrier densities of $10^{18}/\text{cm}^3$ requires a photon density of $10^{18}/\text{cm}^3$. At 100% efficiency, this requires $0.18\text{J}/\text{cm}^3$ of light and to get this into the silicon in 20 psec requires a peak power of $9\text{GW}/\text{cm}^2$. The peak power output of today's mode locked YAG lasers is in the 5 GW range with about 40 watts average power; our calculations indicate that silicon today can effectively control about 5×10^4 watts/cm² average power in the pulsed mode. Thus, using today's technology in both lasers and silicon thyristors will permit significant levels of power to be controlled with comparatively small switches.

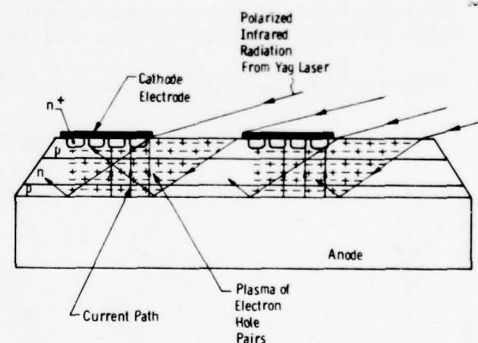


Fig. 9 Schematic cross-section of a fast light activated semiconductor switch.

Average power is not very meaningful when one is talking about pulsed power applications. It provides a measure of the drain on the primary power supply and of the heat to be dissipated. Because the current handling capabilities of the thyristor are thermally limited and because the dissipation increases faster than the square of the current, peak power usage usually results in reduced average power rating.

With support from the USAF-APL, Westinghouse has performed an analytical and experimental investigation of the LASS for high power, high dI/dt applications. The program was started in 1974 with the goal of determining the maximum dI/dt and peak current densities that the thyristor could stand in a low duty cycle mode of operation. Specific performance goals and the corresponding values achieved are shown in Table 2.

Table 2

Performance of Laser Activated Silicon Switches

| Switched Voltage V | Peak Current Amperes | | dI/dt kA/ μ sec | | Pulse Length |
|-----------------------|-------------------------|----------|--------------------------|----------|--------------|
| | Goal | Achieved | Goal | Achieved | |
| 1700 | 20,000 | 24,000 | 20 | 40 | 40 μ sec |
| 1000* | | 10,000 | | 1100 | 100 nsec |

* Extended work done in cooperation with Lawrence Livermore Laboratories.

An analytical investigation was performed of the internal operation of a thyristor during turn-on and conduction of high current pulses initiated by light. Parameters included in the analysis were current density, size and configuration of the illuminated area, path of the internal currents, carrier densities, forward drop, heat generation and removal, effect of temperature on other parameters, and pulse width. A mathematical model of the LASS was constructed and embodied in a computer program that, given the device design and current pulse characteristics, returns a 3-dimensional temporal and spacial map of current density and temperature plus a description of the forward voltage drop throughout the length of the pulse. The details and results of this analysis and computer model have been reported previously. (3)

The above model needed some parameters to be set by measured values because they cannot be derived from first principles. In addition, an experimental verification of the model was desired. Therefore, a test circuit, shown schematically in Figure 10, was fabricated to provide a test bed for LASS units fabricated specifically for this work. Figure 11 is a photograph of one of the thyristor elements; Figure 12 is a photograph of this element with the multifurcated fiber optic cable used to distribute the laser light among the eight windows shown on the LASS element. An overall view of the test set-up, showing the laser output head, the pulse forming network, and the container for the LASS element is shown in Figure 13. The performance of the LASS in this circuit is summarized in the first line of Table 2. It can be seen that the performance goals were met or exceeded in every case.

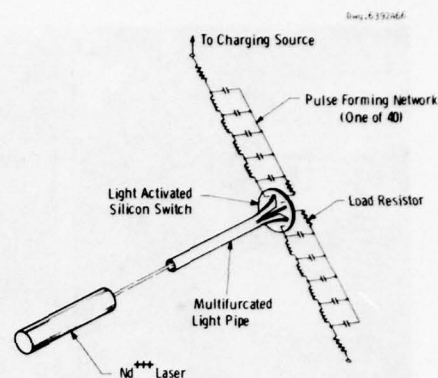


Fig. 10 Schematic of light activated silicon switch test apparatus. When the laser turns on the silicon switch, the energy stored in the pulse forming networks is discharged through the switch into the load resistors.



Fig. 11 Completed light activated semiconductor switch element design for fast turn-on.

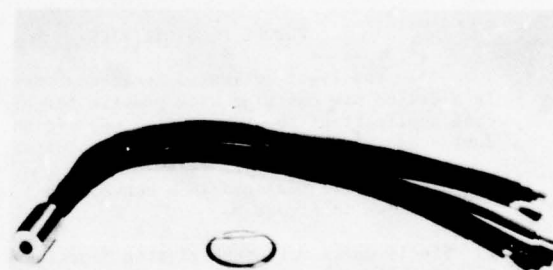


Fig. 12 Multifurcated fiber optic cable used to couple the laser beam into the semiconductor element.



Fig. 13 Experimental set up for measuring LASS performance. The laser is shown on the left and the LASS is located in the center of the fixture on the right. The door has been opened in the photograph to show the pulse forming networks.

At the time that this program was begun, the level of understanding was such that the di/dt and peak current goals seemed formidable and possibly unattainable. The USAF displayed foresight and courage in identifying early the need for a reliable, long lived high power switch and in funding a research program to identify and solve as many problems as possible. Because of this effort, we were able in late 1975 and 1976 to work with the Lawrence Livermore Laboratories of ERDA and extend the demonstration of the di/dt capabilities of the LASS up to 10^{12} A/sec. It is now evident that the value of the di/dt is almost entirely circuit dependent since the thyristor has extremely low self inductance.

This work has demonstrated that a laser activated silicon switch is capable of extremely fast turn-on to very high currents. When coupled with previous work for the United States Navy, it has now been shown that high voltage (tens of kV), high current (10's of kA) switches with rise times of the order of 10^{12} A/sec are feasible.

FUTURE POSSIBILITIES

The light activated semiconductor switch is a device now emerging with promise for significant applications for the 1980's. We see the device evolving into several forms including:

1. Single units packaged in a conventional manner as shown in Figure 8.
2. Single units with much greater blocking voltage capability (up to 10 kV).
3. Modules with high voltage blocking capability that can be integrated into systems.
4. Self-contained assemblies that will block 10's of kV and pass 10's of kA with the light source internal to the assembly.

In addition, as systems designers understand the advantages and disadvantages of the LASS, requests for variations in performance will result in a number of performance improvements such as improved sensitivity to the light triggering signal for phase controlled units and improved light distribution and heat removal for the ultra-fast LASS. Units that block modest voltages (< 5 kV) and switch low currents (< 25 A) at low cost will be desired and will become available. The repetition rate and the reliability of the light sources will increase. We foresee application in such fields as:

- high energy lasers for fusion, weapons, and isotope separation
- simulation of electromagnetic pulse (EMP)
- magnetically confined fusion
- laser or electron-beam compressed fusion
- target designators, man portable and mobile
- aircraft electrical distribution and control systems
- electric utility power conditioning

It is our purpose in this paper to alert the aerospace electronics community that this technology is emerging.

CONCLUSIONS

We have described in some detail two examples of light activated thyristors to illustrate the range of performance capabilities available. The more glamorous example shows a fantastic turn-on speed to very high currents and promises to become important in high power pulse circuits which need the very fast turn-on from high blocking voltages to high current pulses at a low duty cycle. The other example, though prosaic in character, may well prove to be just as useful in aerospace electronics as the utilization of fiber optic cables for control signals increases. This type of thyristor will perform compatibly with such fiber optic cable systems while providing performance comparable to present electrically gated thyristors. This technology is in the early stages of development and a considerable range of performance can be expected to become available in the next few years if you, the users, demand them.

REFERENCES

1. I. V. Grekov et al, "Some New Possibilities of Fast Switching of Large Area PNP Structures," Sov. Phys. Semicond. 10, No. 2, 206 (1976).
2. D. Sibling, W. Winter, and M. Fullmann, "Progress in Light Activated Power Thyristors," IEEE Trans. ED-23, No. 8, 899 (1976).
P. DeBruyne and R. Sittig, "Light Sensitive Structure for High Voltage Light Thyristors," PESC '76 Record, 262.
3. J. R. Davis and J. S. Roberts, "Ultra-Fast High-Power Laser Activated Switches," PESC '76 Record, 272.
J. R. Davis, "A Theoretical Model of Light-Fired Thyristors," PESC '75 Record, 305.

ACKNOWLEDGEMENTS

The authors would like to thank the personnel of the Westinghouse Semiconductor Division for their support in fabricating devices. Thanks are also due to many members of the Westinghouse Research Laboratories for their contributions to this work, in particular to E. S. Schlegel, J. S. Roberts, J. R. Davis, and M. H. Hanes, and to O. Zucker and associates at the Lawrence Livermore Laboratories for special tests demonstrating the very fast rise times.

APPENDIX V-4

Paper Given at Pulsed Power Systems Workshop
White Oak, MD, 1976

FUTURE PROSPECTS FOR FAST, HIGH POWER, LONG LIFE, SOLID STATE SWITCHES

D. J. Page and L. R. Lowry

Westinghouse Research Laboratories
Beulah Road, Churchill Borough
Pittsburgh, Pennsylvania 15235

ABSTRACT

The optically activated thyristor shows great promise in meeting the needs of the pulsed power community for a very fast, high power, high repetition rate, long life switch. This paper describes how conventional and optically activated thyristors operate and why the optically activated unit can perform so well. A calculation of the theoretical upper limits of the device are presented, and the problems that must be solved to obtain a viable switch are discussed.

INTRODUCTION

To generate the electrical pulses needed by pulse power system applications such as lasers, electron beams, and plasma-physics experiments, switches are needed that can operate at reasonable repetition rates for long periods of time. An ideal switch would have the ability to switch high power (gigawatts), fast rise time (nanoseconds), capability of repetitive operation (kilohertz), and an inherently unlimited life.

High-power fast-rise-time devices such as spark gaps and liquid or solid dielectric switches have limited life. Long-life devices with fast rise time (thyratrons, ignitrons, hard tubes, and transistors) are useful only at low or moderate power. The thyristor, a four-layer (PNPN) semiconductor device, has the longevity of solid-state devices and a power-switching capability approaching that of the spark gap. The inherent switching speed of the electrically triggered device is relatively slow, but recent developments have dramatically increased the switch-on speed of thyristor type structures. And, by operating these devices at a low duty cycle, it is possible to achieve simultaneously nanosecond switching times and conduction of tens of thousands of amperes. By turning the thyristor "on" with laser radiation, current rises of the order of 10^6 A/ μ sec have been demonstrated;⁽¹⁾ and it is believed that in all cases to date the current rise has been limited by the test circuit rather than by the switch. This paper reviews the state of the art, describes

the basics of power thyristor operation, and shows why laser firing provides several orders of magnitude of improvement in the switching characteristics. Some experimental results are presented, the upper limitations imposed by the physics of materials are defined, the performance of a particular switch is projected, and the problems that must be solved are enumerated.

STATE OF THE ART OF POWER SEMICONDUCTOR SWITCHES

In recent years the power handling capability of power semiconductor devices, particularly thyristors and rectifiers, has increased significantly.⁽²⁾ With the availability of large diameter silicon crystals, large area devices are being developed. At the present time, commercial devices are available with active areas of nearly 20 cm^2 and devices with over 40 cm^2 are at the development stage. Such devices will be capable of conducting several thousand amperes continuously.

Advances in processing techniques have allowed the voltage rating of power devices to increase to over 3 KV. Still higher blocking voltages are desirable for pulsed power applications. The usual approach to increasing blocking voltage capability also increases forward conduction losses and the turn-off time.

The turn-on time is especially important in high frequency or in very high power pulsed systems. By employing special electrode designs, it has been possible to significantly reduce the turn-on switching losses and to obtain devices which can tolerate a rapid rise in the conduction current. Figure 1 shows one example of such an electrode design. However, there are practical limits to what can be achieved by electrode design improvements.

When a thyristor is turned-on by an electrical gate signal, only a small area of the device is initially conducting, and the power dissipation in the conducting region must be constrained within safe limits. A conventional thyristor is shown in cross section in Figure 2. Assume that the device is in the off state and that the anode contact is at some high positive potential relative to the cathode contact. The central p-n junction is reverse biased and a depletion region exists as shown cross-hatched in Figure 2. To initiate turn-on, a small signal, positive with respect to the cathode, is applied to the gate electrode. The path of the gate current is as indicated from the

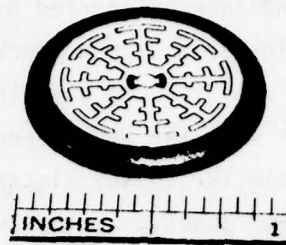


Figure 1. A thyristor chip incorporating an amplifying gate and interdigitated cathode electrode.

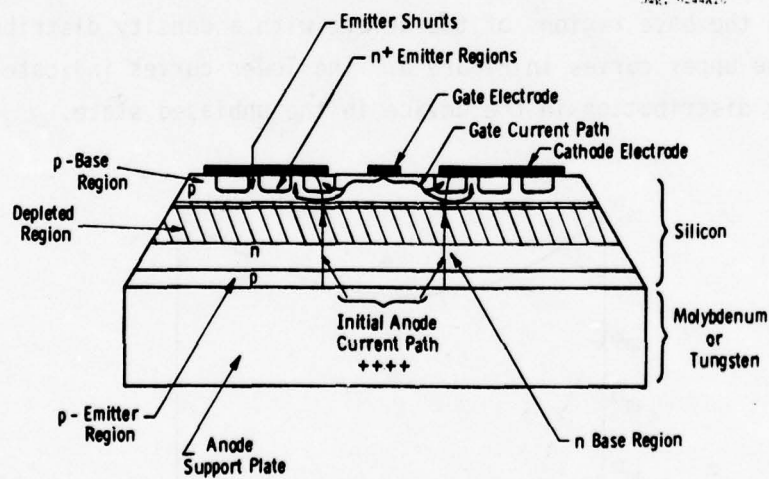


Figure 2. Cross section of a conventional thyristor (not to scale) illustrating the turn-on process.

gate electrode to the cathode electrode. When this current is large enough, the $p-n^+$ junction will be forward biased and electrons will be injected into the base region at the inside edge of the cathode. These electrons will diffuse towards the depleted region and then be carried by drift within the depleted region due to the high electric field. Upon reaching the other side of the depleted region the electrons will forward bias the anode $p-n$ junction, causing the injection of holes into the n -base region. These holes will traverse the device in a manner similar to the electrons and result in further forward bias of the cathode $p-n^+$ junction. This will result in further electron injection from the cathode and hence further hole injection. The net result will be double injection of charge into the base regions and the voltage across the depletion region will collapse. The turn-on process has now commenced and anode current is established at the inside edge region of the cathode as indicated in Figure 2. This "on" region will then spread laterally at about 40 microns per microsecond until the entire cathode region is conducting. However, the anode current must be limited by the external circuit until substantial spreading of the "on region" has taken place.

When the turn-on process is completed, a plasma of electrons and holes exists in the base regions of the device with a density distribution as indicated by the upper curves in Figure 3. The lower curves indicate the free carrier density distribution in the device in the unbiased state.

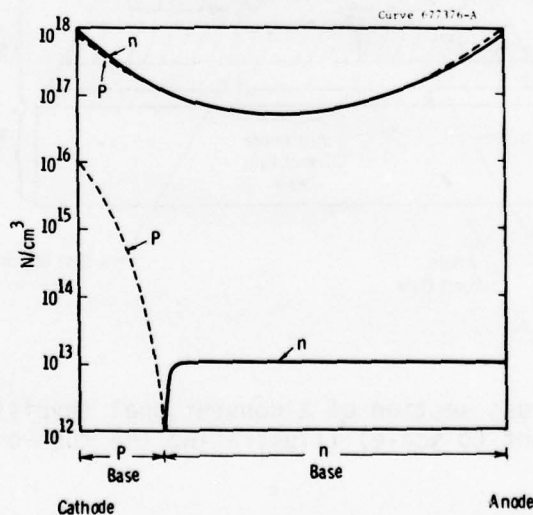


Figure 3. Carrier distribution within a thyristor in the conducting state and in the unbiased state.

The turn-on process just described is, in terms of pulsed power applications, very slow. From the time that the trigger signal is applied until the anode voltage starts to fall is typically one-half microsecond. The fall time is typically one-quarter microsecond. Both of these values can vary widely from unit to unit. This slowness of turn-on results in high power dissipation under large di/dt conditions; the variation in the values results in overvoltageing of and subsequent failure of devices when they are connected in series strings for high voltage applications. In utility and industrial applications, series inductors are installed to limit the di/dt to acceptable values. This approach is intolerable in pulsed power applications.

One approach to partially solving these problems is shown in cross section in Figure 4. This is the Reverse Blocking Diode Thyristor or RBDT, formerly known as the reverse switching rectifier or RSR. This is a two-terminal device which operates as follows: Let the anode electrode be at a high positive potential. Most of the n and p base will be depleted of charge because the voltage is dropped across the reverse biased center p-n junction. In this state the device can be regarded as a capacitor. If now a positive voltage pulse is applied to the anode, charge will flow within the device to further charge the capacitor. This charge will flow in the manner indicated in Figure 4 beneath each of the n emitter regions and hence to the cathode electrode via

Doc. 6244A09

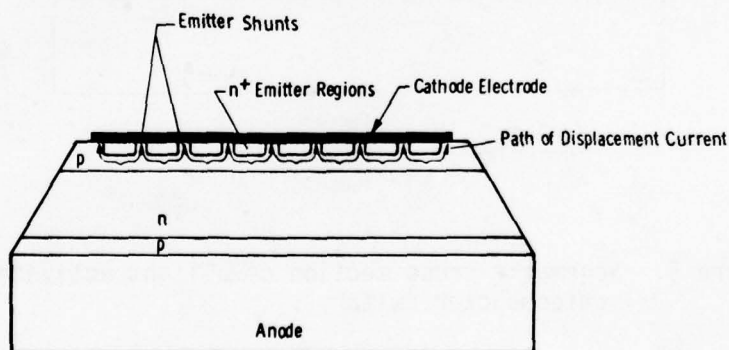


Figure 4. Cross section of a reverse blocking diode thyristor showing the displacement current paths when the anode is subjected to a positive step of voltage. This current causes the emitter junctions to become forward biased and turn on takes place over a large area of the device.

the emitter shunts. If this capacitive current is large enough, it will create a lateral voltage drop sufficient to forward bias the emitter p-n junctions. The emitter regions will become forward biased at a matrix of points interstitial to the emitter shunt pattern. In this manner, a large area of the device can be turned on rapidly. Devices of this type have achieved rates of current rise of 8000 A/ μ sec and are well suited to series stacking because it is not necessary to produce the isolated trigger circuitry that is required for conventional thyristor strings. This device, therefore, shows considerable promise as a high power switch in many pulsed power system applications. It has the additional advantage that it is commercially available in two different sizes.

The approach which has demonstrated the shortest switching time (of the order of 10 nanoseconds) and the highest di/dt capability is optical activation by laser. This is shown schematically and with artistic license in Figure 5. This again is a two-terminal pnpn structure. If a positive

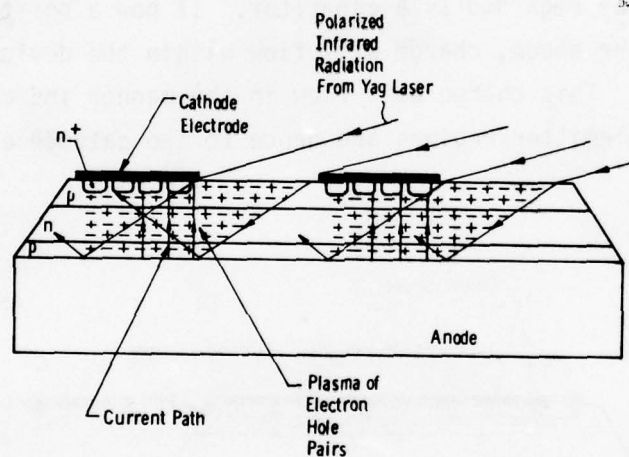


Figure 5. Schematic cross section of a light activated semiconductor switch.

potential is applied to the anode electrode, the center p-n junction will be reverse biased, carriers will be depleted from the central region, and the device will be in the forward blocking (off) state. In all the devices described earlier, turn on involved various means of obtaining injection of electrons and holes from the cathode and anode to achieve the plasma charge density shown in Figure 3. This is a relatively slow mechanism because it

involves diffusion processes which are inherently slow. Optical activation creates all the free carriers necessary for conduction in the bulk of the device by illuminating the device with photons whose energy is closely matched to the silicon band gap, i.e., 1.09 eV. This process is extremely rapid and can be used to create a plasma in the depletion region without having to rely on transverse diffusion of charge from the trigger electrode region. The results with intrinsic silicon indicate that turn-on times on the order of tens of picoseconds are achievable.⁽³⁾

In practice, the required radiation is obtained from a neodymium doped YAG laser and has a wavelength of 1.06 microns. Such radiation is closely matched to the band gap of silicon and results in efficient conversion of photons to electron hole pairs. To maximize the efficiency of the optical coupling to the silicon, the polarized radiation is introduced into the silicon at the Brewster angle.

Using this technique, the plasma of electrons and holes that normally exist in the base regions of a thyristor in conduction can be instantaneously produced. The area of turn on can be large and transit time limitations to establish the plasma by injection from the cathode and anode emitters are greatly reduced. Furthermore, series stacking is greatly simplified by the isolated nature of the trigger system. An optical system for stacking devices to produce a high voltage switch is shown in Figure 6. Here, a single laser beam is split up into a number of beams each of which is applied to a semiconductor device. The scheme ensures simultaneity of switching; and, therefore, only a minimum equalization network is necessary to ensure equal voltage division by the devices. We have demonstrated stacks of devices with only shunting resistors instead of the usual RC networks. Some of the experimental results achieved to date for single devices under various operating conditions are summarized in Table 1.

BASIC LIMITATIONS

Considerable analysis has been performed by Westinghouse under in-house programs and under government contracts. The analysis indicates that there is still room for a considerable increase in the power switching capabilities of silicon semiconductors. For instance, the power gain in the absence of regeneration within the semiconductor can be obtained by considering

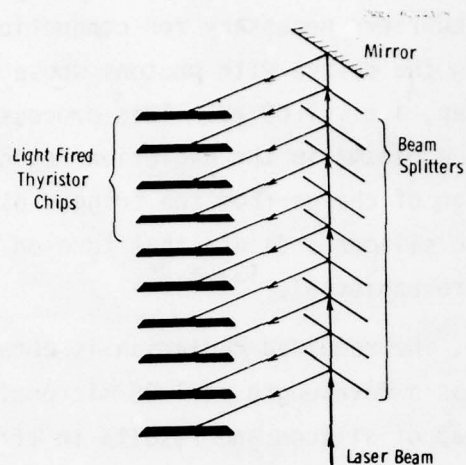


Figure 6. An optical scheme employed to turn on a series stack of thyristors. The beam splitters are designed to equally divide the laser beam.

Table 1. Summary of Experimental Data

| Voltage Switched (KV) | Pulse Current (KA) | Pulse Duration (μ s) | di/dt (KA/ μ s) | Peak Power Switched (MW) | Pulse Repetition Rate (pps) |
|--------------------------|-----------------------|------------------------------|------------------------|-----------------------------|--------------------------------|
| 1.5* | 1.8 | 5 | 4. | 2.7 | 60 |
| .6 | 3. | 1 | 20. | 1.8 | < 1 |
| 1.7 | 20. | 40 | 40. | 34. | 1 |
| 1.02 | 9.82 | 0.1 | 755. | 10. | < 1 |

* Stack of 10 devices operated in series. Voltage limited by power supply availability.

that every free carrier created consumed one photon of 1.06 eV. If the off-state blocking voltage V_0 appears across the load in the on state, then this carrier, falling through a potential V_0 , will deposit V_0 electron volts in the load. Thus, for a 1-eV input and a 1500-V blocking voltage, the output energy would be 1500 eV, yielding a maximum power gain of 1500. Although the efficiency of creating carriers using photons can be arbitrarily high, the process of getting the photons into the depletion region in an efficient manner is an important area for further investigation.

The inherent switching power density (P_{dmax}) of the material can be estimated from

$$P_{dmax} = E_{max} J_{max} \alpha.$$

E_{max} for silicon is 200 kV/cm and α is a form factor (1/2) to take into consideration the nonuniform electric field in the depletion region. J_{max} can be estimated from the equation

$$J_{max} = nev,$$

where n is the carrier density, e is the electronic charge, and v is the carrier velocity. A reasonable figure for maximum optically generated carrier density is $10^{20}/\text{cm}^3$, and the optical phonon velocity limit in silicon is 10^7 cm/s. Thus, $J_{max} = 10^{20} \times 10^7 \times 1.6 \times 10^{-19} = 1.6 \times 10^8$ A/cm²; and $P_{dmax} = \frac{1}{2} \times 2 \times 10^5 \times 1.6 \times 10^8 = 1.6 \times 10^{13}$ W/cm³.

For devices where internal carrier regeneration is provided as in the present experiments, the power gain becomes unlimited since only a trigger is required. For maximum switch power density, the same figures apply except that the normal injection carrier density is approximately $10^{18}/\text{cm}^3$. Thus, the maximum switch power density would be

$$P_{dmax} = 1.6 \times 10^{11} \text{ W/cm}^3.$$

The highest power density achieved to date is of the order of 10^{10} W/cm³. It is expected that this level could be significantly increased with appropriate effort.

THEORETICAL MODELING

An analytical model has been developed to relate the various device parameters that operate during turn-on so as to predict the forward voltage

drop and the spatial and temporal temperature distribution within the device for any given current pulse. This model has been described elsewhere.^(4,5) Experiments have been performed that demonstrate reasonably good agreement of the model with experimental data.

Individual thyristor elements can handle large but limited amounts of power. This is an advantage in pulsed power work because standardized building blocks of reasonable size can be used to assemble a structure capable of switching hundreds of thousands of amperes and volts. Once the basic building block or module is developed, one need develop only the special package configuration to meet the requirements of each application. As an example of what can be done with the present state of the art, we have used the theoretical model described above to predict the performance of one element of an optically fired switch. Each element will block 3000 volts and is to switch a 10,000 ampere peak current with a pulse duration of one microsecond and rise and fall rates of 10^5 A/microsecond. It is assumed that the pulse shape and width is set by a pulse forming network. Figure 7 shows the pulse current and the conducting voltage drop for the thyristor element assuming that the illuminated

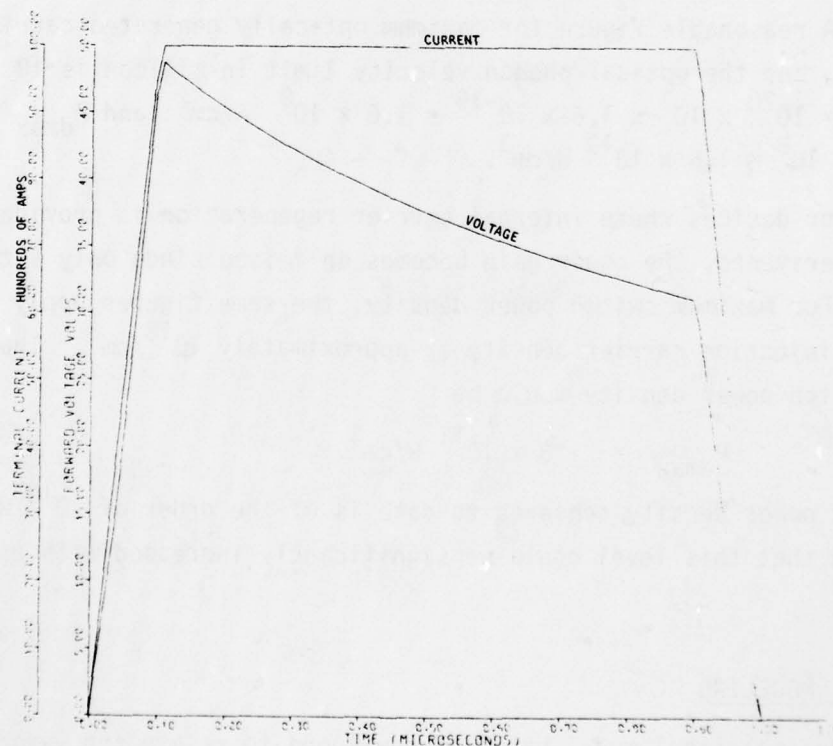


FIGURE 7 - THE CALCULATED VOLTAGE AND THE DRIVING CURRENT WAVEFORMS FOR A 10,000 AMPERE PEAK PULSE FOR A PARTICULAR OPTICAL SLIT DESIGN

slit is 20 cm long. The temperature distribution within the element during the pulse is shown in the three-dimensional plot of Figure 8. Each element will dissipate approximately 0.4 joules/pulse and the average conducting voltage drop is about 40 volts. At a pulse repetition rate of 250 pps this corresponds to a power dissipation of 100 watts. Conventional silicon thyristors can dissipate up to 100 watts/cm². However, a device of several square cm will probably be required to attain the specified voltage drop -- perhaps as large as 5 cm dia.

Now let us extend our projection to include the performance of a switch with the following characteristics:

| | |
|--------------------------|----------------|
| Peak blocking voltage | 42,000 V |
| Working blocking voltage | 30,000 V |
| Pulse current rise | 100,000 A/μsec |
| Pulse current peak | 10,000 A |
| Pulse duration FWHM | 1 μsec |
| Pulse repetition rate | 250 pps |

These switch requirements are not highly ambitious for either pulsed power applications or as goals for semiconductor performance. But such a switch could be formed from 14 elements connected in series (assuming the 3 KV blocking capability initially specified). This leads to about 1400 watts dissipation during conduction and to a 520 volt drop at mid-pulse. Such a switch is well within the present state-of-the-art, but considerable effort will be required to reduce the forward drop by an order of magnitude and to provide appropriate packaging including means of introducing the light.

PROBLEMS TO BE SOLVED

Over the last half century, several billion dollars have been invested by government and industry in solid state research, development, manufacturing facilities, and the resultant products. Without the background of this long-term effort, we could not seriously consider a semiconductor switch for pulse power applications. Even so, pulsed power systems impose on solid state devices regions of operation that have not been adequately investigated, and which will not be pursued for other applications. The pulsed power systems users must face the fact that if they need, as we believe they do, the semiconductor switch, then they must pay the cost of the specialized research and development needed to obtain a viable product.

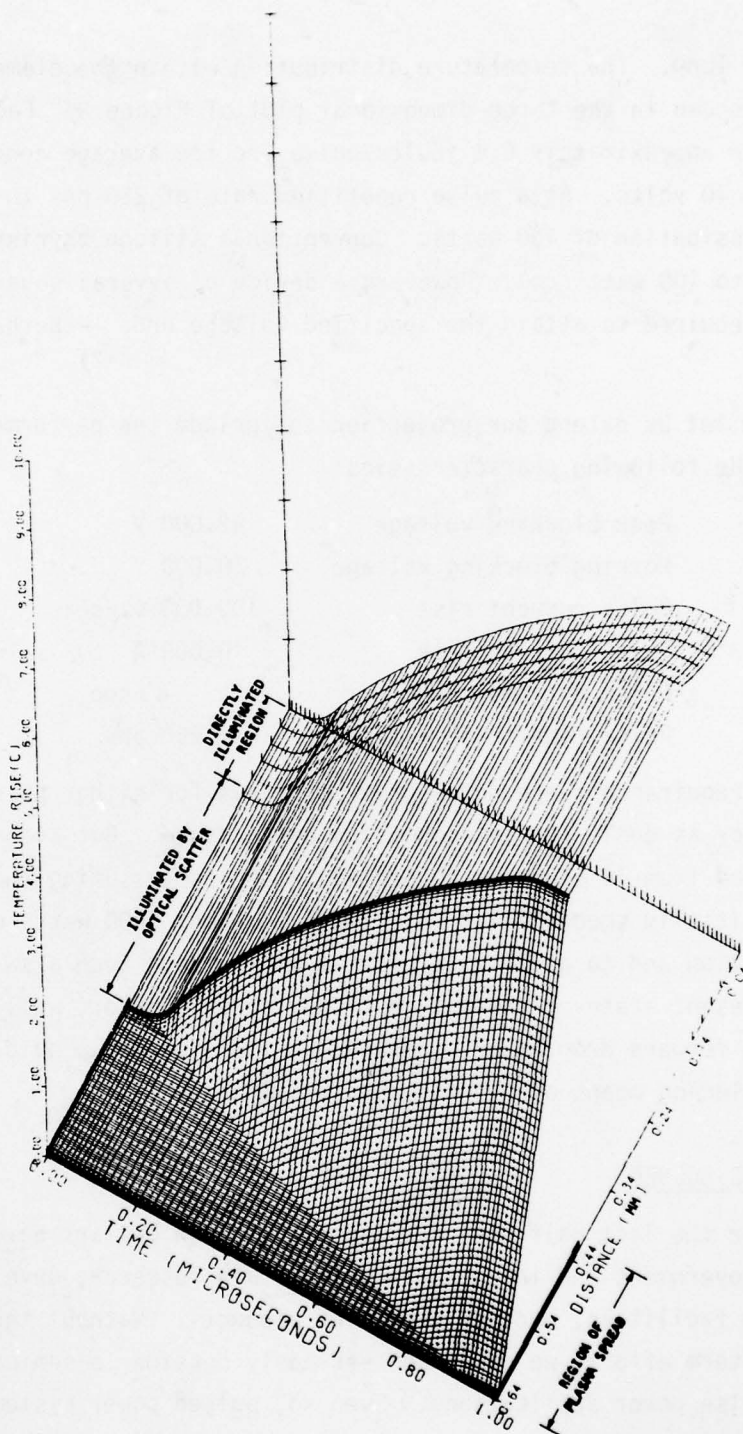


FIGURE 8 - TEMPERATURE PROFILES VERSUSE TIME FOR THE CURRENT PULSE OF FIGURE 7. THE ORIGIN CORRESPONDS TO $t = 0$, THE START OF THE PULSE, AND TO THE CENTER OF THE DIRECTLY ILLUMINATED REGION (SLIT)

Work on improved processing and materials to permit higher blocking voltages and higher current densities will provide improvements that are generic to all pulsed power semiconductor switches. So, too, will work on the related problems of light introduction and electrical and thermal contacting, on passivation techniques, and on improved laser performance, as well as basic work on operating parameters such as the minimum light required, and the influence of design parameters on forward voltage drop and internal temperature rise. Technology improvement programs are appropriate to advance the state-of-the-art in these areas. On the other hand, problems of package size and configuration, although common as problems, will for the foreseeable future require solutions that are specific to each application; and, therefore, design and development programs for each application are the appropriate vehicle to accomplish the desired ends.

SUMMARY

We have described the potential of semiconductor switches for high power pulsed systems. The electrically gated thyristor has limited usefulness in such systems because of the comparatively long and variable turn-on time. A relatively new device, the RBDT, is starting to be used in some applications where faster current rise time is required. The fastest switch of all, the optically fired thyristor, has been described and experimental data have been presented that confirm the theoretical promise of the device. Finally, we have discussed the problems that must be solved before a viable optically fired switch is truly available for pulsed power applications.

ACKNOWLEDGMENTS

We wish to acknowledge Messrs. J. R. Davis and J. S. Roberts and Dr. P. L. Hower for theoretical and experimental data supplied for use in this document.

The work reported herein was partially supported by the United States Air Force, Aeronautical Systems Division, Aero Propulsion Laboratory, under contract F33615-74-C-2029 and by the United States Navy, Naval Electronics Systems Command, under contract N00039-71-C-0228.

REFERENCES

1. O. S. F. Zucker, J. R. Long, V. L. Smith, D. J. Page and P. L. Hower, "Experimental Demonstration of High-Power Fast-Rise-Time Switching in Silicon Junction Semiconductors," *Appl. Phys. Lett.* 29, 261 (1976).
2. D. J. Page, "Some Advances in High Power, High di/dt , Semiconductor Switches," in Energy Storage, Compression, and Switching, edited by W. H. Bostick, V. Nardi and O. S. F. Zucker (Plenum, New York, 1976), p. 415.
3. D. H. Auston, "Picosecond Optoelectronic Switching and Gating in Silicon," *Appl. Phys. Lett.* 26, 101 (1975).
4. J. R. Davis, "A Theoretical Model of Light-Fired Thyristors," *IEEE PESC Record*, 309-311; 1975.
5. J. R. Davis and J. S. Roberts, "Ultra-Fast, High Power Laser-Activated Switches," *IEEE PESC Record*, 272-279; 1976.

APPENDIX V-5

Paper Given at Pulsed Power Systems Conference - 1976

SOLID STATE HIGH POWER PULSE SWITCHING

by

P. F. Pittman and D. J. Page
Westinghouse Research Laboratories
Beulah Road, Pittsburgh, Pennsylvania 15235

ABSTRACT

In this paper, the structural features and the methods of turning on high power thyristors, reverse blocking diode thyristors and light activated silicon switches are reviewed. The advantages and limitations of these devices are described together with a description of the performance achieved to date by the various devices. Finally, the operation of these devices in series strings to form high power switching modules is described.

Introduction

Fifteen years ago, the highest rating of a semiconductor switch was 80 amperes and 1400 volts, and since that time, there has been a steady growth in the power than can be switched. Today, solid state devices capable of switching megawatts of power are commonplace. The highest blocking voltage of these devices has now reached about 5kV, but due to fundamental limitations, significant further improvement is unlikely. Current handling capability on the other hand is likely to grow steadily as devices with ever increasingly larger conducting area are being developed. These devices are operated at an average current density of about 100A/cm² at the present time, and devices with over thirty square centimeters of conduction are available. As the crystal growth techniques are developed and other process improvements are made, we can look forward to even higher current ratings. Devices with over forty square centimeters of conducting area are now under development.

All of these switches have been designed for high duty cycle operation at low frequency. The switching speed of these devices is relatively slow although some devices employing special electrode structures and processing techniques have been designed to operate at frequencies up to tens of kilohertz. However, the inherent switching speed of thyristor type structures is relatively slow when conventional triggering techniques are employed. There have been some recent developments that have dramatically increased the switch-on speed of high power thyristor type devices. By operating these devices at a low duty cycle, it seems possible that nanosecond switching times and conduction of tens of thousands of amperes are feasible. Such extremely high rates of rise and peak current levels of power switching have only been possible

up to the present time by using spark-gaps. These devices suffer from problems of reliability and short operating life, and are confined to very low switching frequencies. The firing techniques and structures described in this paper lead us to conclude that solid state devices can achieve the same high level of power switching as spark gaps and, at the same time, exhibit the reliability and longevity associated with semiconductor devices.

The operation of the basic thyristor is first described and some basic limitations are outlined, and this is followed by a description of the amplifying gate structure with increased di/dt rating. The structure of the RBDT*, an even higher di/dt device, will then be discussed. Finally, the highest di/dt semiconductor structure, the light activated silicon switch, will be described.

The use of these devices in switching circuits will be discussed, together with various techniques to fire the arrays of devices.

Thyristor Operation

When a thyristor is turned on by a pulse of gate trigger current, the rate-of-rise of anode current must be limited by the external circuit. The reason for this is that only a small area of the device is initially turned on and the resultant power dissipation in the "on" or conducting region must be kept down to safe limits. This is best explained by referring to Fig. 1 which shows the cross section of a conventional thyristor. Let us assume that the device is in the off state and the anode contact is at some high positive potential relative to the cathode contact. The central p-n junction is reverse-biased and a depletion region, shown cross-hatched in Fig. 1, exists. The device can be turned on by applying a small positive signal to the gate electrode relative to the cathode. The resultant gate current will flow along the path indicated from the gate to the cathode electrode. If the current is large enough, the voltage drop laterally within the p-base region underneath the n^+ emitter will be sufficient to forward bias the p- n^+ junction and electrons will be injected into the base region at the inside edge of the cathode. These electrons will diffuse towards the depleted region and then be carried by drift within the depleted region due to the high electric field. Upon reaching the other side of the depleted region, the electrons will forward-bias the anode p-n junction, causing the injection of holes into the n-base region. These holes will traverse the device in a manner similar to the electrons and result in further forward bias of the cathode p- n^+ junction. This will result in further electron injection from the cathode and hence further hole injection. The net result will be double injection of charge into the base regions and the voltage across the depletion region will collapse. The turn-on process has now commenced and current flows at the inside edge region of the cathode. This results in anode current flowing in this region as indicated in Fig. 1. This "on" region" will then spread at about forty microns per microsecond until the entire cathode region is conducting. However, the anode current must be limited by the external circuit until the conducting area has grown to such a size that extremely high current densities are not encountered.

When the turn-on process is completed, a plasma of electrons and holes exists in the base regions of the device with a density of about 10^{18} cm^{-3} .

The conducting region in a thyristor can be observed by imaging the infrared radiation emitted from the recombination of electrons and holes

*Formerly known as the RSR.

within the on region in the device. This is done by etching an array of small holes in the cathode electrode to allow the radiation to leave the device. The radiation is observed using an image converter tube, and by gating the imaging system, the turn-on process in a thyristor can be examined in detail.

Figure 2 shows the on region in a thyristor 12 μsec after initiation of turn on carrying 140A, 50 μsec after initiation of turn on carrying 350A, and finally 120 μsec after turn on carrying 400A. Note here the small fraction of the total device area that is initially turned on.

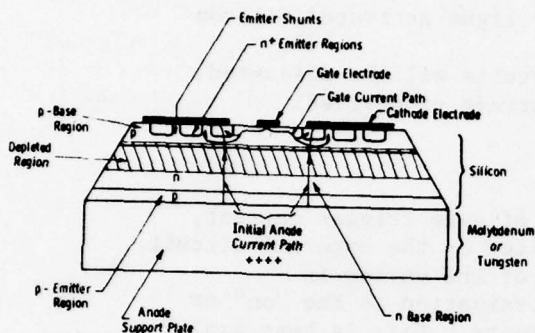


Fig. 1. Cross section of a conventional thyristor (not to scale) illustrating the turn on process.



Fig. 2. Images of the infrared radiation emitted from a conventional thyristor taken at various times after the initiation of turn on. This shows how the spreading of the conduction region takes place from the center of the device.

One way of improving the device is to increase the inside perimeter of the cathode electrode so that the initial on region will be larger and hence the current can be allowed to rise more rapidly. However, if this is done the gate current to fire the device will become excessively large because of the lower lateral resistance of the p-base region. This can be compensated by incorporating an amplifying gate. A cross section of a device with this feature is shown in Fig. 3. Here a small thyristor is integrated into the center of the thyristor. This is the n^+ emitter region beneath the floating pilot cathode electrode. The turn-on of the device is similar to the first case discussed and a gate current is made to flow from the gate electrode to the cathode (labeled 1). The geometry of the n emitter regions is adjusted so that the emitter beneath the floating cathode becomes forward biased before the main emitter region. The gate current then causes injection from the pilot cathode and this area turns on and results in pilot cathode current (labeled 2). This current then supplements the original gate current and assists in turning on the main cathode region, resulting in the flow of main cathode current (labeled 3). The floating pilot cathode electrode and the main cathode can be designed with an interdigitated pattern, giving the desired large cathode perimeter. The current can be allowed to rise fairly rapidly in such devices, typically at the rate of about $2000\text{A}/\mu\text{sec}$. An interdigitated amplifying gate thyristor is shown in Fig. 4.

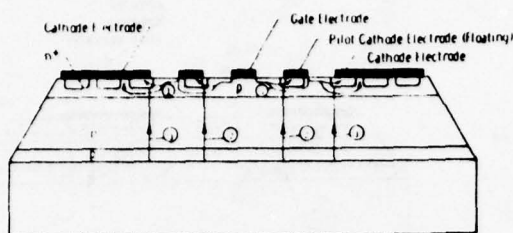


Fig. 3. Cross section of a thyristor incorporating an amplifying gate structure. Here the sequence of turn on is illustrated, starting with a gate current labeled 1, resulting in a pilot anode current 2 which in turn results in a main anode current 3.



Fig. 4. A thyristor chip incorporating an amplifying gate and interdigitated cathode electrode.

Reverse Blocking Diode Thyristor (RBDT)

This two terminal structure is shown in cross section in Fig. 5. The device is switched on by applying a positive pulse to the anode electrode. An explanation of the device operation is as follows: Let the anode electrode be at a high positive potential. Most of the n and p base will be depleted of charge because the voltage is dropped across the reverse biased center p-n junction. In this state the device can be regarded as a capacitor. If now a positive voltage pulse is applied to the anode, charge will flow within the device to further charge the capacitor. This current will flow in the manner indicated in Fig. 5 beneath each of the n emitter regions and hence to the cathode electrode via the emitter shunts. If this capacitive current is large enough, it will create a lateral voltage drop sufficient to forward bias the emitter p-n junctions. The emitter regions will become forward biased at a large number of points in the emitter pattern. In this manner, a large area of the device can be turned on rapidly. These devices are well suited for series stacking because it is not necessary to produce the isolated trigger circuitry that is required for conventional thyristor stacks.

Devices of this type have demonstrated rates of rise of current up to 8000A/ μ sec, and are commercially available in two sizes.*

Light Activated Semiconductor Switch

The fastest turn on is achieved by the light activated silicon switch (LASS) which is shown schematically in Fig. 6. This again is a two-terminal pnpn structure. If a positive potential is applied to the anode electrode, the center p-n junction will be reverse biased and carriers will be depleted

*Westinghouse types T40R and T60R.

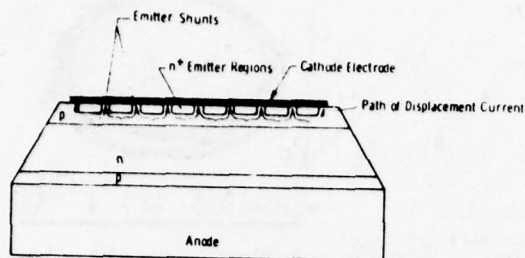


Fig. 5. Cross section of a reverse conducting thyristor showing the displacement current paths when the anode is subjected to a positive step of voltage. This current causes the emitter junctions to become forward biased and turn on takes place over a large area of the device.

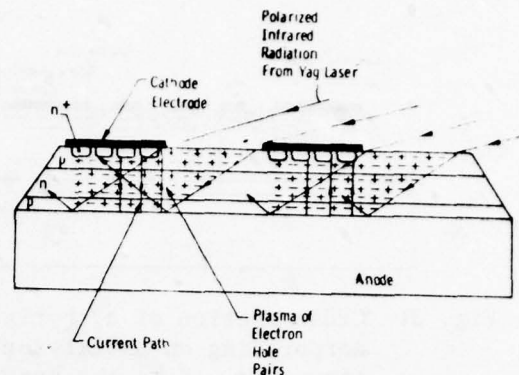


Fig. 6. Schematic cross section of a light activated semiconductor switch.

from the central region and the device will be in the forward blocking (off) state. In all the devices described earlier, turn on involved various means of obtaining injection of electrons and holes from the cathode and anode to achieve a high injected plasma charge density. This is a relatively slow mechanism because it involves diffusion processes which are inherently slow. There is another, much faster, method of creating a plasma of electrons and holes in the base regions and that is by optical absorption. By illuminating the silicon with light, photons can be absorbed and create electron-hole pairs. This process is extremely rapid and can take place within the depletion region, creating a plasma without having to rely on diffusion of charge from the electrode regions.

In practice, the infrared radiation is obtained from a neodymium doped YAG laser and has a wavelength of 1.06 microns. Such radiation is closely matched to the band gap of silicon and results in efficient conversion of photons to electron hole pairs. To obtain more efficient optical coupling to the silicon, the polarized radiation is introduced into the silicon at the Brewster angle.

Using this technique, the plasma of electrons and holes that normally exist in the base regions of a thyristor in conduction can be instantaneously produced. The area of turn on can be large and transit time limitations associated with establishment of the plasma by injection from the cathode and anode emitters are greatly reduced. Furthermore, series stacking is greatly simplified by the isolated nature of the trigger system.

A stack of ten devices fired with a single laser using a beam splitter system has been operated at 4000A/ μ sec with a peak current of 1800 amperes at a 60 Hz repetition rate. The power limit was set by the circuit and not by the devices. Each thyristor was capable of blocking 1200 volts.

A test apparatus designed to produce fast rising current pulses is shown schematically in Fig. 7. This apparatus is composed of 40 pulse

forming networks (PFN's) arranged in parallel to give an effective characteristic impedance of 0.04Ω , the electrical length of the pulse forming network being $40\text{ }\mu\text{sec}$. The circuit is designed to be charged to 2000 volts. A 50 mm diameter light fired semiconductor switch is located at the center of the pulse forming networks and is used to switch the power from the PFN's into the load resistors. The laser on the left of Fig. 7 is directed at the multifurcated light pipe, which in turn is directed through the specially designed window in the silicon switch. Using this technique we have switched peak currents of 25KA at rates up to $40\text{KA}/\mu\text{sec}$. The waveform of such a switching event is shown in Fig. 8.

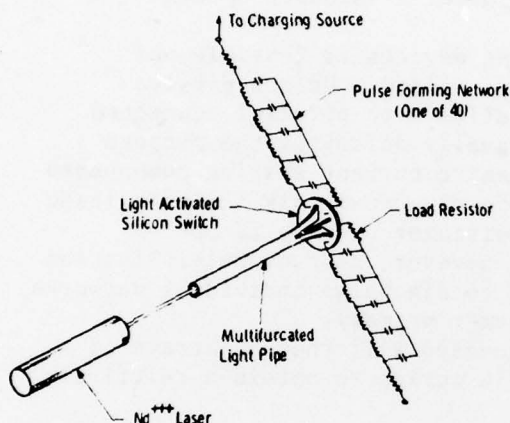


Fig. 7. Schematic of light activated silicon switch test apparatus. When the laser turns on the silicon switch, the energy stored in the pulse forming networks is discharged through the switch into the load resistors.

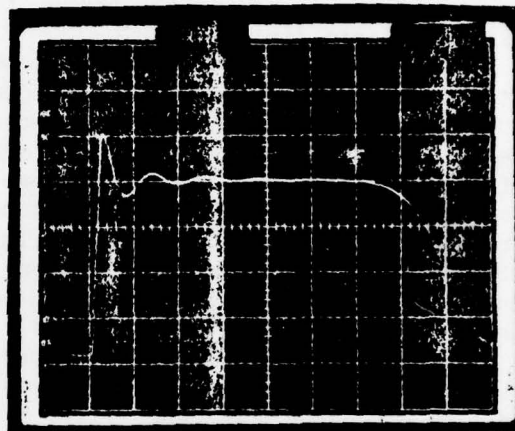


Fig. 8. Current waveform obtained by discharging system in Fig. 7. The time scale is $5\text{ }\mu\text{sec/division}$, current scale 5KA/division .

Even higher rates⁽¹⁾ of current rise have been achieved using parallel connected strip lines and low inductance connections. In this case, peak currents of 10KA and current rates of rise of $750\text{KA}/\mu\text{sec}$ have been measured. Pulse lengths in this case were 100 nsec. The results are summarized in Table 1.

Table 1

| Line Impedance (Ω) | Charge Voltage (V) | Peak Current (A) | Pulse Length | $\frac{di}{dt}$ (KA/ μsec) | Peak Power (MW) |
|-----------------------------|--------------------|------------------|--------------------|--|-----------------|
| 50 | 750 | 16 | 100 nsec | 3.75 | 0.011 |
| 0.104 | 1020 | 9820 | 100 nsec | 755 | 10.0 |
| 0.040 | 1700 | 25000 | 40 μsec | 40 | 42.5 |

Circuit Considerations

Pulse network charging voltages in the multikilovolt range are commonplace in radar modulation circuits, while the most advanced short pulse applications call for switches which can block from 100 kV to 1 MV. Since the basic devices used for switch construction are limited to a few kilovolts, the need for series operation of semiconductor switching devices is obvious.

The modularity of power pulse switching circuitry utilizing semiconductor devices can be of great benefit to the circuit designer because it provides an additional degree of flexibility not otherwise available. A given set of load requirements can be satisfied using a single series string of switching devices, or by combinations of series-connected devices switching individual pulse networks whose outputs are combined and coupled to the load by a pulse transformer. Although this flexibility is not available across the board, it does offer a valuable option within certain limits.

Although series connection of switching devices is feasible and attractive, direct paralleling is generally avoided. Unless passive current sharing components are placed in series with parallel connected devices, current is generally not shared equally defeating the purpose of the parallel connection. The use of passive current sharing components is expensive and results in the introduction of undesirable series voltage drops. Therefore, direct paralleling of switching devices is not considered in subsequent discussions. If, however, current multiplication is needed, individual switches can be used to discharge individual networks into a common load or into a pulse transformer primary.

The types of solid state switches discussed will then be arrays of semiconductor switching devices connected in series to obtain a relatively high voltage blocking capability.

Series Operation Considerations

When a number of switching devices are series-connected to hold off a high PFN charge voltage, a resistor must be connected in parallel with each device to insure uniform division of the PFN voltage between all switching devices when in the off state as shown in Fig. 9. All resistors, R_{a1} to R_{an} , should be equal in value and should be low enough in resistance to swamp out differences in switching device leakage currents over the full range of operating temperatures, but they should be high enough so that the PFN is not discharged appreciably between pulses.

A four layer switching device can be triggered on by a sharply rising voltage transient appearing between anode and cathode. To guard against such an occurrence at an undesirable time caused by a miscellaneous circuit transient, RC networks are sometimes connected across each of the switching devices in the series string as shown also in Fig. 9 as R_{b1} to R_{bn} and C_1 to C_n .

The complexity of the triggering apparatus required depends upon the type of basic device structure used in the switch. The purpose of the triggering circuitry is to turn on at the same instant all individual switching devices which comprise the complete switch. In practice, however, this is impossible to accomplish because all switching devices do not exhibit the same delay time, defined as the interval between receipt of the triggering stimulus and the time when anode voltage begins to fall. The effects of delay time on switch performance are discussed in the following paragraphs.

AD-A080 567

WESTINGHOUSE RESEARCH AND DEVELOPMENT CENTER PITTSBU--ETC F/G 9/1
OPTICALLY ACTIVATED SWITCH.(U)
APR 78 L R LOWRY

UNCLASSIFIED

AFAPL-TR-78-17

F33615-74-C-2029

NL

4 OF 4
AD
A080567



END
DATE
FILMED
3-80
DDC

When a series string of switching devices receives a triggering signal, the devices with shorter turn-on delay times turn on before those whose delay times are longer. When this occurs, the off state voltages formerly blocked by the devices turning on first are shared as increased off state voltages applied to those devices which turn on last. The result of this effect is different for each of the three types of device structures considered, so each one will be discussed in turn.

In a thyristor switch, the result of differences in turn-on delay times between individual devices can be catastrophic failure. If the applied off-state voltages of the devices having longer delay times exceed the maximum forward blocking capability of the device structure before turn-on takes place, catastrophic failure will occur. The presence of the RC snubber network helps to protect against this situation to some extent, but in high power pulse circuitry, the amount of protection the snubber can offer is minimal if other problems are to be avoided. Greater protection is afforded by use of larger values of capacitance, but too large a capacitor increases the turn-on dissipation of the switching device excessively.

The RBDT series string is triggered on by application of a fast-rising, high voltage pulse to all or part of the series string of devices. Devices with short delay times turn on first allowing the triggering voltage they formerly blocked to be applied to the devices with longer delay times. The slower devices then receive added turn-on drive which tends to shorten their remaining turn-on delay time. Because the RBDT turns on as a result of a fast rising high voltage pulse, turn-on delay time phenomena cannot cause catastrophic failure as is the case with the thyristor. If anything, the effects of differing turn-on delay times are minimized by the turn-on mechanism of the RBDT.

The effects on series switch performance of turn-on delay time differences between devices is theoretically the same for the LASS as it is for the thyristor. However, as a consequence of the laser drive used to initiate triggering, turn-on delay time is reduced to a value so small that for all practical purposes it can be ignored. All LASS devices in a series string respond so quickly and uniformly to the laser drive that no voltage increase is observed on any device in the string prior to turn-on.

Circuits which generate high power pulse currents by the discharge of pulse networks in general tend to reverse bias the switching device at the end of the pulse owing to reverse charging of the network. In contrast to the action of a thyatron, a semiconductor switching device will not block reverse voltage immediately following forward pulse current conduction until a reverse current has flowed for a time sufficient to sweep out all stored charge. When this point is reached, reverse current is suddenly interrupted and the device blocks whatever reverse voltage the external circuit impresses on it.

The quantity of stored charge contained in a semiconductor device following forward pulse current conduction varies from device to device. If a switch comprises a series string of semiconductor switching devices, the reverse sweep-out current will be the same for all, but due to stored charge variations, the time duration of reverse current flow before reverse blocking capability is regained will vary from device to device. The device with the smallest amount of stored charge will recover first and then attempt to block the entire voltage impressed upon it by the external circuit. In general, such a condition leads to catastrophic failure in a series switching circuit unless precautions are taken.

For all three device structures considered, turn-off time is minimized when a small amount of reverse bias is applied to the semiconductor switching devices following the end of forward pulse current flow. This can be accomplished by the same circuit techniques used to protect devices against catastrophic reverse voltage transients as shown in Fig. 9. Diode D_R and the resistor R_R serve as a damping network to limit peak reverse voltage applied to the switch overall, as is commonly done in thyatron circuits. Individual stored charge variations between semiconductor switching devices are taken into account by the placement of individual diodes, D_1 to D_n , in antiparallel connection across each switching device. When the device containing the smallest quantity of stored charge recovers, the reverse switch current interrupted by it is diverted to its antiparallel diode which provides a path for it to flow and prevents the generation of a high reverse voltage transient.

In general, semiconductor switching devices tailored for optimum pulse switching do not also exhibit short turn-off time. At present, RBDT devices are manufactured with turn-off times in the range of 100 to 200 μ s at rated junction temperature, and although thyristors can be made with turn-off times much less than these, the thyristors suitable for fast pulse switching have turn-off times between 100 and 200 μ s as well. The situation regarding the turn-off time of the LASS is less clear because LASS has not yet been fully evaluated in pulse circuitry. Present LASS devices are made from thyristor structures with turn-off times ranging from 50 to 100 μ s, but it appears that, in the future, devices with shorter values of turn-off time can be developed.

Comparison of Alternatives

Each of the switching device structures considered offers a certain combination of performance parameters. When a device must be chosen for a given application, the best fit between the requirements of the application and device performance should be obtained.

From the standpoint of voltage blocking capability, there is little to choose from at present between the thyristor, the RBDT, and the LASS. The basic fast switching structures of all three are capable of blocking about the same voltage. In virtually all cases, individual devices must be series-connected to realize a high voltage switch.

For short pulse work (less than 20 μ s), the maximum allowable peak current is related to di/dt , pulse length, and PRF. The thyristor structure is the poorest, in regard to the compromise. The RBDT is next, and the best is the LASS because its turn-on losses are lower.

The maximum allowable di/dt is dependent on peak current, pulse length, and PRF. The larger the initial area turned on, the higher the maximum allowable value of di/dt as discussed earlier. In this regard, the thyristor is the poorest, the RBDT is better, and the LASS the best.

Semiconductor device turn-off time depends upon the combination of parameters chosen for device design, and in addition, it depends on junction temperature. If a hot spot is developed at a given point on the surface of the device owing to small area turn-on, it will be the determining factor for turn-off time. In regard to turn-off time, then, the RBDT is superior to the thyristor. Because it has not yet been fully evaluated, the turn-off time of the LASS operating in fast, high power pulse circuitry has yet to be determined.

Each of the three device structures considered requires a different form of trigger. The simplest to trigger is the thyristor which requires

a relatively small gate current of the order of a few amperes at several volts. In series string connections, however, the current for each device must be supplied by an isolated source. The RBDT requires a high voltage, fast rising voltage pulse of sufficient amplitude to break over all or a substantial part of the series string of devices. The trigger pulse, which must have a leading edge rate-of-rise between 5 and 10 kV/ μ s, need not be more than a few microseconds in duration regardless of load current pulse length. The LASS must be triggered by radiation of a certain wavelength. The required pulse is best produced by a neodymium YAG laser. The radiation can be distributed to the individual devices connected in a series string by use of fiber optics or with conventional optics using beam splitters.

Triggering techniques increase in complexity and cost in going from the thyristor to the RBDT to the LASS. When a device is chosen for use in a given application, the increased system cost resulting from the requirement for a more complex triggering system must be justified by the necessity for the higher di/dt capability obtained.

Basic Circuit Techniques

For the purposes of this discussion, the switch will be assumed to serve as the device which discharges a PFN or line into a load matched reasonably closely to the network or line characteristic impedance. This type of basic circuit configuration covers generally most applications from small radar modulators to high power laser pulsers.

Shown in Fig. 10 is a simplified basic configuration of a discharge circuit using a series thyristor switch. As discussed earlier, shunting diodes, snubber networks and voltage equalizing components may be included if called for in the application. Each thyristor must be gated on by an isolated gating circuit. A common triggering signal must initiate simultaneous gate current injection into all thyristors to minimize turn-on voltage spikes.

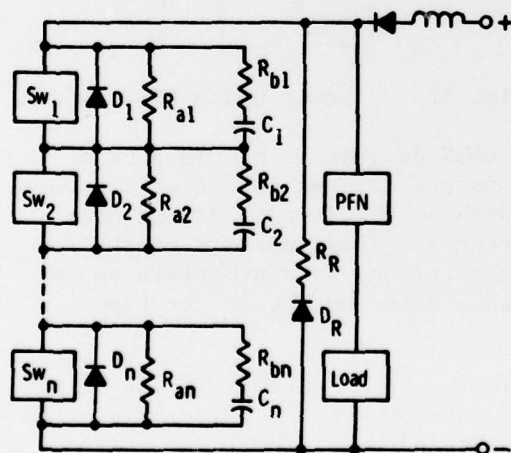


Fig. 9. Basic pulse circuit.

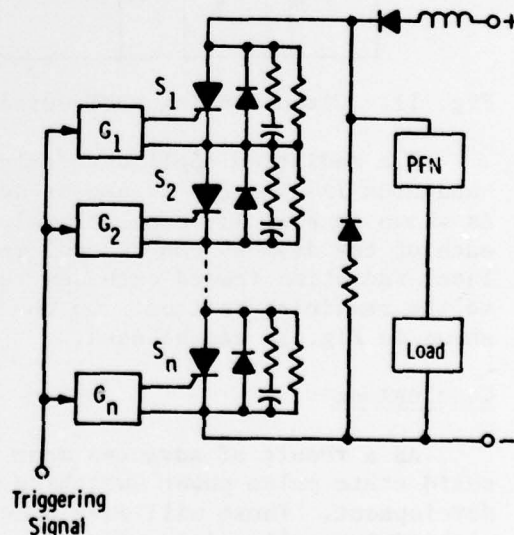


Fig. 10. Circuit using thyristor switch.

Shown in Fig. 11 is a simplified basic configuration of a discharge circuit using a series RBDT switch. Each RBDT device is shunted by a diode,

a snubber network reduced to a small capacitor only, and a voltage equalizing resistor. A short, fast rising high voltage pulse is delivered to the switch by the secondary of the trigger pulse transformer. Diode D_1 prevents the PFN from shorting the trigger pulse to ground, and diode D_2 prevents the PFN from discharging through the pulse transformer. Diode D_3 helps to further limit peak reverse voltage. The trigger pulse must be generated by the discharge of a capacitor into the primary of the trigger transformer by a fast switch such as another RBDT or a thyatron. The trigger pulse is applied to the entire switch by diode D_2 . In other configurations, the pulse can be applied to a portion of the series string as long as the portion is greater than $1/2$.

Shown in Fig. 12 is a simplified basic configuration of a discharge circuit using a series LASS switch. The LASS devices are shunted by antiparallel diodes and voltage equalizing resistors. It appears that in some applications, small snubber networks will be required, but because of the negligibly small turn-on delay times, no dynamic equalizing capacitance is needed.

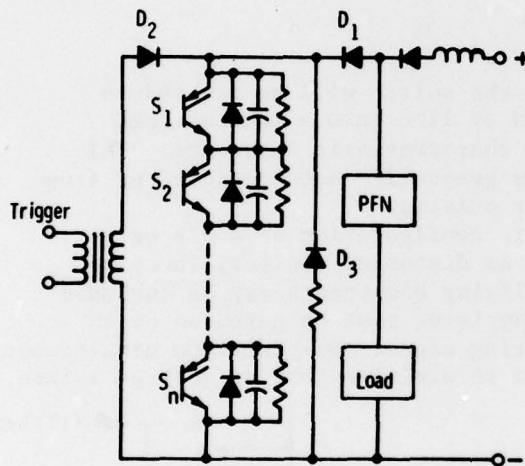


Fig. 11. Circuit using RBDT switch.

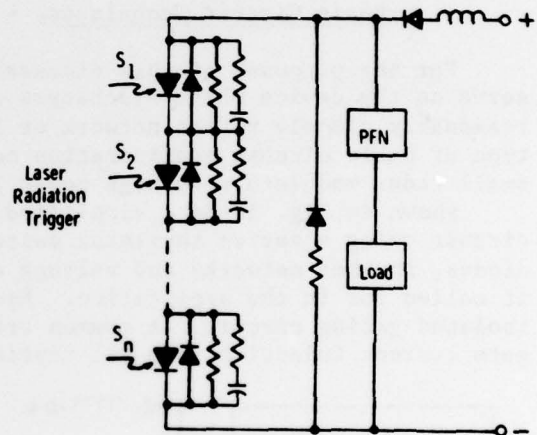


Fig. 12. Circuit using LASS switch.

The radiation applied to trigger the LASS devices is provided by a neodymium YAG laser. It can be delivered to the devices in one of two ways. As shown in Fig. 13, conventional optics with beam splitters located near each of the devices can be employed to direct a certain portion of the laser radiation toward each device while passing on an appropriate amount to the remaining devices. On the other hand, fiber optics of the type shown in Fig. 14 can be used.

Conclusions

As a result of advances made in the semiconductor industry, several solid state pulse power switching devices are now either available or under development. These will make possible pulse generation ranging from negligibly small values of di/dt to levels higher than 10^{12} A/sec. As switching devices with increasingly high di/dt ratings are selected for application, the complexity and cost of triggering increases also. It is important, therefore, to select the device best suited to each application,

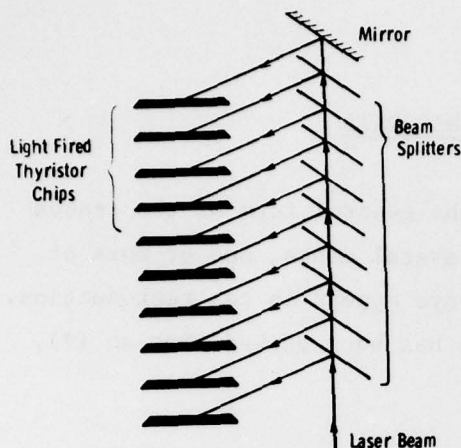


Fig. 13. Beam splitter optical system.

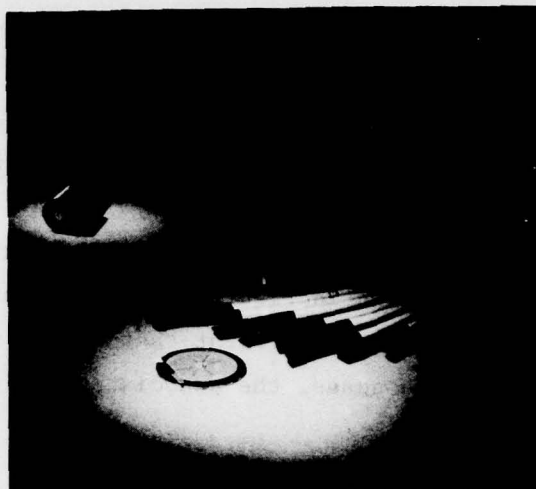


Fig. 14. Fiber optic cables.

and to make sure that the device selected is not overly qualified, because if it is circuit cost will be increased beyond the level where it should be. Thyristors of many types are available now for limited use in pulse switching applications. RBDT devices are available and have been used in a number of radar modulators.² Devices employing the LASS structure are now under development supported by government contracts. Because the LASS is still under development, it has not been fully characterized to determine the ultimate limits of its peak current and di/dt capabilities.

Acknowledgments

The authors would like to express their thanks to many members of the Westinghouse Research Laboratories for supplying material for this paper. In particular to Mr. J. S. Roberts for information on LASS performance and Mr. J. B. Brewster for his information on RBDT devices. Thanks are also due to the US Navy and the US Air Force for support in the area of light triggered thyristors under Contracts N00039-71-C-0228 and F33615-74-C-2029.

References

- (1) Experimental Demonstration of High Power Fastrise-Time Switching in Silicon Junction Semiconductors. O.S.F. Zucker et al Applied Physics Letters, Vol. 29, No. 4, p. 261-263.
- (2) The RSR - Past, Present and Future. R. A. Gardenghi, 1976 Pulsed Power Systems Workshop, White Oak, Maryland. September 1976.

APPENDIX VI
OSCILLOGRAMS OF ORIGINAL DATA

In the following oscillograms, the general form of the traces is as shown in Figure VI-1. However, in several cases, one or more of the traces is so faint that it may not always appear in the reproduction. In these cases, the associated scale value has been marked with an (*).

Dwg. 6415A14

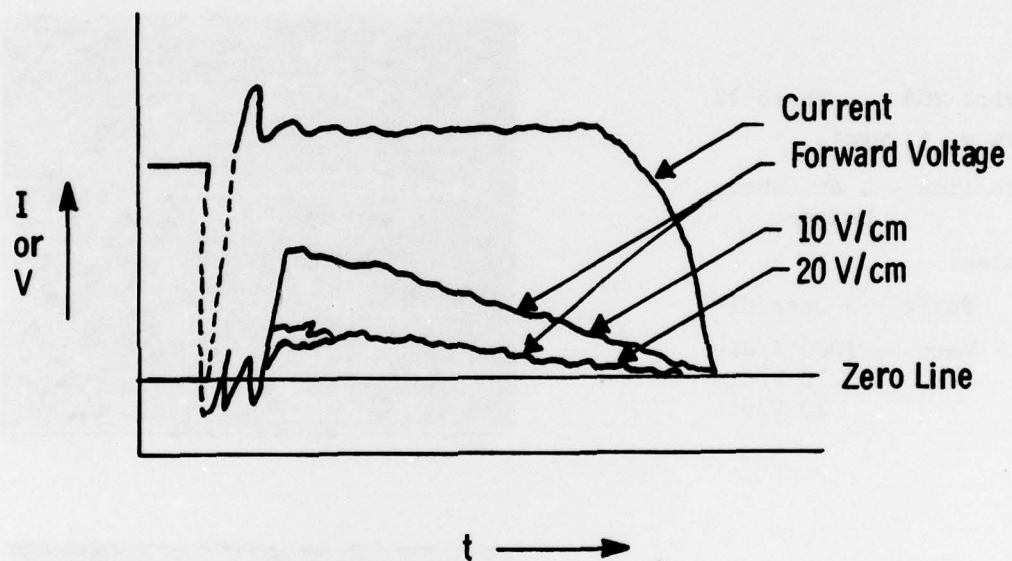
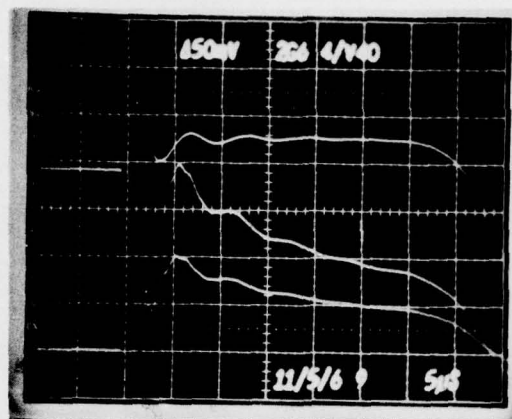


Figure VI-1. General format of the oscillograms. The actual location of the zero line must be carefully established in each instance.

Device 2G6 Photo 5
 1700 V, 40 PFN's
 Zero line - 1 div above
 bottom

Scales:

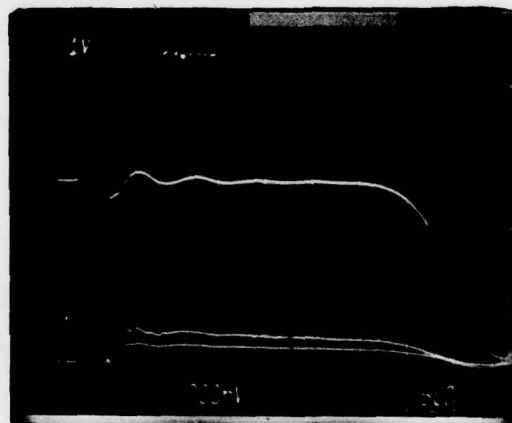
Horiz - 5 μ sec/div
 Vert - 4000 A/div
 10 V/div
 20 V/div



Device 2G4 Photo 12
 1275 V, 11 PFN's
 Zero line - 1 div above
 bottom

Scales:

Horiz - 5 μ sec/div
 Vert - 1000 A/div
 10 V/div
 20 V/div

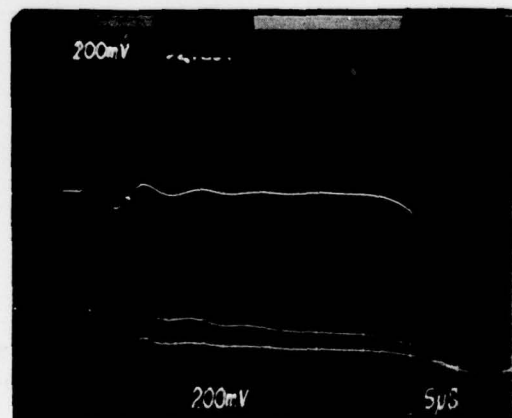


Device 2G4 Photo 13
 1275 V, 20 PFN's
 Zero line - 1 div above
 bottom

Scales:

Horiz - 5 μ sec/div
 Vert - 2000 A/div
 10 V/div
 20 V/div

8 light pipes



Device 2G4 Photo 14

1275 V, 25 PFN's

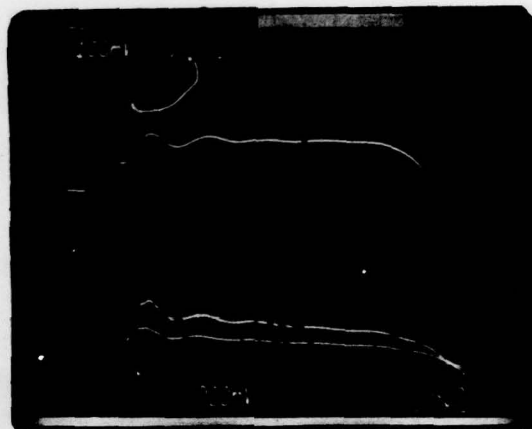
Zero line - 1 div above
bottom

Scales:

Horiz - 5 μ sec/div

Vert - 2000 A/div
10 V/div
20 V/div

8 light pipes



Device 2G4 Photo 15

1275 V, 30 PFN's

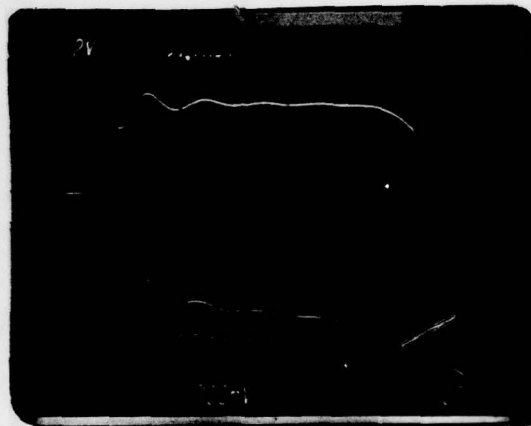
Zero line - 1 div above
bottom

Scales:

Horiz - 5 μ sec/div

Vert - 2000 A/div
10 V/div
20 V/div

8 light pipes



Device 2G4 Photo 16

1275 V, 35 PFN's

Zero line - 1 div above
bottom-V

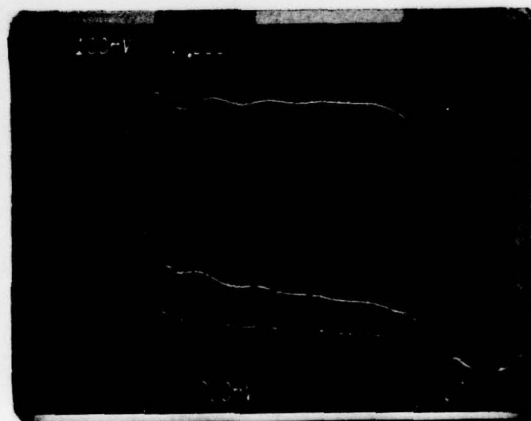
- at bottom-I

Scales:

Horiz - 5 μ sec/div

Vert - 2000 A/div
10 V/div
20 V/div

8 light pipes



Device 2G4 Photo 17

1275 V, 40 PFN's

Zero line - 1 div above
bottom

Scales:

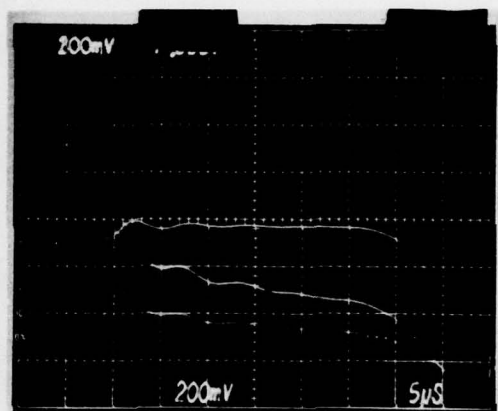
Horiz - 5 μ sec/div

Vert - 5000 A/div

10 V/div

20 V/div

8 light pipes



Device 2G4 Photo 18

1700 V, 20 PFN's

Zero line - 1 div above
bottom

Scales:

Horiz - 5 μ sec/div

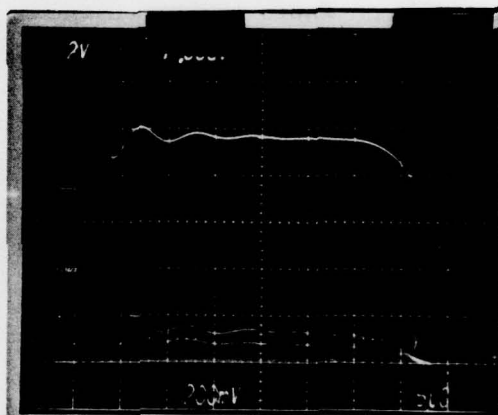
Vert - 2000 A/div

10 V/div*

20 V/div*

Voltage signal clamped

8 light pipes



Device 2G4 Photo 19

1700 V, 25 PFN's

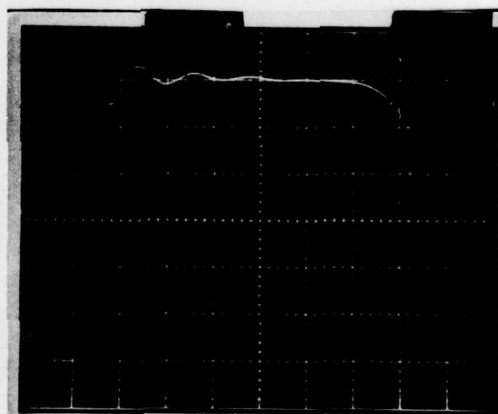
Zero line - 1 div above
bottom

Scales:

Horiz - 5 μ sec/div

Vert - 2000 A/div

8 light pipes



Device 2G4 Photo 20

1700 V, 25 PFN's

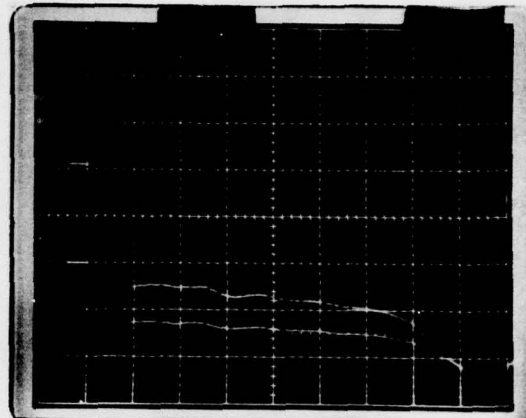
Zero line - 1 div above
bottom

Scales:

Horiz - 5 μ sec/div

Vert - 10 V/div
20 V/div

Voltage clamped
8 light pipes



Device 2G4 Photo 21

1700 V, 30 PFN's

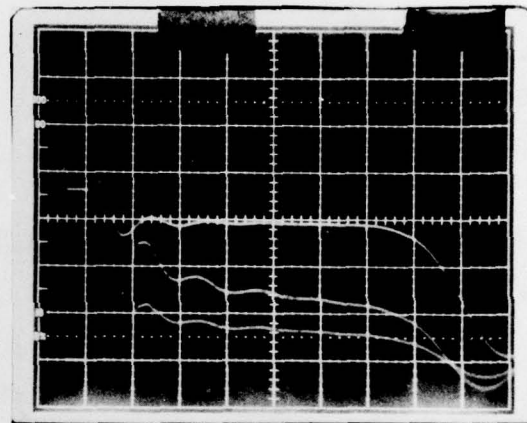
Zero line - 1 div above
bottom

Scales:

Horiz - 5 μ sec/div

Vert - 5000 A/div
10 V/div*
20 V/div*

Voltage clamped at 45 V
8 light pipes



Device 2G4 Photo 22

1700 V, 35 PFN's

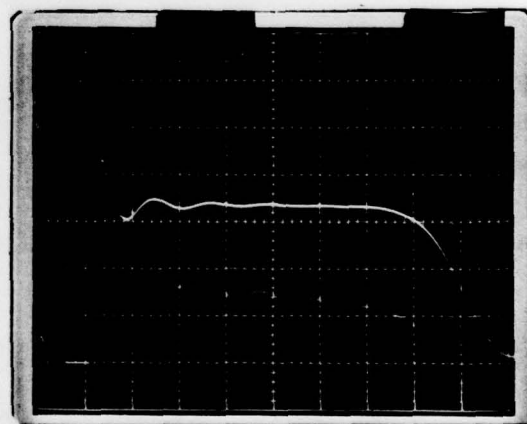
Zero line - 1 div above
bottom

Scales:

Horiz - 5 μ sec/div

Vert - 5000 A/div
10 V/div

8 light pipes



Device 2G6 Photo 97

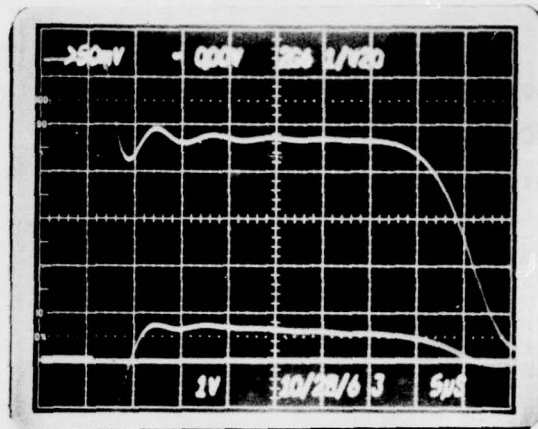
425 V, 20 PFN's

Zero line - 1 div above
bottom

Scales:

Horiz - 5 μ sec/div

Vert - 1000 A/div
10 V/div
20 V/div



Device 2G6 Photo 89

425 V, 20 PFN's

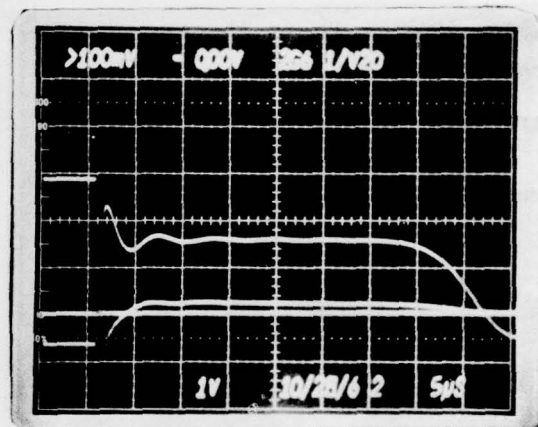
Zero line - 2 div above
bottom-V

- 1.4 div above
bottom-I

Scales:

Horiz - 5 μ sec/div

Vert - 1000 A/div
10 V/div
20 V/div



Device 2G6 Photo 88

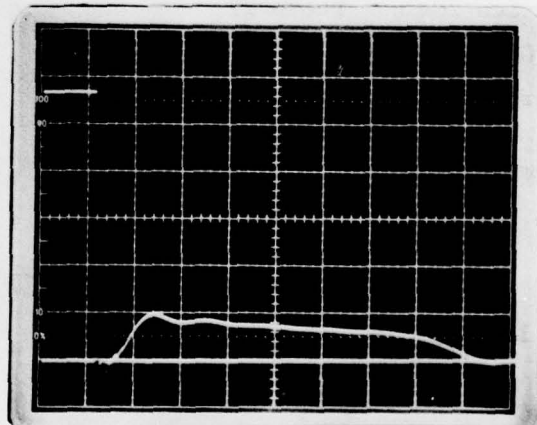
425 V, 39 PFN's

Zero line - 1 div above
bottom

Scales:

Horiz - 5 μ sec/div

Vert - 10 V/div



Device 2G6 Photo 92

425 V, 39 PFN's

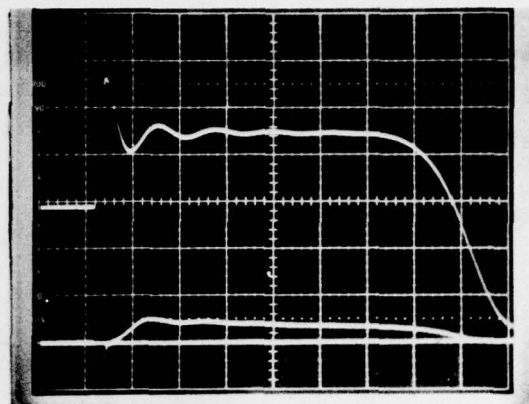
Zero line - 1 div above
bottom

Scales:

Horiz - 5 μ sec/div

Vert - 1000 A/div
20 V/div

8 light pipes



Device 2G6 Photo 83

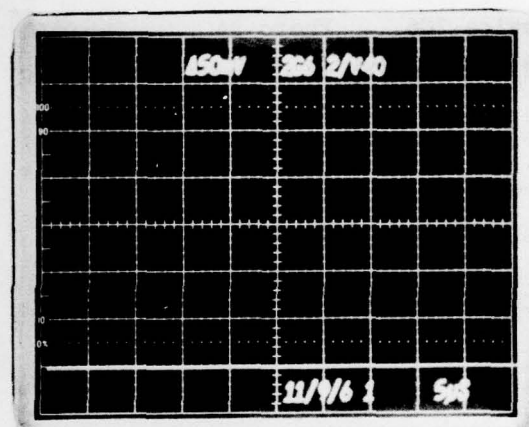
850 V, 40 PFN's

Zero line - 1 div above
bottom

Scales:

Horiz - 5 μ sec/div

Vert - 10 V/div*
20 V/div*



Device 2G6 Photo 83A

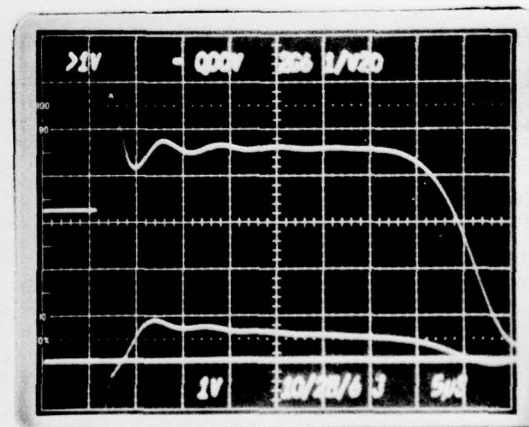
850 V, 40 PFN's

Zero line - 1 div above
bottom

Scales:

Horiz - 5 μ sec/div

Vert - 2000 A/div
20 V/div



Device 2G6 Photo 93

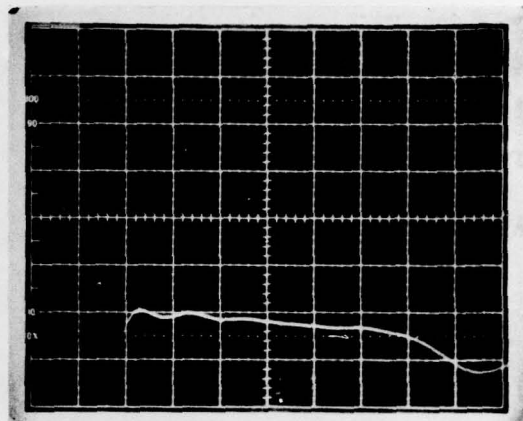
1275 V, 20 PFN's

Zero line - 1 div above
bottom

Scales:

Horiz - 5 μ sec/div

Vert - 10 V/div



Device 2G6 Photo 94

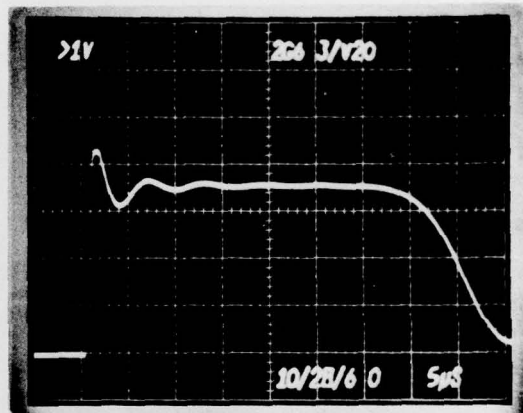
1275 V, 20 PFN's

Zero line - 1 div above
bottom

Scales:

Horiz - 5 μ sec/div

Vert - 2000 A/div



Device 2G6 Photo 96A

1275 V, 25 PFN's

Zero line - 1 div above
bottom

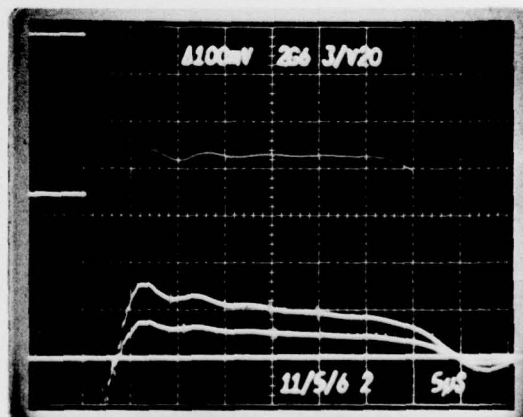
Scales:

Horiz - 5 μ sec/div

Vert - 2000 A/div*

10 V/div

20 V/div



Device 2G6 Photo 150

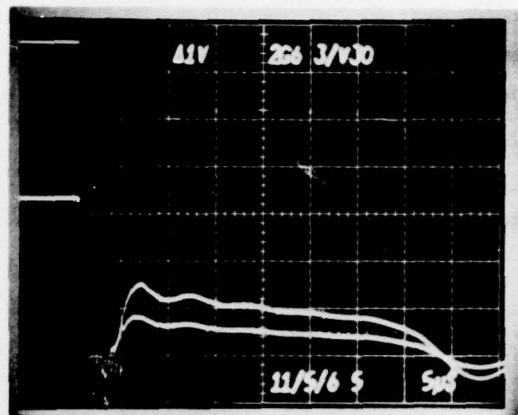
1275 V, 30 PFN's

Zero line - 1 div above
bottom

Scales:

Horiz - 5 μ sec/div

Vert - 2000 A/div*
10 V/div
20 V/div



Device 2G6 Photo 151

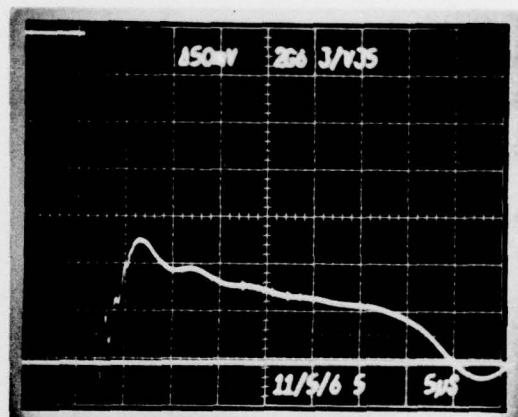
1275 V, 35 PFN's

Zero line - 1 div above
bottom

Scales:

Horiz - 5 μ sec/div

Vert - 2000 A/div
10 V/div
20 V/div*



Device 2G6 Photo 152

1275 V, 40 PFN's

Zero line - 1 div above
bottom

Scales:

Horiz - 5 μ sec/div

Vert - 4000 A/div*
10 V/div
20 V/div



Device 2G6 Photo 153

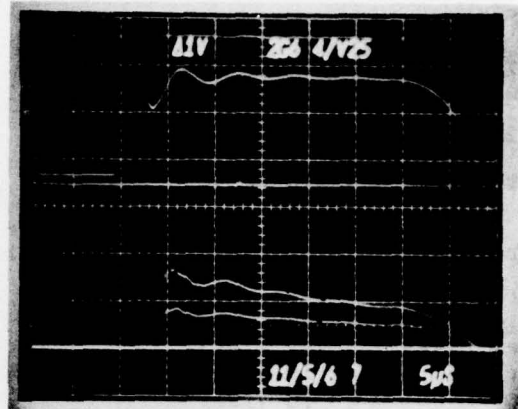
1700 V, 25 PFN's

Zero line - 1 div above
bottom

Scales:

Horiz - 5 μ sec/div

Vert - 2000 A/div
10 V/div
20 V/div



Device 2G6 Photo 154

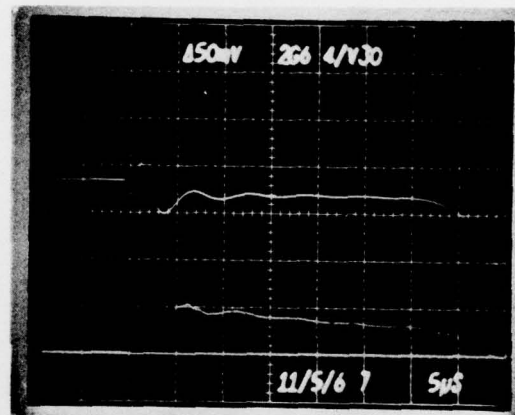
1700 V, 30 PFN's

Zero line - 1 div above
bottom

Scales:

Horiz - 5 μ sec/div

Vert - 4000 A/div
10 V/div*
20 V/div



Device 2G6 Photo 155

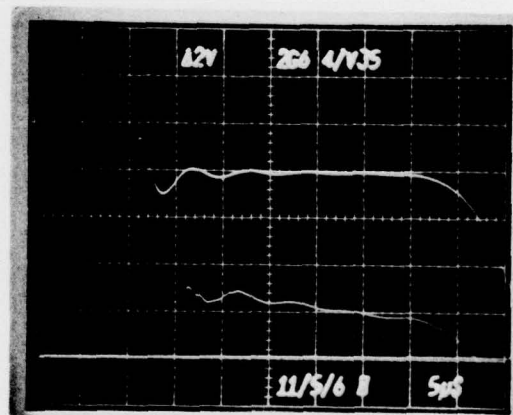
1700 V, 35 PFN's

Zero line - 1 div above
bottom

Scales:

Horiz - 5 μ sec/div

Vert - 4000 A/div
10 V/div
20 V/div*



Device 2G6 Photo 156

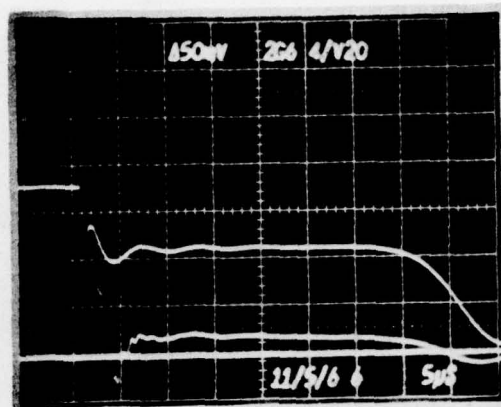
1700 V, 20 PFN's

Zero line - 1 div above
bottom

Scales:

Horiz - 5 μ sec/div

Vert - 4000 A/div
10 V/div*
20 V/div



Device 2G6 Photo 100

850 V, 40 PFN's

Zero line - 1 div above
bottom

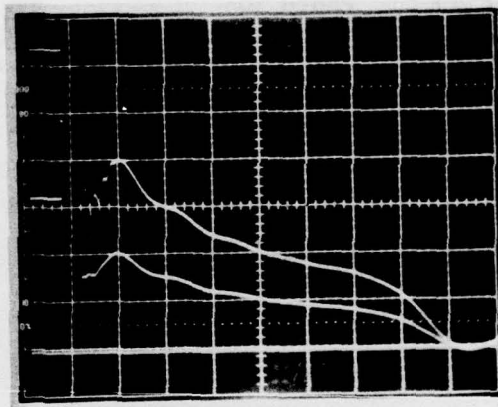
Scales:

Horiz - 5 μ sec/div

Vert - 10 V/div
20 V/div

light pipes 8-1-2-3

in slots 2-4-6-8



Device 2G6 Photo 101

850 V, 40 PFN's

Zero line - 1 div above
bottom

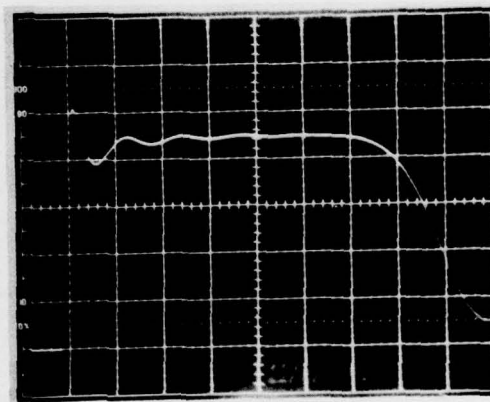
Scales:

Horiz - 5 μ sec/div

Vert - 2000 A/div

light pipes 8-1-2-3

in slots 2-4-6-8



Device 2G6 Photo 103

850 V, 40 PFN's

Zero line ~ 1 div above
bottom

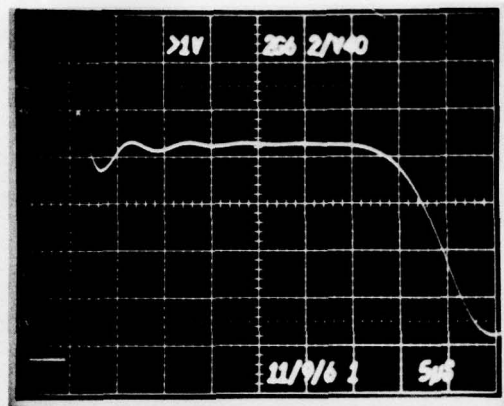
Scales:

Horiz - 5 μ sec/div

Vert - 2000 A/div

light pipes 8-1-2-3-7

in slots 2-4-6-8-7



Device 2G6 Photo 104

850 V, 40 PFN's

Zero line - 1 div above
bottom

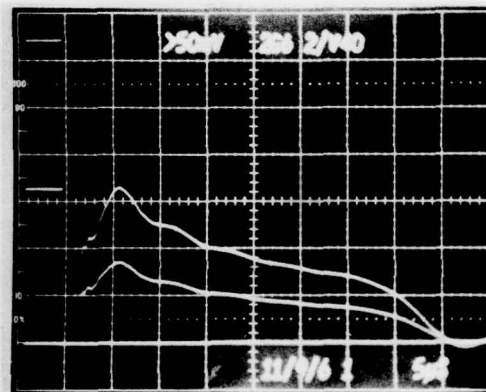
Scales:

Horiz - 5 μ sec/div

Vert - 10 V/div
20 V/div

light pipes 8-1-2-3-7

in slots 2-4-6-8-7



Device 2G6 Photo 105

850 V, 40 PFN's

Zero line - 1 div above
bottom

Scales:

Horiz - 5 μ sec/div

Vert - 2000 A/div

light pipes 2-4-5-6-7-8

in slots 8-1-5-2-7-3



Device 2G6 Photo 108

850 V, 40 PFN's

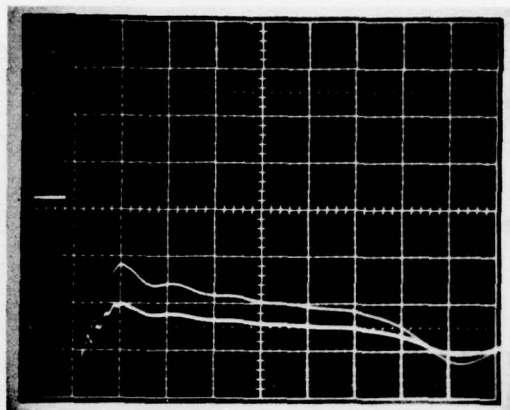
Zero line - 1 div above
bottom

Scales:

Horiz - 5 μ sec/div

Vert - 10 V/div
20 V/div

8 light pipes



Device 2G6 Photo 112

850 V, 40 PFN's

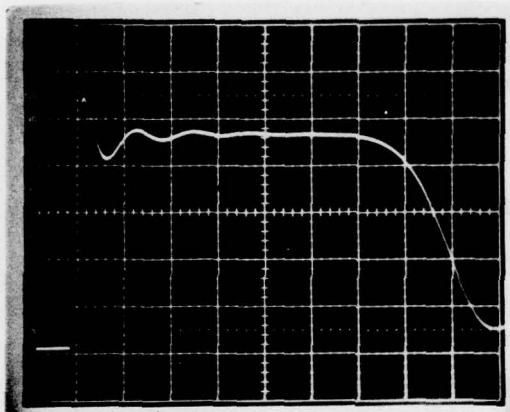
Zero line - 1 div above
bottom

Scales:

Horiz - 5 μ sec/div

Vert - 2000 A/div

8 light pipes



Device 2G6 Photo 106

850 V, 40 PFN's

Zero line - 1 div above
bottom

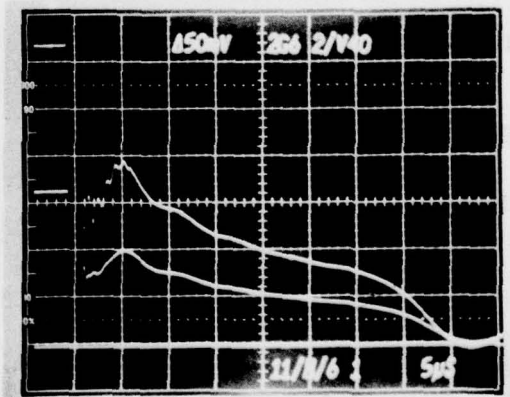
Scales:

Horiz - 5 μ sec/div

Vert - 10 V/div
20 V/div

light pipes 8-1-2-3

in slots 1-3-5-7



Device 2G6 Photo 110

850 V, 40 PFN's

Zero line - 1 div above
bottom

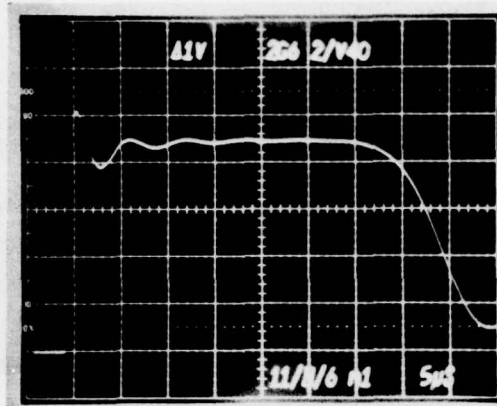
Scales:

Horiz - 5 μ sec/div

Vert - 2000 A/div

light pipes 8-1-2-3

in slots 1-3-5-7



Device 2G6 Photo 109

850 V, 40 PFN's

Zero line - 1 div above
bottom

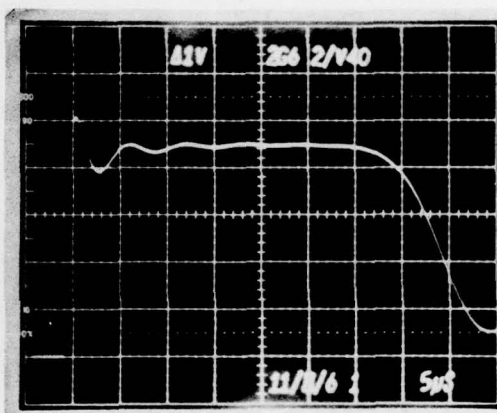
Scales:

Horiz - 5 μ sec/div

Vert - 2000 A/div

light pipes 8-1-2-3

in slots 8-1-4-5



Device 2G6 Photo 113

850 V, 40 PFN's

Zero line - 1 div above
bottom

Scales:

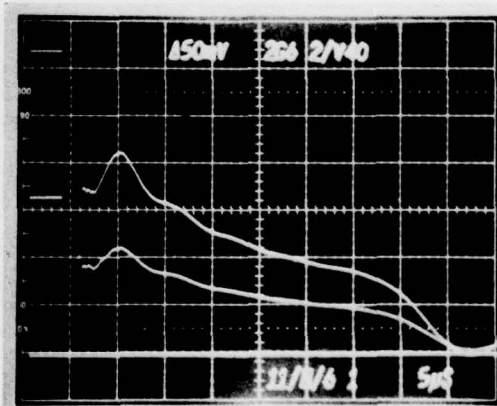
Horiz - 5 μ sec/div

Vert - 10 V/div

20 V/div

light pipes 8-1-2-3

in slots 8-1-4-5



Device 2G6 Photo 114

850 V, 40 PFN's

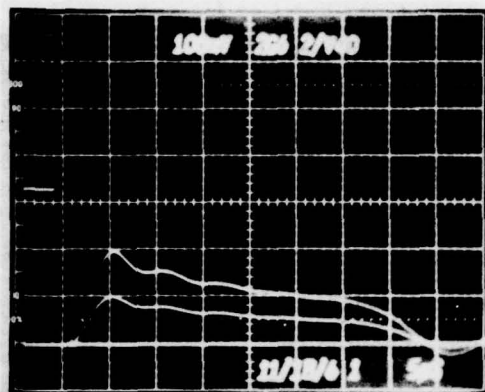
Zero line - 1 div above
bottom

Scales:

Horiz - 5 μ sec/div

Vert - 10 V/div
20 V/div

no attenuation of light



Device 2G6 Photo 115

850 V, 40 PFN's

Zero line - 1 div above
bottom

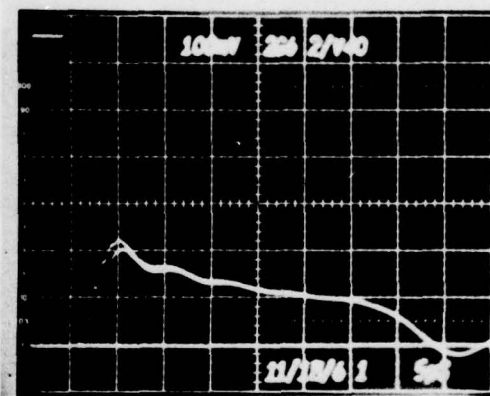
Scales:

Horiz - 5 μ sec/div

Vert - 10 V/div

38% light attenuation

filters CS7-56



Device 2G6 Photo 116

850 V, 40 PFN's

Zero line - 1 div above
bottom'

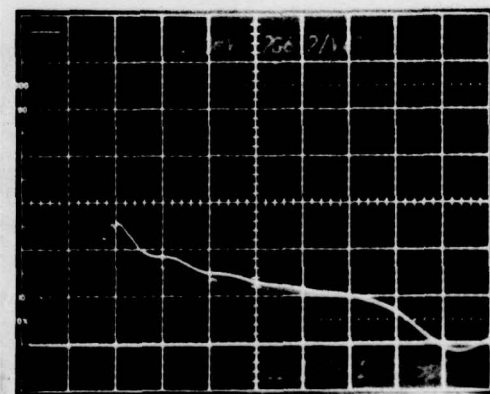
Scales:

Horiz - 5 μ sec/div

Vert - 10 V/div

55% light attenuation

filters CS3-73 & CS7-56



Device 2G6 Photo 117

850 V, 40 PFN's

Zero line - 1 div above
bottom

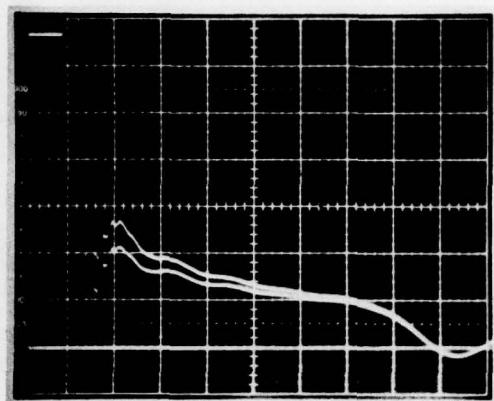
Scales:

Horiz - 5 μ sec/div

Vert - 10 V/div

62% light attenuation

filters CS5-76, CS3-73, &
CS7-56



Device 2G6 Photo 118

850 V, 40 PFN's

Zero line - 1 div above
bottom

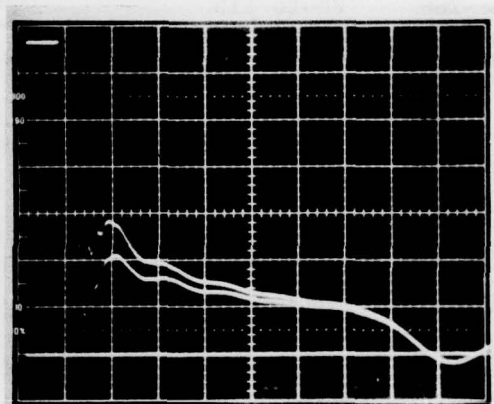
Scales:

Horiz - 5 μ sec/div

Vert - 10 V/div

68% light attenuation

filters CS5-56, CS5-56,
CS3-73, & CS7-56



Device 2G6 Photo 119

850 V, 40 PFN's

Zero line - 1 div above
bottom

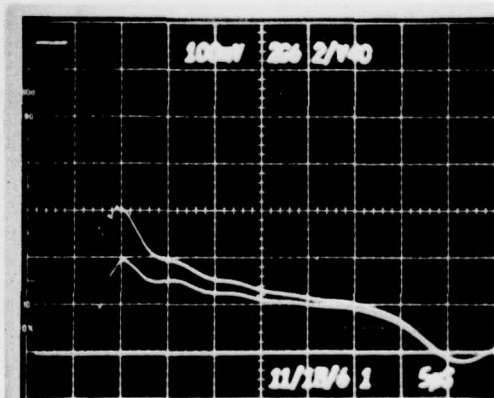
Scales:

Horiz - 5 μ sec/div

Vert - 10 V/div

77.3% light attenuation

filters CS2-61, CS2-58,
CS5-56, CS5-56
CS3-73, & CS7-56



Device 2G6 Photo 120

850 V, 40 PFN's

Zero line - 1 div above
bottom

Scales:

Horiz - 5 μ sec/div

Vert - 2000 A/div

77.3% light attenuation

filters CS2-61, CS2-58

CS5-56, CS5-56

CS3-73, & CS7-56



Device 2G6 Photo 121

850 V, 40 PFN's

Zero line - 1 div above
bottom

Scales:

Horiz - 5 μ sec/div

Vert - 50 V/div

Light unattenuated and
77.3% attenuation

Voltages probes direct -
no clamping circuit

